Electrical resistivity tomography investigations of discontinuous mountain permafrost and its relation to elevation and vegetation, Yukon

Zoé Kuntz

Thesis submitted to the

Faculty of Graduate and Postdoctoral Studies

in partial fulfillment of the requirements

for the degree of Master of Science in Geography

uOttawa

Department of Geography, Environment and Geomatics

University of Ottawa

© Zoé Kuntz, Ottawa, Canada, 2017

Abstract

This study seeks to better understand the relationship between permafrost, elevation and vegetation cover, and to test the hypothesis that changes in mountain permafrost distribution and characteristics occur at vegetation type boundaries, as they do in latitudinal permafrost.

Twelve electrical resistivity tomography (ERT) surveys were completed at vegetation transitions on selected slopes near Whitehorse and Dawson, Yukon, in July 2015. Wenner arrays with 2 m spacing between electrodes were used to complete the 80-280 m long surveys. Organic layer thickness and vegetative species composition were recorded in a transect for each survey. Ground-truthing via frost probing, pit digging, and ground temperature data from past and present weather stations aided in the analysis of ERT profiles.

Several different resistivity patterns are present along the profiles. These patterns indicate some presence of permafrost along most of the slopes sampled. Exceptions include south-facing slopes free of permafrost and a few slopes with inconclusive resistivity interpretations due to complex resistivity patterns and ground-truthing difficulties.

Overall, the results indicate that changes in permafrost distribution and characteristics do not consistently occur at vegetation type boundaries. At the scale examined, treeline is not as important a demarcation point for changes in permafrost as initially thought. Changes in organic mat, surficial geology, and snow cover (via micro-topography) appear to be as important as vegetation variation. These local controls play a significant role on permafrost distribution across both altitudinal and latitudinal forest-tundra ecotones. However, the propensity of alpine environments for cold air drainage and surface lapse rate inversions can create differences between the permafrost trends across altitudinal and latitudinal ecotones.

Acknowledgements

Many, many thanks and heartfelt appreciation to all those who have helped me along this Master's journey so far. First and foremost, I am grateful for the time and effort, wisdom and guidance I have received from my supervisor, Dr. Antoni Lewkowicz. His passion for permafrost, his experience and skill as a researcher and teacher, as well as his good humour and positive attitude have made this instructive experience enjoyable and enriching. I also appreciate the time and expertise of the other members of my thesis committee, Dr. Denis Lacelle and Dr. Sharon Smith.

Financial support came from the University of Ottawa, the Natural Sciences and Engineering Research Council, the Northern Scientific Training Program, and the Ontario Graduate Scholarship Program. My research would not have been possible without this funding. In addition, I am grateful to the Canadian Association of Geographers – Ontario Division and the International Permafrost Association for offering me the opportunity to present parts of my research and exchange with other researchers, as well as to the University Centre in Svalbard for the enriching Permafrost and periglacial landscape course that I was fortunate to attend.

I am indebted to my field assistant and colleagues. Pavel Popov, Jean Holloway, Robert Way, Olivier Bellehumeur-Génier, I salute you. Your help in the field, in the office or over email, for large and small tasks, has saved me much time and stress. Also, Alex Bevington, who has suffered my repeated questions and patiently provided me feedback, I must thank you. Your thesis work compiling the climate database has been invaluable.

To my family and friends, I thank you for encouraging me and listening to me when I needed a friendly ear. To my parents, Ray and Hélène, thank you for your continued guidance and support. Your own journeys as teachers and researchers are inspiring. Max, your arrival in Ottawa could not have been timed better. Having my brother nearby as I powered through those final days of editing was an unexpected gift. Nevenka, thank you for having us over for supper and driving us to the lake. You helped keep me well-nourished and relaxed. Pavel, thank you for helping me keep a good work-life balance and for helping us continue to go running. I sincerely thank all of you for being there and taking care of me when I needed to just "thesis" and juggle nothing else.

Table of Contents

List of figures

List of tables

List of abbreviations

AMAT - annual mean air temperature: the average temperature of the air for a single year.

AMGT - annual mean ground temperature: the average temperature of the ground at a given depth for a single year.

AMGST - annual mean ground surface temperature: the average temperature of the ground surface for a single year.

asl - above sea level

BTS – basal temperature of snow: a method used to infer permafrost presence

bTTOP - blended temperature at the estimated top of permafrost: a blended-year statistic from Bevington's (2016) database that is the average of the twelve monthly mean temperatures of the ground at a given depth, where each monthly mean was calculated by averaging the values for months, from a range of years, that were 90% complete.

bMAAT - blended mean annual air temperature: a blended-year statistic from Bevington's (2016) database that is the average of the twelve monthly mean temperatures of the air, where each monthly mean was calculated by averaging the values for months, from a range of years, that were 90% complete.

bMAGST - blended mean annual ground surface temperature: a blended-year statistic from Bevington's (2016) database that is the average of the twelve monthly mean temperatures of the ground surface, where each monthly mean was calculated by averaging the values for months, from a range of years, that were 90% complete.

ERT - Electrical resistivity tomography

SDD - Snow depth days: a measure of the snow cover calculated by adding the estimated average snowpack height (in meters) of each day of snow cover during a year.

TTOP model – Temperature at the top of permafrost model: a functional model for the mean annual temperature at the top of permafrost proposed by Smith and Riseborough (1996) as a general formulation of the climate-permafrost relationship.

1.0 Introduction

1.1 General

Mountain permafrost conditions vary around the globe and are not always comparable between regions. Many studies of mountain permafrost have been made in Europe (e.g. Isaksen et al. 2002; Harris et al. 2003; Gruber et al. 2004; Gruber and Haeberli 2007) where permafrost currently occurs only above treeline, in the tundra or bare rock areas. In contrast, in North America and Mongolia permafrost extends below treeline in subarctic lowland areas.

The differences in permafrost conditions between vegetation types have been examined in several studies (e.g. Smith 1975; Karunaratne and Burn 2004; Shur and Jorgenson 2007; Roadhouse 2010; Kremer et al. 2011; Bonnaventure and Lewkowicz 2012; Throop et al. 2012), but the transition zones from one type of vegetation cover to another, for instance between tundra and shrubs, or from shrubs to forest, have yet to be studied in detail. These transition zones are particularly important in climate change studies, as they will likely undergo significant change. As the air warms, shrubs may encroach on tundra and forests may encroach on areas with shrub cover (Loranty and Goetz 2012). These changes in vegetation cover will impact the thermal regime controlling the existence and characteristics of any underlying permafrost.

This thesis aims to increase our understanding of permafrost characteristics at the elevation transitions between different types of vegetation. Vegetation cover significantly affects energy exchanges between the air and the ground surface (Brown 1966) and thus the probability of permafrost being present. At high elevations in northern regions where tundra dominates, permafrost may be continuous. But, as one descends, air temperatures generally increase

enabling first shrubs and then trees to grow. In addition, the snowpack changes in thickness and density, affecting the degree of insulation of the ground in winter. Permafrost begins to break down spatially to the point that it may be present only in isolated patches.

This study attempts to characterize patterns of permafrost transitions from continuous permafrost in the tundra through to discontinuous permafrost beneath shrub and forest zones in the mountains in and around Whitehorse and Dawson in the Yukon.

1.2 Research objectives

Much remains unknown about discontinuous permafrost in mountainous environments. For instance, how does permafrost break down spatially from the boundary of continuous permafrost through to the zone of isolated patches? What are the sizes of permafrost bodies and how do they vary along an altitudinal transect through different vegetation zones? Does this change in permafrost contiguity that occurs over a few hundred meters of elevation differ from the change that takes place with latitude over hundreds of kilometers? This thesis demonstrates how electrical resistivity tomography can be used to help answer such questions. The answers to these questions should enable us to better understand future environmental change caused by climate warming combined with translocation of vegetation zones in northern mountains.

The project only provides a snapshot in time of the permafrost contiguity conditions at select locations suspected of featuring zones of transition. Such permafrost transition zones are expected to occur in association with changes in elevation and vegetation cover.

The overarching goals of this project, therefore, are:

1) to gain knowledge about boundaries between permafrost and non-permafrost terrain.
2) to increase understanding of permafrost characteristics at vegetation transitions.

Such knowledge is needed for the development of models representing the responses of the permafrost zone to external change (Lewkowicz et al. 2011). The modeled permafrost responses, in turn, can inform our predictions about changes in mountain hydrology, slope stability and geohazards.

The project objectives more specifically are:

1) to examine how permafrost breaks down spatially at vegetation transitions on select slopes.
2) to test, in select areas, the following hypotheses based on the impact of different vegetation covers on ground thermal regimes as expressed in the literature:
    a. Permafrost characteristics (permafrost thickness, active layer thickness, size and frequency of non-permafrost bodies) change across vegetation cover transitions.
    b. The active layer deepens and permafrost thins or disappears from above to below local treeline.
    c. Changes in permafrost contiguity over a few hundred meters of elevation differ from changes that take place with latitude over hundreds of kilometers.

2.0 Background

2.1 Mountain permafrost

Methodical research on mountain permafrost began around 1970 (Gorbunov 1978; Haeberli 2013). During the last two decades, research has focused increasingly on mountain permafrost due to growing concerns about how permafrost's response to climate change will affect basin hydrology, slope stability, infrastructure investments, and human lives (Lewkowicz et al. 2012). Many studies have been conducted in Europe and central Asia(e.g. Ishikawa and Hirakawa 2000; Isaksen et al. 2002; Harris et al. 2003; Gruber et al. 2004; Etzelmüller et al. 2006; Gruber and Haeberli 2007; Oelke and Zhang 2007; Wu et al. 2007; Harris et al. 2009; Farbrot et al. 2011; Isaksen et al. 2011). In North America, research is also underway (e.g. Lewkowicz and Coultish 2004; Lewkowicz and Ednie 2004; Carey and Woo 2005; Bonnaventure and Lewkowicz 2008; Roadhouse 2010; Smith et al. 2010; Lewkowicz et al. 2012; Bevington 2015).

Research focused on understanding the relationship between permafrost and its explanatory variables is important for improving both permafrost response models and permafrost distributions models. The most important factors explaining the presence of permafrost are elevation and potential incoming solar radiation (PISR) as these strongly influence the air and ground temperatures (Roadhouse 2010). In fact, at the regional scale, if there are no major trends in snowfall, mean annual air temperature is the main determinant of permafrost distribution (Péwé 1973; Lewkowicz et al. 2012).

In mountainous environments, permafrost distribution usually varies with elevation because atmospheric temperature decreases with an increase in altitude, typically at a rate of

around -6.5°C/km. Altitudinal zonation of permafrost consists of vertically dividing mountain permafrost into zones based on the proportion of ground that remains perennially frozen. At sufficiently high elevations, a continuous permafrost (>90%) zone occurs. Downslope discontinuous (50-90%), and sporadic (10-50%) permafrost zones occur and also a zone of isolated patches (<10%). Like permafrost, there is a vertical zonation of vegetation in mountains (see section 2.2). In continental locations in the Yukon, the permafrost zones extend to elevations below treeline and overlap with different vegetation zones (Bonnaventure and Lewkowicz 2012) (Figure 1).

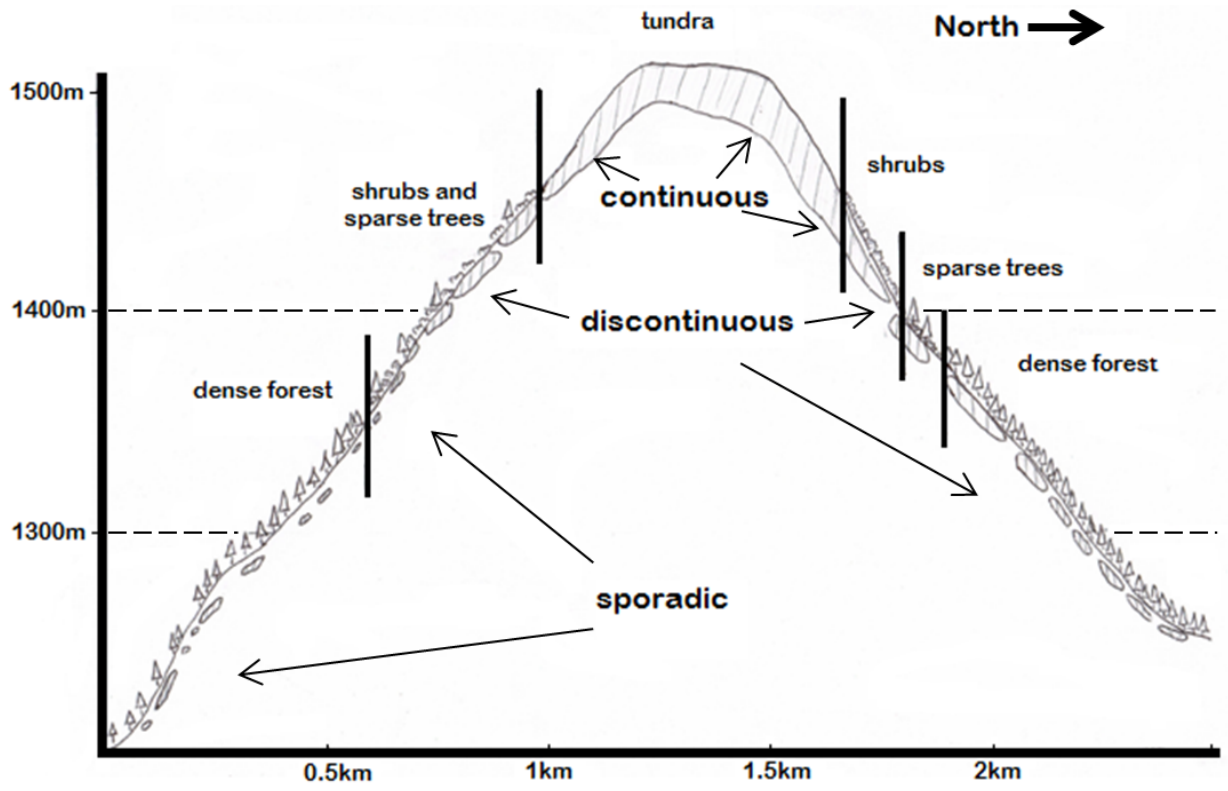

Figure 1: Schematic illustration of the altitudinal zonations of permafrost and vegetation at locations with a negative lapse rate

Ground surface temperatures can vary significantly within short distances in mountainous terrain where changes in elevation, aspect, and topographic shading impact both the amount of incoming radiation and the movement of air masses (Tabony 1985; Thompson 1986; Gustavsson et al. 1998; Colette et al. 2003; Isaksen et al. 2011; Gisnas et al. 2014; Lacelle et al. 2016). As in non-mountainous environments, local variations in snow accumulation and vegetation growth also affect the surface energy balance in mountainous terrain by modifying the surface albedo, moisture availability, and transfers between sensible, latent and ground heat (Smith 1975; Zhang 2005). The local soil properties, notably the thermal conductivity, finally determine the energy transferred from the ground surface to the soil below and consequentially determine its temperature (Figure 2).

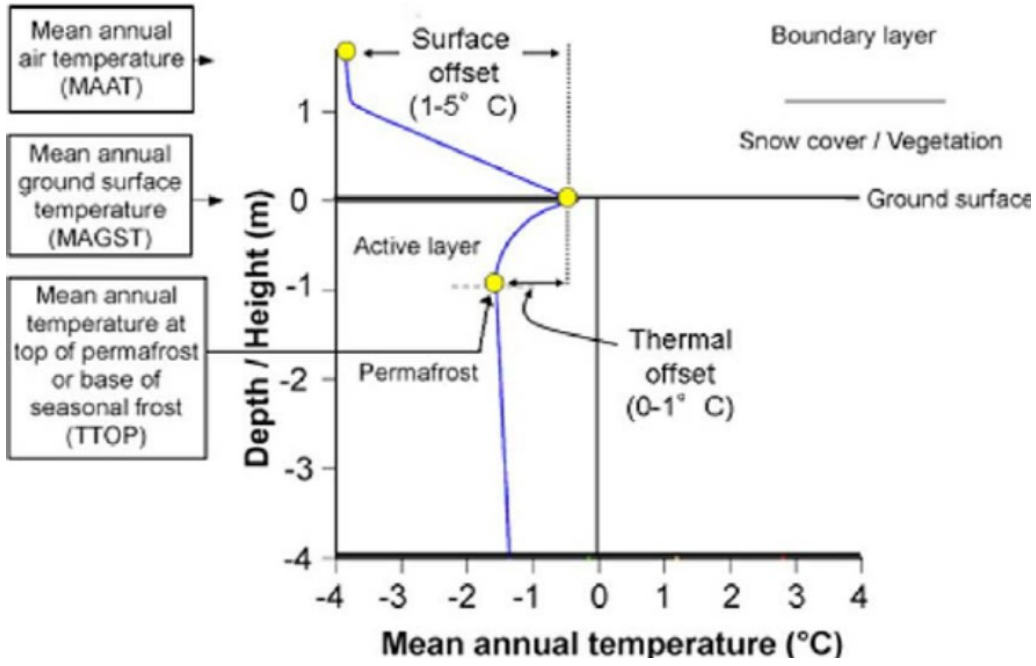

Figure 2: Schematic conceptual mean annual temperature profile through the surface boundary layer, showing the relation between air temperature and permafrost temperature (Bonnaventure and Lamoureux, 2013 after Smith and Riseborough, 2002)

In mountainous watersheds, an additional consideration is the basin's shape which may influence the spatial variations in air temperature as it can promote cold air drainage and pooling (Colette et al. 2003). Cold air pooling and inverted surface lapse rates, as well as shallow snowpacks, and thick organic mats are among the factors contributing to the existence of permafrost below treeline, which is characteristic of certain mountain ranges (Bonnaventure and Lewkowicz 2012). However, the degree of continentality of an area is the main factor explaining permafrost presence below treeline as strong continentality can cause very cold winters that enable mean annual air temperatures much less than 0°C to occur while still having summer temperatures high enough to allow forest growth (Bonnaventure and Lewkowicz 2012). Consequently, permafrost is present in valley bottoms in the Yukon (Bonnaventure and Lewkowicz 2012) and Mongolia (Gorbunov 1978), but absent from the Alps.

2.2 Treeline and climate change

Above a certain elevation no trees can grow irrespective of species. Other low-stature vegetation, such as shrubs, grasses and lichen may cope well at higher elevations; but worldwide, there is a termination of upright tree growth where low temperatures prohibit it (Körner 2012). This termination is known as the treeline. Some individual krummholz type trees act as exceptions existing above treeline; however the "patches of forest consistently positioned along a common isotherm in a given mountain range" are what are used to define treelines (Körner 2012).

Treeline elevation varies with latitude (Figure 3-A). In the Canadian arctic at approximately 68° N, the arctic lowland tundra and the tree limit merge at sea level (Körner 2012).The treeline here is latitudinal rather than altitudinal since the low temperatures are due to

the latitudinal position. At only a few degrees lower latitude, however, treelines can be found at high elevation; and further south, these rapidly rise to above 1000m as is the case in Southern Yukon just north of 60 ° N, where the study areas are located (Figure 3). The elevation where alpine permafrost is present also varies with latitude. The altitude of localities of existing alpine permafrost in the Cordillera of North America similarly increases at lower north latitudes (Figure 3-B). Both of these relations are due to spatial patterns in the global climate system.

Climatic conditions are not the only factors that determine treeline position. Furthermore, the current treeline position is not necessarily a response to the current climatic conditions. Rather, it echoes the combined impact of climatic influences from over several hundred years as well as any significant disturbances (Körner 2012). Additionally, treelines are never truly distinct lines. At a local scale, there are many factors that can modulate treeline including lack of substrate, cold air drainage, and others (Figure 4). Both the local treeline variations produced by these factors and the gradual stand opening typical in treelines (Matyssek et al. 2009 as cited by Körner, 2012) form a transition zone between forest and tundra termed the forest-tundra ecotone (Harper et al. 2011).

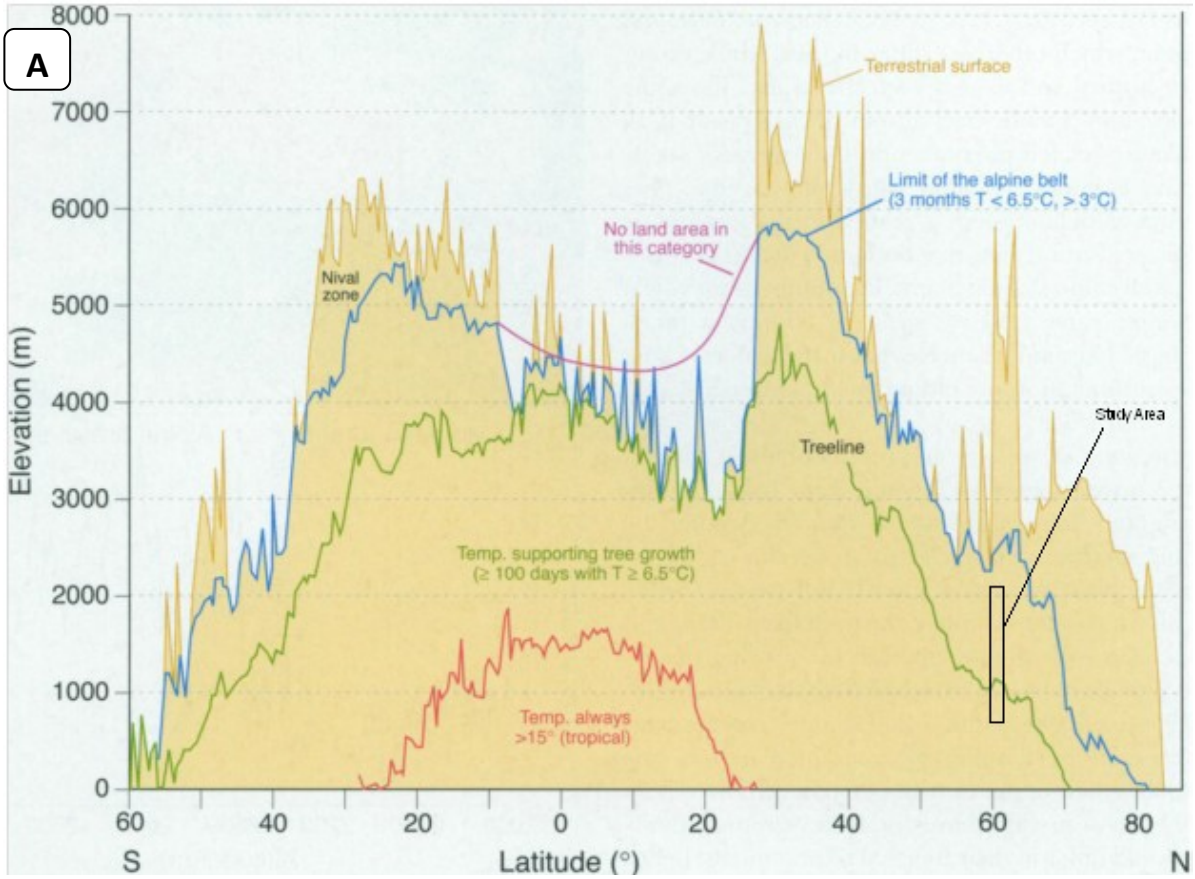

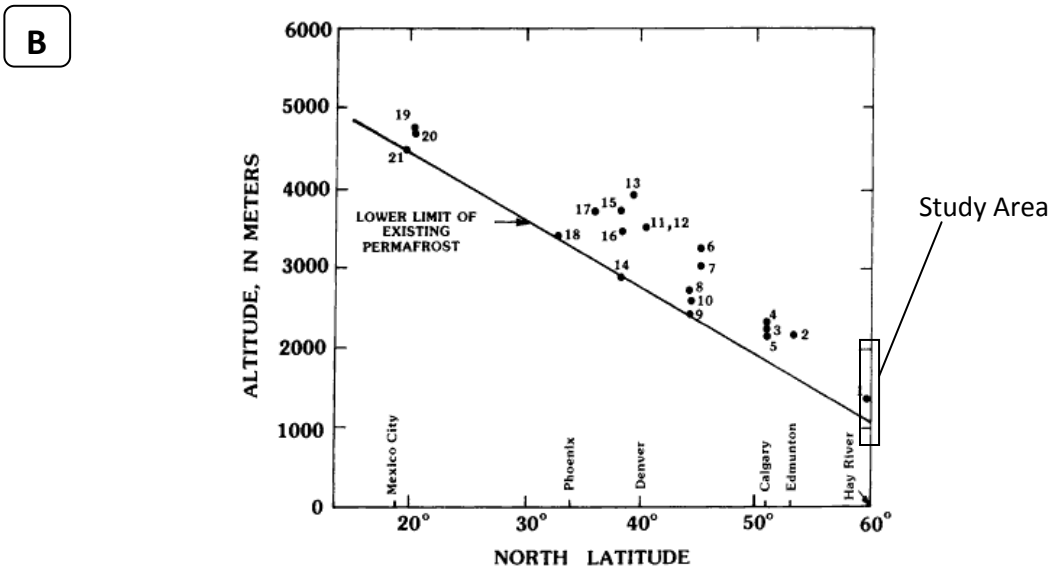

Figure 3: Study area in latitudinal and altitudinal vegetation and permafrost contexts

(A): Latitudinal distribution of maximum elevation of land area, modeled altitudinal position of treeline and upper limit of the alpine belt with the nival belt above (Körner 2007)and box marking study area range

(B): Relation between latitude and altitude of reported localities of existing alpine permafrost in the Cordillera of North America (Péwé 1983)

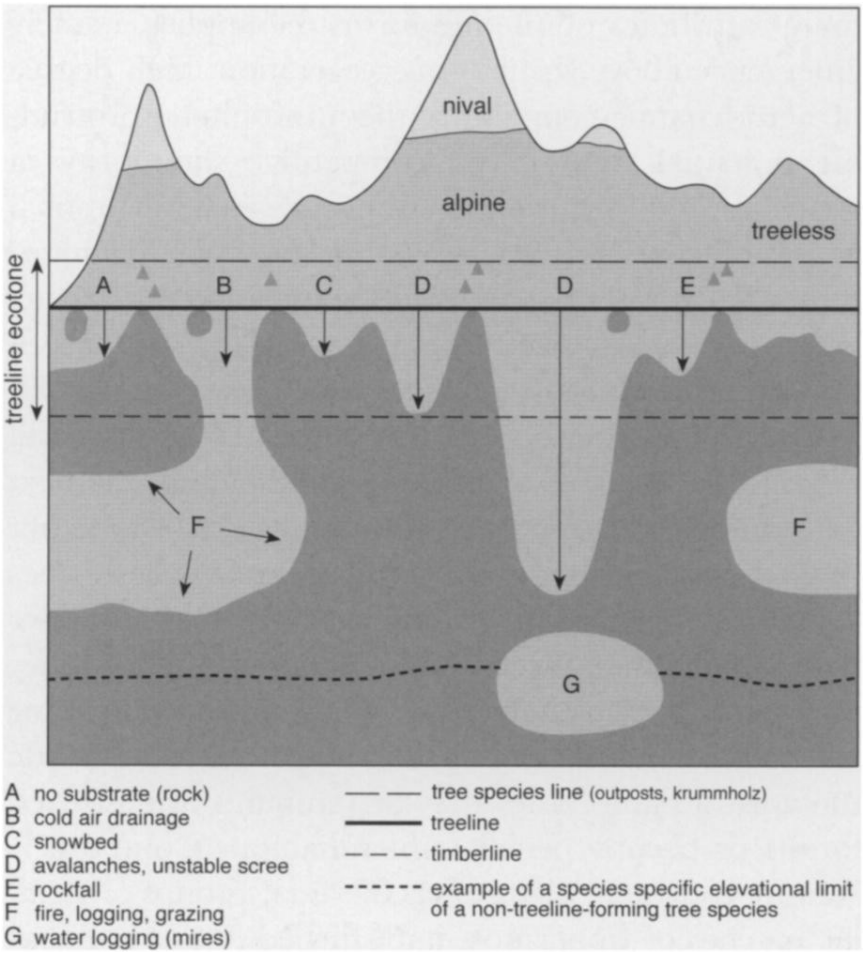

Figure 4: A schematic illustration of various factors that may modulate the forest and tree limit at a local scale compared to the limit set globally by thermal conditions alone (Körner 2007)

Researchers have renewed interest in both treeline and forest-tundra ecotone because of the possible effects of climate change on treeline movement and forest densification which have implications for the global carbon cycle, ecotone biodiversity, and livelihoods linked to montane landscapes (Grace et al. 2002; Danby and Hik 2007a; Harper et al. 2011; Danby 2011). Climate warming is known to impact treeline. Positive growth responses of trees near the treeline in the last decades of the twentieth century have been identified in North America (LaMarche et al. 1984; Payette et al. 1985; Cooper et al. 1986; Danby and Hik 2007b), the Alps (Nicolussi et

al.1995; Paulsen and Weber 2000), and the Patagonian Andes (Villalba et al. 1997; Salzer et al. 2009). Some photographic evidence and remotely sensed data suggest a rapid advance of treeline in certain areas (Grace et al. 2002). Some alpine treelines have shifted upslope by up to 30m of elevation while others have changed very little (Walther 2003; Harsch et al. 2009). In reaction to climate warming, the forest-tundra ecotones may shift poleward or upward without any changes in its spatial configuration; or forest density might increase without the forest-tundra ecotone shifting spatially thus causing the vegetation pattern to change (Harper et al. 2011). A treeline's response depends on the site-specific factors affecting tree establishment such as the width of the forest-tundra gradient, aspect, tree species, microclimate and microtopography (Harper et al. 2011).

Overall, future treeline positions will be mostly determined by the degree of climatic warming, but regional cloudiness and snowpack may delay or balance the climatic signals (Körner 2012). Palaeo-data suggests altitudinal treeline positions will track climate change eventually since temperatures set the ultimate biological limit to tree growth at high elevations. According to Reasoner and Tinner (2009) the maximum treeline elevation in North America during the Holocene was 180 m above current treeline elevation.

Recent changes have been observed in treeline and the forest-tundra ecotone in northern Canada, In southwest Yukon, increases in treeline elevation and stand density occurred during the early to middle of the 20th century and appeared to relate to a 30-year period of above average temperatures, which began in 1920 (Danby and Hik, 2007 a & b). Recent expansions of dwarf shrub cover have also been observed across the Tuktoyaktuk Coastlands, Northwest Territories (Moffat et al. 2016).

The influence of these forest-tundra ecotone changes on permafrost are still unknown, but they are likely to be significant. Vegetation cover has been shown to affect energy exchanges between the air and the ground surface and thus the probability of permafrost being present (Brown 1966; Smith 1975; Karunaratne and Burn 2004; Kremer et al. 2011; Lewkowicz et al. 2012). Consequently, any changes in vegetation cover patterns should impact the permafrost thermal regime. Tape et al. (2006) deem the relation between snow accumulation and shrub distribution to be critical for assessing the impact of climate change on permafrost in the forest-tundra ecotone. Research in northern Canada also revealed the importance for ground temperatures of vegetation related snow cover changes (Palmer et al. 2012; Burn and Kokelj, 2009) Climate change-induced forest densification at treeline may also have a signficant impact on permafrost because the interception of snow in closed canopy forests promotes heat loss and lower ground temperatures (Jean and Payette 2014).

2.3 Permafrost detection and ERT

Detecting permafrost in the field can be done by directly measuring ground temperatures in boreholes at different depths over several years as is exemplified by the Global Terrestrial Network on Permafrost (e.g. Smith et al. 2005; Isaksen et al. 2007; Biskaborn et al. 2015). Alternatively, the presence of permafrost can be inferred in areas with shallow active layers by probing the ground with a frost probe during late summer when the active layer has almost or completely thawed (Brown et al. 2000). When the probe reaches frozen ground it is incapable of penetrating deeper into the ground, signaling the presence of ice-bearing ground. This technique has limitations since bedrock or clasts-rich soils cannot be probed. Moreover, permafrost may be present at depths exceeding the length of the probe. Thus, probing should be used in combination with other detection methods. Digging pits in summer can reveal the presence of near-surface

permafrost (e.g. Lewkowicz and Ednie 2004). Ground coring at various times of year can also reveal frozen ground and ice layers (French 1998).

Without penetrating the ground surface, permafrost can be inferred using the basal temperature of snow (BTS) technique (Haeberli 1973) in which ground surface temperatures measured under a snowpack at least 80 cm thick that are below-3°C are indicative of permafrost being probable (Hoelzle 1992). This technique also has limitations, especially spatially since not all environments have the required stable 80 cm or greater snowpack. Furthermore, it is difficult to make inferences with BTS results across landscapes since deeper snow may reduce the chances of permafrost being present and permafrost may be more likely where snow is too thin for BTS measurements (Lewkowicz and Ednie, 2004).

Direct current electrical resistivity tomography (ERT), a non-invasive geophysical technique that produces images of sub-surface structures, can be used to infer permafrost conditions (Hauck and Kneisel 2008). The technique works by injecting DC electrical current into the ground between one pair of electrodes in an array while measuring the voltage between another pair (Lewkowicz et al. 2013; Figure 5). This difference in voltage in used to calculate resistivity (Hauk and Kneisel 2008):

$$\rho_a = K\frac{\Delta V}{I}$$

Where:

ρ_a is the apparent resistivity (Ω.m)

ΔV is the difference in voltage (V)

I is the current (A)

K is a geometric factor dependant on the electrodes' configuration

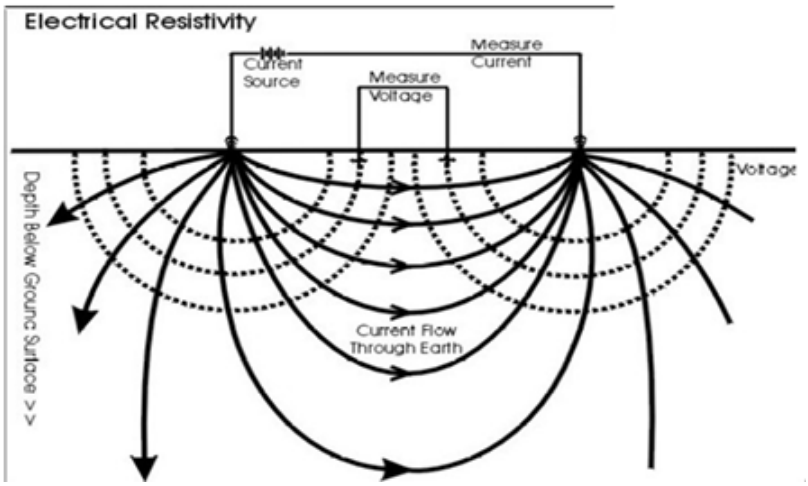

Figure 5: Schematic illustration of electrical resistivity tomography (Echotech 2005)

ERT investigations rely on different earth materials having different resistivity values (Table 1). Since the electrical resistivities of ice and water differ by orders of magnitude, permafrost bodies can generally be detected (Figure 6). However, the large difference in resistivity between thawed and frozen states does not manifest for dry or non-porous materials, such as massive bedrock, with little to no ground water. Furthermore, even though Hauck and Kneisel place the range of frozen sediments between 1 kΩm and 1000 kΩm (Table 1), lower resistivity values may occur in areas of warm fine-grained permafrost with high unfrozen water contents (e.g. Lewkowicz et al. 2011).

Table 1: Resistivity values for different earth materials (Hauck and Kneisel 2008)

Material	Range of Resistivity (Ωm)
Clay	1 - 100
Sand	100 - $5x10^3$
Gravel	100 - $4x10^3$
Granite	$5x10^3$ - 10^6
Gneiss	100 - 10^3
Schist	100 - 10^4
Groundwater	10 - 300
Frozen sediments (ground ice, **mountain permafrost**)	$1x10^3$ - 10^6
Glacier ice (temperate)	10^6 - 10^8
Air	Infinity

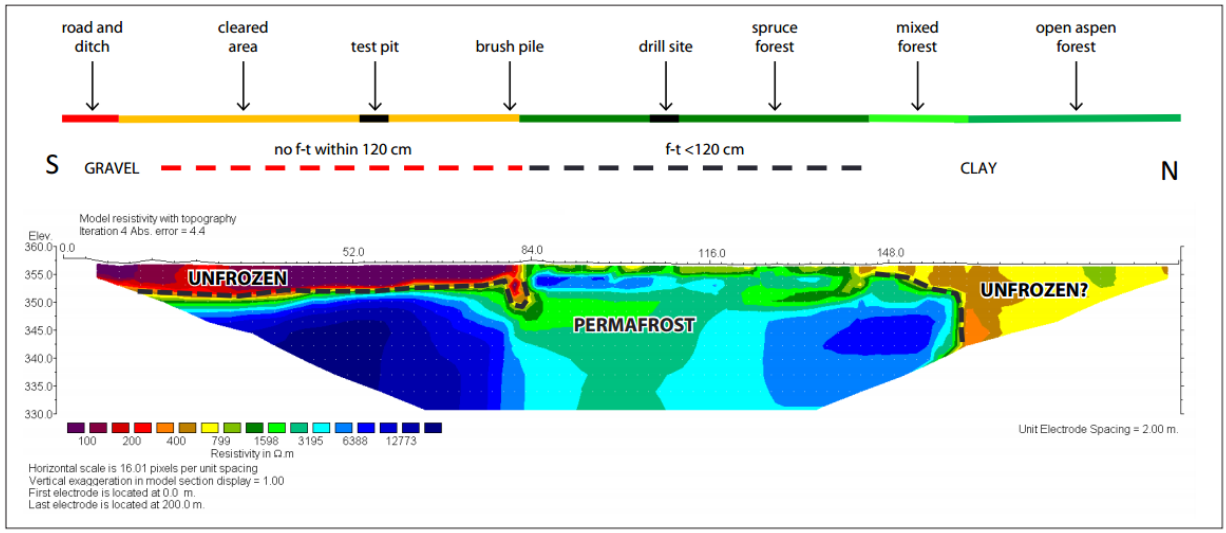

Figure 6: Example of ERT survey over permafrost and unfrozen ground

Survey to 25 m depth at Dawson, Yukon, showing newly thawed zone due to anthropogenic clearing (left in red), permafrost body (blue) under coniferous forest and unfrozen ground (green at right) under deciduous forest (Benkert et al. 2015).

ERT has been used to study permafrost in several previous investigations in the Yukon, in eastern Canada, as well as in Europe and elsewhere (e.g. Isaksen et al. 2002; Lewkowicz et al. 2011; Way and Lewkowicz 2015). It is an essential and cost-efficient tool for investigating discontinuous permafrost (Lewkowicz et al. 2013). The electrodes can be placed in different arrays to detect different subsurface structures more effectively. Typically 2-D profiles produced with a Wenner array are used for permafrost investigations. Since the Wenner array has the smallest geometric factor of any array (Hauck et al. 2003), the signal strength is stronger than the other common arrays (Loke 1999). The Wenner array has a moderate depth of investigation, but due to electrode spacing, no data are collected in the lower areas under the edges of the array (Loke 1999).

2.4 Permafrost at latitudinal and altitudinal treelines

Few studies have examined permafrost at latitudinal and altitudinal treelines. Typically, near arctic treelines, tree cover declines northward, stands open and spacing between individual trees increases. These characteristics are due to the low solar angle, resulting in colder temperatures, at high latitudes and the presence of permafrost (Körner 2012). A negative cold root-zone feedback as well as impeded drainage can prevent tree stands from closing in permafrost (Körner 2012). This is one example of how permafrost affects treeline. Treeline and its division of the forest-tundra ecotone also impacts permafrost.

At latitudinal treelines, the forest-tundra ecotone can be an important transition zone for snow cover and ground temperatures. In the Mackenzie Delta, tree cover, shrub height and shrub density decrease northward causing the snow cover to decrease. This contributes to a decrease in annual ground surface temperatures across treeline, where the steepest gradient occurs near the northern limit of trees (Palmer et al. 2012). Indeed, the tundra exhibits colder annual ground surface temperatures than south of treeline, which explain the general northward thinning of the active layer (Burn and Kokelj 2009; Kokelj et al. 2014). Also, the occurrence of thermal contraction cracking, the density of polygonal terrain and the size of ice wedges all increase northward as the ground temperatures decrease (Kokelj et al. (2014).

In mountainous terrain, the active layer similarly tends to thin as altitude increases. Harris (1987) notes that field measurements have demonstrated such a trend in Northern Tien Shan (Gorbunov 1978 cited by Harris 1987; Marchenko et al. 2007), the Andes (e.g. All cited by Harris, 1987 - Lliboutry 1961; Marangunic 1976; Corte 1985), and the Rocky Mountains of Alberta (Harris and Brown 1978). Harris' (1987) findings on the northwest-facing slope of

Outpost Mountain, Kluane Lake, however, show an anomalous relationship between the active layer thickness and altitude, suggesting that the organic mat thickness is the dominant factor controlling active layer thickness rather than altitude(Harris 1987). In contrast, Farbrot et al. (2011) found snow distribution within the transition zone of mountain permafrost to be the primary controlling factor for permafrost occurrence along elevation gradients in southern Norway.

Altitudinal treeline elevation was used in the demarcation of differences in processes affecting permafrost in the Wolf Creek Basin near Whitehorse. For instance, thawing of the active layer began earlier and occurred more intensely (i.e. with more thawing degree days) below treeline (Lewkowicz et al. 2012). Furthermore, during winter, surface lapse rates often inverted below treeline. Additionally, significant differences were found in surface offset values (MAAT-MAGST see Figure 2, p.17) for alpine tundra and forested sites in the study area as well as between the n-factors of sites with different types of vegetation cover (Roadhouse 2010; Lewkowicz et al. 2012). Roadhouse (2010) reported freezing factors (nf) that were significantly greater for tundra sites than for forested sites, and thawing factors (nt) for tundra sites that were slightly lower than for the forested sites.

Despite all these investigations, there is little in the literature concerning permafrost temperatures and the arrangement of non-permafrost bodies at altitudinal treeline or within the forest-tundra ecotone in mountains.

3.0 Study areas

This study focused on two areas within the Boreal Cordillera in the Yukon. One area south of Whitehorse is within the sporadic discontinuous permafrost zone, while the other, near Dawson, is within the extensive discontinuous permafrost zone (Figure 7).

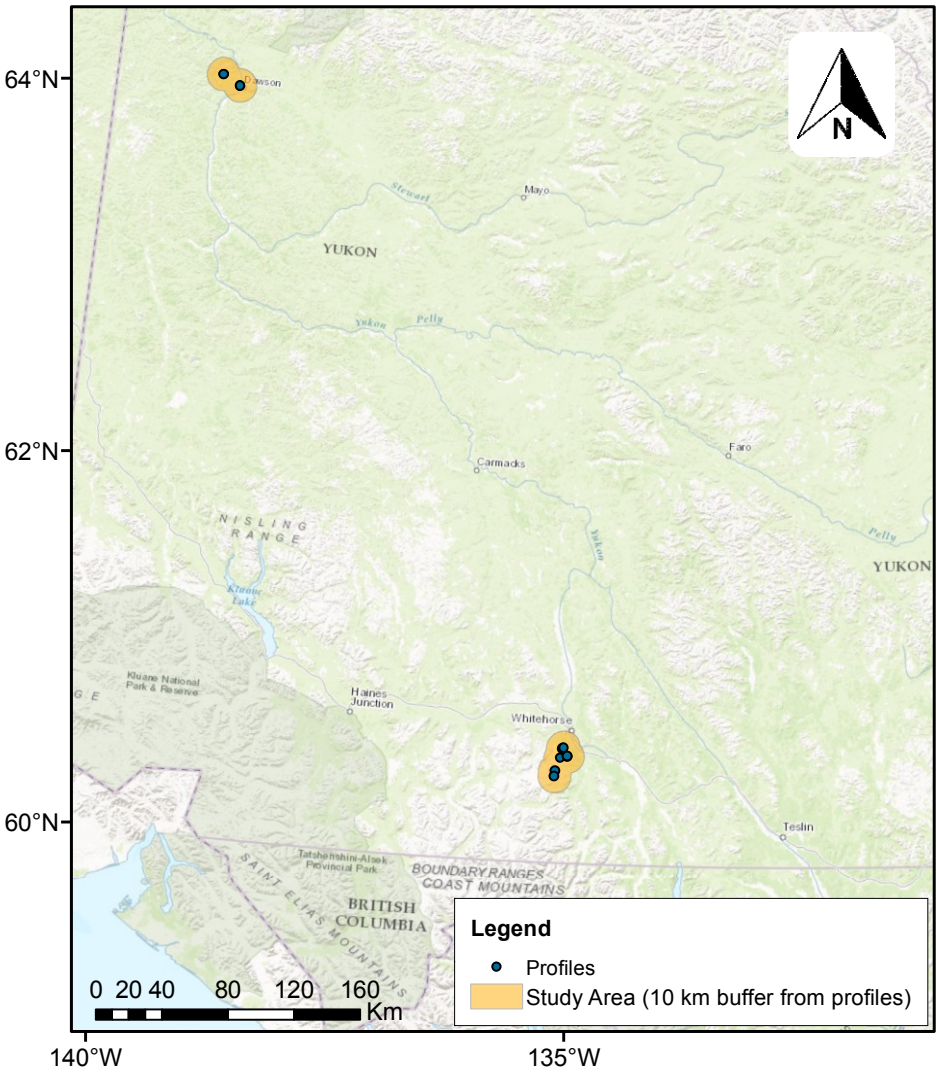

Figure 7: Location of study areas near Whitehorse and Dawson, Yukon

The locations of the profiles within each study area appear in more detail in Figure 18 (Whitehorse area) and Figure 58 (Dawson area)

The extent and distribution of permafrost in North America has varied considerably during the Quaternary, and the age, growth and distribution of permafrost are closely related to the glacial and postglacial history (Mackay and Black 1973). Since the Dawson study area remained unglaciated, permafrost is likely older and deeper there than in the Whitehorse area, where the permafrost may be as young as the Little Ice Age. Both areas are within the discontinuous permafrost zone where much of the permafrost is believed to be either ecosystem protected or degrading (Shur and Jorgenson 2007).

3.1 Whitehorse study area

3.1.1 Physiography and glacial history

The Whitehorse study area (2,975 km^2, centred on 60.6°N, 135.1°W) is located within the Yukon Southern Lakes ecoregion. Elevations within the study area range from less than 600 m above sea level (asl) to more than 2000 m asl. The complex terrain, with gentle to rugged topography that include high peaks and U-shaped valleys, results from past glacial action (Yukon Ecoregions Working Group 2004b; Roadhouse 2010; Bonnaventure and Lewkowicz 2011). The Cordilleran ice sheet repeatedly covered the study area during glacial periods over the last 2.6 million years (Duk-Rodkin and Barendregt 2011), though the area has been ice-free for approximately the last 10,000 years (Bond 2004).

3.1.2 Geology

The bedrock geology of the Whitehorse study area includes part of the Stikine terrane composed of Mesozoic sedimentary rock. It also includes plutonic and volcanic rocks of Cretaceous or younger age (Gordey 2008). Cobble conglomerates with sandstone interbeds, shales and siltsones, as well as greywacke and mudstone underlie much of the study area but; the

Mount McIntyre and Whitehorse plutonic suites, rich in adamellite and granite, make up a large part of the geology, particularly in the northern half of the study area (Gordey 2008).

Morison and Klassen (1991) mapped the surficial geology around Whitehorse. Their map indicates that within the study area the surficial geology is mostly composed of various combinations of bedrock and bedrock rubble, moraine tills, reworked glacial deposits, and colluvium. Some glaciofluvial deposits are present and a few alluvial, colluvial and glacial deposits complexes of variable thickness are found in the valley bottoms (Morison and Klassen 1991). Indeed, the latest deglaciation (McConnell) was highlighted by periods of differential retreat and fluctuating ice fronts that produced systems of pro-glacial lakes in southern Yukon suitable for deposition (Bond 2004). In the early Holocene, the glacial lakes drained, glaciolacustrine fill was incised and aeolian activity increased (Bond 2004).

3.1.3 Climate

The climate is cold and semiarid in the study area since it is located in the rain shadow of the St. Elias Mountains (Yukon Ecoregions Working Group 2004; Lewkowicz et al. 2012). Total annual precipitation regionally is less than 325 mm and mean annual air temperatures near -1°C to -4°C were reported in the Southern Lakes ecoregion (Yukon Ecoregions Working Group 2004b). The Whitehorse study area is only a small part of the ecoregion. Still, elevation controls contribute to a large range of temperatures. The daily average air temperature for the most recent climate normal, from 1981 to 2010, was -0.1°C at the Whitehorse airport station, 706 m asl, (Environment Canada). In contrast, it is much lower at 2066 m asl on Mt Granger where the mean annual air temperature is about -7°C (Bevington 2015). The climate in the study area has

warmed. The daily average air temperature at Whitehorse increased by almost 1°C from 1961-1990 to 1981-2010 (Environment Canada).

Mean monthly air temperature normals for 1981 to 2010 indicate a daily average temperature of 14.3°C in July, and of -15.2°C in January (Environment Canada 2016). The Whitehorse study area also encompasses twenty eight University of Ottawa climate stations, several of which have been operating since August 2006. The mean monthly temperatures calculated for these stations from 2006 to 2011 range from approximately -16°C during the winter to approximately 13°C during the summer (Lewkowicz et al. 2012). Strong topoclimatic variability is noted within short distances in the study area (Lewkowicz and Ednie 2004). In addition, temperature inversions can occur in both the valleys and in the mountains, with especially large and persistent inversion episodes during the winter (Lewkowicz et al., 2012).

3.1.4 Permafrost

The Whitehorse study area is located within the sporadic discontinuous permafrost zone (Heginbottom et al. 1995). Results of modelling studies indicate that permafrost distribution ranges from isolated patches at lower elevations to continuous on mountain peaks. (Lewkowicz and Ednie 2004; Lewkowicz et al. 2012; Bonnaventure and Lewkowicz 2012). According to Lewkowicz and Ednie's (2004) work in the Wolf Creek basin, which overlaps with much of the study area, permafrost distribution is mainly elevation-controlled with slope orientation and angle also affecting permafrost limits. In addition, cold air drainage, resulting in temperature inversions, influences the distribution of permafrost by maintaining permafrost in certain valleys (Lewkowicz and Ednie 2004). Ground ice contents are believed to be low in the coarse sediments covering much of the study area. Excess ice is present mainly in glaciolacustrine

sediments or moist, silty soils covered by peat. In the valley between Mt Granger and Coal Ridge, multiple mineral-cored palsas are present (Lewkowicz and Coultish 2004).

The active layer thickness is commonly greater than 1.5 m in mineral soil, but may be less than 1 m in wet organic terrain (Yukon Ecoregions Working Group 2004b). When permafrost was encountered in Whitehorse, it was only 2 or 3 m thick (Burgess et al. 1982; EBA 1995 as cited by Yukon Ecoregions Working Group 2004), whereas permafrost is more than 20 m thick on Mt McIntyre (Lewkowicz et al. 2011) and probably more than 100 m thick on Mt Granger.

3.1.5 Vegetation

Vegetation in the study area forms three ecological zones. Above 1500 m asl, the ground is either unvegetated or supports alpine tundra vegetation communities including *Salix* sp. (willow) and *Betula nana* (dwarf birch) shrubs, grasses and lichens (Francis et al. 1999). Below that, a subalpine zone vegetated by shrubs and sparse trees, especially *Picea glauca* (white spruce), forms a broad ecotone between the unvegetated alpine areas and the forested lowlands. Within this ecotone the altitudinal treeline occurs at about 1300 m asl (Lewkowicz and Ednie 2004; Bonnaventure and Lewkowicz 2012b; Lewkowicz et al. 2012). Finally, the boreal zone, characterized by conifer forests communities dominated *Pinus* sp. (pine), *Picea glauca* and/or *Populus* sp. (aspen) generally occurs below 1100 m asl (Francis et al. 1999). Other tree species potentially occurring within the study area include *Abies lasiocarpa* (subalpine fir), which can be associated to cooler conditions such as cold air drainage, and *Picea mariana* (black spruce), which is often found at sites with near-surface permafrost. Understory vegetation may include mosses, lichens, and species such as *Linnaea borealis* (twinflower), *Arctostaphylos uva-ursi*

(kinnikinnick), *Vaccinium vitis-idaea* (lingonberry), and *Betula glandulosa* or *nana*[1] among others (Yukon Ecoregions Working Group 2004b).

3.2 Dawson study area

3.2.1 Physiography and glacial history

The Dawson study area (2,828 km^2, centred on 64.1°N, 139.6°W) is located within the Klondike Plateau ecoregion. Elevations within the study area range from less than 300 m asl to slightly more than 1200 m asl. The ecoregion's physiography consists of "smooth topped ridges dissected by deep, narrow, V-shaped valleys [,] characteristic of an area that has not been glaciated in the recent past" (Yukon Ecoregions Working Group 2004a). In fact, the Dawson study area is part of a larger region which remained unglaciated during the maximum extent of glacial coverage in the Yukon from the Late Pliocene to Late Pleistocene. Neither the Cordilleran nor the Laurentide ice sheets covered the study area (Duk-Rodkin and Barendregt 2011). The "area was exposed and deeply weathered for at least 15 million years" (Yukon Ecoregions Working Group 2004a).

3.2.2 Geology

The bedrock geology of the Klondike Plateau ecoregion is comprised of the Yukon-Tanana Terrane, a composite of crustal blocks that includes former volcanic island arc and continental shelf deposits (Yukon Ecoregions Working Group 2004a). Metamorphic volcanic rocks, as well as metamorphic clastic and igneous rocks characterize the bedrocks of Top of the World and King Solomon's Dome ecodistricts (McKenna et al. 2010). Klondike schist, which

[1] *Betula glandulosa* (resin birch) and *Betula nana* (dwarf birch) are very difficult to distinguish, as both can grow as prostrate shrubs. For simplicity, *Betula nana* refers to both species in the remainder of this text.

includes quartz-muscovite-chlorite schist, chloritic quartzite and intermediate rock types, dominates in the study area (Green and Roddick 1961).

Duk-Rodkin (1996) mapped the surficial geology near Dawson. Colluvial deposits occupy most of the study area. They consist of diamicton, rubble, organic-rich silt and sand derived from bedrock and surficial material. This colluvium forms veneers or blankets from 1 m to more than 3 m thick with some exposed bedrock at prominent ridges and escarpments (Duk-Rodkin 1996). Slope complexes and pediment rubble occupy valley sides and tributary valley bottoms can have meters-thick colluvial silt deposits covered by peat and muck (Yukon Ecoregions Working Group 2004a). In addition, several alluvial plains, glaciofluvial terraces, and mine tailings occur around the Klondike and Yukon Rivers (Duk-Rodkin 1996).

3.2.3 Climate

The Dawson study area has a more continental climate than the Whitehorse study area. Total annual precipitation ranges from 300 to 500 mm and mean annual air temperatures are near -4°C, with air temperatures varying considerably during the year (Lewkowicz et al. 2012). Mean monthly air temperature normals from 1981 to 2010 for the Environment Canada station that is close to the study area range from 15.7°C for July to -26.0°C for January (Environment Canada 2016). Up to twelve University of Ottawa climate stations have been operating since August 2007. The mean monthly temperatures recorded for some of these stations between 2007 and 2011 ranged from approximately -27°C during the winter to 15°C during the summer (Lewkowicz et al. 2012).

3.2.4 Permafrost

The Dawson study area falls within the extensive discontinuous permafrost zone (Heginbottom et al. 1995; Bonnaventure et al. 2012). Permafrost has survived in this area since at least the early-Middle Pleistocene. In fact, the oldest ice known in North America was found near Dawson (Froese et al. 2008). The presence of relict permafrost and the occurrence of cold-air drainage in interior basins and valleys complicate the permafrost distribution (French and Heginbottom 1983). Continuous permafrost is present at higher elevations, but large bodies of permafrost also occur in valley-bottoms. Permafrost is usually thicker under north-facing slopes, and it is often absent beneath south-facing slopes (Figure 8).

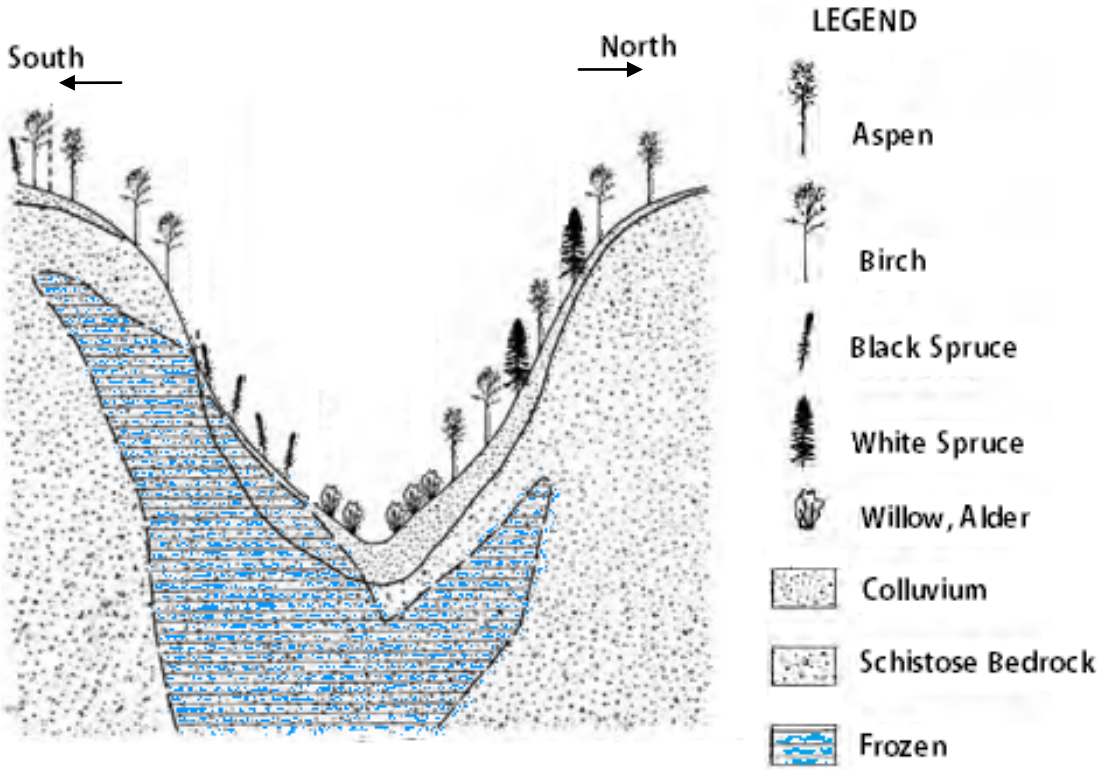

Figure 8: Schematic landscape cross-section showing the influence of aspect on permafrost and vegetation in the Klondike Plateau ecoregion (adapted from Yukon Ecoregions Working Group 2004a)

The absence of permafrost on well drained slopes regardless of their aspect and the frequent presence of ice-rich permafrost in valley-bottoms or uplands characterize the area (EBA Engineering Consultants Ltd 1989as cited by Yukon Ecoregions Working Group 2004a). “In general permafrost is markedly less prevalent in the coarse soils of the central Yukon than in the fine-grained soils” (Hughes and Van Everdingen 1978, p.4).

Early research in and around the study area indicated that permafrost thickness varies up to 60 m (McConnell 1905 as cited by Yukon Ecoregions Working Group 2004a). The active layer thickness reportedly ranges from 30 or 40 cm in ice-rich peat and up to 2 m in dry sand, while it is relatively thin in alpine tundra, above treeline (Yukon Ecoregions Working Group 2004a).

3.2.5 Vegetation

Vegetation in the study area ranges from boreal forests to subalpine tundra. The Subalpine bioclimatic zone above 1000 m asl exhibits ground covers mainly composed of herbaceous vegetation, low shrubs, sparse short conifers, with some bare surfaces (McKenna et al. 2010). Below 450m asl, open stands of sparse conifers with low shrubs and water characterize the Boreal-Low bioclimatic zone (McKenna et al. 2010). Active riparian and wetlands are widespread in this zone and abundant tree species include *Picea glauca*, *Picea mariana*, and *Populus* sp. (McKenna et al. 2010). Between these two zones, the Boreal-High bioclimatic zone exists where low shrubs and sparse or open conifer stands dominate. Common species in this zone include *Picea glauca*, *Picea mariana*, and *Betula* sp., while *Populus* sp. is infrequent (McKenna et al. 2010).

Altitudinal treeline occurs at approximately 1000 m asl (Yukon Ecoregions Working Group 2004a). Generally, the vegetation patterns below treeline follow the distribution of permafrost with stunted *Picea mariana* stands on colder, north-facing sites underlain by permafrost changing to mixed forests on warmer south-facing slopes devoid of permafrost (Yukon Ecoregions Working Group 2004a).

4.0 Methods

This chapter describes site selection, field techniques, and the methods used to interpret the data collected.

4.1 Site selection

Sites were selected based on their accessibility, proximity to existing climate stations, and potential for sampling vegetation transitions on a variety of slopes. Attempts were made to maximize the number of transects completed while also sampling slopes with differing elevations, inclinations and aspects. Google Earth satellite images and aerial photographs were initially used to identify accessible slopes with various aspects and inclinations in the study area near Whitehorse. The elevations of key features such as the local summit, valley floor, and vegetation transitions were identified. The ERT surveys planned for each slope were chosen to capture the zones of transition in vegetation within the available field work timeframe. Changes were made to the initial list of selected sites while in the field once a better understanding of the terrain and logistics involved for some sites was acquired. Proposed sites on Mt Granger and Haeckle Hill were dropped while sites near Dawson were added to include more sites with climate station data and to offer a comparison with an area unglaciated during the last glacial maximum. A complete list of sites is available in Appendix A.

4.2 Resistivity surveys

An ABEM terrameter LS system (Figure 9) was used to perform the ERT surveys. This system includes the terrameter, four 40 m long cables with 21 electrical take-outs, and stainless steel rods, or long nails, which were inserted into the ground to about 30 cm depth and connected to the cables' electrical take-outs by jumper cables.

Figure 9: ABEM Terrameter LS being used in the field to complete electrical resistivity tomography surveys (Lewkowicz et al. 2013)

Field notes and photographs were used to record the vegetation cover along each survey line while slope angle, organic layer thickness and frost probe refusal depth were measured every 4 m along the profile as described below.

4.2.1 Wenner array and profile settings

The cables were laid out with electrodes spaced at 2 m in 160 to 280 m long Wenner arrays (Figure 10). For the first and last cable of the profiles, the electrodes were inserted into the ground at 4 m intervals and connected to every second electrical take-out. For the two middle cables, the electrodes were inserted into the ground at 2 m intervals and connected every electrical take-out. This configuration allows 14 levels of depth to be modeled between 0.5 m and about 26 m. The precise settings used are listed in Appendix C.

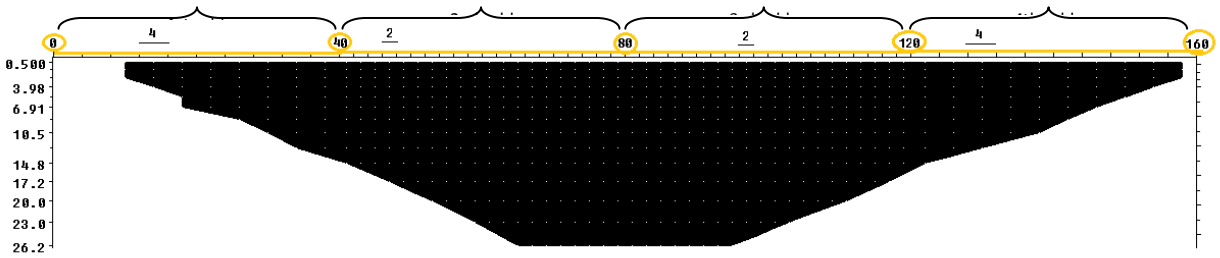

Figure 10: Diagram of the layout for a 160 m ERT survey using a Wenner array.

4.2.2 Elevation and slope measurements

Elevation was recorded every 40 m along the profile using a handheld Garmin Etrex vista global positioning system (GPS, ±5 m precision). The GPS was simultaneously used to record the latitude and longitude according to the North American Datum of 1983 (NAD 83) of these same points. These coordinates were copied in the field notes.

Slope angle was measured with an Abney level. Researchers determined one another's eye height and sighting spot on level ground then placed themselves 4 m apart along the survey (two electrical take outs away) and sighted the level to their designated eye height/sighting spot. The Abney level then indicated the angle between the two points 4 m apart along the profile.

4.2.3 Organic layer thickness and frost probe record

A frost probe and tape measure were used to determine the organic mat thickness and frost probe refusal depth. Every 4 m along the profile, the 120 cm long metal probe was gently inserted into the ground surface until inorganic resistance is felt; the depth attained was measured and recorded as the organic mat thickness. Then the probe was inserted more forcefully into the ground until it went no deeper. The depth attained was again measured and recorded as the probe refusal depth. The type of resistance felt at the point of refusal; gravel, rocks or other clasts (G), compact ground refusal (R), or permafrost (pf), was also noted. If probe refusal was not encountered within 120 cm, the probe refusal depth was recorded as 120+ cm.

4.2.4 Field notes and photographs

Field notes for each survey included the date and weather, GPS coordinates, photograph list, data for every 4 m along the transect (Table 2) and other important details pertaining to pits dug, climate station serviced, or aerial photographs taken.

Table 2: Example of typical table used to record field notes

Electrical Take-Out number	Probe refusal depth (cm)	Abney level slope angle (°)	Organic mat thickness (cm)	Vegetation and other
1-1	40G	12↓	5	Tall shrubs (birch, willow.)
1-3	10G	24↓	1	Approx. 10m birch
…	…	…	…	…
4-19	120+	0	18	Stunted black spruce, moss
4-21	110R	1↑	13	Black spruce, coltsfoot...

Photographs from a handheld camera as well as aerial photographs were taken in the field. A shock and waterproof Panasonic Lumix DMC-TS1 12 mega pixel digital camera was used to take pictures of vegetation and other features of interest along the profile. Photographs at the beginning and end of the survey as well as at the junctions between ERT cables were taken for reference. The number of each photograph was noted in the field notes along with a brief description of the photographs contents. Unknown types of vegetation were photographed in more detail and later identified using Cody's (2000) book *Flora of the Yukon Territory* and Long's (2016) website *Yukon Views -- Yukon plant photographs*.

To produce high-resolution aerial image mosaics of ERT profile sites, an Unmanned Air Vehicle (UAV), the Phantom 2 Vision+, was used (Figure 11). This quadracopter aerial photographic platform was equipped with a 14 megapixel camera which can take 4384 x 3288 pixel resolution photographs with a 85°/110° field of view (DJI, 2014). The aerial photographic platform was suitable as shots could be taken perpendicular to the ground by tilting the gimbal to

90° (DJI 2014). Also, since the Phantom 2 Vision+, weighing 1284g (DJI 2014), met the exemption requirements for UAVs of 2kg or less, permission from Transport Canada was not required to fly the UAV (Transport Canada 2015). Still, several rules needed to be followed when flying, including not flying higher than 90m above the ground (Transport Canada 2015).

Figure 11: Phantom 2 Vision+ (DJI 2014)

With this restriction in mind, the UAV was manually flown over the survey site, and high resolution photographs of the ground were taken with a field of view of 85° and a gimbal angle of 90°. The photographs were taken from varying heights above the ground depending on site conditions, notably the slope angle, and flight starting point. Thus, the dimensions and scale of the photographs varied (Figure 12). Due to the fact that an entire ERT profile could not be captured by a single picture, successive overlapping photographs covering the entire ERT profile area were taken and then processed in Photoshop to remove lens distortion and create mosaics (Bellehumeur-Génier 2014).

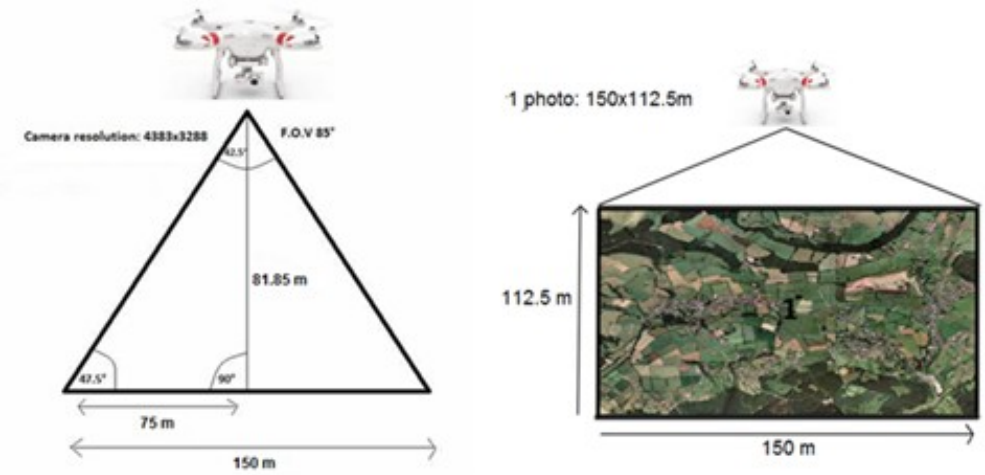

Figure 12: Dimensions of aerial photographs taken around 80 m above the ground (modified from Bellehumeur-Génier 2014)

4.3 Ground-truthing

To help interpret the ERT modeled resistivity profiles in terms of the presence of permafrost, various methods of ground-truthing were utilized. These included frost probing, digging pits, taking near-surface ground temperature measurements, and examining ground temperatures at depth in locations where boreholes with thermistors were present. Frost probing data were collected at 4 m intervals along all profiles (see Section 4.2.3). The data collected could confirm the presence of frozen or unfrozen ground in the near-surface, and if the probing data provided information between 0.5 m and 1 m depth it could be compared with the resistivity modeled in that depth range. Similarly, excavated pits up to 1 m deep could confirm the presence of frozen or unfrozen ground in the near surface. Climate stations equipped with thermistors (±0.2°C to ±0.5°C accuracy) at the ground surface and a various depths, from 25 to 100 cm (see Appendix B), provided temperature data for past years and could assist in understanding the ground thermal regime which in turn supports interpretations that permafrost is either present or absent in the near surface. Live temperature readings of near-surface ground temperatures were also recorded in some cases, by attaching a thermistor to a thin pole, inserting

the pole in a hole made by the frost probe and manually recording the temperatures that appeared on the real-time display of a four-channel Onset Hobo UX120-006M analog data logger (±0.2°C accuracy) once thermally equilibrated. Only where boreholes were present could ground temperatures be obtained for greater depths.

4.4 Climate station data collection

Several University of Ottawa climate stations are present along or near some of the profiles (Appendix B). These stations are generally equipped with thermistors and Onset Hobo Pro data-loggers (±0.2°C to ±0.5°C accuracy) recording hourly or bi-hourly air temperature, near-surface ground temperature and temperature in the ground near the estimated top of permafrost. The stations also include a snow stake equipped with Thermochron iButtons (±0.5°C accuracy), which are used to interpret the snowpack thickness throughout the winter. Figure 13 illustrates a typical climate station and its different components. Lewkowicz et al. (2012) explain in detail the climate station installations.

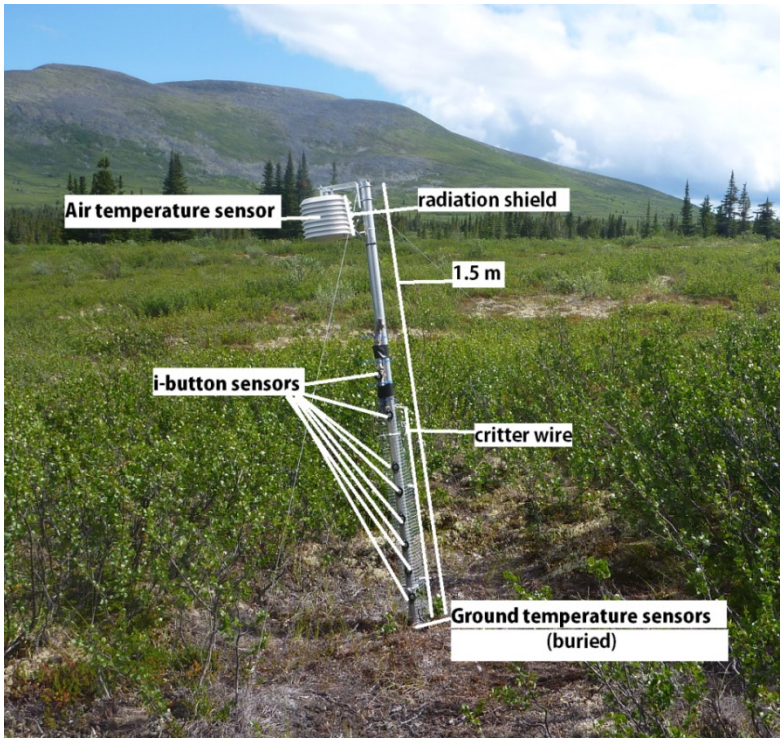

Figure 13: Typical climate station with components

Data from the climate stations were collected in two ways. First, the most recent data were downloaded on site during the fieldwork. A field laptop equipped with the HOBOware or Onset Boxcar softwares was used with the respective interface cables to download the data from the climate station loggers. Downloaded data were then saved and later processed in Microsoft Excel. Second, data from previous years were extracted from an unpublished database (Bevington 2016). The database includes a wide range of data, from raw files to calculated daily and monthly averages, as well as blended-year statistics. Some of the sites have data from as far back as 2006. The most recent data downloaded on site during the fieldwork was added to the database by Alexander Bevington in order to have up-to-date statistics.

4.5 Data processing and interpretation

4.5.1 Resistivity data

After the field ERT survey, apparent resistivity values must be converted into a resistivity model that can be used for geological interpretation (Loke 2004). A software package, RES2DINV by Geotomo Software, is used to remove bad data points manually, incorporate topography data, perform a robust inversion, and export data from the model selected.

Hauck and Vonder Muhll (2003, p.307) describe in detail how the RES2DINV program applies a smoothness-constrained least-squares method to solve the tomographic inversion problem. Due to the iterative nature of the inversion process, different resistivity models are produced with different root-mean square (RMS) errors. The model selected for each profile was selected based on the following rules. Regardless of any subsequent rules no iteration past the 5th was selected. The 5th iteration model was selected unless the RMS error of an earlier iteration was below 5%. In that case, that iteration's model was selected unless the RMS error in subsequent iterations continued to decrease by more than 1% between iterations. If that was the case, then the model from the last iteration to exhibit and decrease in RMS greater than 1% was selected.

Virtual boreholes were produced by exporting the selected models data in XYZ format and using SPSS statistics or Microsoft Excel to graph the modeled resistivity by depth for a given point along the survey (Figure 14). Virtual boreholes were produced for locations that represented different types of resistivity transitions, such as very rapid changes in magnitude or more gradual changes.

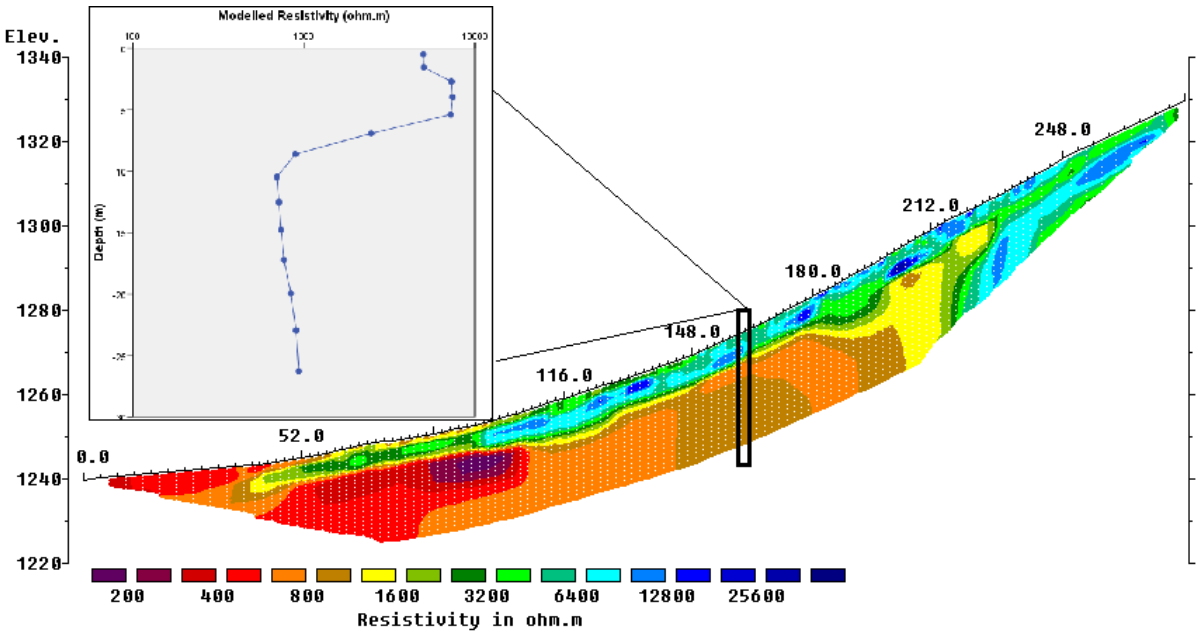

Figure 14: Example of ERT profile and virtual borehole interpretation (The sharp transition from high to lower resistivity is interpreted as permafrost boundary around 1000 Ωm)

Finally by using the virtual boreholes and examining the selected model's resistivity patterns in conjunction with ground-truthing data, i.e. frost probe data, climate station data, pits etc., the profiles were interpreted in terms of permafrost occurrence. High resistivity values and sharp resistivity transitions were considered potential indicators of permafrost. Possible changes in permafrost presence and contiguity are summarized in Figure 15-A.

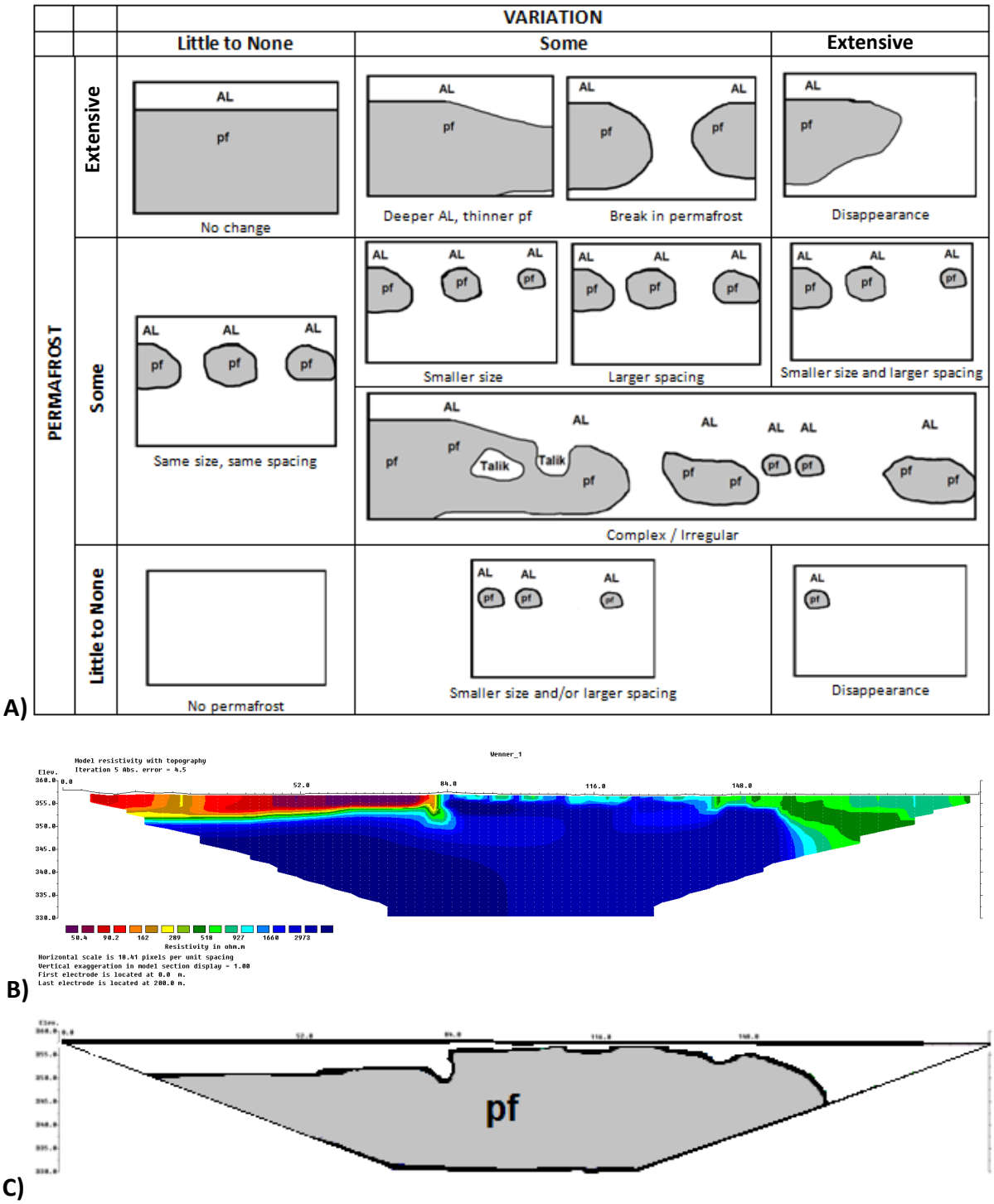

Figure 15: Interpreting changes in permafrost presence and contiguity from resistivity profiles

A) Schematic representation of changes in permafrost contiguity potentially represented in ERT profiles. pf=permafrost, AL=Active Layer (not to scale)

B) Example of modeled resistivity of a profile.

C) Permafrost interpretation for the modeled resistivity indicating extensive permafrost with some change in active layer thickness and possible permafrost disappearance on the right.

4.5.2 Aerial photographs

Adobe Photoshop Lightroom5 software was used to remove the lens distortion from aerial photographs taken in the field. Adobe Photoshop CC software was then used to auto-align, auto-blend and merge multiple photographs taken along a single profile. Once a new object was created from the merged layers, the image was annotated in Photoshop with lines depicting the location of the ERT cables and squares representing the start and end of the profile. Distances along the profile were noted every 40 m and climate stations, where present, were circled. The entire process is summarized in Figure 16.

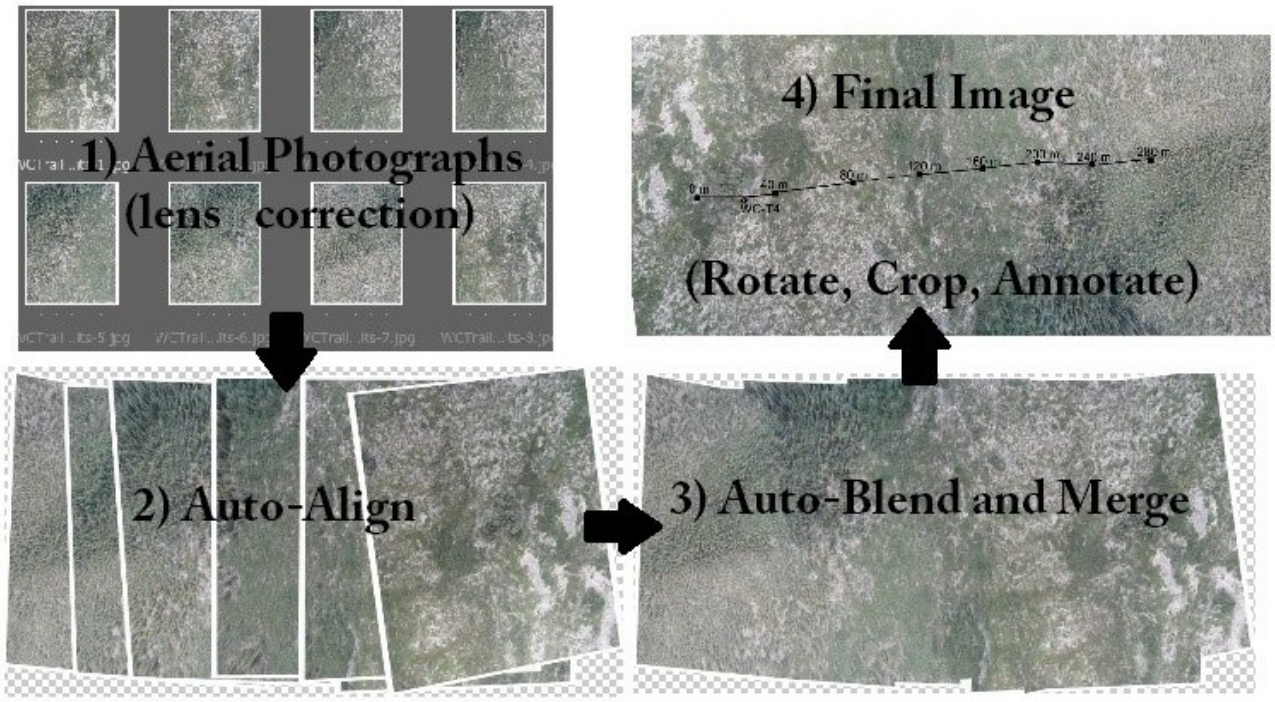

Figure 16: Example of aerial photograph processing steps

4.5.3 Organic layer thickness and frost probe record

The organic layer thickness and frost probe record were manually copied from the field notes into Excel spreadsheets and later digitally copied into SPSS statistics to produce graphs.

4.5.4 Climate station data

The climate station thermistor data were transferred from its original formats into Excel and added into an existing database (Bevington 2016). Values extracted from this database include mean January and July air temperatures, annual mean air temperatures (AMAT), annual mean ground surface temperature (AMGST) and annual mean ground temperatures (AMGT), The ground temperatures were measured at different depths across the sites and are sometimes referred to as temperatures at the estimated top of permafrost, although they were not necessarily measured at this depth. Blended mean annual temperatures for the air, ground surface and "top of permafrost" were also extracted from the database. The blended-year method creates a single year of data based on the mean of all months that are more than 90% complete. The blended-year approximates the climate at each site based on as much of the available data as possible (Bevington 2016, p.29). Snow stake iButton data were processed in Excel using a new semi-automated technique (Kuntz 2016) that calculates snow depth days and produces graphs of the estimated snowpack evolution through the winter (see Appendix D).

5.0 Results

This section presents the results obtained after processing and examining the data collected for twelve study sites. The results for eight sites within the Whitehorse study area are presented first followed by the results for four study sites within the Dawson study. For each profile, site characteristics are described and vegetation cover is examined. Where on site climate data are available, the relationships between air and ground temperature, and snow cover are examined. Each site's ERT data are summarized and presented in various forms. Most sites have an annotated modeled resistivity profile image, and a permafrost classification image. Sites also have virtual borehole figures when these appear relevant.

When resistivity patterns are described in the results, resistivity values are classified according to categories based on the data distribution (Figure 17). Medium resistivity refers to values between 1.1 kΩm and 3.5 kΩm. Low resistivity refers to resistivity values below 1.1 kΩm. High resistivity refers to values above 3.5 kΩm. Very low refers to resistivity values below 0.5 kΩm. Very high refers to values above 9.8 kΩm.

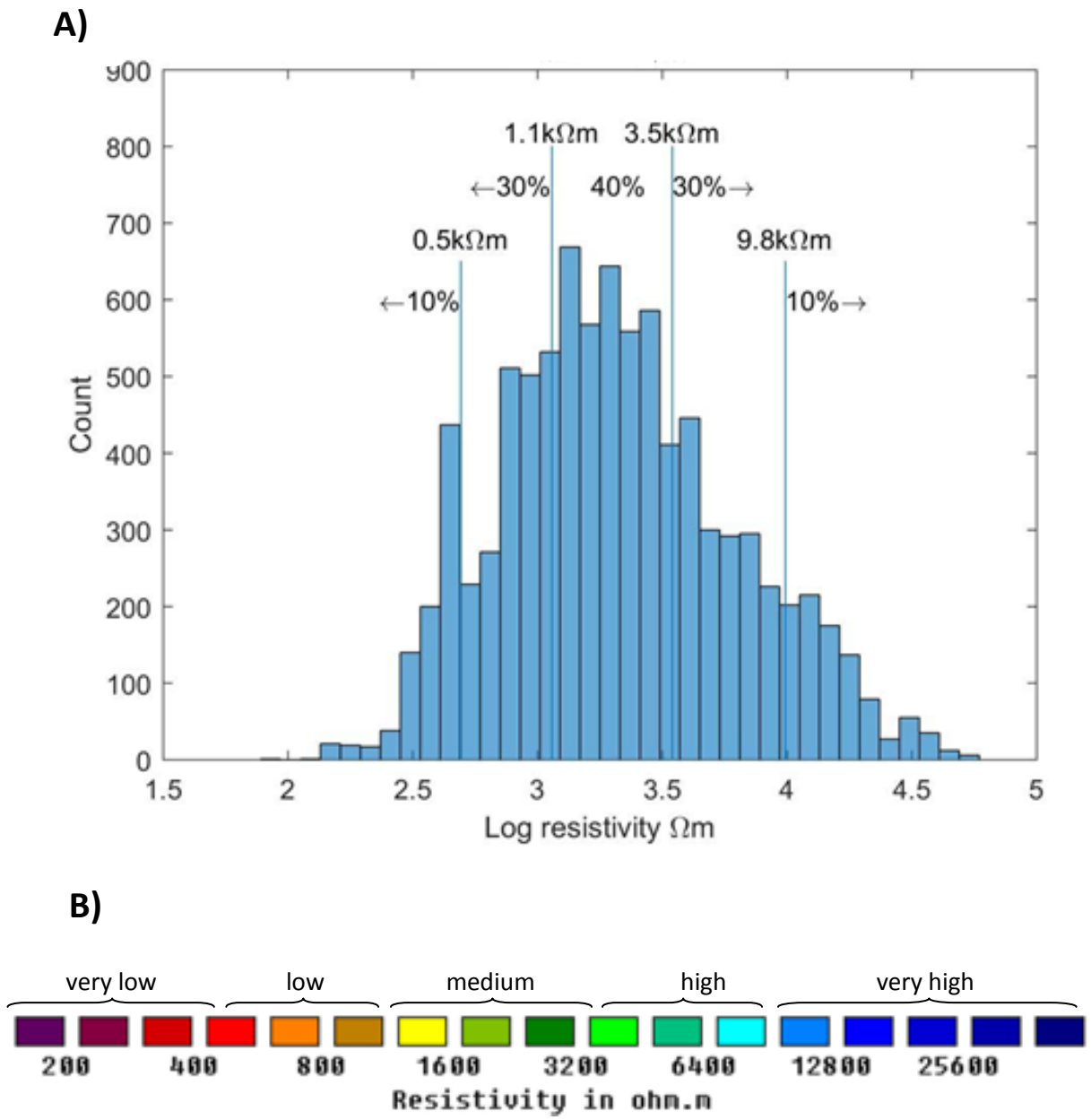

Figure 17: Modeled resistivity distribution and classification.

(A) Histogram of all modeled resistivity value in log scale. Resistivity values in kΩm are shown for the 10th, 30th, 70th, and 90th percentiles.

(B) Resistivity magnitude classification in relation to the colour scheme used in the tomograms. Five classes from very low to very high span the 17 colours.

5.1 Whitehorse study area sites

Eight ERT profiles were completed in the Whitehorse area (Figure 18). The first was completed at an alpine site in the Wolf Creek basin, the second along the northwest-facing slope of Coal Ridge, and the third on a south-facing slope in the basin. Profiles 4 and 5 were completed at treeline near the Mt Sima trail while the last three profiles were completed along a transect on Mt McIntyre.

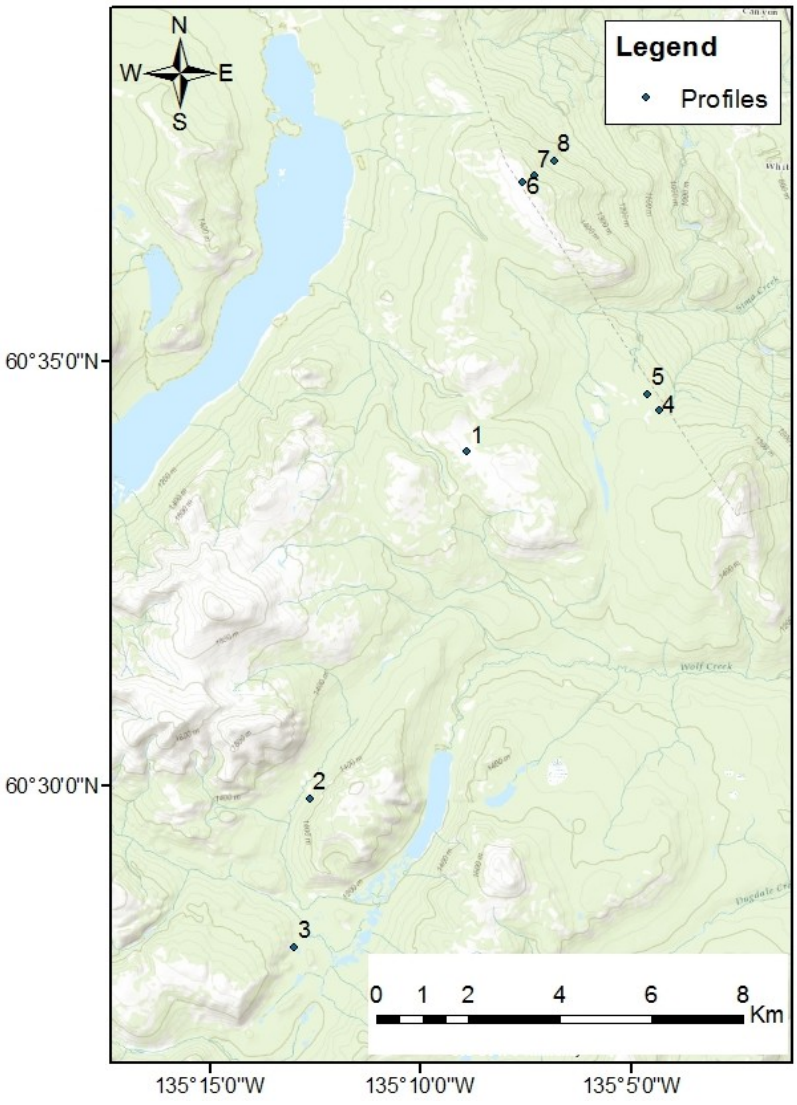

Figure 18: Map showing the location of the ERT profiles 1 - 8 in the Whitehorse area

Most of the sites in the Whitehorse study area are situated in areas of extensive discontinuous permafrost (Figure 19). Sites 1, 6, 7 and 8 are in areas where permafrost is expected to be extensive. Sites 3 and 5 are in areas where permafrost is modeled to be sporadic and thus is expected to be minimal or absent while sites 2 and 4 should sample the transition between sporadic and extensive discontinuous permafrost.

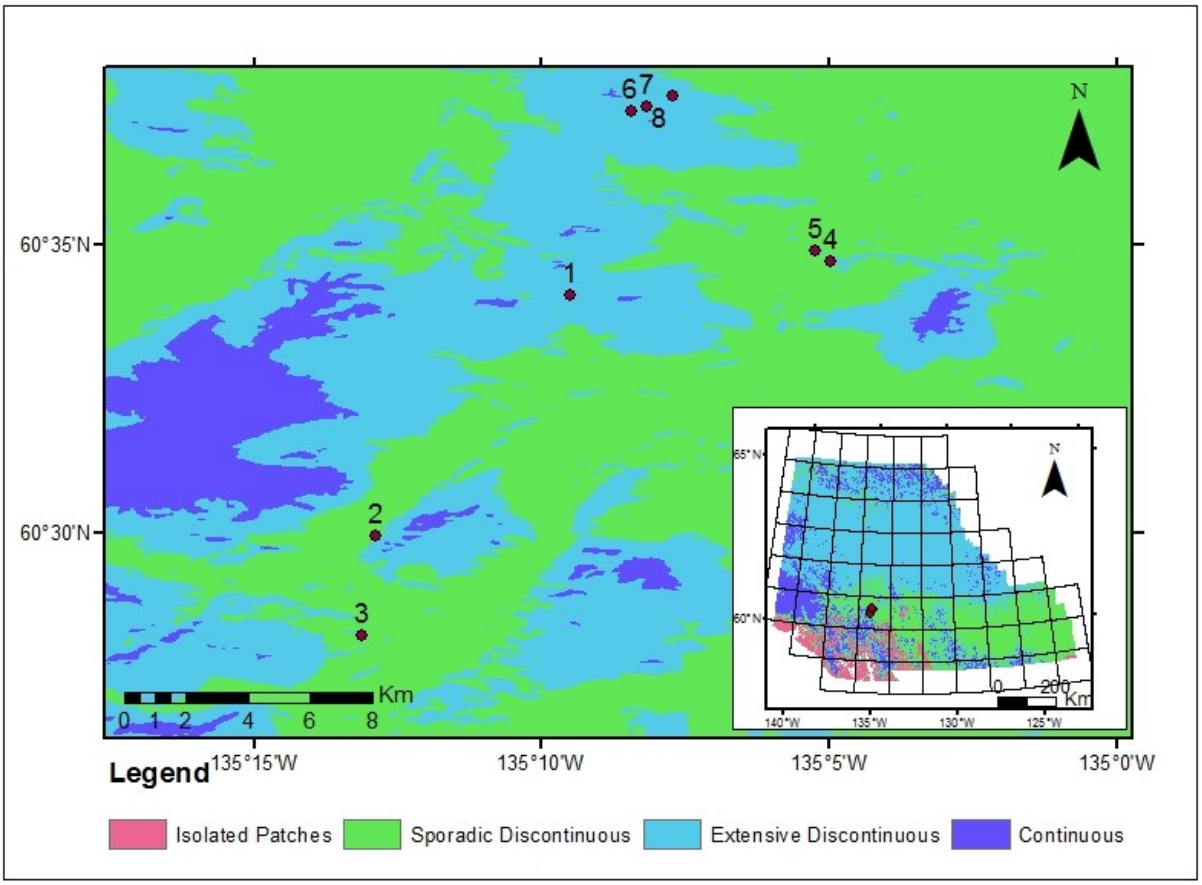

Figure 19: Whitehorse area sites in relation to the *Yukon Permafrost Probability Map* (Bonnaventure et al., 2012)

5.1.1 Site 1

Site 1 is on a gentle slope near the crest of a ridge in the Wolf Creek basin. The profile (Figure 20) begins at approximately 1494 m asl and extends down the gentle west-facing slope to approximately 1472 m asl.

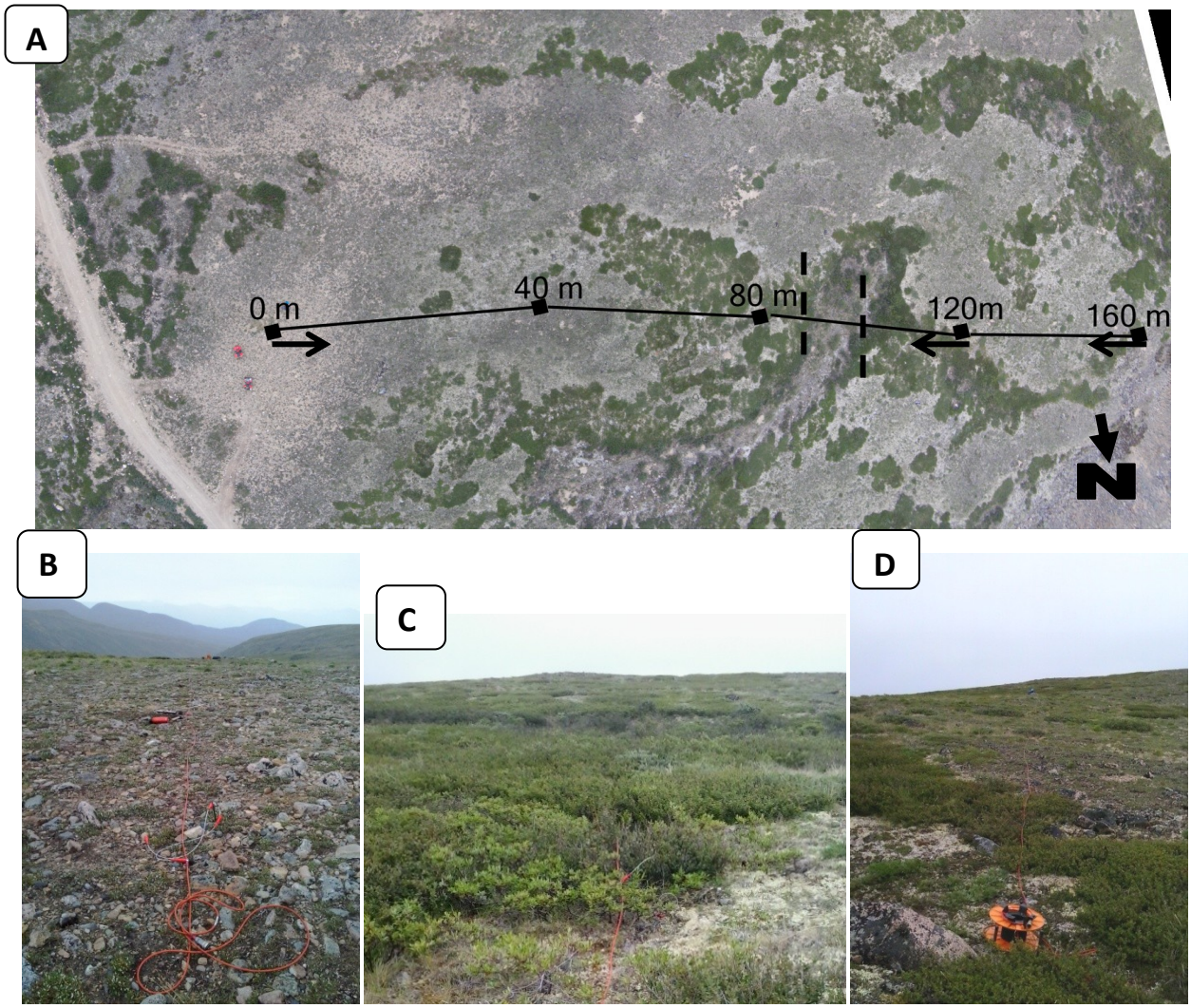

Figure 20: Aerial image mosaic and photographs for Site 1
A) Aerial image mosaic of Site 1, with the profile traced in black and the distance along profile noted every 40 m. Dashed lines mark a depression and arrows indicate direction of photographs.
B) Photograph from 0 m along the profile
C) Photograph from 120 m along the profile
D) Photograph from 160 m along the profile

Vegetation

This profile is located well above treeline and covers bare ground, tundra vegetation and patches of low shrubs (Figure 20). Very few shrubs occur in the first 60 m along the profile. Dense *Salix* sp. and *Betula nana*, up to 88 cm tall, occur between 100 and 120 m. The shrubs then become shorter and sparser until lichen- and moss-covered rocks dominate the surface.

The distribution of shrubs appeared to impact the organic mat thickness, which ranged from 0 to 19 cm. Where shrubs were absent, the organic mat was absent or minimal (mostly < 5 cm). Where shrubs were dense or tall, the organic mat thickness was greater.

A channel-like depression with large rocks, grasses and sparser shrubs is present between 92 m and 106 m along the profile. The photograph taken around 120 m along the profile (Figure 20 B) captures the break in slope that occurs at 96 m.

Climate

This site does not include any climate stations. However, based on the surface lapse rate and data from nearby climate stations, WC-T4 and WC2006-01, the mean annual air temperature is estimated to be in the range between -3.5°C to -4°C. Snow cover likely varies along the profile. Less snow is expected on the windswept section near the crest. However, snow may accumulate around taller shrubs and in the channel-like depression.

Resistivity and Permafrost

The fifth iteration with a 4.1% RMS error was selected as the modeled resistivity profile for this site (Figure 21).

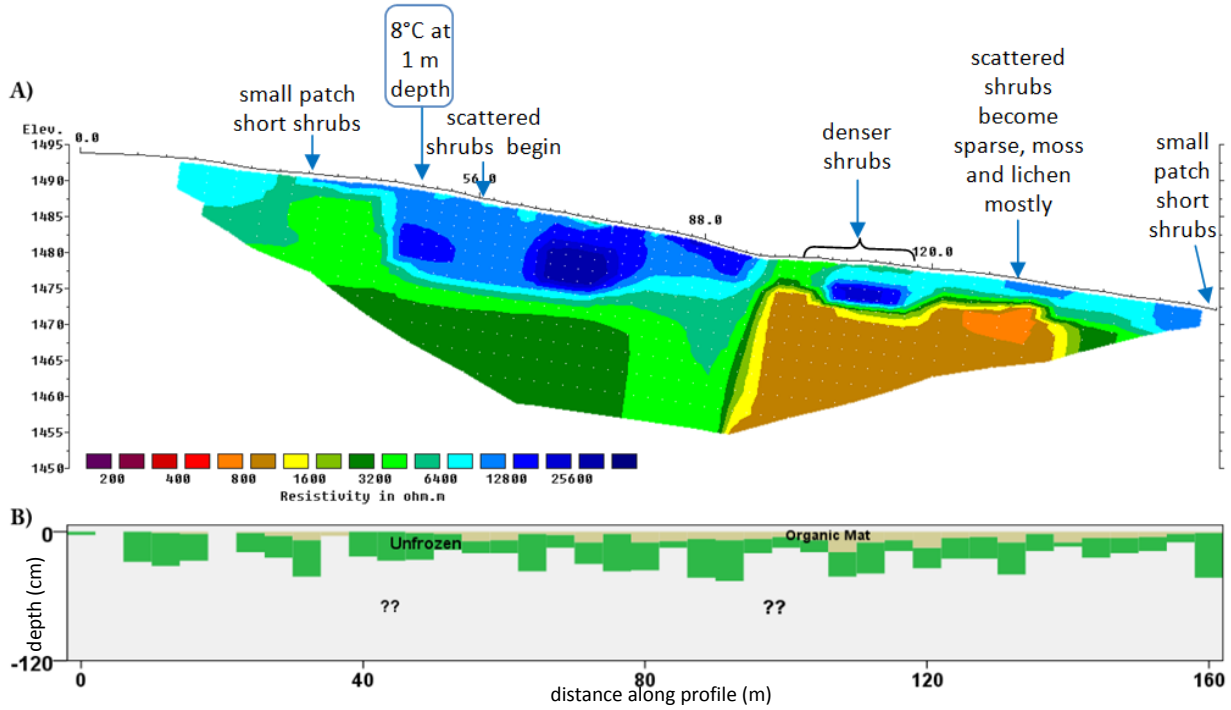

Figure 21: Combined results for Site 1.

(A): Modeled resistivity profile annotated with changes in vegetation and live temperature readings on day of the survey.
(B): Frost probe measurements (in cm) including organic mat thickness (in beige)and refusal depth (in green) with instances where refusal was interpreted as frozen ground (in blue).

Modeled resistivity values vary across the tomogram from approximately 0.6 kΩm in some areas to 31 kΩm in others. Low modeled resistivity values all occur from 92 m to 140 m along the profile. These values begin mostly from 5 m depth or more and extend to the maximum modeled depths. Resistivity values modeled near the surface are always high or very high. The lowest values near the surface are from 98 m to 108 m along the profile.

A few places along the profile display modeled resistivity values near the surface that are lower than values modeled below. In the section between 32 m and 96 m along the profile, there are four occurrences of such a pattern. In addition, a pattern of high resistivity values between lower resistivity values occurs from 106 m to 116 m. From about 3-8 m depth, an area with

values above 10 kΩm overlies a thick layer of low resistivity with a very sharp boundary. Resistivity values change from less than 1 kΩm to more than 10 kΩm within a few meters (Figure 22-B).

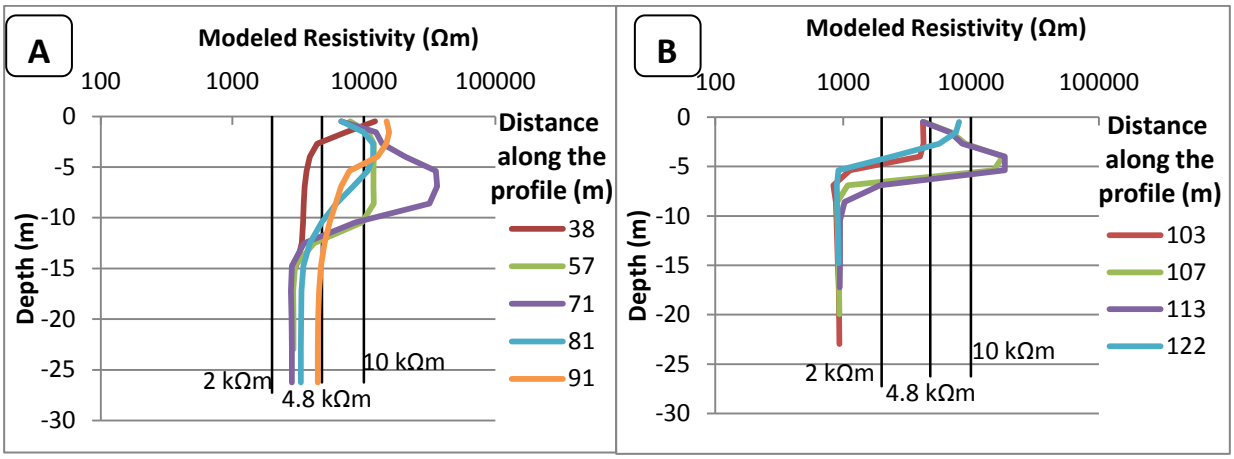

Figure 22: Virtual boreholes for Site 1
A) All values greater than 2 kΩm B) Section with low resistivity values

The resistivity patterns are used to interpret permafrost conditions. The highest resistivity areas (>13 kΩm) with sharp transitions to lower resistivity values above and below them are interpreted as indicating probable permafrost, while permafrost is interpreted to be improbable in the area of low resistivity. With the exception of this area, permafrost is deemed possible for most of the profile. However it is rarely interpreted with complete confidence (Figure 23).

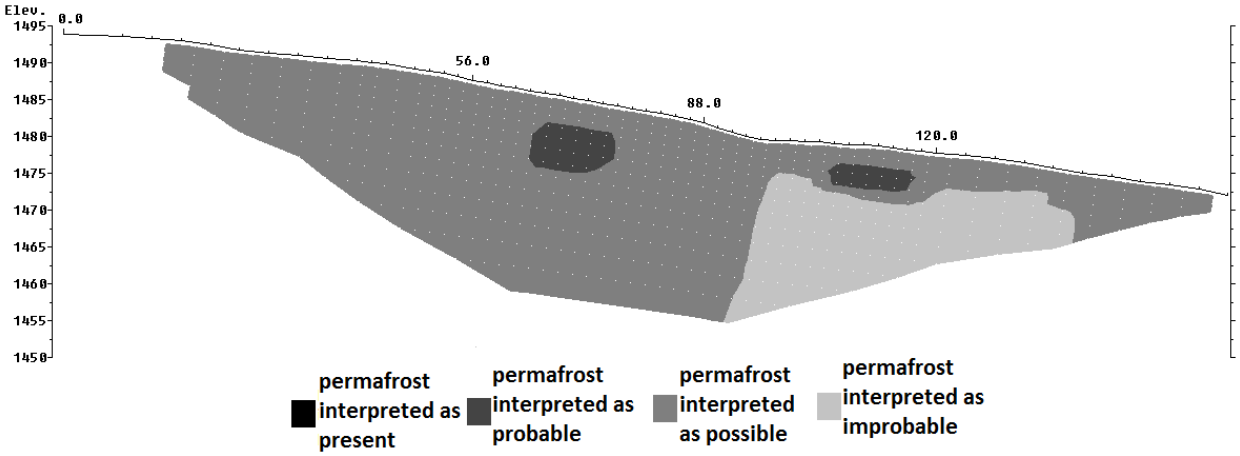

Figure 23: Permafrost interpretation image for Site 1

Several factors complicate the profile interpretation. These factors include the complex patterns in modeled resistivity, the highly resistive surficial material, and the lack of ground-truthing data. Probe refusal, reached at depths ranging from 0 cm to 46 cm, was always interpreted as caused by clasts. Also, only one temperature measurement of was obtained. Permafrost extent is difficult to interpret because the resistivity of the ground material likely varies across the profile regardless of temperature. High resistivity values modeled where the ground was proven unfrozen, 48 m along the profile, speak to the imprudence of using high resistivity values as unequivocal indications of frozen ground.

A deep active layer is expected at this site, but cannot be confirmed due to the surficial materials. Lewkowicz et al. (2011) reported an active layer of 6.4 m in 2009-10 on the bare windswept crest of Mt McIntyre. Similar conditions are expected to occur at Site 1. The tomogram does not reveal the thick lower resistivity layer near the surface expected of a thick unfrozen active layer. The coarse and blocky surface material of this site, which included rocks as large as 1 m long, likely prevents the active layer from being discernible in the tomogram. In addition, numerous ground squirrel holes are present at this site. Their presence suggests a network of air-filled channels below the surface which could also increase the near surface resistivity.

In conclusion, the ERT indicates deep permafrost in the first part of the profile and thin permafrost between 98 and 140 m along the profile where shrubs are denser. The active layer, expected to be thick, is not discernible from the profile.

5.1.2 Site 2

Site 2 is located on the northwest-facing slope of Coal Ridge (Figure 24). The profile begins at approximately 1240 m asl on a gravelly fan with some grass and *Salix* sp. The profile ends at about 1330 m asl on a steep slope with dense shrubs, large boulders and stunted type *Picea* sp.

Figure 24: Upslope view from start of the profile at Site 2. The approximate line of the profile is shown by a white dashed line.

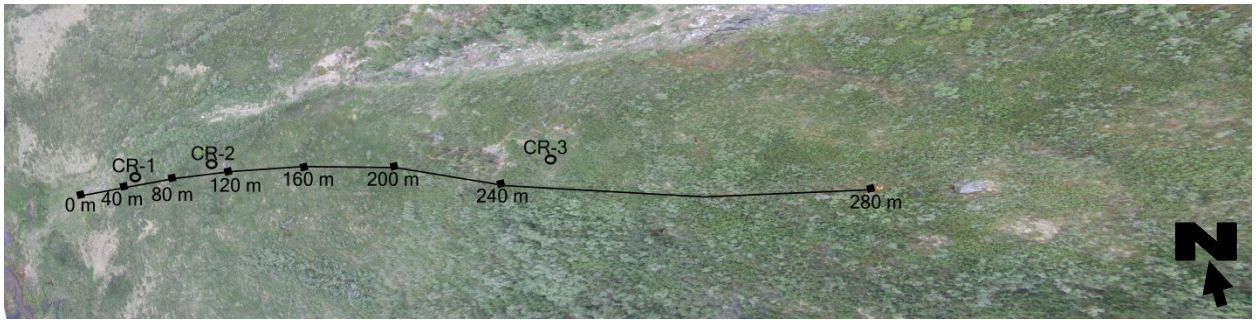

Figure 25: Aerial image mosaic of Site 2, with the profile traced in black and the distance along profile noted every 40 m. Climate stations CR-1, CR-2 and CR-3 are circled.

Vegetation

The profile was intended to capture the vegetation transition for a lower treeline around 1250 m asl, at about 78 m from the start. However, because trees are so scattered on this slope, the first trees adjacent to the profile actually occur at 218 m from the start at a distance of roughly 3 m from the profile line. Tree and shrub species occurring along the profile include *Picea* sp., *Salix* sp., and *Betula nana*. Ground cover species include *Delphinium sp.*, *Potentilla* sp., *Ledum* sp., *Salix reticulata*, *Petasite s*sp. (coltsfoot), and *Epilobium angustifolium* (fireweed). Mosses, lichens, grasses, and berry-bearing plants also occur. The organic mat thickness ranged between 0 cm and 40 cm.

Climate

Three climate stations (CR-1, CR-2, and CR-3) are present near the profile (Figure 25). They have been operating from 2004 through to present but with some gaps in the data. Their data were used to calculate mean annual temperatures for the air and the ground as well as snow depth days (Figure 26, Figure 27, and Figure 28). These climate variables could not always be calculated for each year due to gaps in the dataset. Nonetheless, sufficient data were available to characterize some of the local topoclimatic variability.

The blended-year statistics for the climate stations (Table 3) highlight how the variables change with elevation. The blended mean annual air temperature is around -3°C across the profile. The similar annual air temperatures result from winter inversions in the surface lapse rate that occur at this site due to cold air pooling in the valley. Indeed, the mean January air temperatures are lower toward the valley bottom than upslope in contrast with the trend shown in July of air temperature decreasing with elevation.

Table 3: Summary statistics for stations CR-1, CR-2, and CR-3

	CR-1	CR-2	CR-3
Elevation (m asl)	1249	1262	1324
Blended mean annual air temperature[1] (°C)	-2.9 (n=70)	-3.1 (n=66)	-2.8 (n=89)
Blended mean annual ground surface temperature[1] (°C)	0.8 (n=94)	0.3 (n=97)	-0.5 (n=98)
Blended temperature at the top of permafrost[1] (°C)	0.1 (n=84)	-0.4 (n=85)	-0.6 (n=73)
2006-15 mean snow depth days[2] (m.days)	115 (n=8)	71 (n=8)	62 (n=8)
2006-15 mean surface offset[2] (°C)	3.9 (n=5)	3.4 (n=5)	2.2 (n=6)
2006-15 mean thermal offset[2] (°C)	-0.6 (n=6)	-0.8 (n=7)	-0.3 (n=5)
2006-15 mean January air temperature[2] (°C)	-12.4 (n=6)	-13.3 (n=6)	-11.8 (n=8)
2006-15 mean July air temperature[2] (°C)	10.4 (n=5)	10.2 (n=5)	9.6 (=8)

[1]Blended-year statistic obtained from Bevington's (2016) Database, calculated from data for *n* number of months.
[2]Means calculated by averaging the values obtained for *n* number of years during the defined period

The snow accumulation is greatest in the valley bottom and decreases further upslope. Annual ground surface and ground temperatures are warmest at station CR-1, and decrease upslope to be colder at station CR-2 and coldest at station CR-3. The negative mean ground temperatures and thermal offsets confirm the presence of permafrost. The surface offsets calculated for station CR-1 average almost 4°C. The mean surface offsets decrease with elevation for the remaining two climate stations. The small and negative mean thermal offsets do not show a pattern with elevation.

Annual data from all three stations provide insight into the interannual variability of the measured variables and their interrelationships, specifically the impact of differing numbers of snow depth days (SDD). The year 2007-08 was, at all three stations, the year with the lowest number of SDDSDD. 64 m.days were calculated for station CR-1, while only 33 m.days were calculated for station CR-3. The year 2007-08 was also the year with the lowest annual mean ground surface temperature (AMGST) and the lowest annual mean ground temperature close to the top of permafrost (AMGT). The years with the largest number of SDD differed among the stations. Still, the year 2010-11 was among the three years with the largest SDD values at all

three stations. Over 150 m.days were calculated for station CR-1 that year, and over 70 m.days were calculated for station CR-3. The years with greater SDD did not always correspond with the years with larger surface offsets.

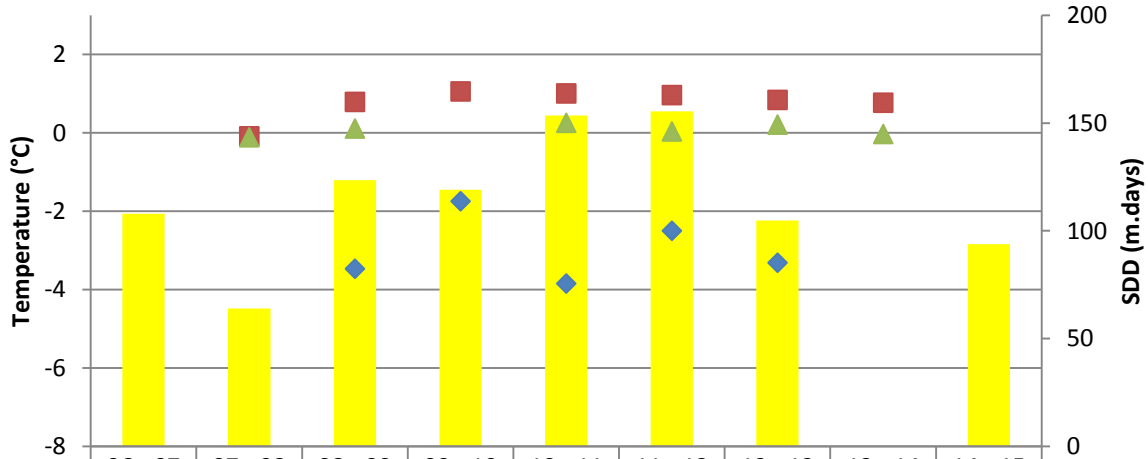

Year	06 - 07	07 - 08	08 - 09	09 - 10	10 - 11	11 - 12	12 - 13	13 - 14	14 - 15
SDDs	108	64	124	119	154	156	105		94
AMAT			-3.5	-1.7	-3.8	-2.5	-3.3		
AMGST		-0.1	0.8	1.1	1.0	1.0	0.8	0.8	
AMGT		-0.1	0.1		0.3	0.0	0.2	0.0	

*SDD-Snow Depth Days, AMAT-Annual Mean Air Temperature, AMGST-Annual Mean Ground Surface Temperature, AMGT-Annual Mean Ground Temperature at the estimated top of permafrost

Figure 26: Climate Station CR-1 Data (1249 m asl)

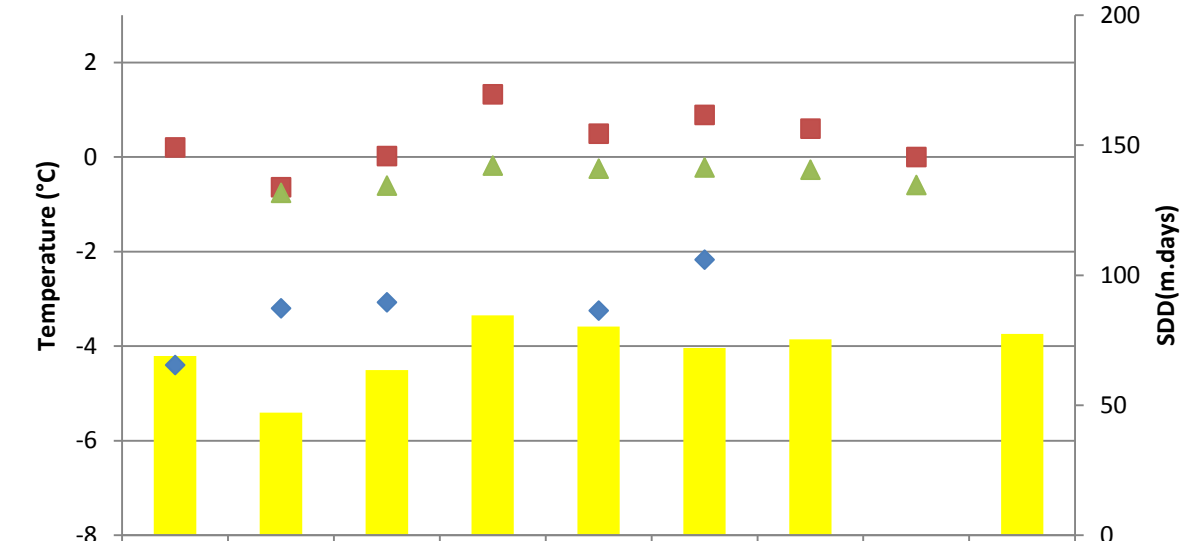

Year	06 - 07	07 - 08	08 - 09	09 - 10	10 - 11	11 - 12	12 - 13	13 - 14	14 - 15
SDDs	69	47	64	85	80	72	75	0	77
AMAT	-4.4	-3.2	-3.1		-3.2	-2.2			
AMGST	0.2	-0.6	0.0	1.3	0.5	0.9	0.6	0.0	
AMGT		-0.8	-0.6	-0.2	-0.2	-0.2	-0.3	-0.6	

*SDD-Snow Depth Days, AMAT-Annual Mean Air Temperature, AMGST-Annual Mean Ground Surface Temperature, AMGT-Annual Mean Ground Temperature at the estimated top of permafrost

Figure 27: Climate Station CR-2 Data (1262 m asl)

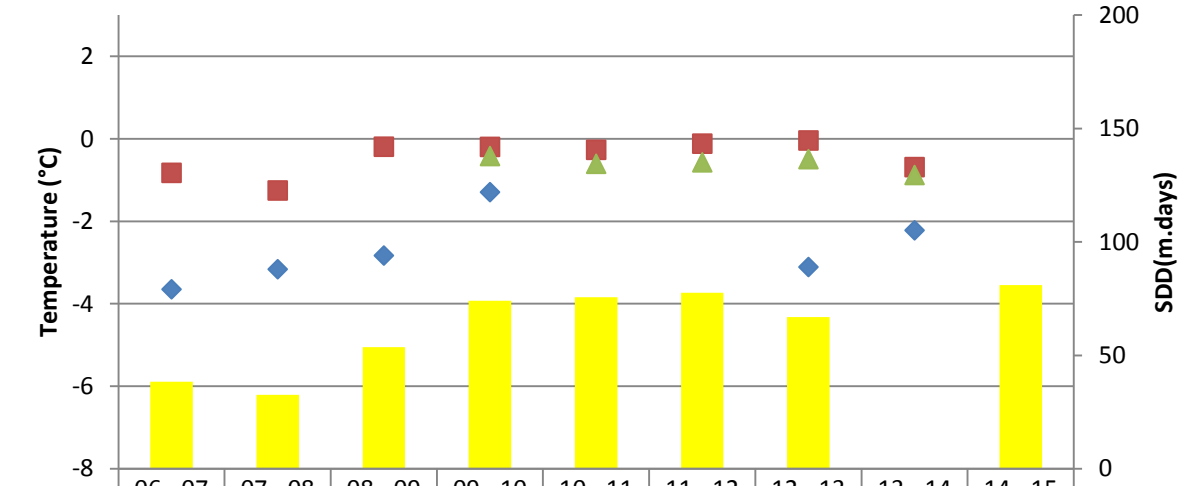

	06 - 07	07 - 08	08 - 09	09 - 10	10 - 11	11 - 12	12 - 13	13 - 14	14 - 15
SDDs	38	33	54	74	76	78	67		81
AMAT	-3.6	-3.2	-2.8	-1.3			-3.1	-2.2	
AMGST	-0.8	-1.3	-0.2	-0.2	-0.3	-0.1	0.0	-0.7	
AMGT				-0.4	-0.6	-0.6	-0.5	-0.9	

*SDD-Snow Depth Days, AMAT-Annual Mean Air Temperature, AMGST-Annual Mean Ground Surface Temperature, AMGT-Annual Mean Ground Temperature at the estimated top of permafrost

Figure 28: Climate Station CR-3 Data (1324 m asl)

Resistivity and Permafrost

The fourth iteration with a 3.5% RMS error was selected as the modeled resistivity profile (Figure 29).

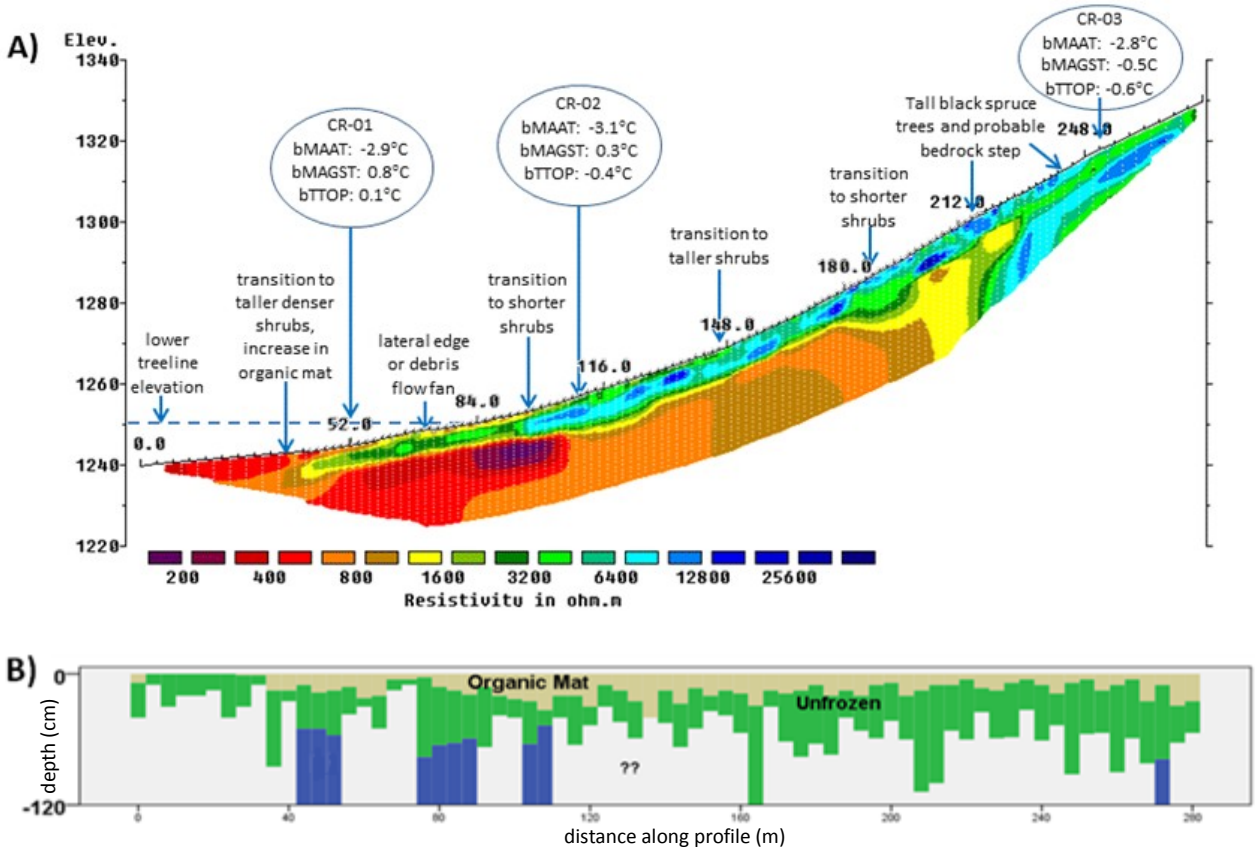

Figure 29: Combined results for Site 2

(A): Modeled resistivity profile annotated with changes in vegetation and temperature data. (B): Frost probe measurements (in cm) including organic mat thickness (in beige) and refusal depth (in green) with instances where refusal was interpreted as frozen ground (in blue).

Resistivity values range from less than 200 Ωm to more than 20 kΩm. The following paragraphs describe the different resistivity patterns which appear in four different sections of the profile : from 6 m to 36 m along the profile, from 36 m to 180 m, from 180 m to 220 m, and from 220 m to 278 m.

A one layer system of low resistivity is modeled until 36 m along the profile. The organic mat is absent or minimal in this section as the profile traverses a gravelly fan that shows signs of ongoing surface runoff. Probe refusal was reached at depths ranging from 10 cm to 40 cm and interpreted as clasts. Permafrost was interpreted as improbable.

From 36 m to 180 m along the profile, a three layer system occurs. A thin lowerresistivity layer is present over a layer of higher resistivity that is underlain by a thick layer of low and very low resistivity. Within this three layer system, resistivity values tend to increase the further they are along the profile. Probe refusal in this section was reached at varying depths, ranging from 10 cm to 85 cm, depending on the location of clasts and peat. For most measurements, refusal was interpreted as being caused by clasts. However, refusal was interpreted as being caused by frozen ground in nine instances at depths ranging from 50 cm to 76 cm. These instances of probe refusal, the three layer system, and the temperature data from the climate stations CR-1 and CR-2 support the interpretation that permafrost is almost certainly present in this section of the profile. The results also suggest that permafrost is thinner and warmer at the lower elevation. The organic mat thickness measurements in this section varied from 3 cm to 40 cm, with the majority of values recorded between 10 cm and 20 cm.

From 180 m to 220 m along the profile, the resistivity values depict mostly a two layer system of high resistivity over lower resistivity but they also resemble the previous three layer system in a small section between 200 m and 210 m.

Lastly, high resistivity values without a distinct layered pattern occur from 220 m to 278 m along the profile. Visual observations in this section indicate that bedrock steps are possible.

Thus, the high and very high resistivity values modeled at depth may be indications of bedrock. Temperature data from the climate station CR-3 indicate permafrost presence in the near surface.

The resistivity patterns and transition between resistivity layers can be examined in more detail with virtual boreholes (Figure 30). The lower part of the profile generally has lower resistivity values than the upslope portion of the tomogram. The transition from near surface low or medium values to higher resistivity values is evident in the lower part of the profile, and generally occurs around the same depth. Even though the near surface values are mostly all high resistivity values, some areas, like at 155 m or at 205, still reveal a noticeable increase in resistivity. In both the upper and lower parts of the slope, a sharp decrease in resistivity is present around 5 m depth.

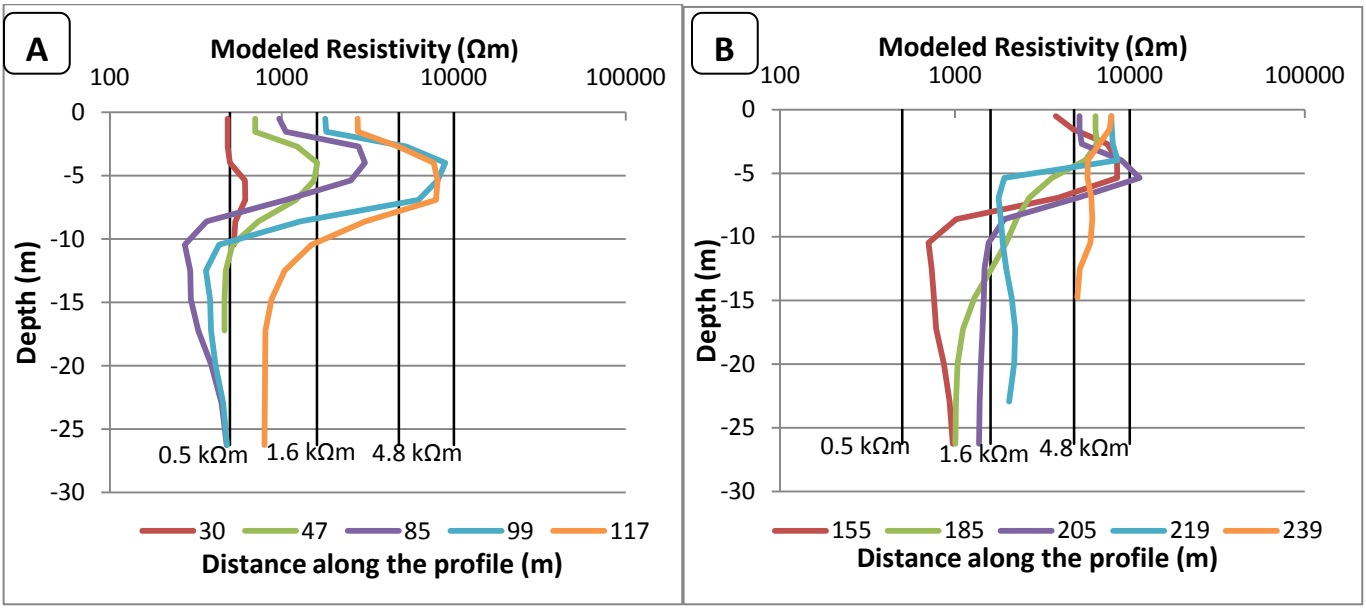

Figure 30: Virtual boreholes for Site 2
A) Lower part of the profile B) Upslope portion of the profile

Combining all of these results, at thin layer of continuous permafrost is interpreted with confidence throughout most of the slope (Figure 31). Permafrost is deemed improbable where resistivity values are low. Where a bedrock step is interpreted to be likely, permafrost is possible.

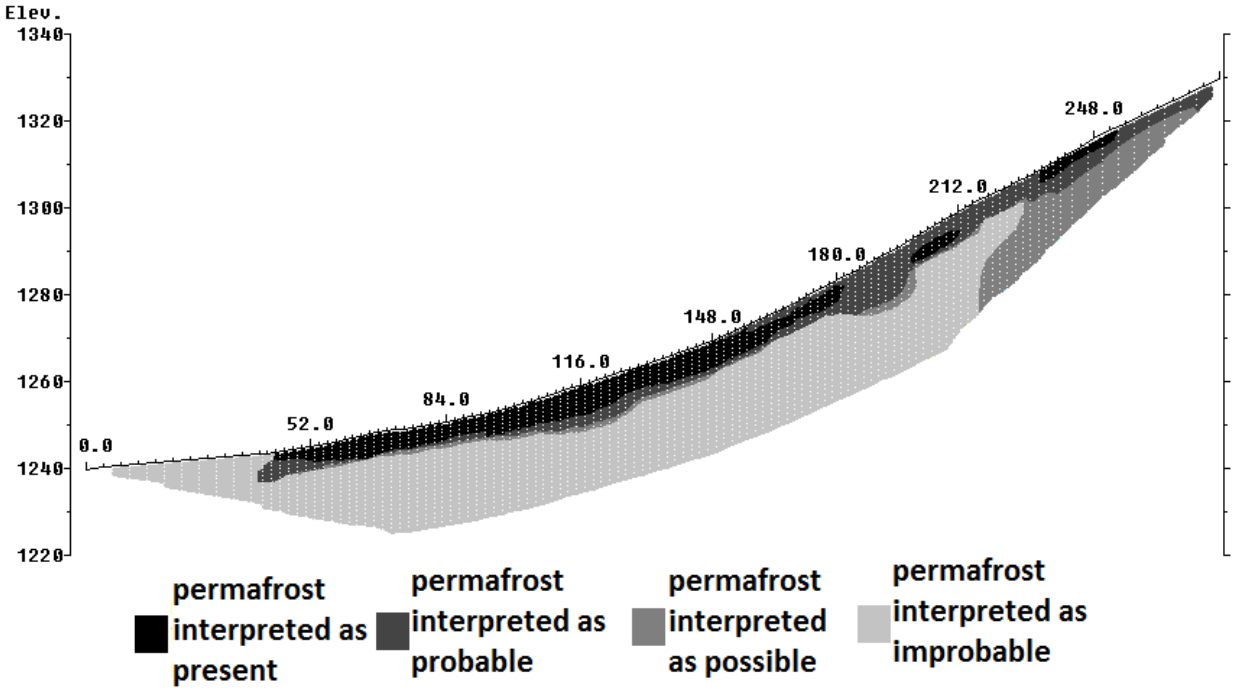

Figure 31: Permafrost interpretation image for Site 2

5.1.3 Site 3

Site 3 is located on a south-facing slope in the Wolf Creek basin (Figure 32). Due to time constraints aerial imagery was not obtained for this site while in the field. The 160 m long profile begins at approximately 1214 m asl and extends upslope to approximately 1250 m asl.

Figure 32: View of Site 3 from satellite imagery.

Vegetation

Vegetation cover at this site varies from shrubs and open mixed forest (Figure 33). Trees include *Pinus banksiana* (jack pine), *Picea* sp., and *Populus tremuloides* (trembling aspen), while shrubs include *Juniper* sp., *Salix* sp. and *Betula nana*. Grasses, mosses and lichens are also present along with plants such as *Epilobium angustifolium*, *Petasites sp.*, *Potentilla sp.*,

Delphinium sp., *Achillea millefolium* (common yarrow), *Senecio* sp. (groundsel), *Empetrum nigrum* (crowberry), and *Arcto staphylos* sp., either *uva-ursi* or *alpina* (kinnikinnick or alpine bearberry). An unvegetated ATV trail, which predates 2000, traverses the profile at 20 m (Figure 33-E). The first *Picea* sp. tree along the profile occurs at 54 m and past 102 m along the profile *Pinus banksiana* begins to occur.

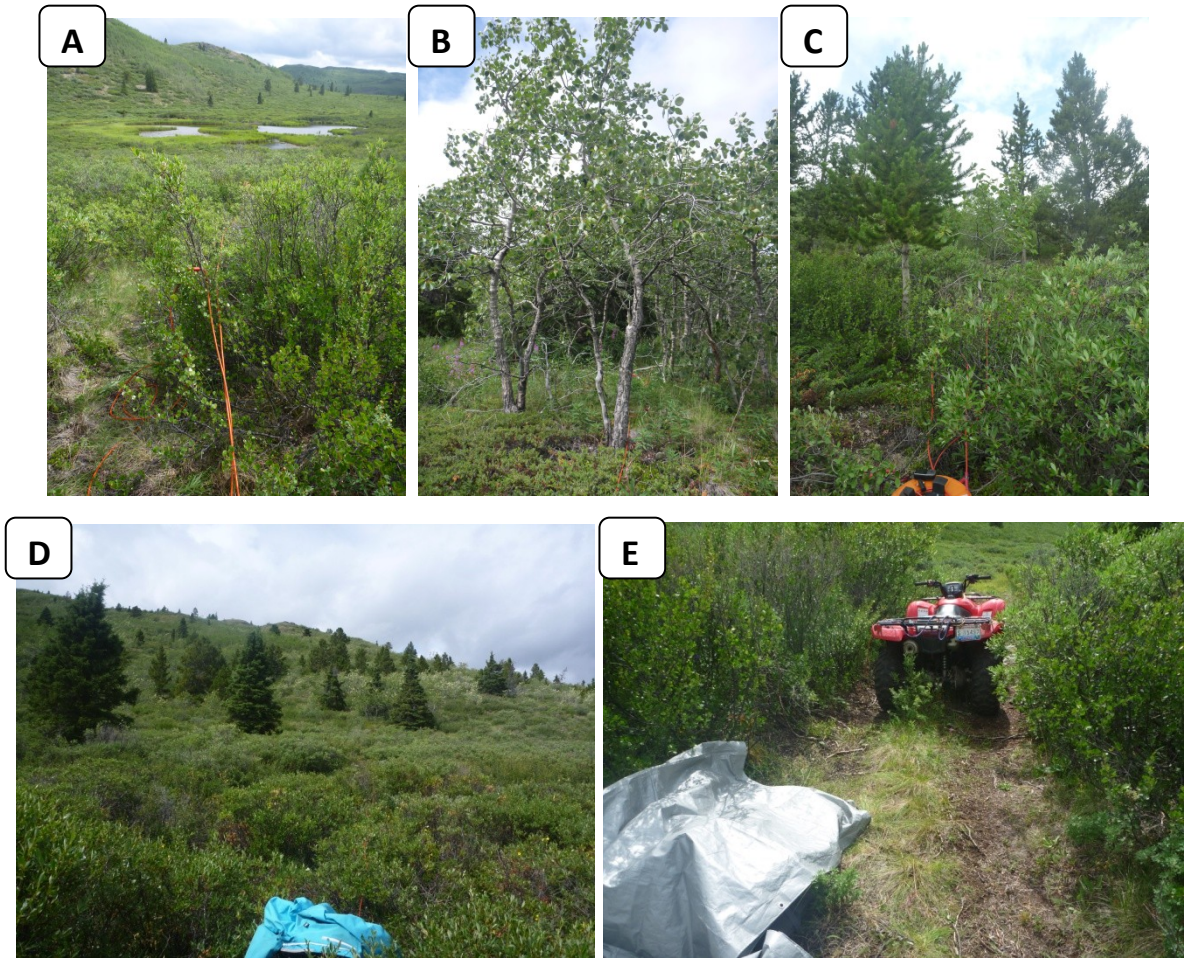

Figure 33: Site 3 photographs

A) Downslope view of *Salix* sp. and *Betula nana*. Water body appears in the distance.
B) Upslope view of *Populus tremuloides*, *Juniper* sp., and *Epilobium angustifolium*.
C) Upslope view of *Pinus banksiana*, *Picea* sp., and *Salix* sp.
D) Upslope view of slope and beginning of trees
E) Unvegetated ATV trail

The vegetation changes around 40 m along the profile (1217 m asl): dense tall shrubs and mosses in the lower part of the slope transition to scattered trees over bare ground, grasses, or very sparse shrubs, 1 to 2 m in height. This transition may correspond to a lower treeline due to cold air drainage, as at Site 2. Alternatively, the change in vegetation may simply result from changes in surficial material or drainage. According to satellite imagery, the lower limit of trees on this slope does not follow a constant elevation. Rather the lower treeline seems modulated by local factors. The proximity to a water body at the base of a slope (Figure 33-A) may be one of these factors.

Climate

Climate data are unavailable for this site but data from nearby climate stations, WC-DR and WC-APM-WS can provide information on conditions for the area. The blended mean annual air temperature (bMAAT) at these stations are within the range from -3°C to -4°C and the blended mean annual ground surface temperatures (bMAGST) are between 1°C and 2°C. On this south-facing slope the mean ground temperature may be greater due to the increased incoming solar radiation. Snow cover at this site is difficult to estimate, but in general, less is expected due to the aspect. The dense shrub area at the base of the slope may have more snow than the steeper part of the slope.

Resistivity and Permafrost

The fifth iteration with a 5.1% RMS error was selected as the modeled resistivity profile (Figure 34).

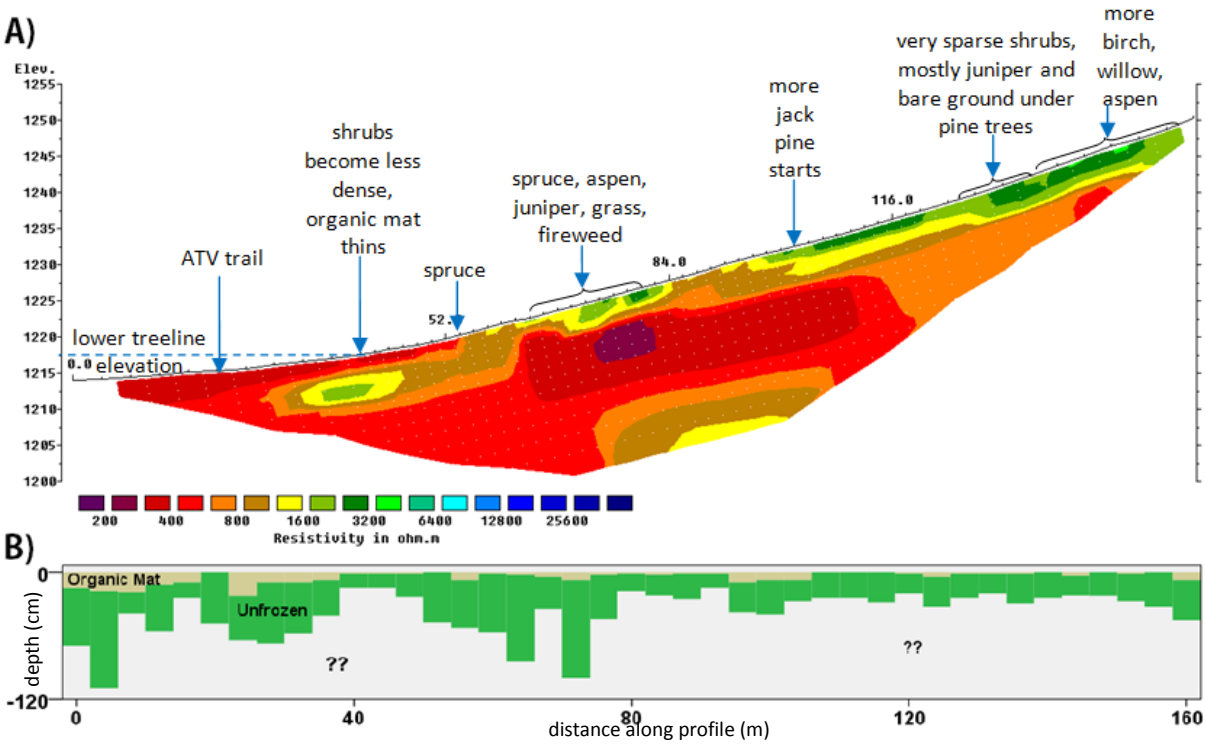

Figure 34: Combined results for Site 3.

(A): Modeled resistivity profile annotated with changes in vegetation.
(B): Frost probe measurements (in cm) including organic mat thickness (in beige) and refusal depth (in green) with instances where refusal was interpreted as frozen ground (in blue).

Modeled resistivity ranges approximately from 0.2 kΩm to 3.2 kΩm. The highest resistivity values occur mainly within the first 5 m of depth forming a near surface low/medium resistivity layer. Down slope from 54 m along the profile, this layer continues beneath low/very low near-surface resistivity values. Some medium resistivity values also occur at depth near the base of the tomogram.

For all probe measurements, refusal is attributed to clasts. The organic mat thickness ranges from 0 cm to 23 cm. Values greater than 10 cm occur only in the first 40 m of the profile in the area of dense shrubs.

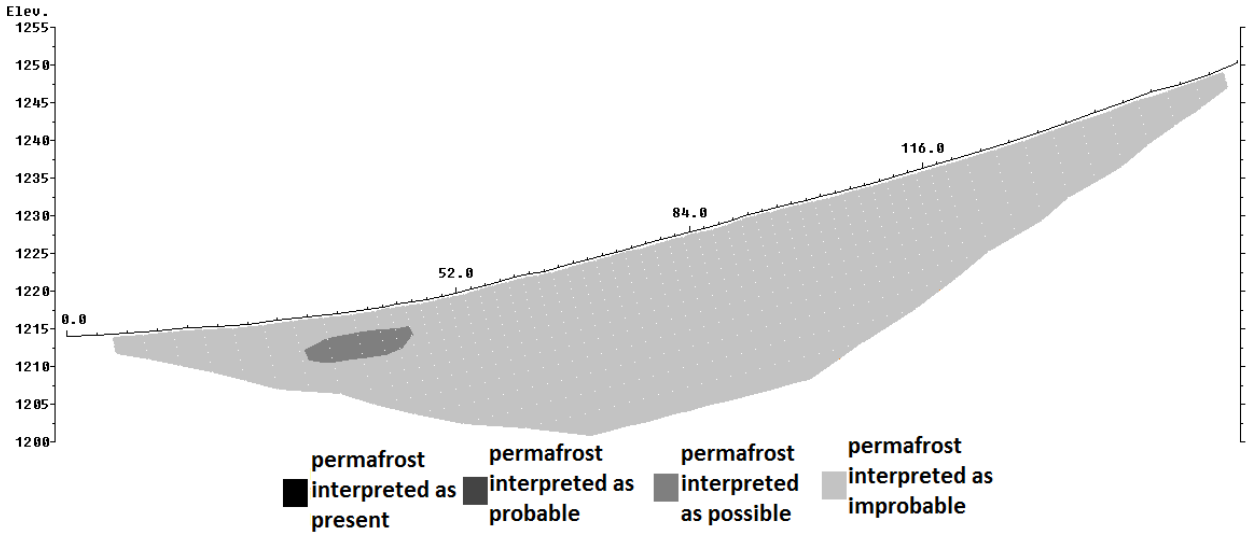

Figure 35: Permafrost interpretation image for Site 3

The resistivity patterns in this site's profile can be interpreted several ways. The transition between the resistivity layers values could be caused by a boundary between frozen and unfrozen ground or it could result from a change in moisture content and grain size. The higher near surface resistivity layer possibly results from drier coarser material on the slope.

Much of the site informations support this second interpretation. Permafrost presence is known to be less probable on south-facing slopes than on north-facing slope in this area (Lewkowicz and Ednie, 2004). The difficulty clasts caused during frost probing highlight the presence of coarse surficial material and the presence of *Pinus banksiana* suggest dry soil. A consideration of all this information leads to the interpretation that permafrost is improbable for most of this site.

Toward the base of the slope, however, different ground conditions may be present and thus permafrost is deemed possible. The organic mat is thicker and shrubs are denser. The higher resistivity layer is deeper and is overlain by low resistivity values.

No ground temperature measurements were taken at this site. Nor were any pits dug. Both may have helped validate this interpretation, but difficulties in equipment logistics prevented such data collection at this site.

5.1.4 Site 4

Site 4 is located near the top and to the east of the Mount Sima trail. The profile at this site is 280 m long (Figure 36). It begins at approximately 1302 m asl and extends down the northeast-facing slope to approximately 1270 m asl.

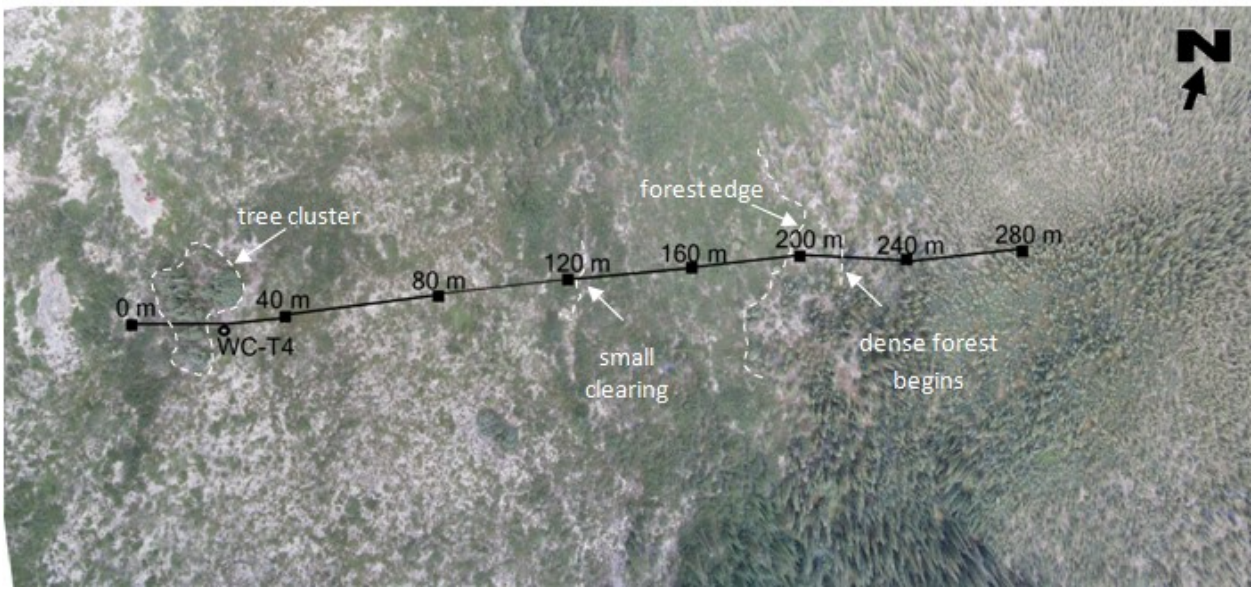

Figure 36: Aerial image mosaic of Site 4, with the profile traced in black and the distance along profile noted every 40 m. Climate station WC-T4 is circled and key vegetation features are indicated in white.

Vegetation

The profile samples a vegetation cover transition around 1275 m asl from shrubs and scattered trees to a coniferous forest (Figure 37-A). A cluster of trees also occurs near the start of the profile (Figure 37-B). Trees along the profile include *Abies lasiocarpa* (subalpine fir). Shrubs are primarily *Betula nana* while the ground cover includes mosses, lichens, *Ledum* sp., *Vaccinium vitis-idaea minus* (mountain cranberry), *Empetrum nigrum*, and *Cornus canadensis* (bunchberry).Organic mat thickness and shrub height and density vary, but generally increase down slope.

Shrubs are generally short and sparse in the first half of the profile but some patches of taller shrubs are present such as around 40 m and 80 m along the profile. These increases in shrub height, like others, generally coincide to increases in slope.

There are two instances where dense shrubs open into small clearings. First, a clearing that resembles a trail is present at 120 m. After this small clearing, dense shrubs, approximately 1.5 m tall, resume along with lichens, mosses, berry-bearing plants and *Abies lasiocarpa* saplings. Older individual *Abies lasiocarpa* also begin to occur along the profile. Second, a clearing with saplings is adjacent to the edge of the forest (Figure 37-C). Trees taller than 2 m begin to occur on both sides of the profile at 208 m, while 216 m marks the start of dense forest.

Figure 37: Site 4 photographs

A) Treeline seen from up slope; B) Cluster of trees near climate station WC-T4; C) Clearing at forest's edge; D) Pit dug in forest.

Conifers, at times quite dense, with a few to no shrubs in the understory, dominate the forest. There are both old and young trees, including fallen trees. At 248 m along the profile the organic mat thickness increases, nearing 30 cm.

Climate

Climate station WC-T4, located 24 m along the profile, has intermittently recorded temperatures since the summer of 2006 (Table 4). The blended mean annual air temperature is -3.3°C while with the blended mean annual ground surface temperature is 1.6°C. The consistently high number of snow depth days (SDD) (Figure 38) is likely responsible for the large surface offset. The climate station is near a cluster of trees that may trap snow so the remainder of the profile may have a lower snow cover than that recorded at WC-T4.

Table 4: Summary statistics for station WC-T4

	WC-T4 (n)
Elevation (m asl)	1290
Blended mean annual air temperature[1] (°C)	-3.3 (59)
Blended mean annual ground surface temperature[1] (°C)	1.5 (87)
Blended temperature at the top of permafrost[1] (°C)	0.9 (56)
2006-15 mean snow depth days[2] (m.days)	132 (9)
2006-15 mean surface offset[2] (°C)	4.7 (3)
2006-15 mean thermal offset[2] (°C)	-0.6 (3)
[1]Blended-year statistic obtained from Bevington's (2016) Database, calculated from data for *n* number of months. [2]Means calculated by averaging the values obtained for *n* number of years during the defined period	

The three annual mean ground temperatures reported (Figure 38) are all greater than 0.2°C, but less than 1°C. Values in this range signify that permafrost is not present at the depth of the sensor, but permafrost may occur at slightly greater depths.

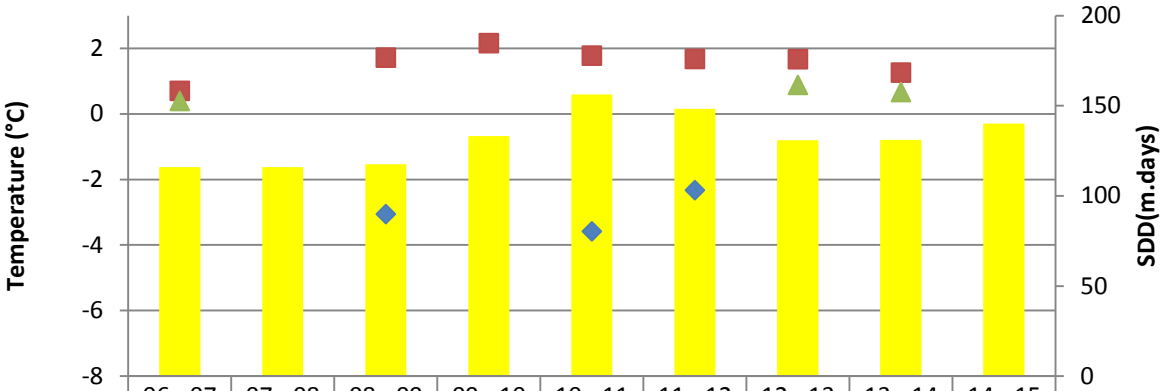

	06 - 07	07 - 08	08 - 09	09 - 10	10 - 11	11 - 12	12 - 13	13 - 14	14 - 15
SDDs	116	116	118	133	156	148	131	131	140
AMAT			-3.1		-3.6	-2.3			
AMGST	0.7		1.7	2.2	1.8	1.7	1.7	1.3	
AMGT	0.4						0.9	0.7	

*SDD-Snow Depth Days, AMAT-Annual Mean Air Temperature, AMGST-Annual Mean Ground Surface Temperature, AMGT- Annual Mean Ground Temperature at the estimated top of permafrost

Figure 38: Climate Station WC-T4 Data (1290 m asl)

Resistivity and Permafrost

The fifth iteration with a 6.3% RMS error was selected as the modeled resistivity profile (Figure 39).

Resistivity values range from very low to very high. A distinct high/very high near-surface resistivity layer is present across the entire profile. In places, however, the high resistivity layer thins and the modeled resistivity values decrease. These sections occur around 20 m, 64 m, 120 m and 175 m along the profile. They sometimes correspond with changes in vegetation.

Below the high resistivity layer, resistivities abruptly transition from greater than 10 kΩm to medium to very low values less than 2 kΩm across only a few meters of depth. In most of the profile, the transition occurs at a depth of 4-5 m, but towards the end of the profile the transition

occurs at greater than 5 m (Figure 40 C). This may be the result of the larger electrode spacing at the end of the profile, or ground resistivity may actually be greater at those depths.

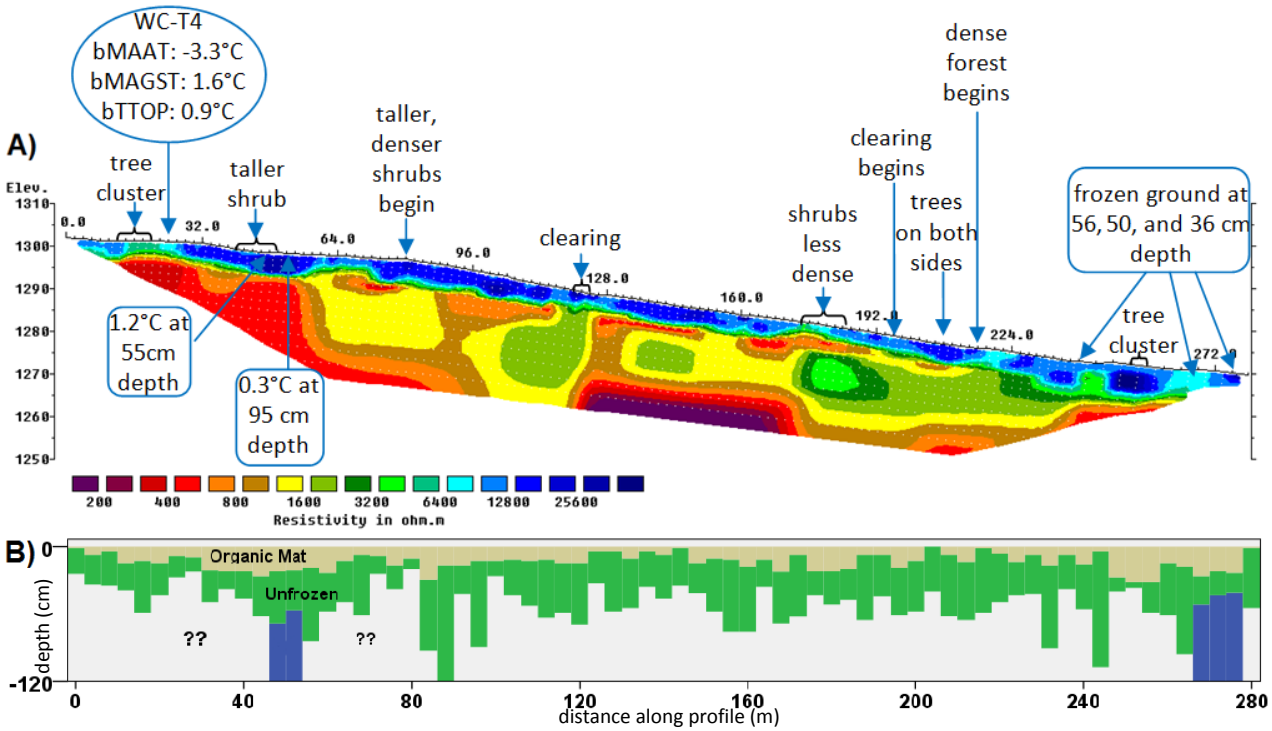

Figure 39: Combined results for Site 4.

(A): Modeled resistivity profile annotated with changes in vegetation and temperature data and live temperature readings on day of the survey.
(B): Frost probe measurements (in cm) including organic mat thickness (in beige) and refusal depth (in green) with instances where refusal is interpreted as frozen ground (in blue).

Within the high to very high resistivity layer, there are at least 16 sections where slightly lower resistivity values are modeled above higher resistivity values. They are quite subtle and several sections are visible only when applying a vertical exaggeration to the tomogram or examining virtual boreholes (Figure 40 C).

These areas are interpreted as unfrozen ground in the active layer overlaying frozen ground. Probing confirmed unfrozen ground to a depth of more than 1.2 m at 88 m along the profile where lower resistivity was modeled above higher resistivity.

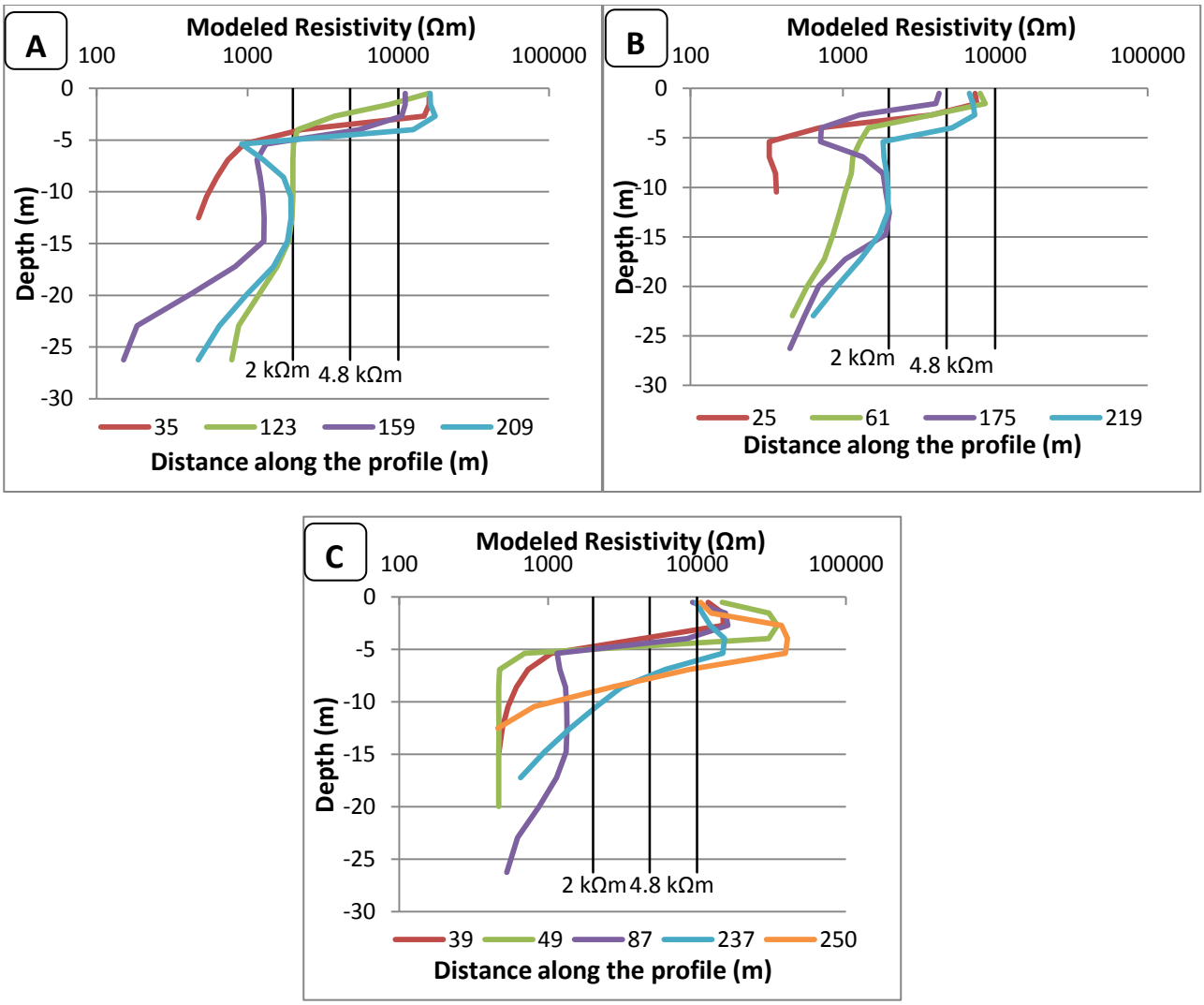

Figure 40: Virtual boreholes for Site 4.

A) Abrupt transitions from over 10kΩm to less than 2 kΩm; B) Values always below 10 kΩm; C) Instances with lower resistivity above higher resistivity in near surface.

Clasts prevented probing to depth greater than 50 cm in many parts of the profile. However, frozen ground was interpreted from probing in a few instances and this was confirmed with a few pits. At 48 m and 52 m along the profile, frozen ground caused probe refusal at 69 cm and 57 cm, respectively. Here permafrost presence is interpreted with confidence. Both the probing data and resistivity profile support the same interpretation: an active layer 0.5 m to 1 m thick over permafrost extending to 5 m depth. From 268 m to 276 m along the profile, frozen

ground caused probe refusal at depths between 40 cm and 52 cm. A pit dug at 276 m along the profile revealed well bonded frozen ground at 36 cm depth. Micro-lenticular cryostructures and ice coating were visible. The shallow depth at which this frozen ground was found relatively late in the thaw season demonstrates the efficacy of a thick organic mat and dense vegetation in shading and insulating the ground. Seasonal frost would be expected to have thawed to a greater depth or entirely by mid-July so the shallow depth suggests that this frozen ground is perennial. Permafrost was also found in a second pit dug at 268 m along the profile. In a third pit, dug at 240 m along the profile, frozen ground at a depth of 56 cm was found to be only 20 cm thick indicating that it was seasonal in nature. This location on the profile shows a much thinner very high resistivity layer than elsewhere.

Two additional pits were dug in the unforested part of the slope and some ground temperatures were measured with a thermistor equipped probe. Frozen ground was not found within the 40 cm deep pit dug 3 m from the climate station, nor was permafrost found 48 m along the profile at 55 cm depth. However, a ground temperature near zero was found at 95 cm depth, 52 m along the profile.

A challenge with the interpretation at site 4 is the possibility that the high to very high resistivity layer results not from permafrost, but rather from the site's surficial geology. The surficial geology mapped for Site 4 includes a soliflucted blanket (>1 m) of rock rubble and reworked glacial deposits (Morison and Klassen 1991) that, in theory, could exhibit high resistivity values. However, the fact that frozen ground was found through probing and in pits, the active layer signal seen with lower resistivity values above higher resistivity values, and the

near zero shallow ground temperatures measured all support the interpretation of permafrost presence.

Taking all the observations into account, a thin body of near-surface permafrost is interpreted as being almost continuously present along profile 4 (Figure 41). Ground where resistivity is modeled below 2 kΩm is interpreted as being unfrozen, so permafrost improbable. Resistivities above 5 kΩm are considered permafrost probable, unless other data, such as probing, suggests otherwise.

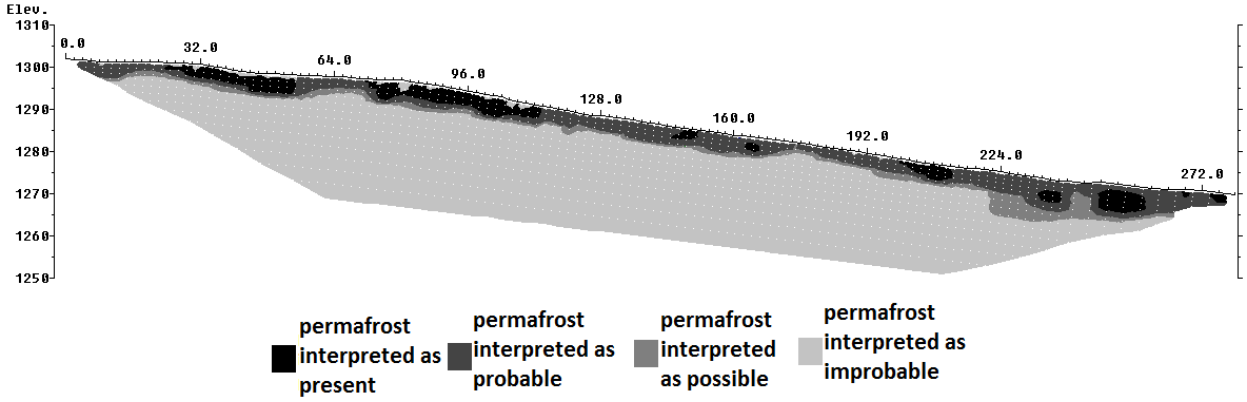

Figure 41: Permafrost interpretation image for Site 4

Though continuous permafrost is deemed possible, permafrost is only interpreted with confidence to be present in some sections. A break in permafrost might be present around 170 m along the profile. Permafrost does not disappear or thin within the forested part of the profile, rather permafrost may even be thicker and colder there than in the unforested parts of the slope.

5.1.5 Site 5

Site 5 is located less than 500 m west of Site 4. The 160 m long profile (Figure 42) begins at approximately 1269 m asl and extends up the northeast-facing slope to approximately 1297 m asl.

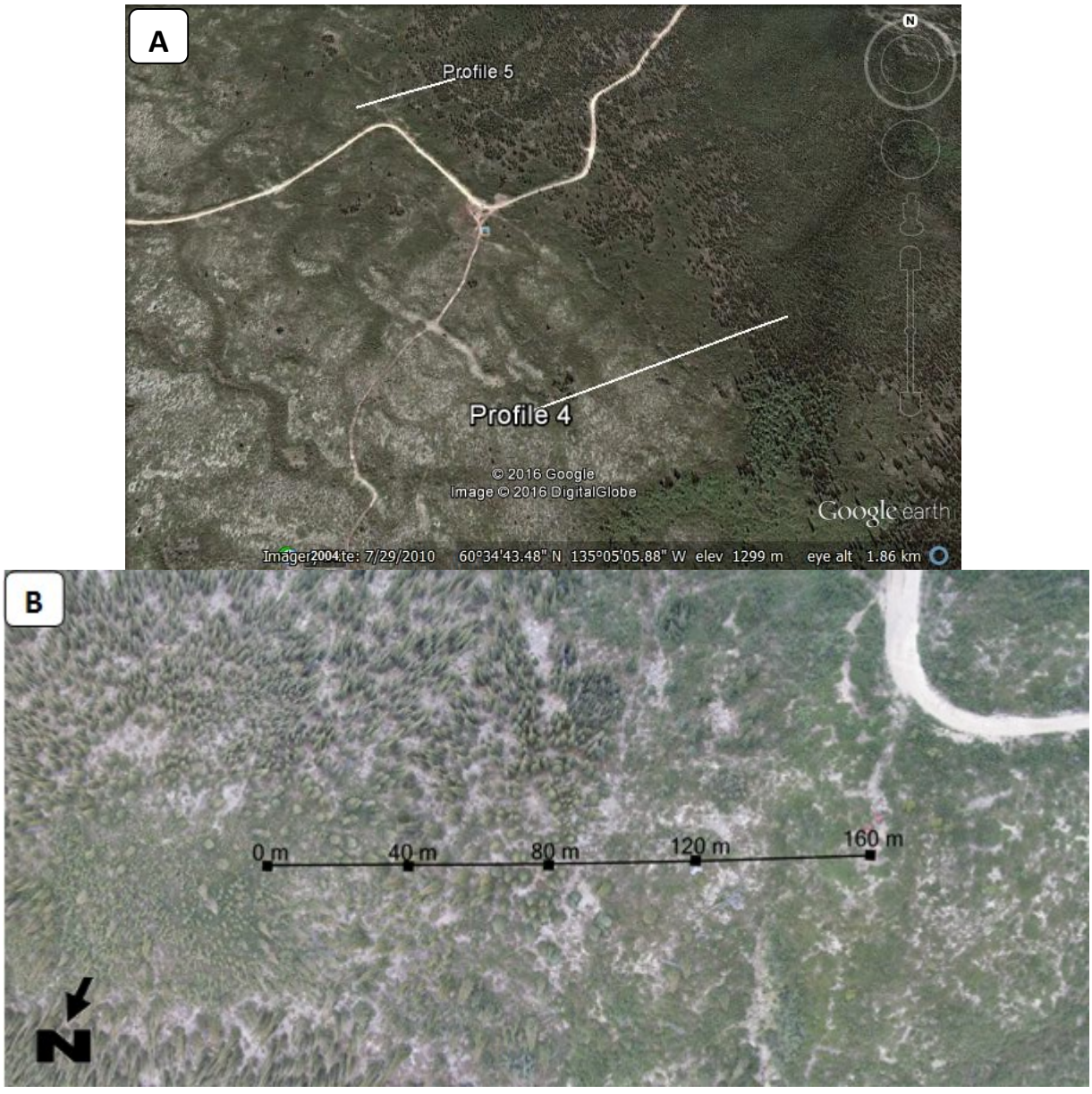

Figure 42: A) Google earth image showing profiles 4 and 5; B) Aerial image mosaic of Site 5, with the profile traced in black and the distance along profile noted every 40 m.

Vegetation

The profile samples the same type of vegetation transition, from shrubs to open forest, as the profile at Site 4 but from low to high instead of high to low. The first 92 m of Site 5's profile are within the open conifer forest. Past that, above 1282 m asl, the vegetation is dominated by shrubs with scattered trees. Site 5 vegetation includes *Abies lasiocarpa* (subalpine fir) trees and saplings, *Betula nana* and *Salix* sp. shrubs, mosses, lichens, and ground cover species such as *Ledum* sp., S*alix mytrillifolia* (blueberry willow), and *Vaccinium vitis-idaea minus*. Some *Pinus banksiana* was also noted at this site. The forested portion of the profile is more open than the forested portion of the profile at Site 4. On average the organic mat is thicker within the open forest than within the shrub-dominated portion of the profile (Figure 43).

Climate

There are no climate stations located at this site. The nearest climate station, WC-T4 is located at Site 4. The mean annual air temperatures at Site 5 can be expected to be similar to the -3.3°C calculated at WC-T4. Snow cover may vary and is presumed to be slightly less than the average SDD of 132 m.days calculated at WC-T4 except in locations likely to trap snow.

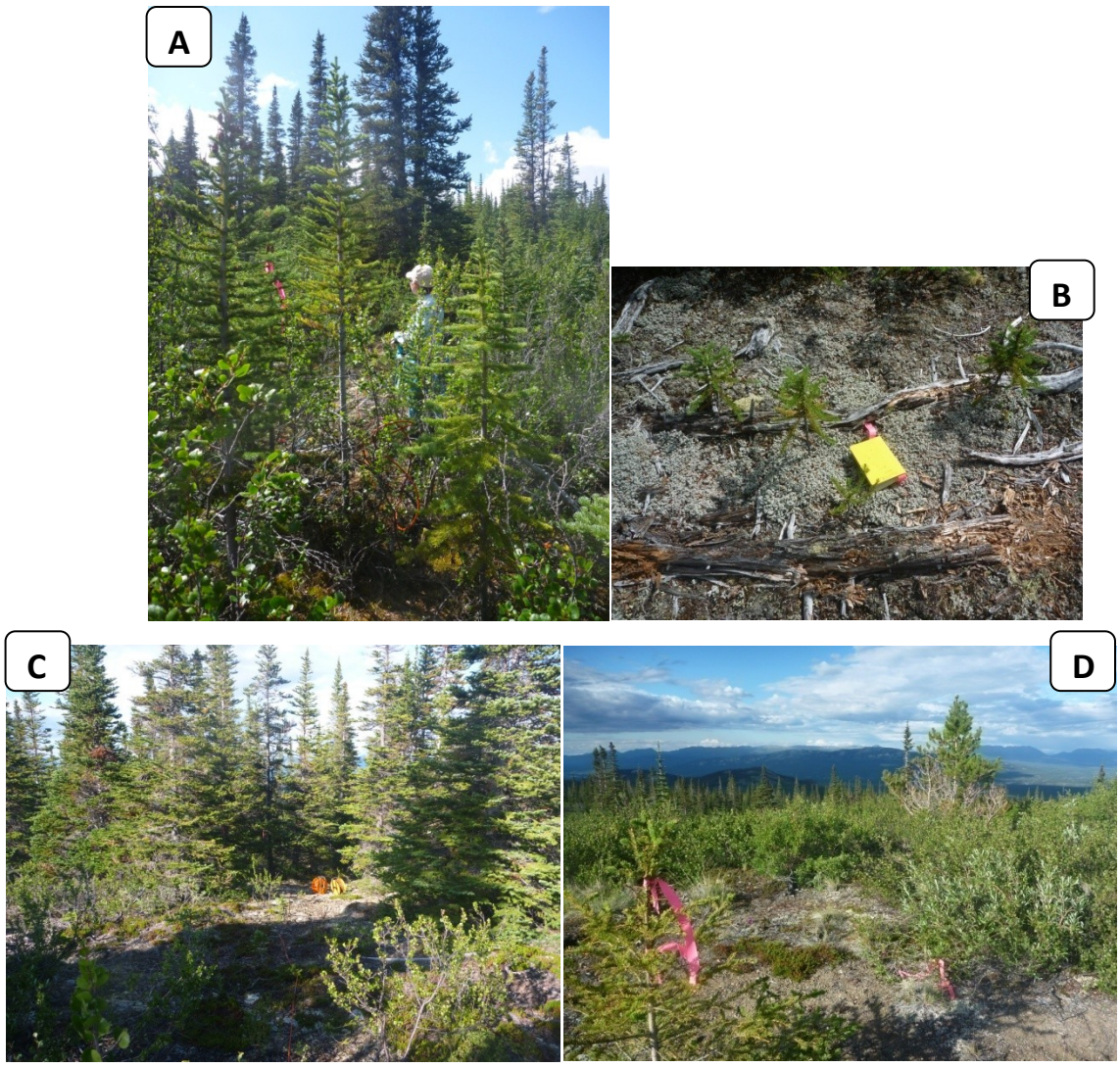

Figure 43: Site 5 photographs

A) Open canopy forest; B) Saplings within the forest; C) Downslope view of transition from sparser trees to forest; D) Down slope view from end of profile, shrubs and sparse trees in the foreground and forest visible in the distance.

Resistivity and Permafrost

The fourth iteration model with a 4.9% RMS error was selected to produce the modeled resistivity profile (Figure 44).

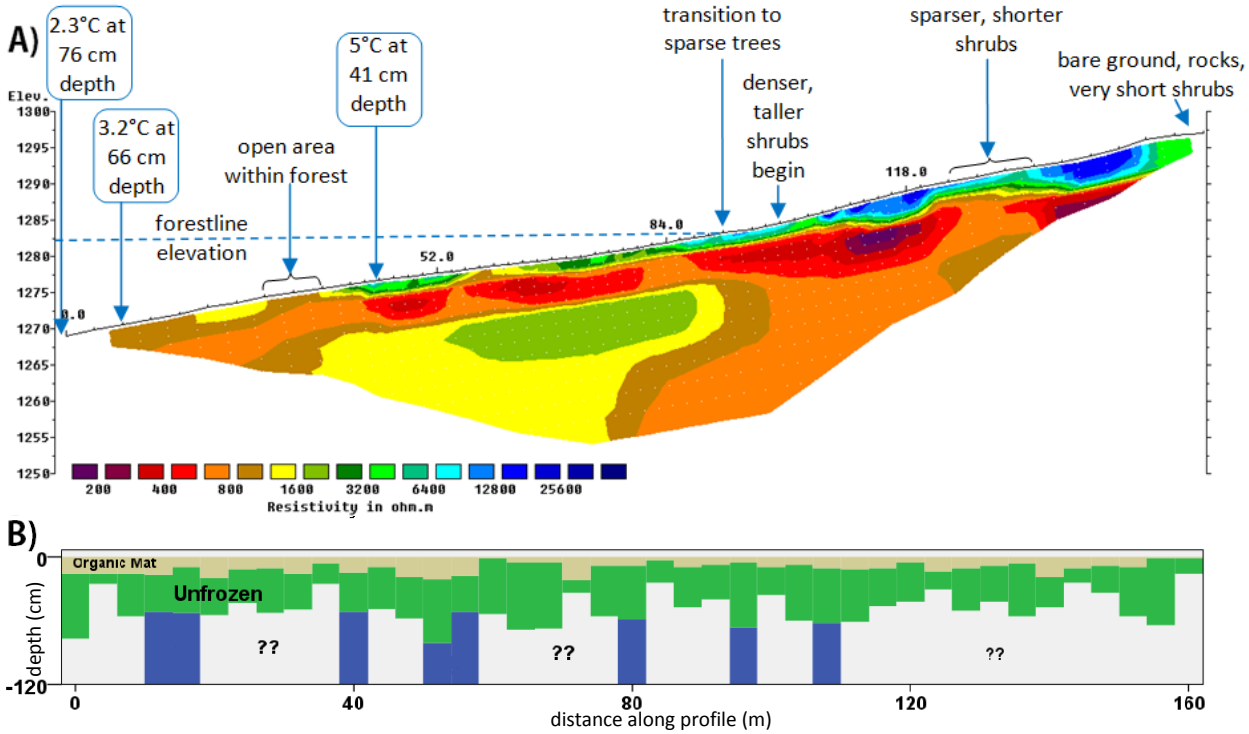

Figure 44: Combined results for Site 5.

(A): Modeled resistivity profile annotated with changes in vegetation and live temperatures readings on day of the survey.
(B): Frost probe measurements (in cm) including organic mat thickness (in beige) and refusal depth (in green) with instances where refusal was interpreted as frozen ground (in blue).

Resistivity values range from very low to very high. The modeled resistivity values greater than 2.4 kΩm are all present in the top few meters, with very high resistivity values occurring up slope in the second half of the profile. The lowest resistivity values occur immediately beneath the highest modeled resistivity values creating very sharp transitions and clear boundaries between areas of modeled resistivity of different orders of magnitude (Figure 45). There are no instances in this profile of near-surface comparatively lower resistivity values being modeled above higher resistivity values, as is the case at Site 4.

Low and medium resistivity values are modeled at depth, with the highest of these in the first 90 m of the profile. There is another sharp transition around 7 m depth (Figure 45).

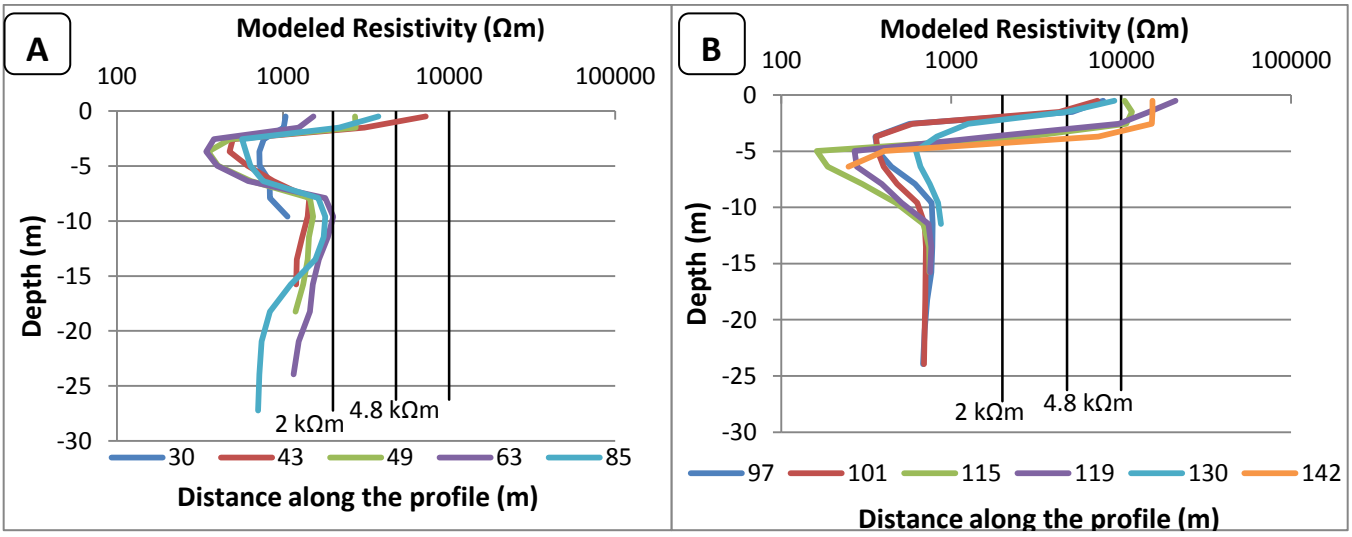

Figure 45: Virtual boreholes for Site 5

A) The forested part of the profile; B) The shrub-dominated part of the profile

Resistivity patterns differ between the forested and the shrub-dominated parts of the profile. In the forested part of the profile, all modeled resistivity values are well below 10 kΩm. There are two sharp transitions: first, a decrease in resistivity around 2 m depth; second, an increase in resistivity from approximately 5 m to 7.5 m depth. In the shrub-dominated portions of the profile, most near-surface values are greater than 4.8 kΩm, some exceed 10 kΩm and the sharp decrease in resistivity occurs either around 2 m or 4 m depth. The increase in resistivity at depth is not as great as in the forested part of the profile.

Probing did not provide reliable information regarding permafrost at this site. Probe refusal was interpreted to be caused by frozen ground in 11 instances, but two attempts to verify this interpretation gave temperature values that suggest its absence.

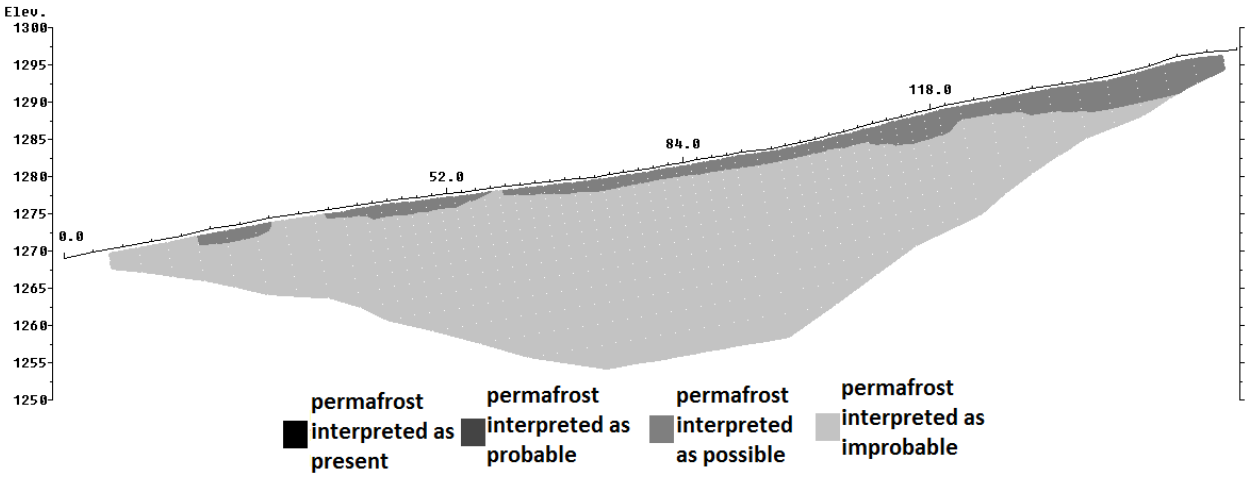

Figure 46: Permafrost interpretation image for Site 5

Considering all this information, permafrost is interpreted to be possible in parts of the near-surface and improbable throughout most of remainder of the profile (Figure 46). If probing had provided more reliable information or if negative ground temperatures had confirmed the presence of frozen ground, permafrost might have been interpreted as present or probable in some areas. Nonetheless, the sharp transition in the near-surface from medium and high resistivity values (> 2.4 kΩm) to lower values may result from a boundary between frozen and unfrozen ground. Alternatively, the transition could reflect a change in the earth's moisture content and grain size. Probing results do not provide compelling evidence for one interpretation or the other because of the unreliable probe refusal interpretations and the fact that shallow probing depths could result from either clasts or near surface permafrost. Thus, this transition supports the interpretation that permafrost is possible in parts of the near-surface, but without additional supporting evidence it cannot be said to be probable. The predominantly low resistivity values at depth suggest permafrost to be improbable.

5.1.6 Comparison of Sites 4 and 5

Even though Sites 4 and 5 are located on the same hillslope and have the same aspect, their profiles provide quite different results. Permafrost is improbable in most of the forest at Site 5, unlike at Site 4. The forest at Site 5 was quite open, with many saplings and the organic mats were not as thick as those recorded at Site 4. The surficial geology is also different between the sites even though they are on the same slope. The surficial geology at Site 5 consists of a veneer (< 1 m) of till, channeled post-deposition, while the surficial geology at Site 4 includes a soliflucted blanket (>1 m) of rock rubble and reworked glacial deposits (Morison and Klassen 1991). Not only do the different surficial materials have different resistivities, they also likely have different thermal conductivities that can impact the probability of permafrost presence. The thermal conductivity is related to the moisture/ice content. The climate data for WC-T4 indicates a MAGST greater than 0°C. Therefore a significant thermal offset is required for permafrost to be present. Higher moisture contents would favour a greater thermal offset, while at Site 5, better drained ground could cause permafrost to be absent. This could be one of the reasons why the tomograms are so different.

5.1.7 Site 6

Site 6 is located on Mt McIntyre's northeast-facing slope. The profile (Figure 47) begins around 1569 m asl and extends downslope to about 1554 m asl. The slope steepness varies forming a series of down-slope steps of varying sizes. These may reflect Mt McIntyre's solifluction landforms, bedrock structure, or glacial history.

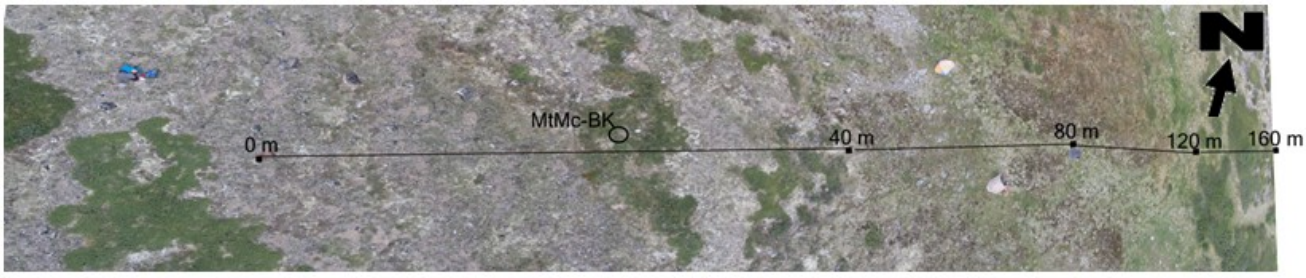

Figure 47: Aerial image mosaic of Site 6, with the profile traced in black and the distance along profile noted every 40 m. Climate station MtMC-BK is circled.

Vegetation

The treeless vegetation cover varies. Some rocky areas are covered mainly by lichens and mosses, while other areas exhibit more grass and *Cassiope* sp. Short dense *Betula nana* and *Salix* sp. shrubs dominate some areas between 20 m and 40 m. Taller shrubs, greater than 1 m in height, begin to appear after 108 m.

Organic mat thickness generally varies according to the type of vegetation cover. The mat is minimal to non-existent in the shrubless area at the beginning of the profile. It increases in thickness down slope, but rarely surpasses 20 cm.

Climate

Site 6 is located near two climate stations. Station MtMC-BK is located 19 m along the profile less than 2 m from the survey line. Station MtMC is further away on Mt McIntyre's crest. The low mean annual air and ground temperatures reported (Table 5) reflect the high elevations of these stations.

Table 5: Summary statistics for stations MtMC-BK and MtMC

	MtMC-BK (n)	MtMC (n)
Elevation (m asl)	1565	1567
Blended mean annual air temperature[1] (°C)	-3.6 (69)	-3.5 (69)
Blended mean annual ground surface temperature[1] (°C)	-1.1 (69)	-2.2 (81)
Blended temperature at the top of permafrost[1] (°C)	-1.4 (29)	-1.7 (56)[3]
2009-15 mean snow depth days[2] (m.days)	111 (6)	17 (5)
2009-14 mean surface offset[2] (°C)	2.7 (4)	1.3 (5)
2009-14 mean thermal offset[2] (°C)	-0.1 (1)	0.5 (4)[3]

[1]B-blended-year statistic obtained from Bevington's (2016) Database, calculated from data for *n* number of months.
[2]Means calculated by averaging the values obtained for *n* number of years during the defined period
[3]Deeper measurements taken at 4 m depth, top of permafrost at MtMC around 6 m depth.

The two stations have very different snow covers. On the windswept crest, very little snow accumulates while, just below the crest, more than 100 m.days of snow cover occurs on average (Table 5). This increases the surface offset and the mean annual ground surface temperature at station MtMC-BK.

Station MtMC-BK has only been operating since 2009, and has not consistently recorded data for all variables. Snow depth days were calculable for each year and ranged from 66 m.days to 157 m.days. AMAT and AMGST, however, were only calculable from 2010 to 2013, and AMGT was only calculable for 2013 (Figure 48). AMAT ranged from -5.1°C to -3.7°C. AMGST ranged from -2.2°C to -0.8°C.

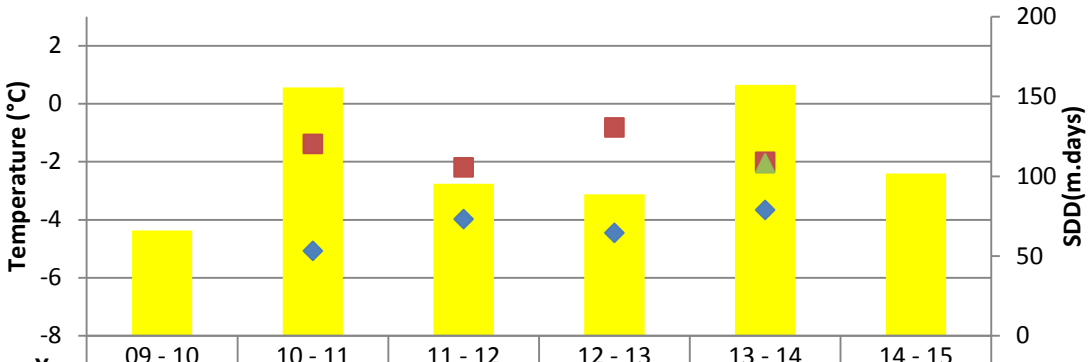

Year	09 - 10	10 - 11	11 - 12	12 - 13	13 - 14	14 - 15
SDDs	66	156	95	89	157	102
AMAT		-5.1	-4.0	-4.5	-3.7	
AMGST		-1.4	-2.2	-0.8	-2.0	
AMGT					-2.1	

*SDD-Snow Depth Days, AMAT-Annual Mean Air Temperature, AMGST-Annual Mean Ground Surface Temperature, AMGT-Annual Mean Ground Temperature at the estimated top of permafrost

Figure 48: Climate Station MtMC-BK Data (1565 m asl)

Station MtMC has been operating since 2008. All annual variables are calculable from 2009 to 2013, except for AMGT, which was could not be calculated for 2013-14 (Figure 49). The SDD at this station range from 2 m.days to 28 m.days. The AMAT ranges from -4.9°C to -2.5°C. The AMGST ranges from -3.1°C to -0.7°C.

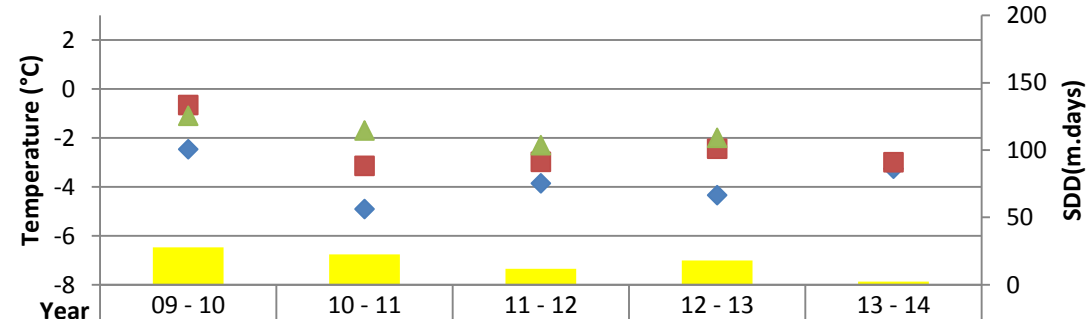

Year	09 - 10	10 - 11	11 - 12	12 - 13	13 - 14
SDDs	28	23	12	18	2
AMAT	-2.5	-4.9	-3.9	-4.3	-3.3
AMGST	-0.7	-3.1	-3.0	-2.4	-3.0
AMGT	-1.1	-1.7	-2.3	-2.0	

*SDD-Snow Depth Days, AMAT-Annual Mean Air Temperature, AMGST-Annual Mean Ground Surface Temperature, AMGT-Annual Mean Ground Temperature at 4 m depth

Figure 49: Climate Station MtMC Data (1567 m asl)

Overall, the consistently negative AMGT and AMGST values confirm permafrost presence at these stations. In addition, a borehole at the MtMC station, clearly indicates deep permafrost with an active layer that was 6.4 m deep in 2009-10 (Lewkowicz et al. 2011). The borehole data show that permafrost extends to depths greater than 29 m since temperatures at that depth remained around -1.7°C between 2011 and 2015 (Figure 50).

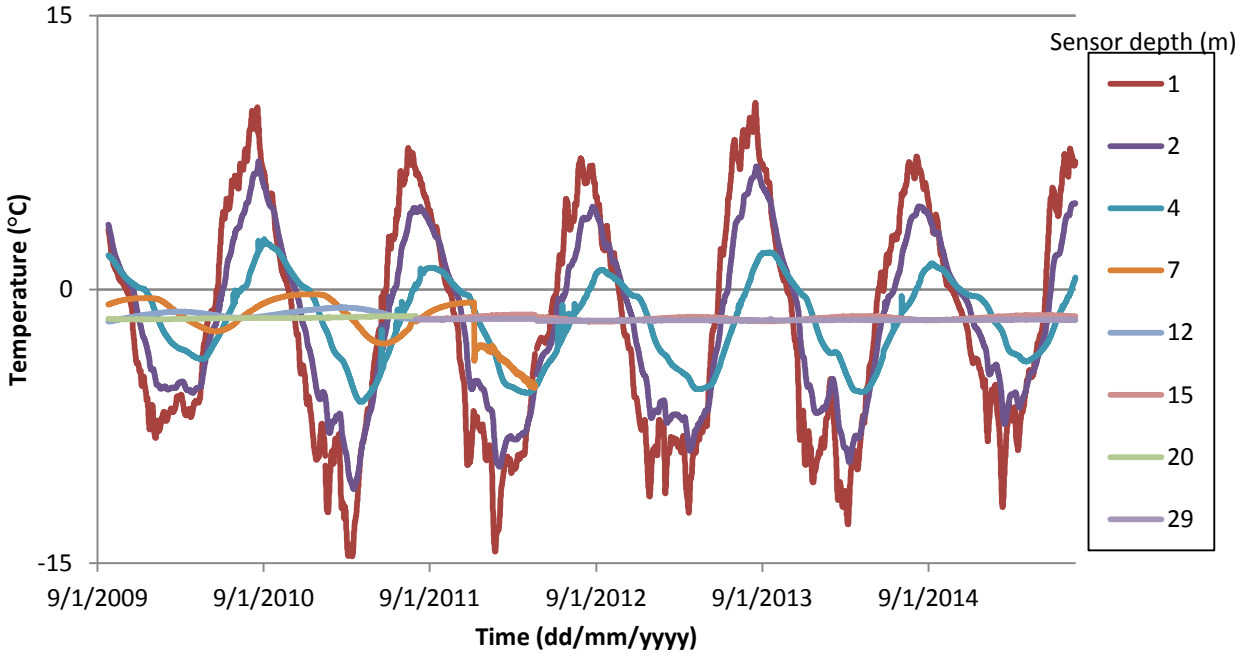

Figure 50: Temperature data from MtMC station borehole. The thermistor cable was changed in 2011 alterning the depth of the lowest thermistors.

Resistivity and Permafrost

The third iteration model with a 4.8% RMS error was selected to produce the modeled resistivity profile (Figure 51).

Medium resistivity values are modeled for most of the tomogram, although low, high and very high values are also present. Some high resistivity values are modeled in first 5 m of depth

near the climate station and to about 10 m depth in the last part of the profile. An area of low resistivity occurs beneath higher resistivity in the first part of the tomogram. This area nears the surface and, in the tomogram's second half, low resistivity values are modeled just below the surface.

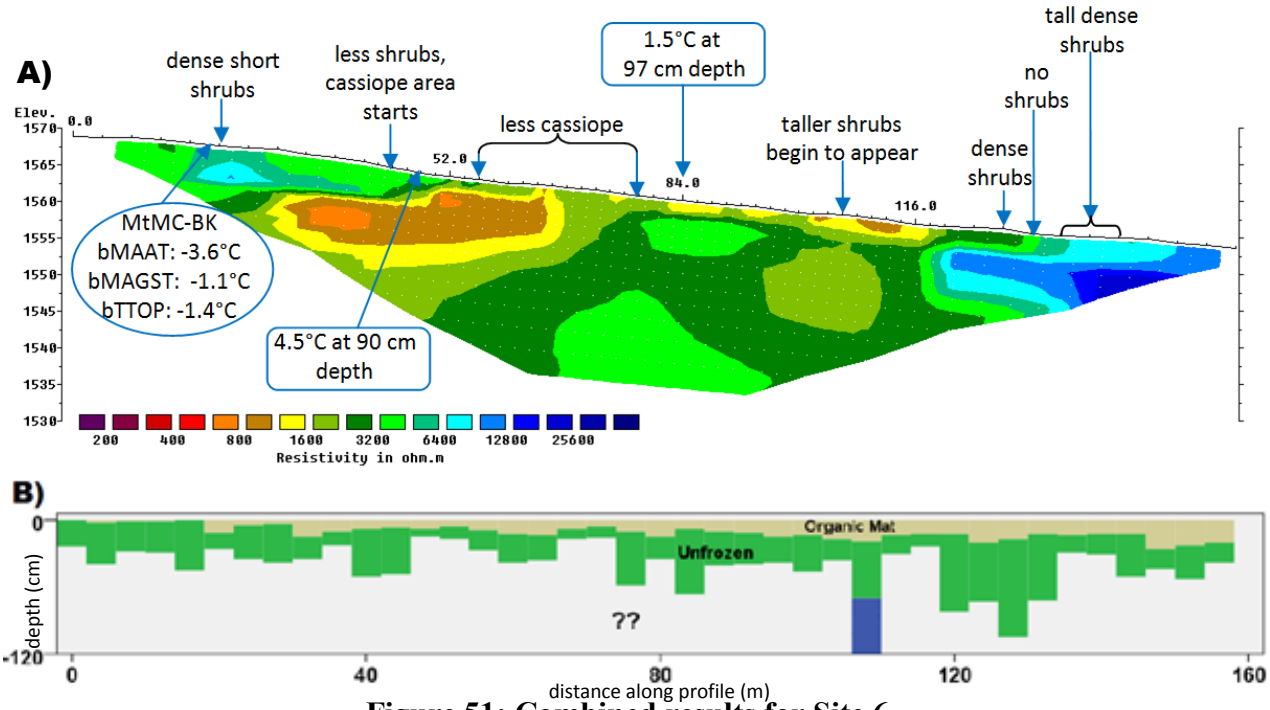

Figure 51: Combined results for Site 6

(A): Modeled resistivity profile annotated with changes in vegetation and live temperature readings on day of the survey.
(B): Frost probe measurements (in cm) including organic mat thickness (in beige) and refusal depth (in green) with instances where refusal was interpreted as frozen ground (in blue).

During probing, clasts were encountered at shallow depths, mainly less than 50 cm (Figure 51-B). Frozen ground was thought to be encountered only twice at 84 m and 108 m along the profile. At 84 m, a pit dug revealed there was no frozen ground present in the top 97 cm but the temperature of 1.5°C at the base of the pit means that it could have been present at greater depth (Figure 51). The tomogram suggests that the frozen ground at 108 m may be a false

positive since the profile is very similar to that at 84 m where frozen ground was not found at such a shallow depth. A second pit dug up slope at 48 m exposed large rocks, cobbles, and gravel, and also revealed positive ground temperatures (Figure 51).

Permafrost is only interpreted present in a small area near the beginning of the profile where negative mean ground temperatures were recorded (Figure 52). The lack of actual ground temperatures in the last forty meters of the profile and the existence of a block stream downslope whose blocky material could have a buried extension prevent permafrost presence from being interpreted with confidence in that area even though very high resistivity values that are modeled. Permafrost is deemed probable there, as in most of the profile. The only areas where permafrost is interpreted improbable (light grey in Figure 52) are where resistivity is modeled less than 1.6 kΩm. These areas may correspond to a closed talik and areas of the active layer. Alternatively, if the area where permafrost is interpreted possible is in reality unfrozen, then an open talik may be present.

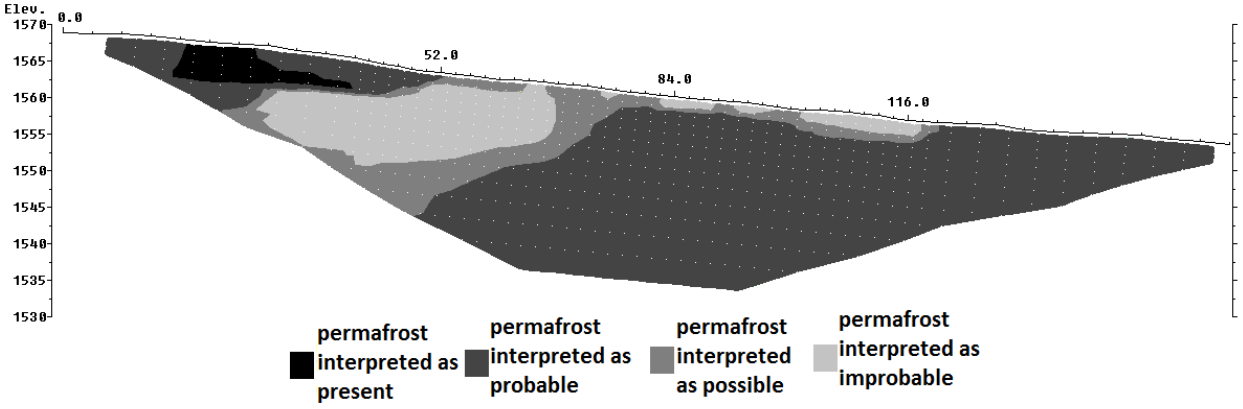

Figure 52: Permafrost interpretation image for Site 6

5.1.8 Site 7

Site 7 is located down slope from Site 6 and exhibits similar slope gradient changes across steps. The profile (Figure 53) begins around 1547 m asl and extends to about 1519 m asl.

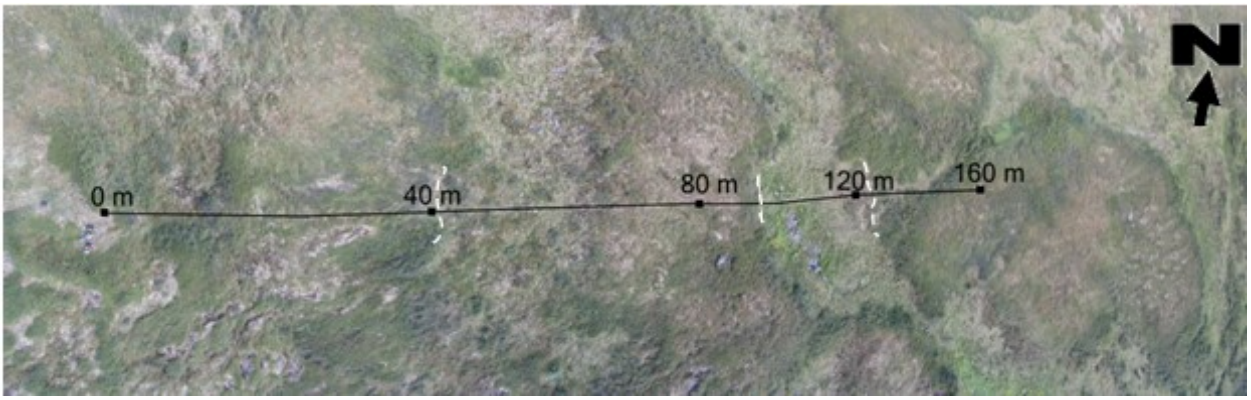

Figure 53: Aerial image mosaic of Site 7, with the profile traced in black and the distance along profile noted every 40 m. The edge of three steps formed by changes in slope gradient are marked by white dashed lines.

Vegetation

Shrub and grass vegetation covers dominate at this site. No major altitudinal vegetation transition is crossed since this is the second of three profiles in a transect down Mt McIntyre. Shrubs at this site include *Salix* sp. and *Betula nana*. Ground cover includes grasses, lichens, mosses, and berry-bearing plants. *Petasites* sp., *Lycopodium* sp. (clubmoss), *Cassiope* sp., *Epilobium anagallidifolium* (alpine willowherb), *Delphinium* sp., *Ledum* sp. and a few other species also occur along the profile. Sometimes large rocks are present.

Shrub height and density vary. Initially, shrubs are mostly short and dense with some sections of taller shrubs occurring. Shrubs are mostly absent from 96 m until 124 m. Then, shrubs of varying height dominate the remainder of the profile. There, a few *Abies lasiocarpa*, 1 m to 3 m tall, also begin to appear near the profile.

Climate

No climate stations occur along the profile. The nearest climate station is MtMC-BK. Based on that station's data and the standard environmental lapse rate, the mean annual air temperature is estimated around-3.5°C at Site 7.

Resistivity and Permafrost

The fourth iteration model with a 4.0% RMS error was selected as the modeled resistivity profile (Figure 54).

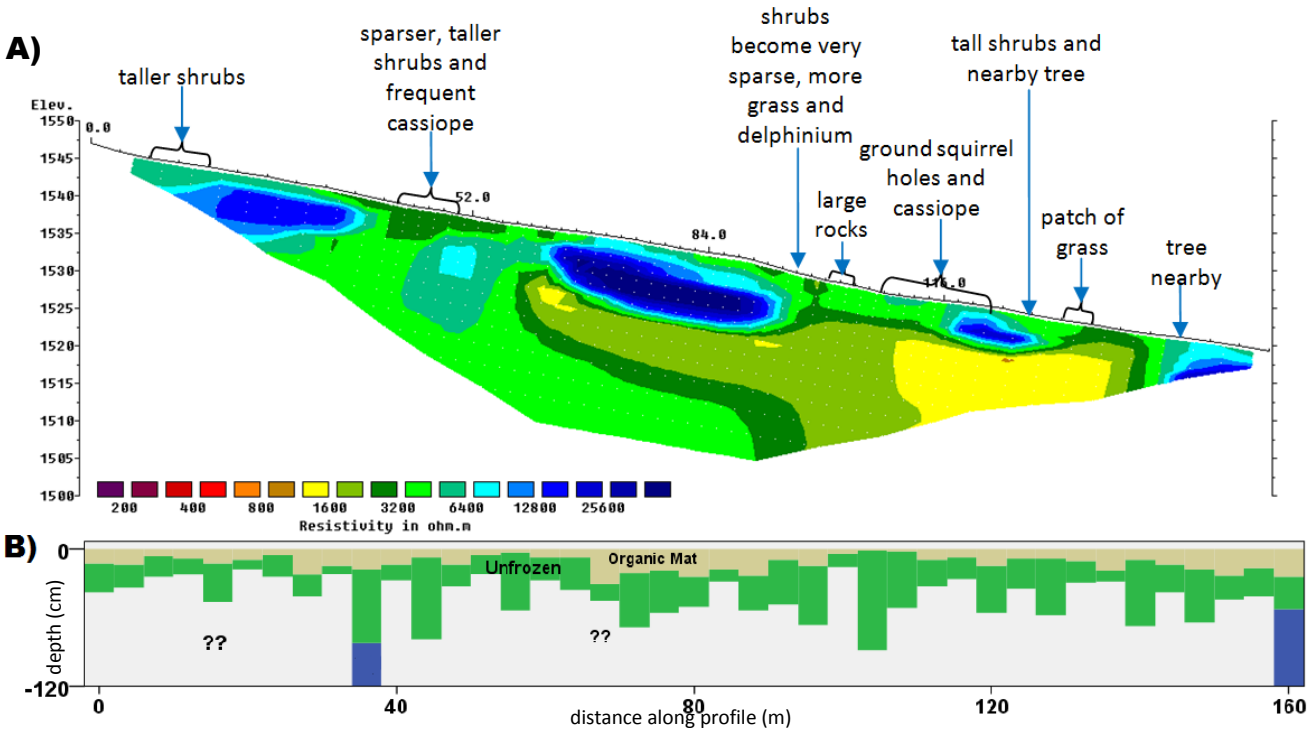

Figure 54: Combined results for Site 7

(A): Modeled resistivity profile annotated with changes in vegetation.
(B): Frost probe measurements (in cm) including organic mat thickness (in beige) and refusal depth (in green) with instances where refusal was interpreted as frozen ground (in blue).

Medium to very high resistivity values are modeled forming different areas. Four high/very high resistivity areas of different sizes are distinguishable. All occur within the upper

10 m. A single large area of values less than 2.4 kΩm also occurs beneath the two middle high resistivity areas.

Along the profile many prominent transitions between higher and lower resistivity values are visible. Several transitions occur at depth of 2 to 3 m with medium resistivity values near the surface and high resistivity values beneath. Other transitions occur at 5 m to 8 m depth with medium or low resistivity values at depth.

During probing, clasts were encountered at less than 50 cm depth in most cases. Frozen ground was thought to have been detected at two points along the profile (Figure 54-B).

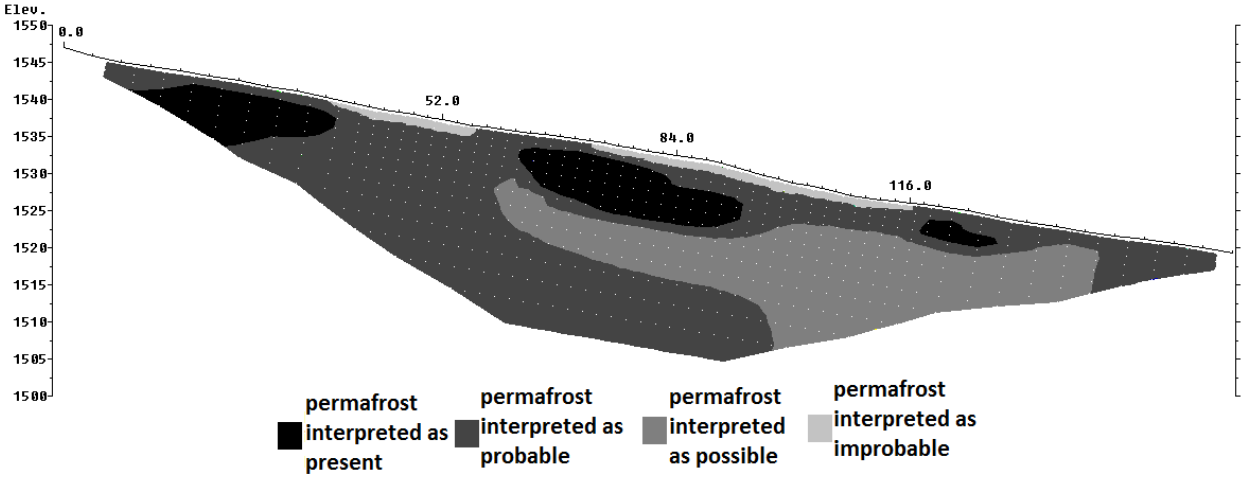

Figure 55: Permafrost interpretation image for Site 7

Permafrost is interpreted to be present in the near surface in parts of this site and probable for much of the remainder (Figure 55). However it is not certain that the permafrost is continuous. There is a surface layer of lower resistivities where the active layer is at least 0.5 m or 1 m depth and permafrost is improbable. A large area of resistivity values less than 2.4 kΩm represents possible permafrost with the alternative being a talik. Permafrost is interpreted as being present in the few separate areas that correspond to the high/very high resistivity areas.

Since permafrost is still deemed probable in many of the adjacent areas, these very high resistivity areas likely represent areas of higher ice content or lower temperatures causing lower unfrozen moisture contents.

5.1.9 Site 8

The third profile in the Mt McIntyre transect starts 1415 m asl and extends to 1385 m asl. The profile samples the downslope transition, around 1400 m asl, from tall dense shrubs to dense forest (Figure 56). No climate stations are present at this site. The mean annual air temperature is estimated to be in the range of -2.5°C to -3°C, by applying the environmental lapse rate to MtMC-BK's data. Unfortunately, the tomogram obtained at this site was too flawed to be analysed. A large number of measurements had to be eliminated during the modeling due to poor contact with the ground, which prevented the creation of a resistivity model with a reasonable RMS error. Probing results were inconclusive regarding permafrost presence since clasts limited probing depth (Figure 57).

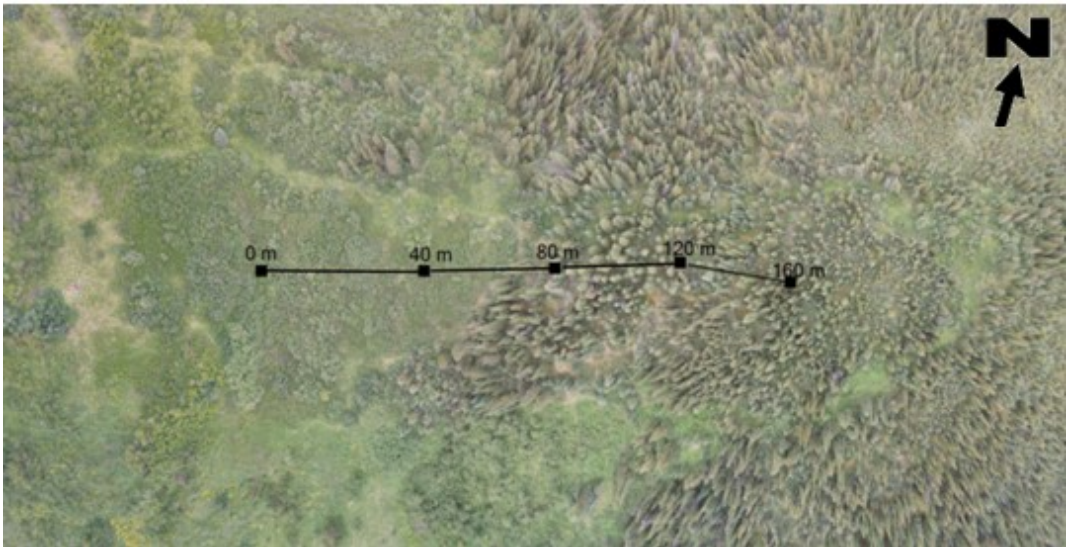

Figure 56: Aerial image mosaic of Site 8, with the profile traced in black and the distance along profile noted every 40 m.

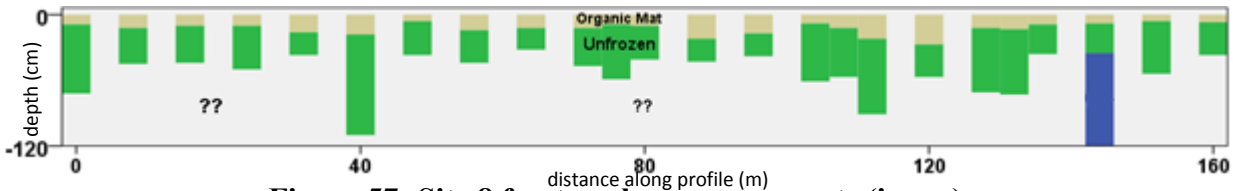

Figure 57: Site 8 frost probe measurements (in cm) including organic mat thickness (in beige) and refusal depth (in green) with instances where refusal was interpreted as frozen ground (in blue).

5.2 Dawson study area sites

Four ERT sites were surveyed in the Dawson study area (Figure 58). Two of these sites (Sites 9 and 10) are located at elevations above 1000 m asl and sample a vegetation cover transition from forest to shrubs. The other two sites (Sites 11 and 12) are located at lower elevations, near and below 500 m asl. They sample slopes descending into a valley with stunted *Picea mariana*.

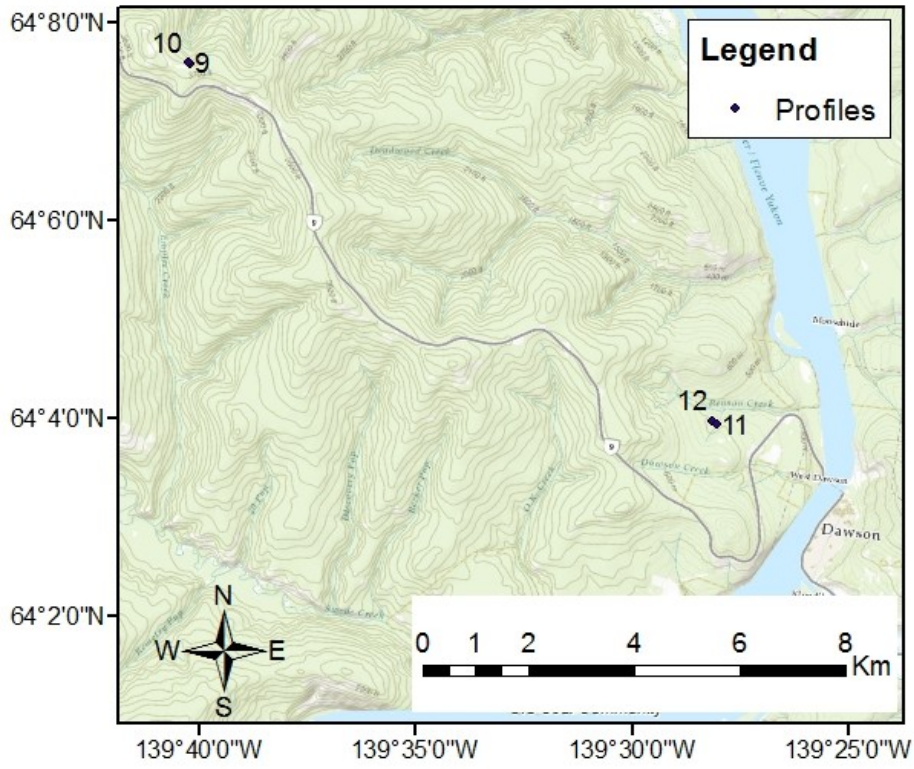

Figure 58: Map showing the location of the ERT profiles 9 - 12 in the Dawson area

The Dawson sites sample areas of extensive discontinuous permafrost (Figure 59). Profiles 9 and 10 are near a small area close to treeline modeled as sporadic discontinuous permafrost.

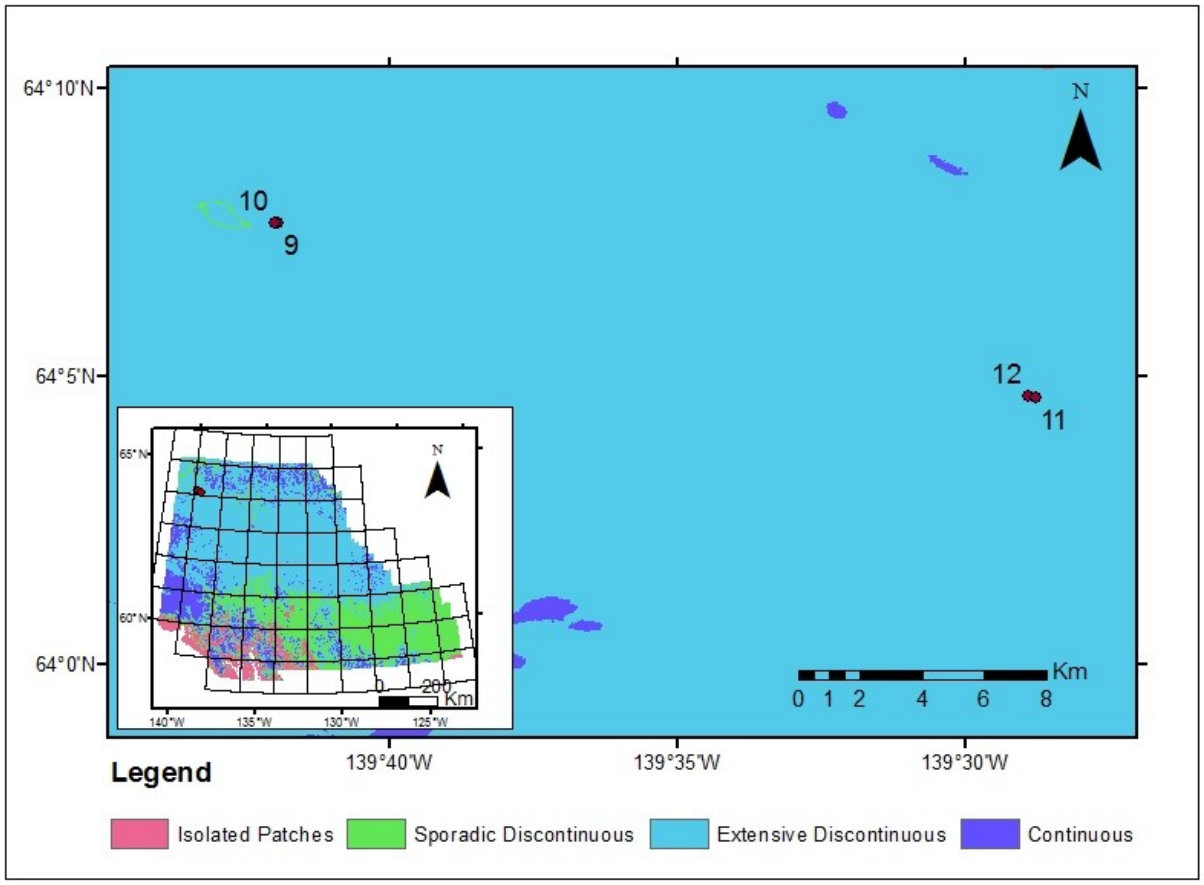

Figure 59: Dawson area sites in relation to the *Yukon Permafrost Probability Map* (Bonnaventure et al. 2012)

5.2.1 Site 9

Site 9 is located on a north-facing slope near a gravel road running parallel to the Top of the World Highway. The profile begins 1134 m asl and extends down the slope to 1088 m asl.

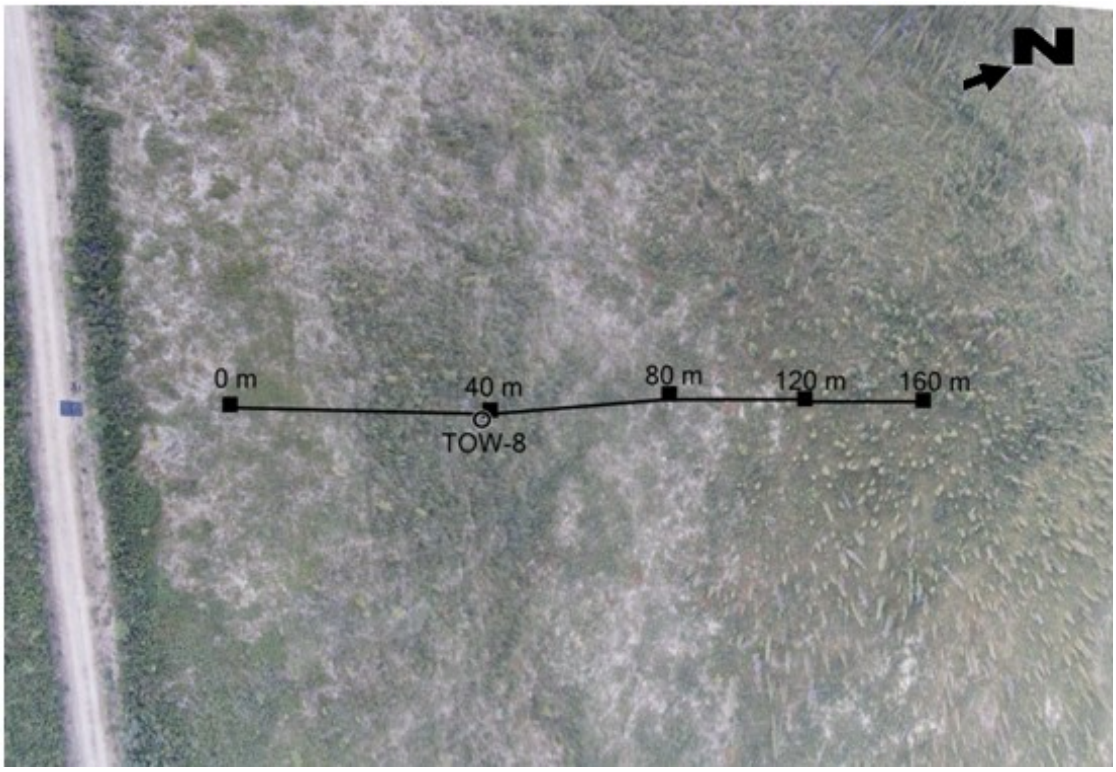

Figure 60: Aerial image mosaic of Site 9, with the profile traced in black and the distance along profile noted every 40 m. Climate station TOW-8 is circled.

Vegetation

The profile remains below the altitudinal treeline for the area (1300 m asl), but it samples a vegetation cover transition, at roughly 1100 m asl, from an area of shrub patches and sparse conifer trees to an open mixed forest downslope (Figure 60). Shrubs along the profile include *Salix* sp. and *Betula nana*. Shrub height varies but overall seems to increase downslope. Trees include *Picea* sp. and *Alnus* sp. (alder) while ground cover includes lichens, grasses, *Cassiope* sp., *Ledum* sp., *Equisetum* sp. (horsetail), *Sphagnum* sp., *Lycopodium* sp., *Arctostaphylos* sp., and

Salix mytrillifolia. Lichens and *Cassiope* sp. are mainly present in the first part of the profile where the slope is steepest. Mosses become more prominent and thicker organic mats appear at lower slope angles. Individual *Picea* sp. are scattered along the entire slope, but few trees occur before 112 m along the profile where an open canopy *Picea mariana* stand begins. *Alnus* sp. begin to be present from 136 m.

Climate

Climate station TOW-08 is located about 1 m from the profile line (Figure 60). The station has been operational since 2007, and all variables are calculable until 2011. After that, only the SDD are calculable (Figure 61). The blended mean annual air temperature for that period was around -3.5°C (Table 6).

Table 6: Summary statistics for station TOW-08

	TOW-08
Elevation (m asl)	1119
Blended mean annual air temperature[1] (°C)	-3.5 (n=71)
Blended mean annual ground surface temperature[1] (°C)	-0.7 (n=74)
Blended temperature at the top of permafrost[1] (°C)	-0.2 (n=66)
2007-15 mean snow depth days[2] (m.days)	117 (n=7)
2007-11 mean surface offset[2] (°C)	2.8(n=4)
2007-11 mean thermal offset[2] (°C)	0.2 (n=4)

[1]Blended-year statistic obtained from Bevington's (2016) Database, calculated from data for *n* number of months.
[2]Means calculated by averaging the values obtained for *n* number of years during the defined period

The snow cover is significant with a mean SDD value greater than 100 m.days. However, the data (Figure 61) reveal considerable inter-annual variability in snow cover. The years 2007-08 and 2008-2009 had the least snow cover with only 86 and 72 m.days respectively. These were also the years with the coldest annual ground temperatures.

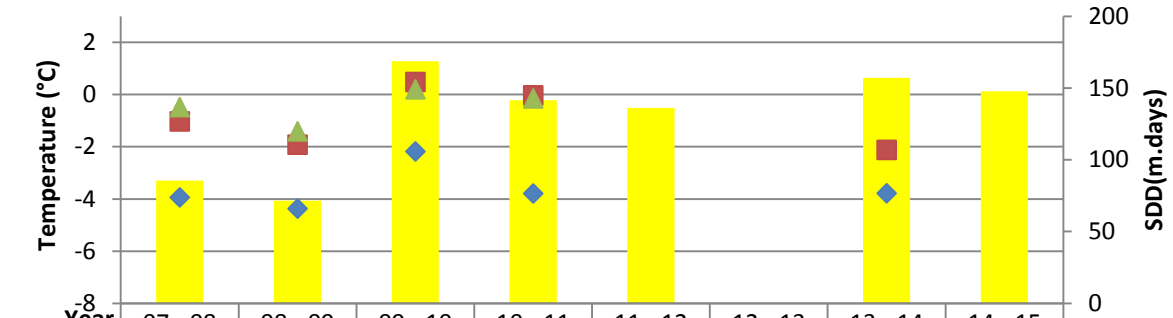

Year	07 - 08	08 - 09	09 - 10	10 - 11	11 - 12	12 - 13	13 - 14	14 - 15
SDDs	86	72	169	142	136		157	148
AMAT	-3.9	-4.4	-2.2	-3.8			-3.8	
AMGST	-1.0	-1.9	0.5	0.0			-2.1	
AMGT	-0.5	-1.4	0.2	-0.2				

*SDD-Snow Depth Days, AMAT-Annual Mean Air Temperature, AMGST-Annual Mean Ground Surface Temperature, AMGT- Annual Mean Ground Temperature at the estimated top of permafrost

Figure 61: Climate Station TOW-08 Data (1119 m asl)

Overall, the negative bTTOP value and AMGT values consistently near or below zero support an interpretation of permafrost presence, with the caveat that data are not available for the most recent years. Given that the AMGST is negative for 2013-14, and was never greater than 0.5°C for the calculated years only a small thermal offset is required for permafrost to be present.

Resistivity and Permafrost

The fifth iteration model with a 5.0% RMS error was selected for the modeled resistivity profile (Figure 62).

Modeled resistivity values are mostly medium or low, although some high and very low values are present. The highest resistivity values are modeled in two very small areas: near the start of the tomogram around 5 m depth, and very near the surface close to the climate station. A much larger low/very low resistivity area, with values <0.8 kΩm, appears in the second half of the tomogram between higher resistivity values near the surface and at depth.

Frozen ground was interpreted from probing in the last 12 m of the profile at 57, 86, 59, and 59 cm. A thick organic mat was also recorded in this section.

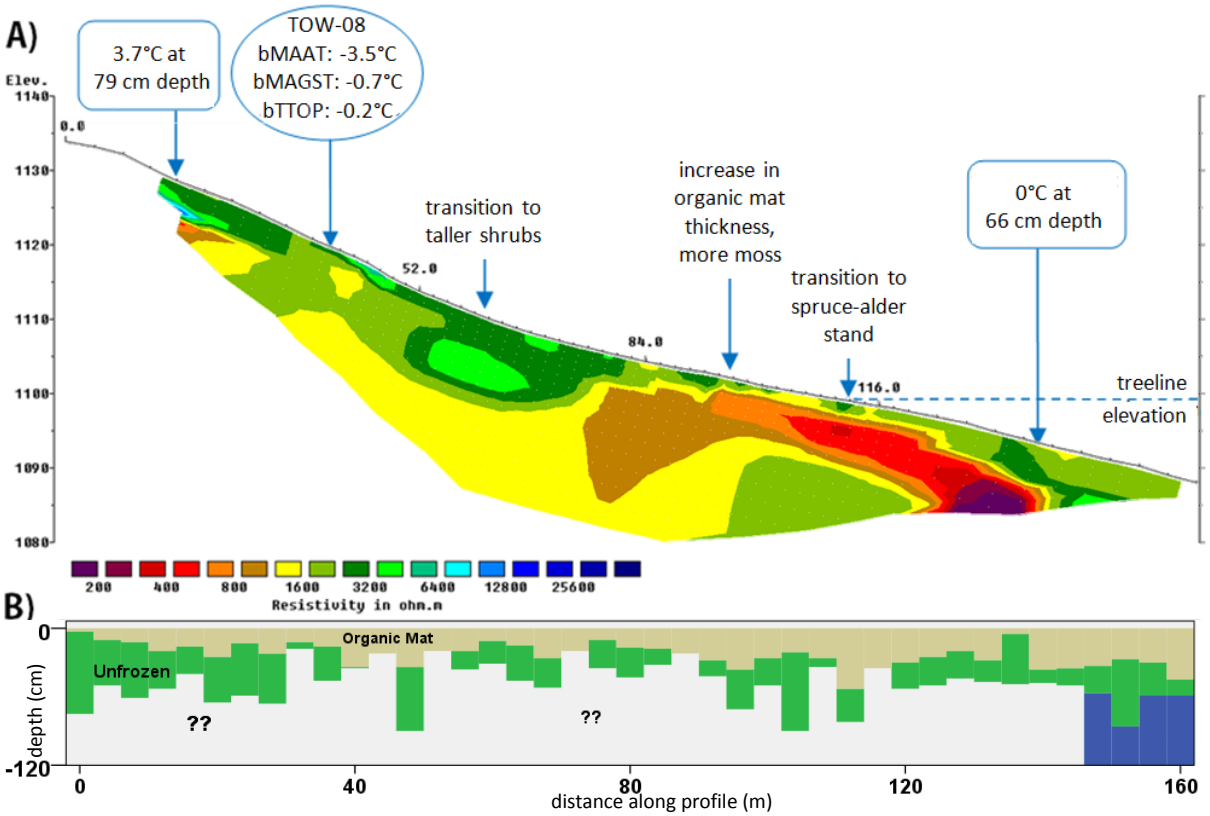

Figure 62: Combined results for Site 9

(A): Modeled resistivity profile annotated with changes in vegetation and temperature data and live temperature readings on day of the survey.
(B): Frost probe measurements (in cm) including organic mat thickness (in beige) and refusal depth (in green) with instances where refusal was interpreted as frozen ground (in blue).

Two ground temperature measurements were recorded. They revealed unfrozen ground at 79 cm depth 16 m along the profile and frozen ground at 66 cm depth 138 m along the profile.

These observations indicate permafrost presence where resistivity is modeled to be less than 2.4 kΩm, but also permafrost absence elsewhere where resistivity values are modeled to be greater than 2.4 kΩm. Thus, high resistivity values along certain parts of profile result from

causes other than permafrost.

The steeper part of the profile generally has a thinner organic mat with more *Cassiope* sp. and lichens, fewer trees and high resistivity values even where permafrost is absent. The climate station provides AMGT values below zero in previous years, however it lacks data for the year the ERT profile was completed and ground conditions may have changed. Thus, permafrost is interpreted possible, yet remains unconfirmed in this part of the profile (Figure 63). The less steep part of the profile is characterized by thicker organic mats, more moss and trees, and a large area of low/very low resistivity values. Permafrost is interpreted present near the end of the profile. In the low/very low resistivity area, permafrost is deemed improbable. A talik, possibly even an open talik, may occur here.

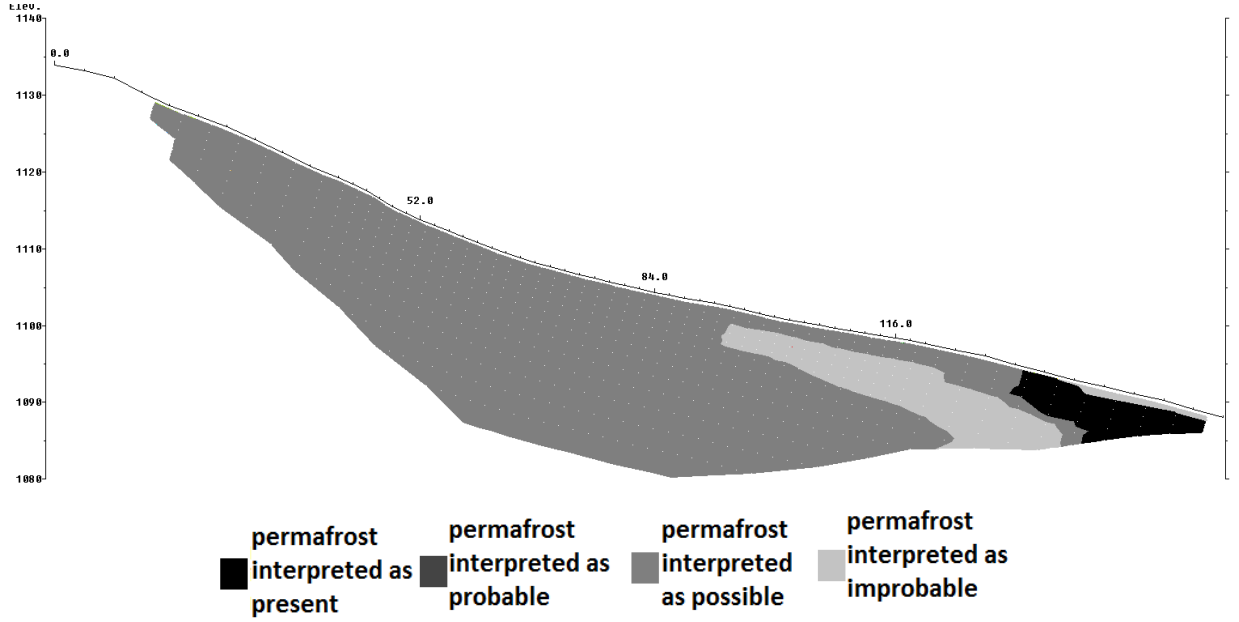

Figure 63: Permafrost interpretation image for Site 9

5.2.2 Site 10

Site 10 is located on the same north-facing slope as Site 9, about 40 m away (Figure 65). The profile extends from 1091 m asl to 1134 m asl (Figure 64).

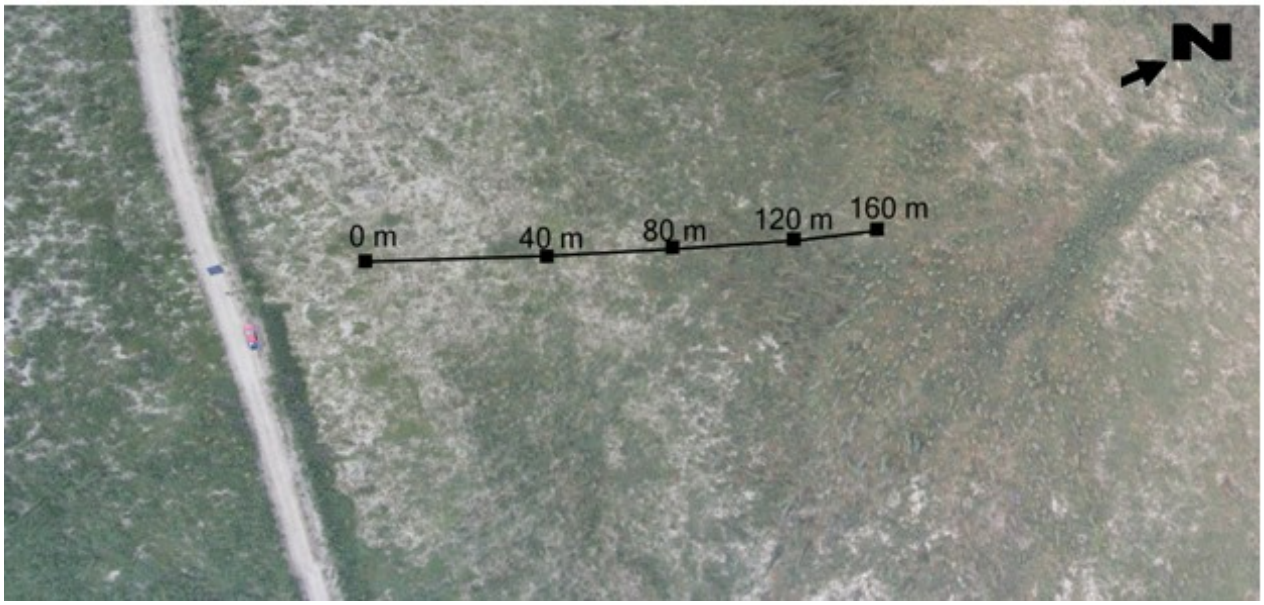

Figure 64: Aerial image mosaic of Site 10, with the profile traced in black and the distance along profile noted every 40 m.

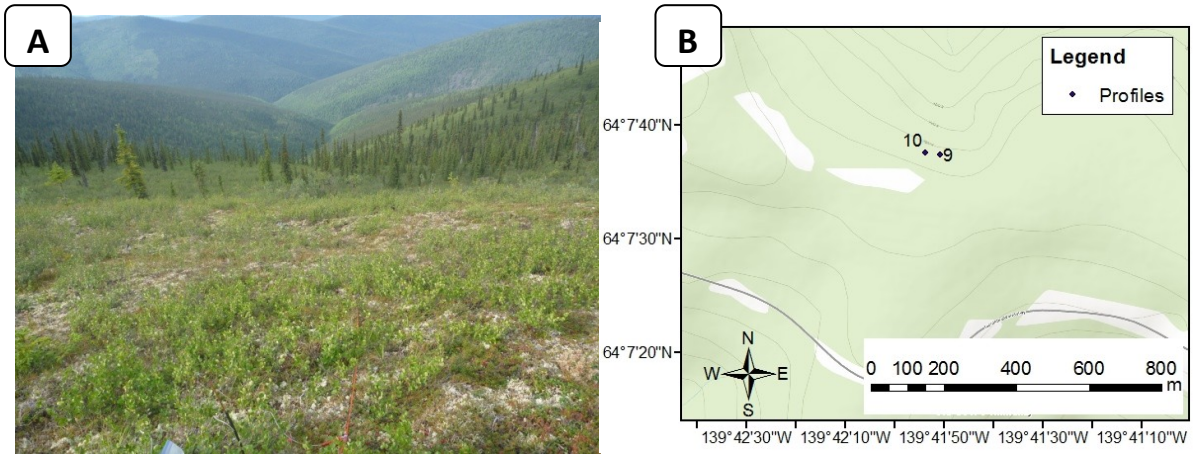

Figure 65: A) Site 10 viewed from the beginning of the profile looking downslope;

B) Enlarged map showing the locations of Site 9 and Site 10

Vegetation

Site 10 samples the same vegetation cover transition from shrubs and sparse trees to open mixed forest as Site 9 (Figure 65). The same vegetative species are reported with the addition of a few more types of berry-bearing plants. *Cassiope* sp. and *Empetrum nigrum* are noted mainly in the second half of the profile. Shrub height frequently varies, within the range of <0.5 m to 2 m, but generally increases as the profile proceeds down slope. A few transitions in shrub density are also noted (see Figure 66-A).

Climate

The nearest station is TOW-08 at Site 9. The air temperature and snow cover conditions are assumed to be similar (see Table 6).

Resistivity and Permafrost

The fourth iteration model with a 4.8% RMS error was selected for the modeled resistivity profile (Figure 66).

Low and medium resistivity values are modeled in most of the tomogram without any layering. Yet, a thin layer of high/very high resistivity appears near the surface in the first part of the tomogram where the slope is steeper.

During probing, frozen ground was interpreted as causing refusal in six instances. The depth reached in these cases ranges from 71 cm to 108 cm. The frost probe findings suggest that frozen ground is present both where high and where low resistivity is modeled.

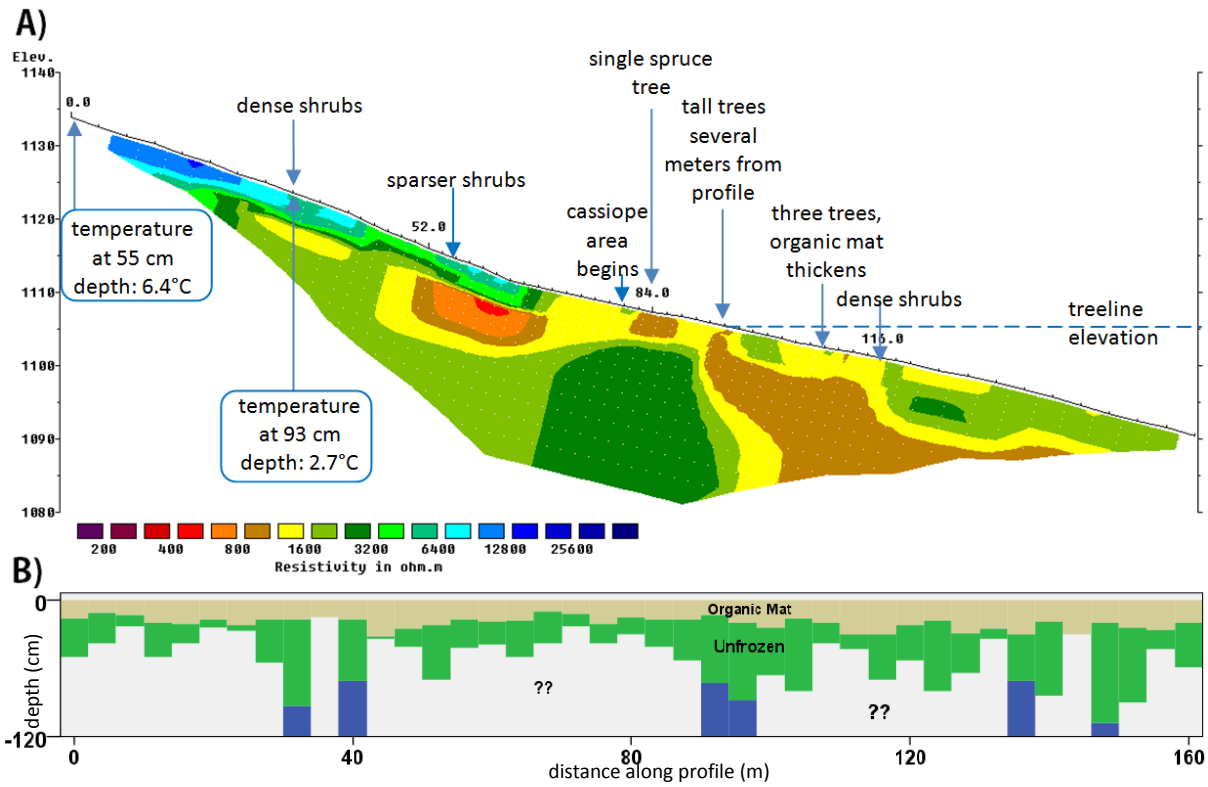

Figure 66: Combined results for Site 10

(A): Modeled resistivity profile annotated with changes in vegetation and live temperature readings on day of the survey.
(B): Frost probe measurements (in cm) including organic mat thickness (in beige) and refusal depth (in green) with instances where refusal was interpreted as frozen ground (in blue).

Assuming an accurate interpretation of probe refusal and properly modeled resistivity, permafrost is deemed possible along the entire tomogram (Figure 67). However, the possibility of false positive frozen ground interpretations from probing and the lack of validation from temperature data prevent permafrost from being interpreted with more confidence. The near-surface high resistivity values and the rapid transition to lower resistivity values are interpreted as indicating a transition in surficial geology from drier, coarser colluvium material to less resistive material beneath and down slope.

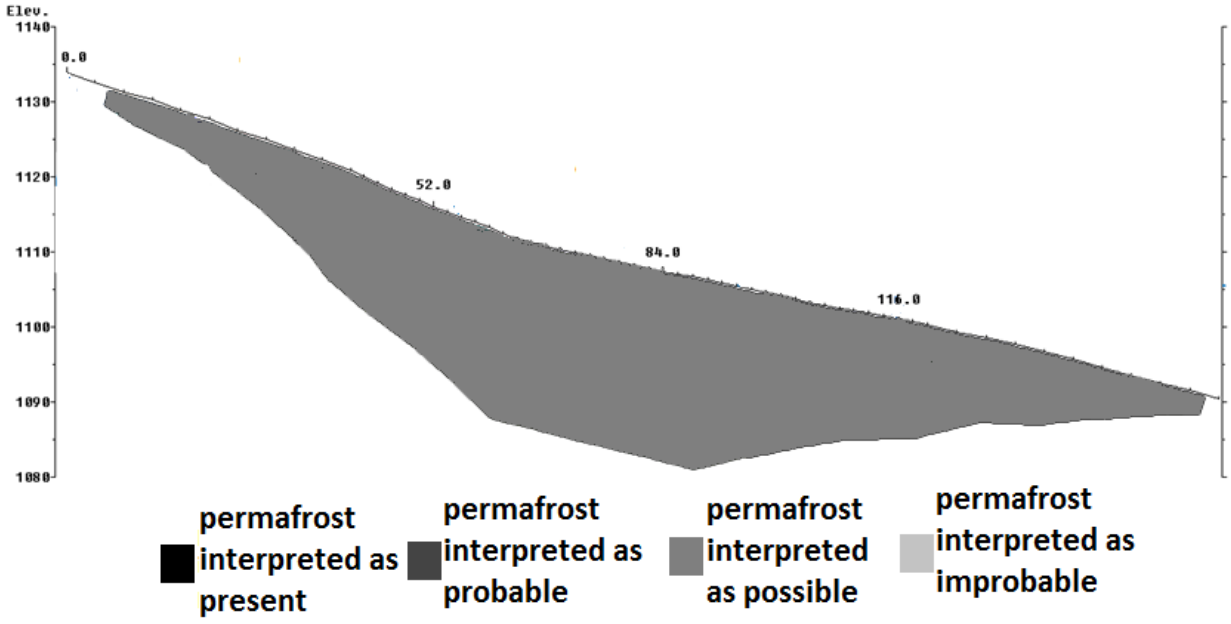

Figure 67: Permafrost interpretation image for Site 10

5.2.3 Site 11

Site 11 is located on a northwest-facing slope near Dawson. Two ERT surveys were completed at this site. The main profile runs from approximately 500 m asl down to about 458 m asl while a secondary shorter, 80 m long, profile overlaps the first 40 m of the main profile (Figure 68).

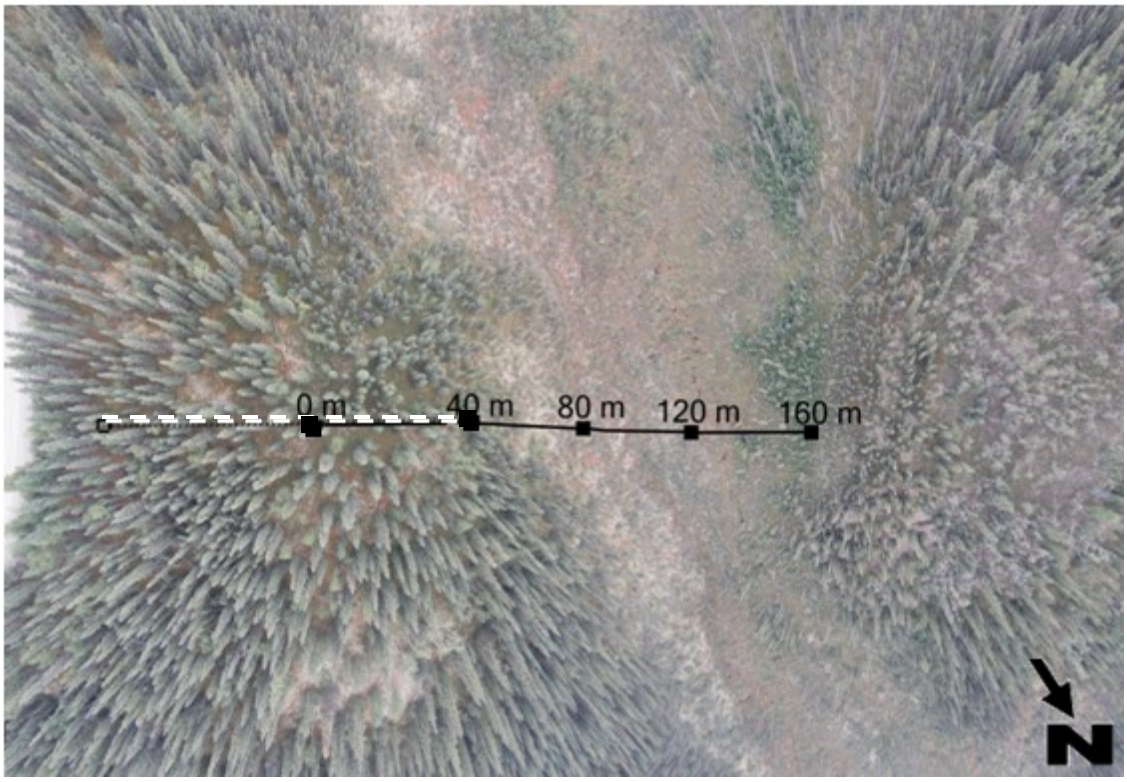

Figure 68: Aerial image mosaic of Site 11, with the main profile traced in black and the distance along profile noted every 40 m. The secondary profile is shown by the white dashed line.

Vegetation

Different forest covers are present at this site and form two distinct areas. For the first 55 m along the main profile, the vegetation cover is composed of an open canopy *Picea* sp. forest with a few *Betula papyrifera* (paper birch) trees, many dying or dead (Figure 69-B), and an understory dominated by *Equisetum* sp., moss, *Vaccinium vitis-idaea*, and *Geocaulon lividum*

(northern comandra). Around 60 m, the vegetation transitions as the slope sharply increases. The trees change. *Betula papyrifera* is absent. *Picea* sp. are much shorter due to stunted growth. *Salix* sp. and *Alnus* sp. shrubs begin to be noted, often less than 1 m tall; while in the understory, *Equisetum* sp. is much less present, *Cladina* sp. (reindeer lichen) and mosses increase and *Sphagnum* sp. begin to be noted. This section of vegetation continues for the remainder of the profile. In addition, various areas of standing water appear between 100 m and 145 m along the profile (Figure 69-A) and coincide with the appearance of *Salix mytrillifolia* shrubs. In approximately the last 5 m of the profile, shrubs also become quite dense.

Figure 69: Site 11 photographs

A) Large pool of standing water near profile;
B) Shrubless tall *Picea* sp. stand with few senescing *Betula papyrifera*;
C) Burrowed mound occurring at 8 m along the profile;
D) Burrow entrances

Other understory species found at this site include grass, *Ledum* sp., *Petasites* sp., *Arctostaphylos* sp., *Peltigera* sp. (felt lichen), *Rubus chamaemorus* (cloudberry), and *Rosa acicularis* (prickly rose).

Climate

Climate stations TOW-04 and TOW-05 are not on the profile (Figure 70), but they aptly capture the variation between the climate in the valley bottom and the climate upslope.

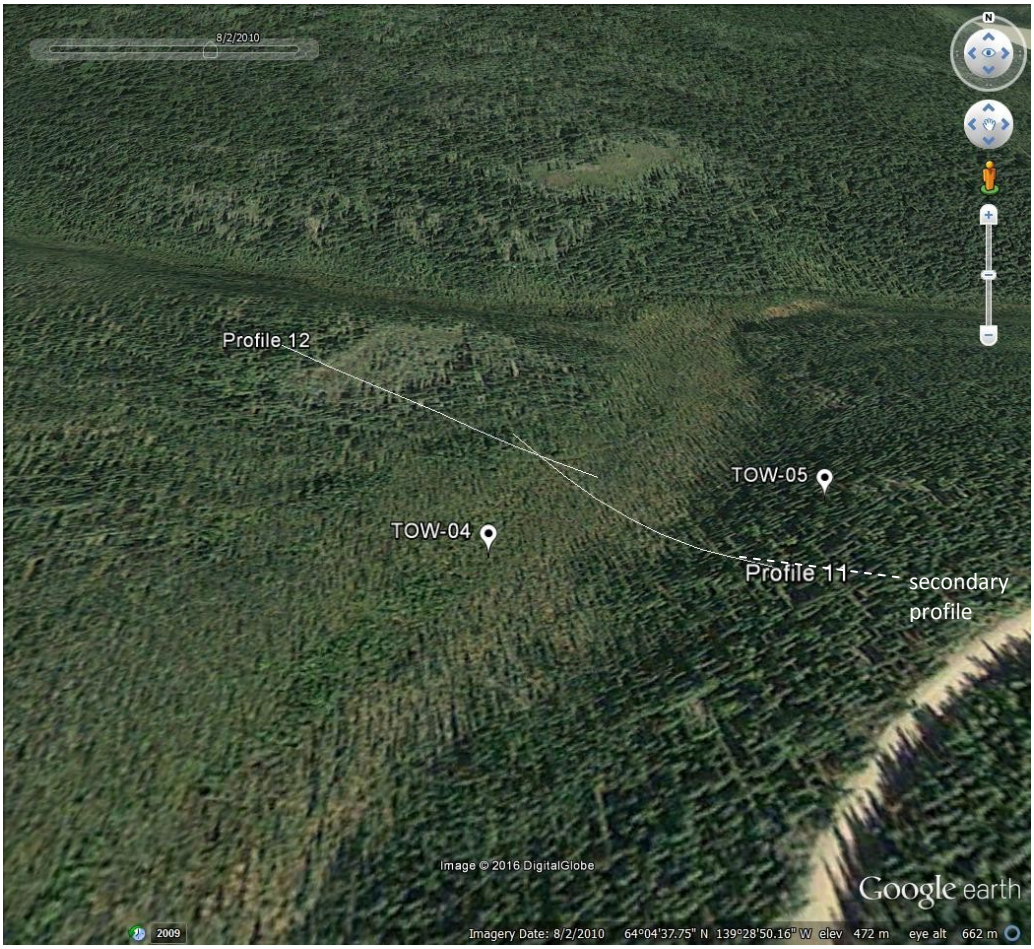

Figure 70: The locations of the climate stations TOW-04 and TOW-05 are shown on a satellite image in relation to the Sites 11 and 12. The dashed line marks the secondary profile at Site 11.

The stations have been operational since 2007. According to summary statistics for both stations (Table 7), the blended mean annual air temperature is around -4.5°C in the valley bottom and -3.5°C upslope. The snow cover is generally less at the upslope station, TOW-05, than at the valley station, TOW-04. However, annual data reveals that the difference in SDD values for both sites is less than 3 m.days for some years (Figure 71 and Figure 72). The blended mean annual ground surface temperatures are near zero for both stations, while the blended TTOP values are quite different. The bTTOP for TOW-04 is almost -1.5°C, but the bTTOP for TOW-05 is just above 0°C (Table 7). The fact that the AMGT values are consistently near or below zero supports the interpretation that permafrost is present, certainly in the valley bottom and possibly under the north-facing slope also.

Table 7: Summary statistics for stations TOW-04 and TOW-05

	TOW-04	TOW-05
Elevation (m asl)	484	503
Blended mean annual air temperature[1] (°C)	-4.9 (n=91)	-3.5 (n=81)
Blended mean annual ground surface temperature[1] (°C)	0.1 (n=94)	-0.1 (n=81)
Blended temperature at the top of permafrost[1] (°C)	-1.5 (n=94)	0.1 (n=81)
2006-15 mean snow depth days[2] (m.days)	90 (n=6)	71 (n=6)
2006-15 mean surface offset[2] (°C)	4.9 (n=6)	3.5 (n=5)
2006-15 mean thermal offset[2] (°C)	-1.6 (n=7)	0.2 (n=5)

[1]Blended-year statistic obtained from Bevington's (2016) Database, calculated from data for *n* number of months.
[2]Means calculated by averaging the values obtained for *n* number of years during the defined period

The annual ground temperatures at TOW-04 appear to be increasing (Figure 71). Still, the timescale is too short to confirm a climatic trend.

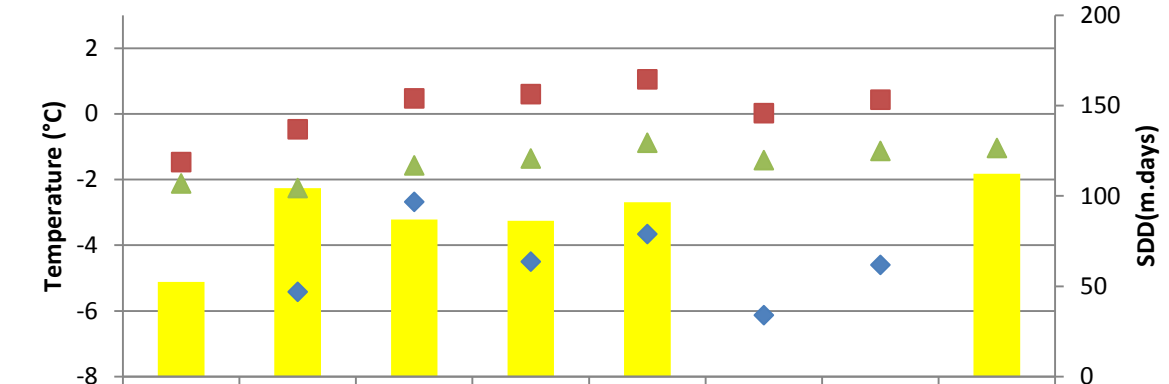

Year	07 - 08	08 - 09	09 - 10	10 - 11	11 - 12	12 - 13	13 - 14	14 - 15
SDDs	52	104	87	86	96			112
AMAT		-5.4	-2.7	-4.5	-3.7	-6.1	-4.6	
AMGST	-1.5	-0.5	0.5	0.6	1.1	0.0	0.4	
AMGT	-2.1	-2.3	-1.6	-1.4	-0.9	-1.4	-1.1	-1.0

*SDD-Snow Depth Days, AMAT-Annual Mean Air Temperature, AMGST-Annual Mean Ground Surface Temperature, AMGT-Annual Mean Ground Temperature at the estimated top of permafrost

Figure 71: Climate Station TOW-4 Data (484 m asl)

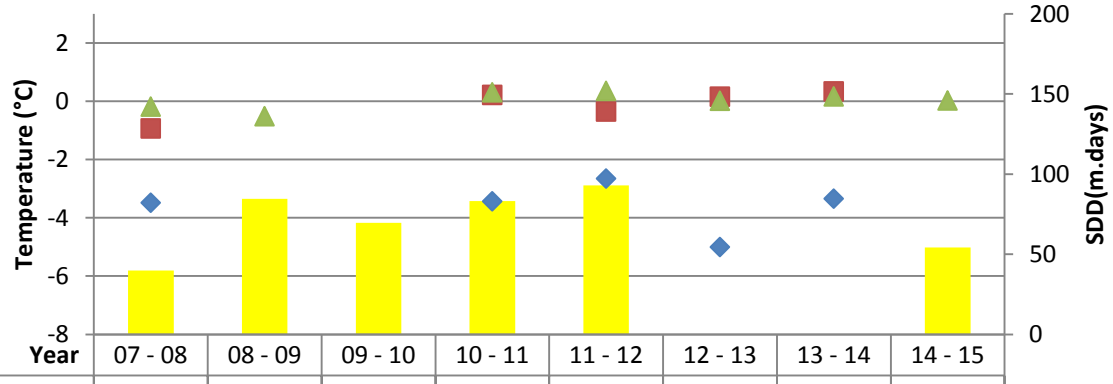

Year	07 - 08	08 - 09	09 - 10	10 - 11	11 - 12	12 - 13	13 - 14	14 - 15
SDDs	40	85	70	83	93			54
AMAT	-3.5			-3.4	-2.7	-5.0	-3.3	
AMGST	-0.9			0.2	-0.4	0.2	0.3	
AMGT	-0.2	-0.5		0.3	0.4	0.0	0.2	0.0

*SDD-Snow Depth Days, AMAT-Annual Mean Air Temperature, AMGST-Annual Mean Ground Surface Temperature, AMGT-Annual Mean Ground Temperature at the estimated top of permafrost

Figure 72: Climate Station TOW-5 Data (503 m asl)

Resistivity and Permafrost

The fourth iteration model with a 4.1% RMS error was selected for the main modeled resistivity profile (Figure 73).

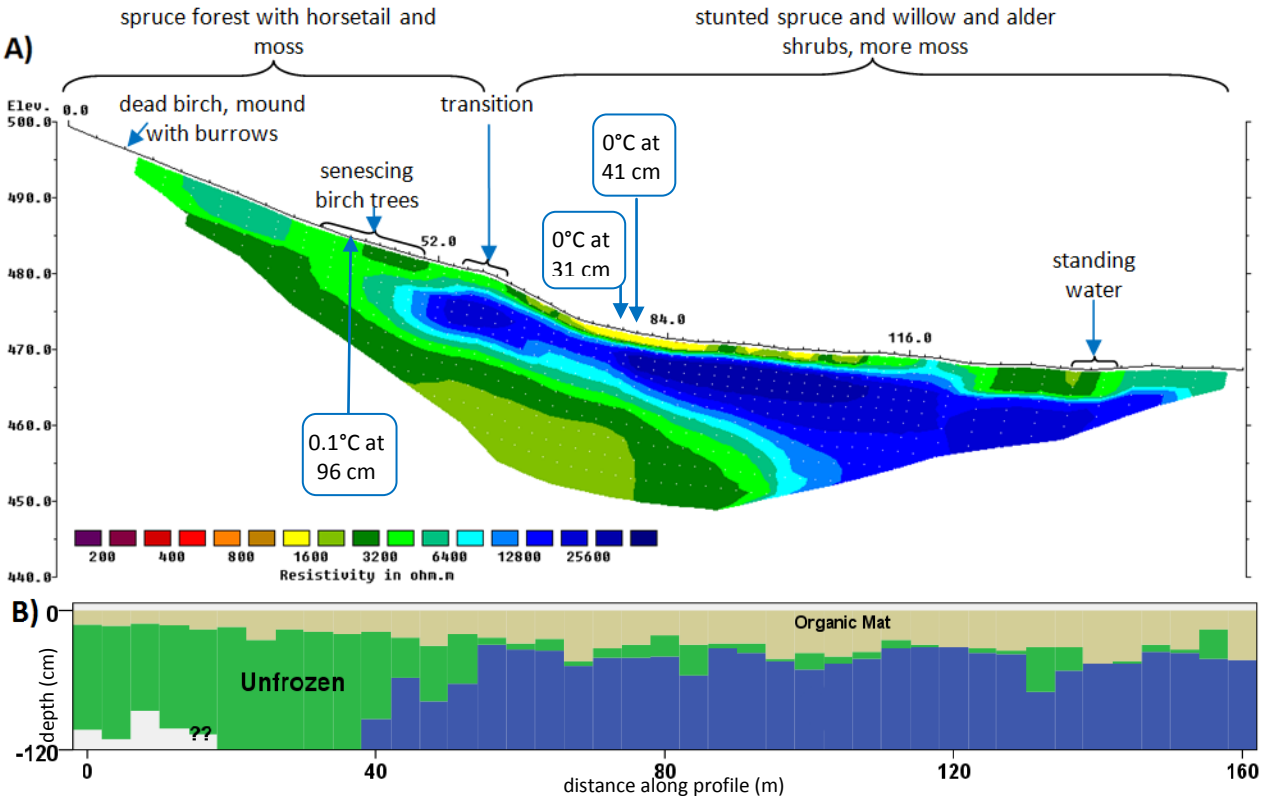

Figure 73: Combined results for Site 11.

(A): Modeled resistivity profile annotated with changes in vegetation and live temperature readings on day of the survey.
(B): Frost probe measurements (in cm) including organic mat thickness (in beige) and refusal depth (in green) with instances where refusal was interpreted as frozen ground (in blue).

Medium to very high resistivity values are modeled forming a three-layer system in the center of the tomogram. An area of very high resistivity is present below medium resistivity values that are in the first meter of depth. The sharp transition between these two areas is shown in a virtual borehole (Figure 74). Below the very high resistivity area, the modeled values

decrease more gradually with depth, but still transition from very high to medium in a about 6 meters. Halfway along the profile, however, the high/very high resistivity values extend to greater depths so that in the last part of the tomogram, the resistivity values at the maximum modeled depths remain very high.

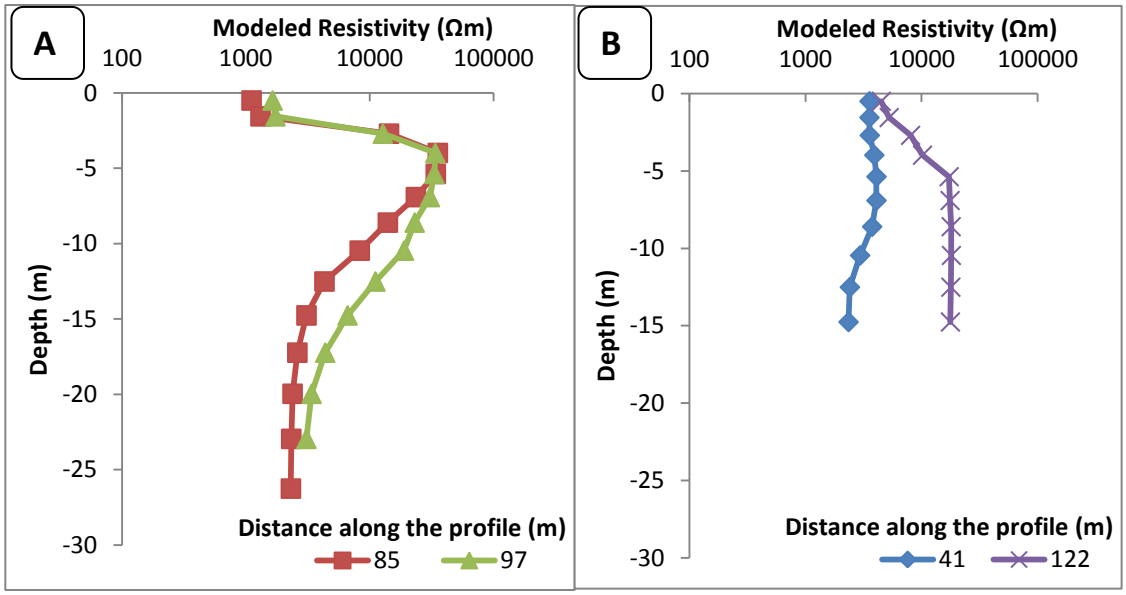

Figure 74: Virtual boreholes for Site 11
with (A) and without (B) sharp transitions through resistivity layers of different magnitude

A very clear pattern emerges from the frost probe data indicating near-surface frozen ground in the valley and unfrozen ground at least 1 m deep in the first part of the profile. Frost probe refusal depth is around 1 m depth for the first 20 m of the profile and refusal is interpreted to be caused by dense ground resistance (R). Past that, refusal is not encountered within the length of the probe (1.2 m) until 40 m along the profile where frozen ground is first detected. The depth at which the frozen ground is encountered decreases at the slope and vegetation transition and is almost always less than 0.5 m depth in the remainder of the profile.

The organic mat is thinner at the beginning of the profile but gradually increases. In the second half of the profile, the organic mat thickness is nearly always greater than 25 cm. Almost all the points along the profile where frozen ground is interpreted from frost probing have organic mat thicknesses of 20 cm or more. While nearly the entire remainder of the profile has organic mats less than 20 cm thick.

Temperature measurements confirmed frozen ground at 31 cm depth 78 m along the profile and at 41 cm 80 m along the profile. Frozen ground may also be present around 1 m depth 40 m along the profile.

A secondary ERT survey was completed to better inform the permafrost interpretation for the first 40 m of the profile (see Figure 68). The 5th iteration with a 7.8% RMS error was selected as the modeled resistivity profile (Figure 75).

The second half of this model (40-80 m) reveals a two layer resistivity system that was not shown in the first 40 m of the main profile (see Figure 73-A). This system does not appear in that profile probably because of the electrode spacing for that section and the shallow maximum depth modeled. The sharp transition between the very high resistivity values near the surface and medium and low resistivity values at depth in the secondary survey may represent the base of permafrost that extends up slope. Alternatively, permafrost maybe absent and the mound and burrows in this section (see Figure 69) might indicate air-filled cavities causing higher resistivity near the surface. Several details suggest the first interpretation to be more plausible. The very high resistivity layer extends considerably beyond the area where the burrows were noted and to a significant depth. Furthermore, lower resistivity values above higher resistivity values are modeled at the very near surface within this layer and these may indicate the presence of an

unfrozen active layer. If this is the case, the different electrode array used from this shorter survey and a change in surficial material could explain why the active layer resistivity in this profile remains very high while medium values are modeled in the valley portion of the main survey.

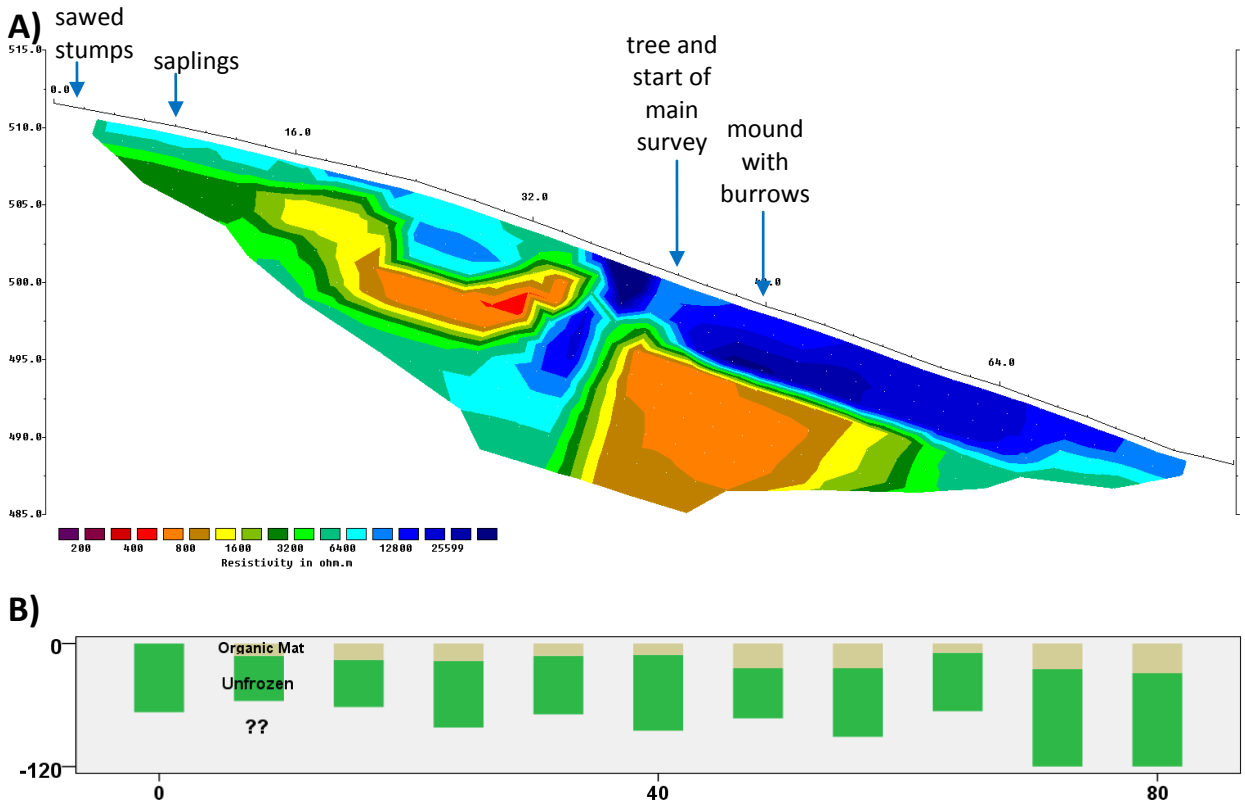

Figure 75: Combined results for the secondary survey completed at Site 11

(A): Modeled resistivity profile annotated with changes in vegetation.
(B): Frost probe measurements (in cm) including organic mat thickness (in beige) and refusal depth (in green) with instances where refusal was interpreted as frozen ground (in blue).

The first part of the secondary profile is less clear. High resistivity values are present near the surface. A layer of medium and low values is present beneath, but at depth high values are present. Permafrost conditions are not evident. Nonetheless, some change in surficial material seems to occur up slope. Not only does the resistivity pattern change, the frost probe refusal depth and the organic mat thickness generally decrease up slope.

A possible explanation for a change in surficial material is the increased proximity to the road whose construction may have added coarser materials to the adjacent areas or otherwise altered them. Sawed tree stumps and clusters of saplings (Figure 76) also suggest human intervention may have impacted this part of the slope.

Figure 76: Site 11 secondary survey photographs

A) Stumps at the beginning of the survey; B) Saplings near the beginning of the survey and road embankment seen behind; C) View upslope from start of main survey.

Taking all the observations into account, permafrost is interpreted as present or probable along most of the main profile (Figure 77). A layer of permafrost several meters thick is interpreted to be present where modeled resistivity is high/very high and where probing confirmed unfrozen ground. This permafrost deepens and eventually reaches the maximum depth modeled. Permafrost is interpreted to be improbable in the very near surface where modeled resistivity values are medium or where probing did not encounter frozen ground. Permafrost is possible at depth where resistivity values are medium.

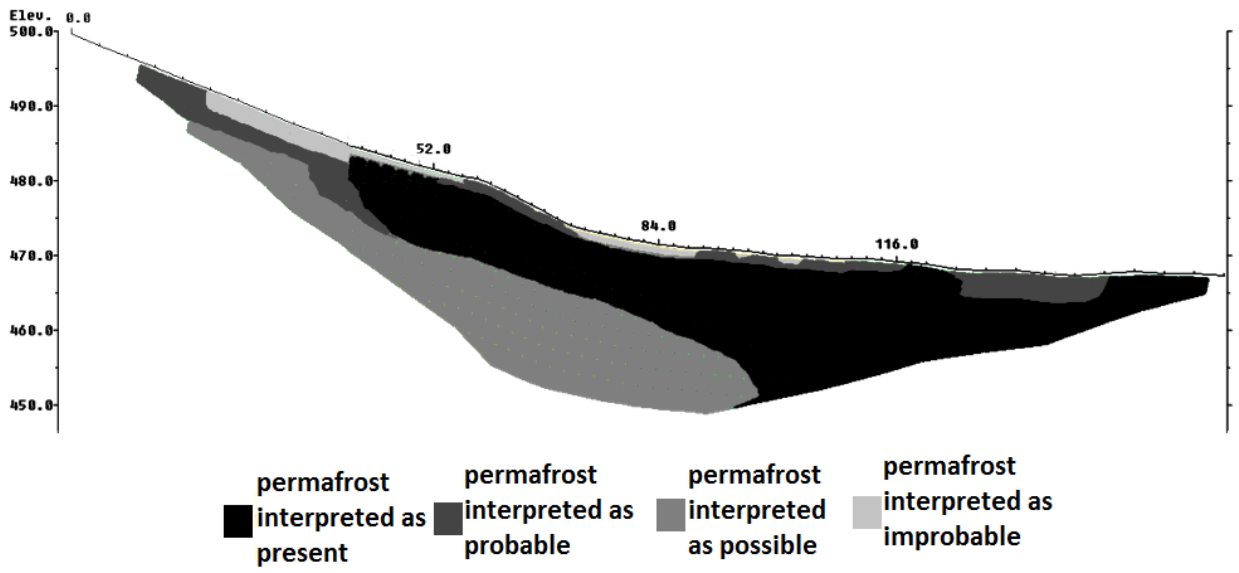

Figure 77: Permafrost interpretation image for Site 11 (not including the secondary survey)

5.2.4 Site 12

Site 12 is located in the same valley as Site 11 but extends along its' southeast-facing slope. The profile (Figure 78) runs from approximately 501 m asl down to about 471 m asl.

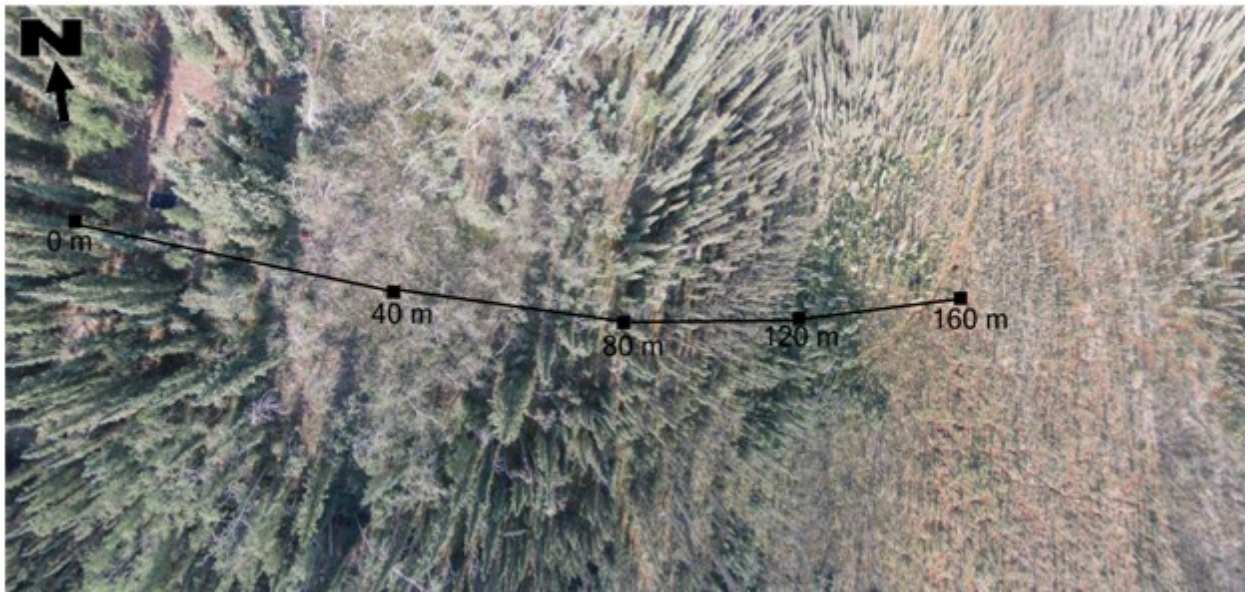

Figure 78: Aerial image mosaic of Site 12 with the profile traced in black and the distance along profile noted every 40 m.

Vegetation

Different forest covers are present at this site. Trees along the profile include *Picea* sp., *Betula papyrifera*, and *Alnus* sp. *Salix* sp. shrubs are present in some sections and the understory includes lots of *Geocaulon lividum*, *Vaccinium vitis-idaea*, *Epilobium anagallidifolium*, *Ledum* sp., *Sphagnum* sp., *Cladina* sp., grasses and mosses. Other understory vegetation species common in various areas along the profile include *Equisetum* sp., *Petasites* sp., *Salix mytrillifolia*, *Rubus chamaemorus*, *Rosa acicularis* and *Saxifraga tricuspidata* (prickly saxifrage).

Several important vegetation cover transitions occur along this profile (Figure 79 A-E).

At 28 m along the profile, the forest (see A) dominated by *Picea* sp. clears and a sandy, steep-sloped area dominated by *Betula papyrifera* begins (see B). At 70 m along the profile, tall *Picea* sp. trees begin to regain prominence and the slope gradient decreases (see C). Past 96 m, the organic mat is much thicker and *Picea* sp. are generally shorter. A tangle of dense *Betula* sp. and *Alnus* sp. is present from 124 m to 128 m along the profile (see D); an open stand of stunted *Picea* sp. and *Salix* sp. shrubs is present for the remainder of the profile (see E). In addition, *Salix mytrillifolia* plants and areas of standing water are noted in the last 12 m of the profile (see F).

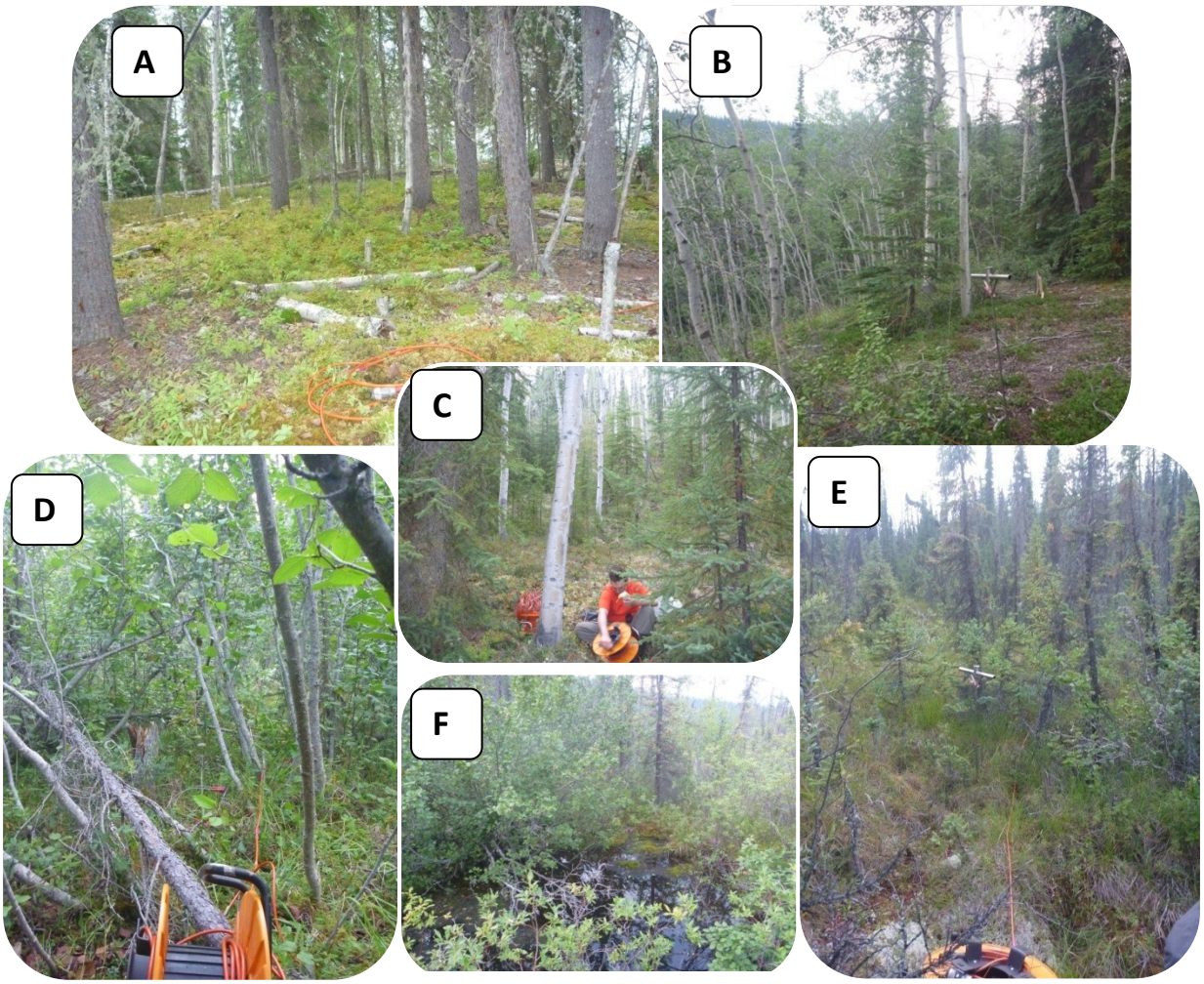

Figure 79: Site 12 photographs

A) *Picea* sp. dominated forest; B) Transition to *Betula papyrifera*; C) *Picea* sp. regains prominence; D) Dense *Alnus* sp.; E) Stunted *Picea mariana*; F) Standing water.

Climate

The nearest climate stations are TOW-04 and TOW-05 (see Table 7) roughly 80 m and 90 m away, nearer to Site 11. TOW-04, in the valley bottom, is likely fairly representative of conditions in the lower part of the slope, but TOW-05, on the opposite northwest-facing slope, likely records colder conditions than those occurring at Site 12's southeast-facing slope.

Resistivity and Permafrost

The third iteration model with a 4.4% RMS error was selected for the modeled resistivity profile (Figure 80).

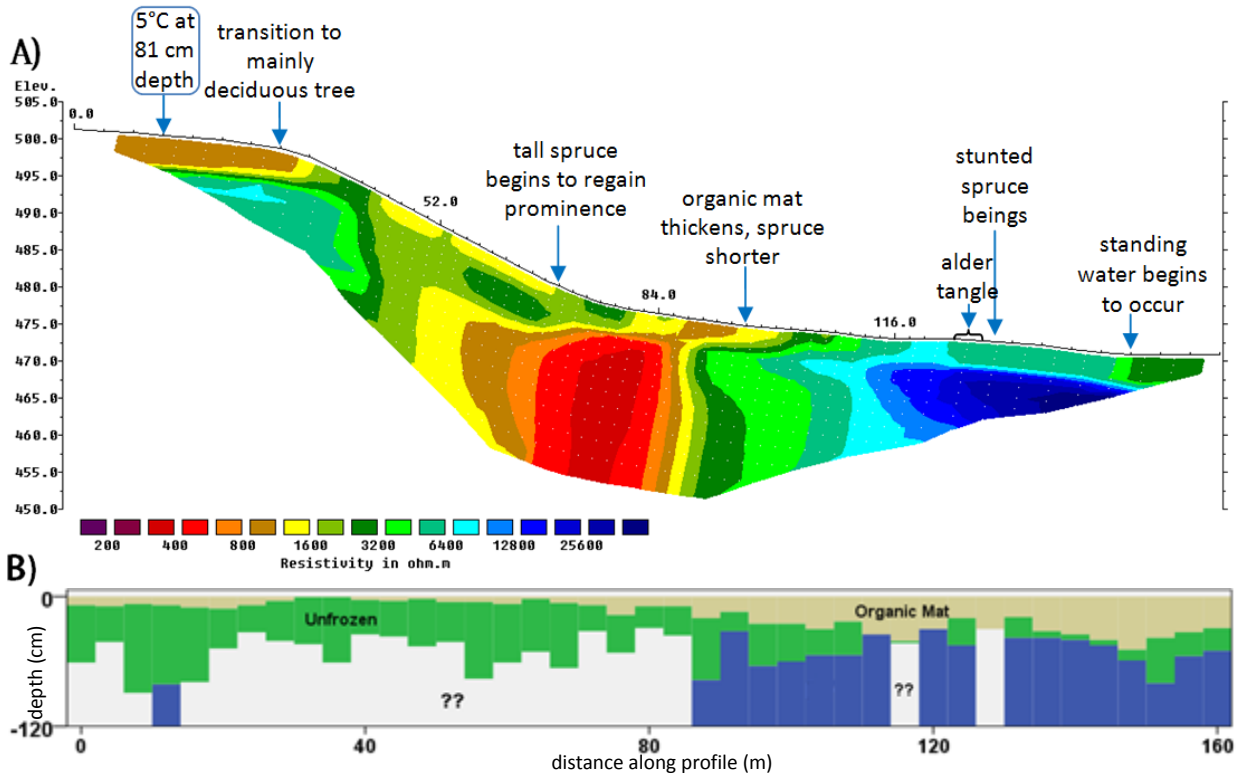

Figure 80: Combined results for Site 12

(A): Modeled resistivity profile annotated with changes in vegetation and live temperature readings on day of the survey.
(B): Frost probe measurements (in cm) including organic mat thickness (in beige) and refusal depth (in green) with instances where refusal was interpreted as frozen ground (in blue).

Very low to very high resistivity values are modeled forming several different patterns. At the start of the tomogram, a two-layer pattern is distinguishable. Low resistivity values are modeled above high resistivity values. The transition from the low resistivity values to high resistivity values is very abrupt, with about a 4 times increase in resistivity values occurring over less than 2 m of depth. Past 40 m, the high resistivity area ends and a different resistivity pattern emerges. Medium resistivity values surround a large area of low/very low resistivity. This large area of low/very low resistivity consistently reaches the maximum depth modeled and joins a smaller low resistivity area near the surface. A significant transition between medium and lower values emerges at the end of the low/very low resistivity area. In the last 60 m of the profile, modeled resistivity values are almost all high or very high.

The organic mat thickness measurements range from 0.5 cm to 49 cm and vary with the slope gradient. At the beginning of the profile, where the slope is gentle, the organic mat is around 10 cm. Where the slope increases considerably, the organic mat is at its thinnest. Past that, the slope gradient lessens and the organic mat thickness increases until it is mostly at or greater than 30 cm.

In the second half of the profile (starting at 88 m), frozen ground was almost always interpreted from probing, with refusal depths ranging from 30 cm to 80 cm. Frozen ground was also believed to be encountered 12 m along the profile, at 81 cm of depth. However, an attempt to verify this interpretation gave a temperature value that suggests unfrozen ground at that depth. The remaining frost probe measurements recorded probe refusal depths ranging from 29 cm to 79 cm. Refusal in most of these instances was caused by clasts and a in few locations, at the start

of the profile, refusal was caused by compact ground resistance.

Taking all the observations into account, and the fact that climate data also indicated permafrost presence in the valley bottom (see Table 7), deep permafrost is interpreted to be present in the last 70 m of the profile and permafrost is interpreted to be improbable in most of the remainder of the profile, with two exceptions (Figure 81). Permafrost probably extends several meters upslope from the high/very high resistivity area, and permafrost is possible around 5 m depth near the beginning of the profile where an area of high resistivity is present under low resistivities.

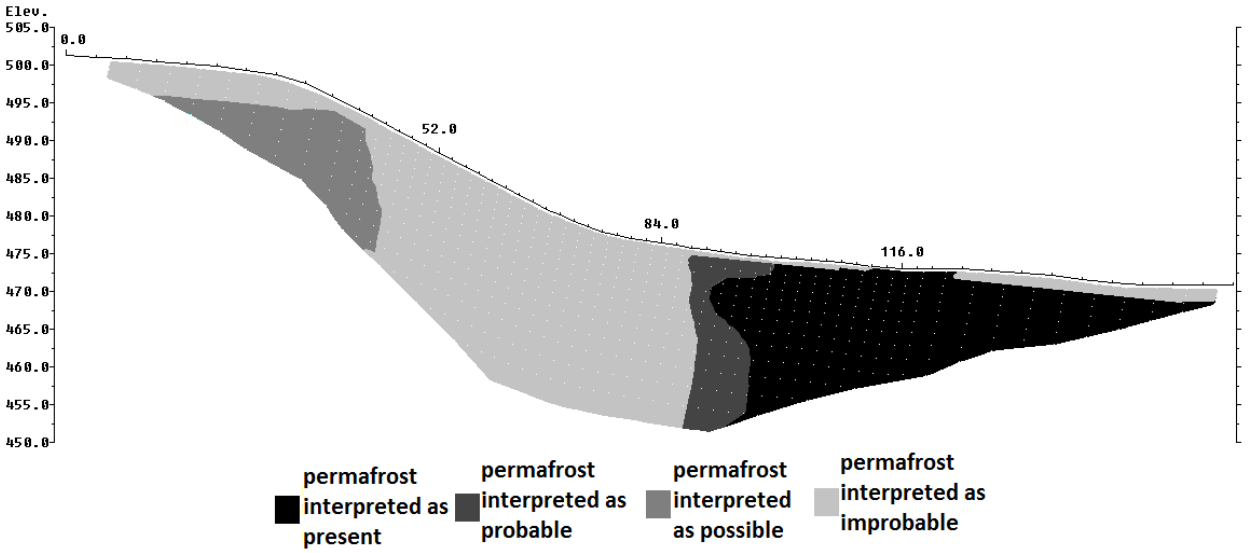

Figure 81: Permafrost interpretation image for Site 12

The strength of the supporting evidence in each case justifies the interpretations. The high and very high resistivity values combined with the frost probe measurements support with confidence the interpretation that permafrost is present in the valley bottom. The consistent probe results suggest near-surface permafrost even where near-surface modeled resistivity values are lower in the last 14 m. A possible explanation is the visible bodies of surface water in that area,

and the fact that conductive water can lower modeled resistivity values. Probe measurements from 88 m to 96 m along the profile suggest frozen ground was encountered in the near-surface where low and medium resistivity values are modeled. Permafrost is deemed probable in this location, but the low resistivity values modeled and the possibility of false positive frozen-ground probe interpretations or of seasonal frost occurrences prevent a confident interpretation of permafrost presence. Near the beginning of the profile, the transition between low and high resistivity layers could be an indication of permafrost or of some stratigraphic change, such as bedrock. Without more evidence permafrost is deemed possible. Finally, several observations support the interpretation that permafrost is improbable along the steeper portion of the southeast-facing slope. The low and medium resistivity values and the lack of any layered patterns or sharp transitions do not suggest permafrost presence. The absence of frozen ground in the probing results, the minimal organic mat and the expected increase in incoming solar radiation due to the slope aspect all suggest that efficient ground warming occurs here during summer months, which would be unfavorable for permafrost.

6.0 Discussion

Prior to fieldwork, it was hypothesised that frozen ground characteristics would change across a transition in vegetation cover. This hypothesis was based partly on vegetation's impact on the thermal regime through shading and snow capture (Brown 1966; Smith 1975; Karunaratne and Burn 2004; Lewkowicz et al. 2012; Jean and Payette 2014). In addition, a change in vegetation can reflect a change in other site factors affecting permafrost, such as air temperature, earth materials and soil moisture (Shur and Jorgenson 2007; Körner 2007; Körner 2012) and this was expected to increase the likelihood of vegetation cover transitions coinciding with changes in permafrost.

The results indicate, however, that the complex interactions between site factors (Jorgenson et al. 2010) can prevent changes in permafrost from consistently coinciding with vegetation cover transitions at the scale examined. They show that the frozen ground characteristics examined often do not differ greatly from one vegetation zone to another across the few hundred meters spanning the transition and that where changes do occur, other factors should be considered. These observations reflect the complexity of the relationships among vegetation, permafrost and other factors (Figure 82). Vegetation covers impact the thermal regime in many different ways and can have cumulative impacts that are difficult to assess. In addition to their impacts on shading and snow cover, vegetation covers alter soil moisture and organic matter decomposition (Jorgenson et al. 2010) in ways that depend on the vegetation type and density. There are also feedbacks between several factors affecting permafrost (Jorgenson et al. 2010) and these may enhance the influence of local scale factors.

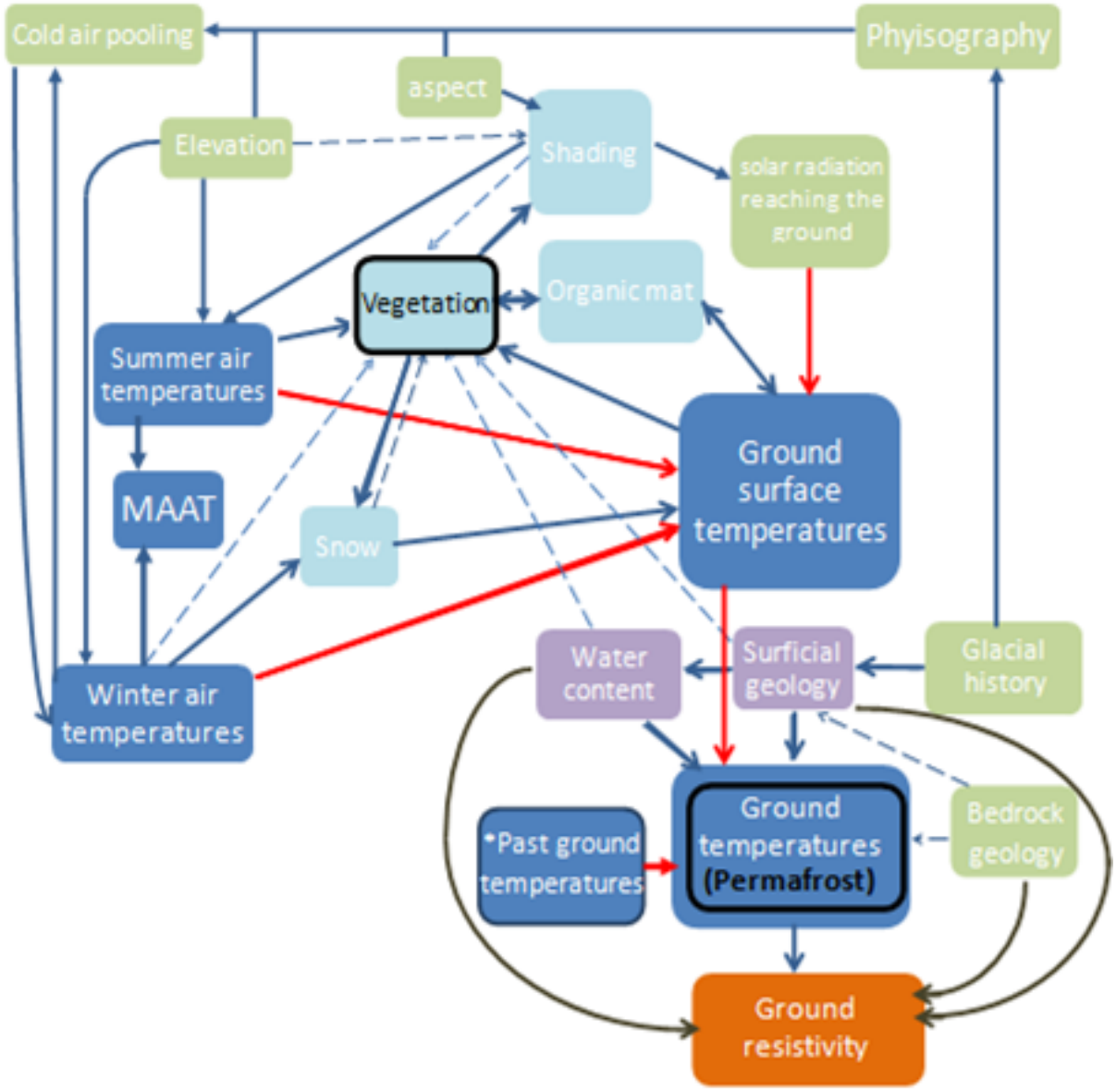

Figure 82 A schematic representation of the interactions between air and ground temperatures, site factors, and ground resistivity. Temperatures are shown in dark blue. Influences on thermal energy fluxes are indicated with red arrows. Site factors associated with the surface offset are light blue, while those associated with the thermal offset are purple. Less direct factors are green. Influences between different factors and temperatures are indicated with blue arrows. Influences on ground resistivity, other than temperature, are indicated with brown arrows.

Much of the permafrost variation that does occur within the vegetation cover transition area may be more closely related to changes which are independent of the altitudinal zonation of vegetation. These changes include differences in earth materials, organic mat thickness, micro-topography, or small-scale changes in vegetation. The results suggest that even though changes in permafrost probability correspond with changes in vegetation in certain locations, such associations do not occur consistently across the landscape and are more evident for some types of vegetation transitions than for others.

6.1 Vegetation assemblages indicative of permafrost presence or absence

Some of the slope aspects and vegetation covers in the study sites were consistently associated with either permafrost presence or absence. For instance, areas of stunted *Picea mariana*, both in valleys (Sites 11 and 12) and on slopes (Site 2), were consistently underlain by permafrost (Figure 83). Elsewhere, permafrost was absent on south-facing slopes with deciduous trees, such as *Populus tremuloides* and *Betula papyrifera*, (Site 3 and Site 12). Vegetation assemblages dominated by either stunted *Picea mariana* or deciduous trees, are therefore considered to be permafrost indicators.

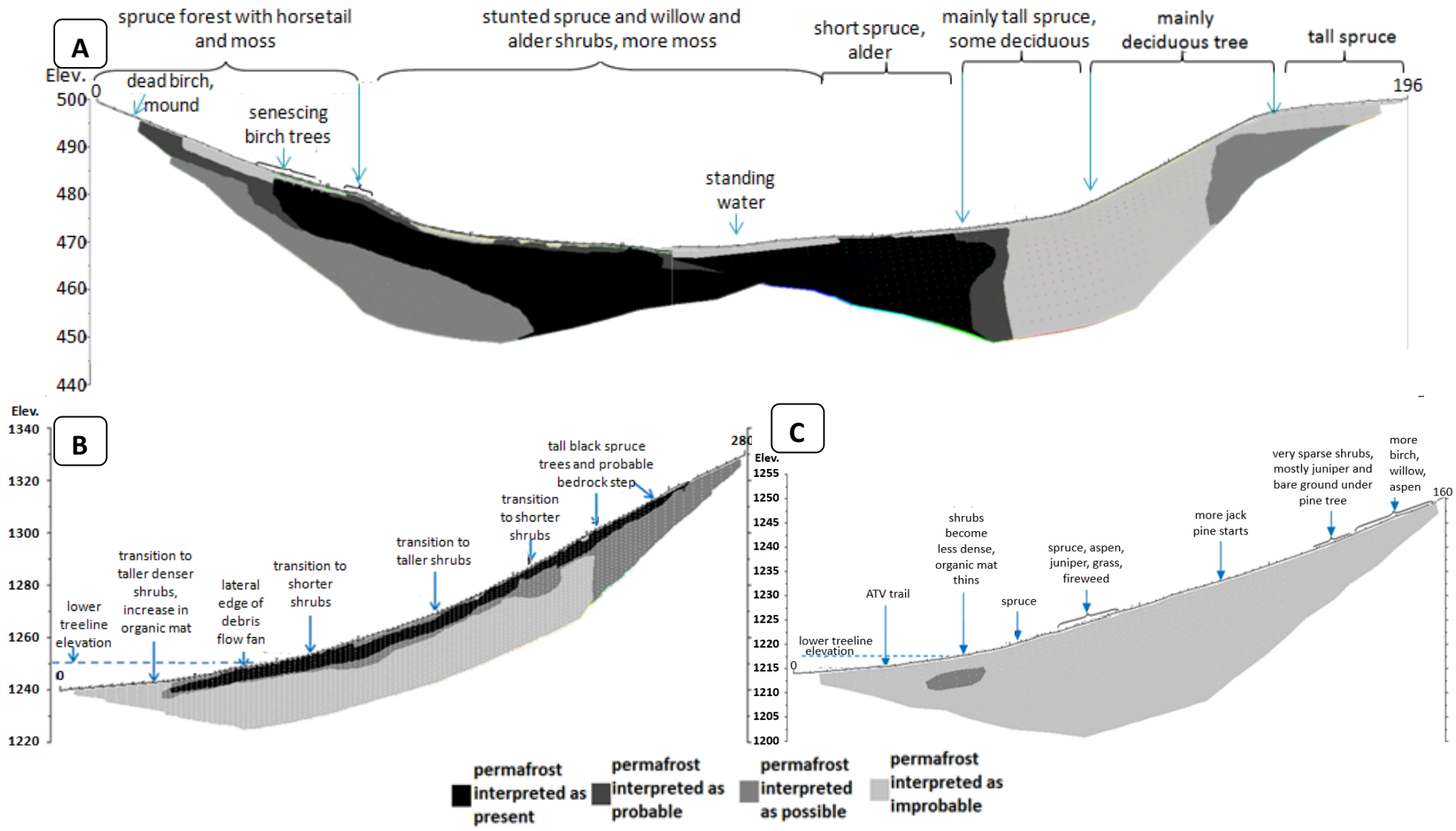

Figure 83: Permafrost interpretation images annotated with vegetation notes in areas of cold air drainage for (A) north-facing Site 12 and south-facing Site 11; (B) north-facing Site 2; and (C) south-facing Site 3.

The findings for these four sites (Figure 83) are consistent with the literature. Slope aspect is one of the most important factors governing the distribution and thermal conditions of mountain permafrost in the northern hemisphere, and its relation is strongest in continental areas (Etzelmller and Frauenfelder 2009). In the study areas, previous work indicates that permafrost is less probable on south-facing slopes than on north-facing slopes (Lewkowicz and Ednie 2004; Yukon Ecoregions Working Group 2004a). Kremer (2010) modeled permafrost presence or absence in several areas of the Yukon and found dominant species to be the most useful variable. However, only *Picea mariana* was consistently classified as permafrost probable, and only *Pinus contorta* and *Populus tremuloides* were consistently classified as permafrost improbable (Kremer 2010). Additionally, *Betula papyrifera* was a dominant species for permafrost absence specifically in the Dawson study area (Kremer 2010). These results support the idea that in Yukon's discontinuous permafrost zone, particular vegetation assemblages can indicate current permafrost presence or absence.

Nonetheless, the field observations provide multiple examples of how interpreted permafrost boundaries do not directly correspond to the limits of these indicator vegetation assemblages. At Site 3, the ground is permafrost improbable even where the vegetation is no longer dominated by *Populus tremuloides*, but by shrubs. Similarly, at Site 2, permafrost extends below the lower treeline and only where the organic mat thins or disappears is the ground interpreted to be permafrost-free. On the north-facing slope at Site 12,permafrost is improbable even where the *Betula papyrifera* stand transitions downslope to a stand of tall *Picea* sp. Permafrost is interpreted as beginning where the organic mat thickens but before the stunted *Picea mariana* stand truly begins. On the south-facing slope at Site 11, permafrost possibly

continues upslope even where *Picea* sp. are no longer stunted. Thus, the boundaries of an area of indicator vegetation may not correspond to the limits of permafrost bodies.

Changes in observed and inferred permafrost conditions sometimes occur within the transitions to and from the areas of indicator vegetation, specifically areas of stunted *Picea mariana*. Observed changes include changes in ground resistivity and frost table depths, while inferred changes include alterations in ground temperature, permafrost depth, active layer thickness, or ice content. For example, modeled resistivity values decrease and the frost table depth increases at Sites 11 and 12 as the vegetation cover transitions from the open stand of stunted *Picea* sp. with *Salix* sp. and *Alnus* sp. shrubs to denser *Picea* sp. forests. The decrease in resistivity values may represent a warmer conditions and a greater unfrozen moisture content. Thus, changes in permafrost characteristic correspond with changes in vegetation in this particular environment, but how do these changes fit in with the altitudinal zonation of permafrost?

The results from the four sites in Figure 83 generally do not correspond to a simple altitudinal zonation for permafrost, in which permafrost is continuous at high elevations, then discontinuous, sporadic and absent as the elevation decreases (Gravis et al. 1978; King 1986; King 1990; Bonnaventure and Lewkowicz 2013). Figure 84 presents a conceptual model of how this simple zonation might apply to a mountainous landscape as well as the changes that occur when the influence of slope aspect is included in the model. The extent of the permafrost zones is then limited to the highest elevations on south-facing slopes and the zones no longer correspond to the same elevations found on north-facing slopes (Noetzli et al. 2007; Gruber and Haeberli 2007). This conceptual model matches the observations made at the south-facing slope at Site 3.

However, the possibly continuous permafrost down the northwest-facing slope of Coal Ridge and the deep continuous permafrost in the valley bottom sampled at Sites 11 and 12 signal additional complexities that are not included in this simple model (Figure 84).

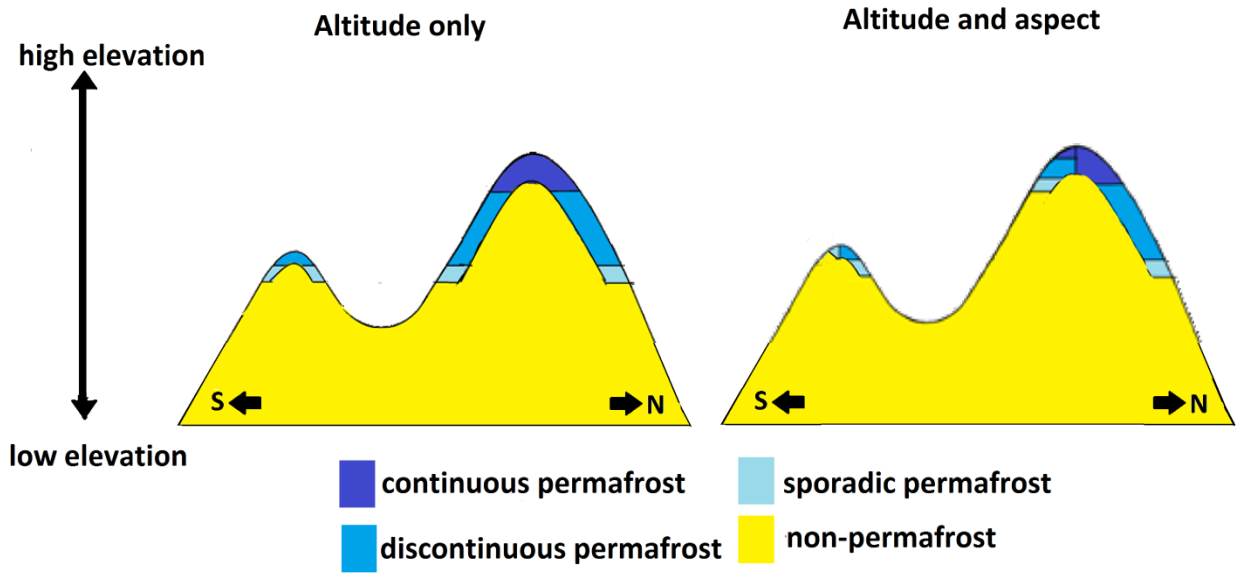

Figure 84: A simple conceptual model of the altitudinal zonation of mountain permafrost.

This model is not to scale and excludes multi-dimensional subsurface heat transfers. (See Noetzli et al. 2007 for more detailed models of subsurface ground temperatures and heat fluxes in idealized ridges with permafrost).

Cold air drainage, an important element of the complex topoclimatic system, explains the presence of both permafrost and its indicator vegetation at elevations lower than would be expected by a simple altitudinal zonation model (Bonnaventure et al. 2012; Bonnaventure and Lewkowicz 2013). The simple model assumes a negative surface lapse rate, like the widely used -6.5°C/km. However, the actual lapse rate varies and temperature along altitudinal gradients can increase with elevation rather than decrease (Lewkowicz and Bonnaventure 2011; Bonnaventure

et al. 2012; Graae et al. 2012; Bonnaventure and Lewkowicz 2013). These inversions occur most frequently in winter because cold air pools in valley bottoms (Graae et al. 2012).

All of the study sites examined are within a region that experiences winter-time inversions in surface lapse rates through the forested zone (Lewkowicz and Bonnaventure, 2011). These inversions are known to increase permafrost probabilities in valley bottoms in areas of high continentality (Bonnaventure and Lewkowicz 2013). Hourly temperature data from climate stations both at Site 2 and near Sites 11 and 12 reveal inversions in the surface lapse rate.

By lowering the mean annual air temperatures, these inversions create conditions at lower elevations that are favourable for permafrost aggradation and/or persistence. The temperature of the cold air that pools in a valley bottom, the depth of the inversion and the duration for which inversions persist all affect the extent and characteristics of the permafrost. In certain circumstances, permafrost may only exist sporadically at the lower elevations where the cold air pools. Under other conditions, permafrost may be continuous along an entire slope.

The inclusion of cold air drainage in the altitudinal zonation model (Figure 85) produces potential permafrost distributions that correspond well with findings from Sites 2, 11 and 12.

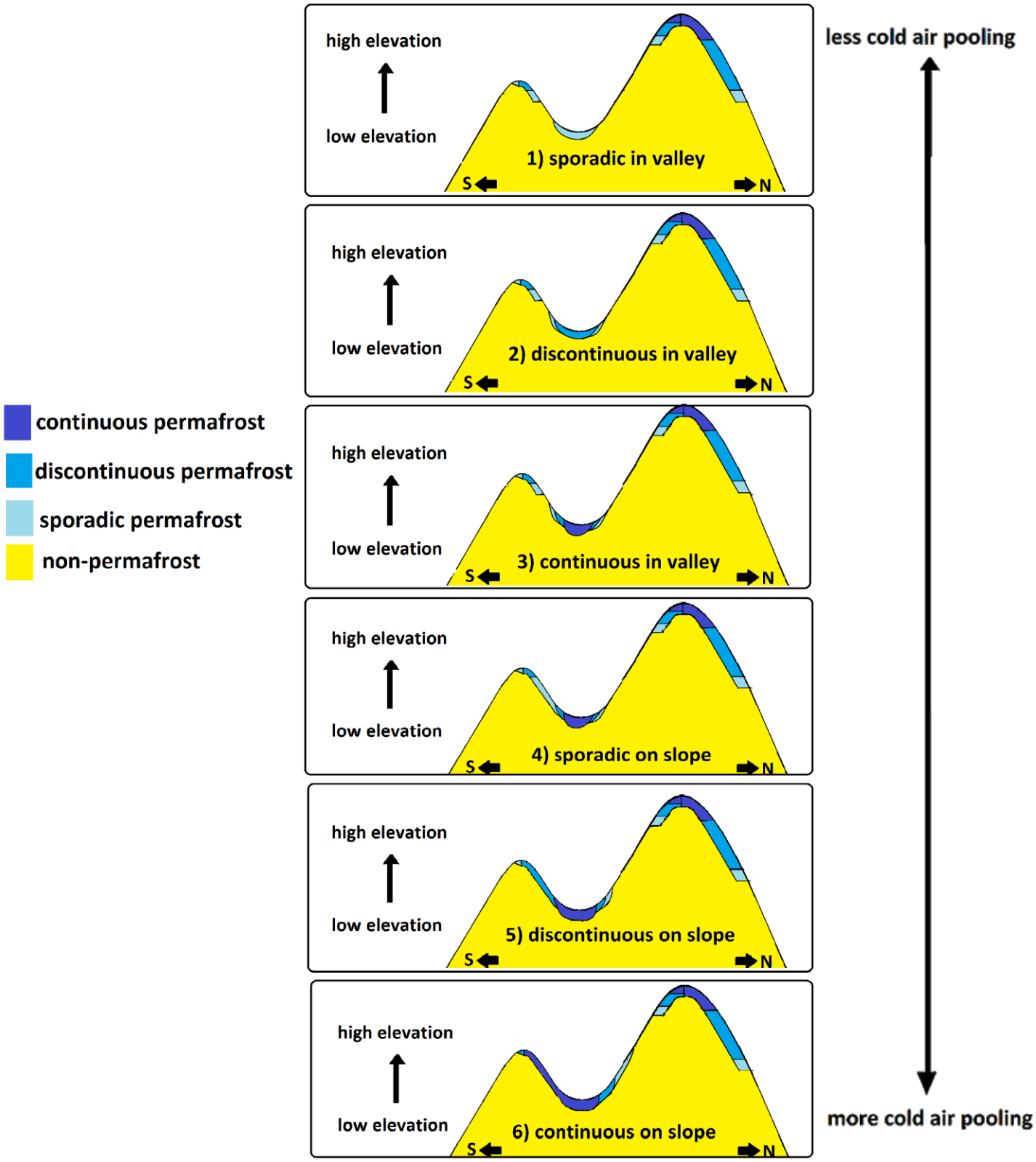

Figure 85: A conceptual model of some of the possible variations in the altitudinal zonation for mountain permafrost impacted by cold air drainage

The inclusion of cold air drainage or indicator vegetation assemblages in permafrost distribution models is challenging. In recent permafrost modeling efforts, the issue of incorporating the effects of inverted or weak surface lapse rates has been addressed at the regional scale (e.g. Bonnaventure and Lewkowicz 2012). In contrast, the dominant species variable has not been used in most permafrost distribution models since its inclusion is feasible only for small areas (Kremer et al. 2011). This is because species composition can vary over short distances and is generally not mapped or modeled at larger scales. The indicator deciduous trees and the stunted *Picea mariana* in the study sites were found across a variety of elevation ranges depending on the specific conditions of each study site. This variety of elevations shows that indicator vegetation assemblages do not fall into specific altitudinal vegetation zones, as do the other vegetation covers whose transitions are discussed below.

In summary, even though transitions to indicator vegetation assemblages differ from the other vegetation transition examined, where permafrost occurs, changes in permafrost characteristics likely occur at their boundaries. Specifically, the results suggest that permafrost conditions can be expected to change at the boundaries of a vegetation cover dominated by stunted *Picea mariana*. Vegetation dominated by stunted *Picea mariana* is not part of the typical altitudinal zonation of permafrost. When such vegetation cover occurs at lower elevations, it is likely linked to cold air drainage. However, the knowledge that permafrost conditions change with these vegetation transitions is of limited use for large scale modeling where species composition is not specified. Model inputs such as treeline and shrub limit elevation are more feasible at larger scales, but the results indicate that permafrost conditions do not necessarily change at these vegetation transitions.

6.2 Transition from tundra to shrubs

Two of the sites sample the vegetation transition from tundra to shrub patches and provide insight into the changes in permafrost conditions. The sites appear to be generally underlain by deep permafrost with some notable changes in the permafrost extents, either in the form of possible localized taliks, sections of thinner permafrost or breaks in the permafrost (Figure 86).

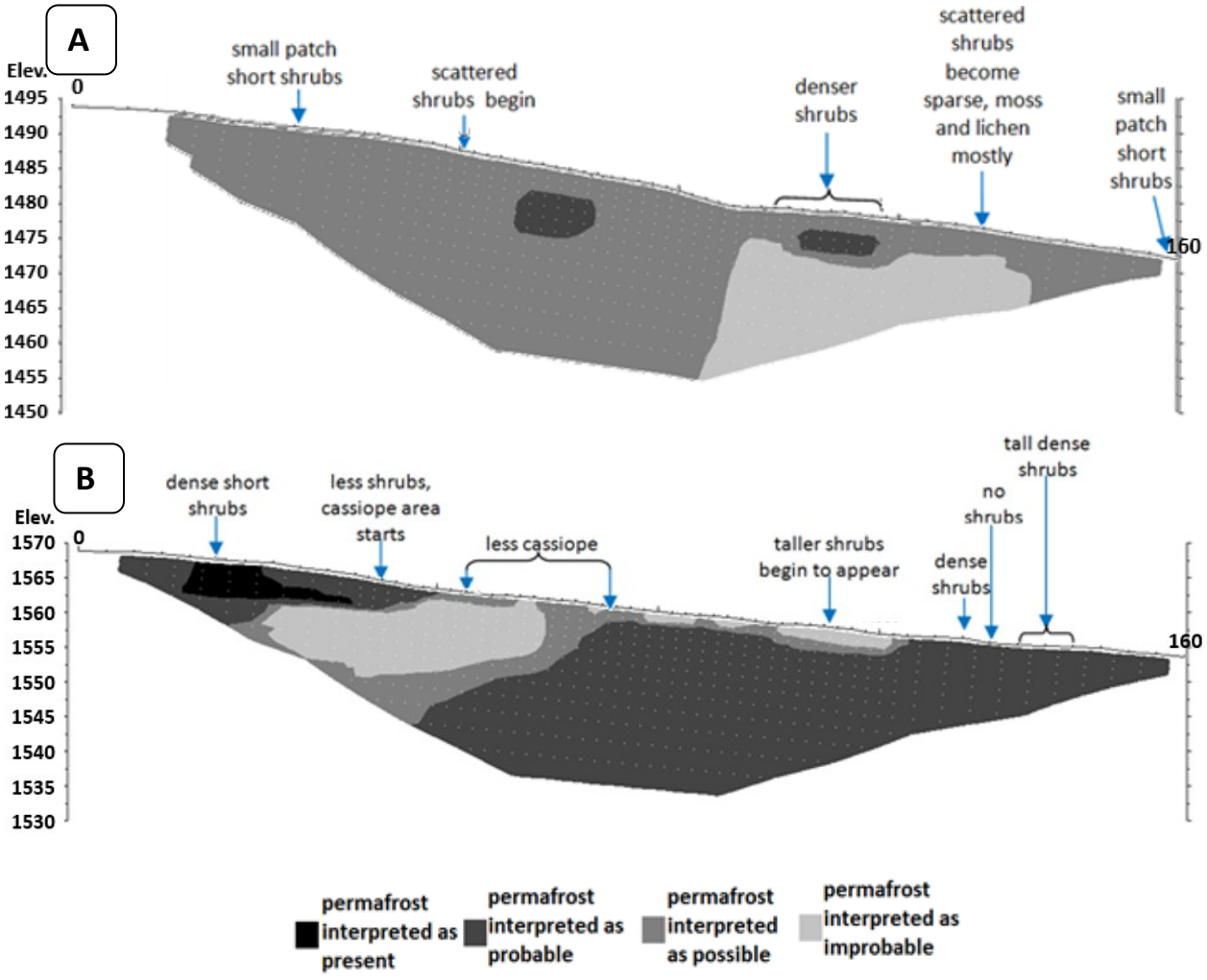

Figure 86: Permafrost interpretation image annotated with vegetation for tundra/shrub transitions at (A) Site 1 and (B) Site 6

The areas inferred to be permafrost improbable (light grey in Figure 86) relate to differing vegetation and surficial conditions. At Site 1, denser shrubs begin near the start of the permafrost improbable area, but the more prominent change is the sharp alteration in slope that may act as a snow-trap (Palmer et al. 2012). A greater snow cover would insulate the ground and could explain the thinner permafrost and sub-permafrost talik interpreted in this section. Other possible explanations include ground water flow within the permafrost improbable area. Such a network might even reach the ground surface and be replenished by runoff if a break in permafrost occurs in the area above it, classified as permafrost possible. At Site 6, fewer *Cassiope* sp. and shrubs occur where the inferred talik initially reaches the ground surface. Fewer *Cassiope* sp. might signal a slightly longer snow-free period while fewer shrubs would likely provide less shade, both producing warmer ground temperatures in the summer.

The only area where permafrost is interpreted to be present with confidence at the two sites also relates to vegetation and slope changes. Permafrost is confirmed at Site 6 in a small topographic hollow near the start of the profile with dense short shrubs. Climate station data indicate a considerable snowpack is usually present in this hollow from October to late May.

The conditions under which permafrost and possible taliks are inferred to occur at these two sites underline the importance of micro-topography, snow cover, and ground water flow on permafrost distribution. Topography may have complex influences on permafrost. For instance, the decrease in slope at Site 1 is associated with the inferred thinning of permafrost; while the hollow at Site 6 is associated with the presence of permafrost. Micro-topography and slope aspect can create wind protected hollows that favour snow accumulation. Snow cover and its insulating properties can either reduce heat entering the ground or exiting it depending on the

snow cover thickness and the timing of snow coverage (Matsuoka 2001). A thin early winter snow cover (<15 cm) results in greater heat loss from ground leading to intense ground cooling in autumn which can be preserved by a deeper snow cover in winter which acts as a thermal insulator and shields energy exchange between the ground and atmosphere (Otto et al. 2012). Heat transfer is also influenced by moisture contents, notably due to the difference in frozen and unfrozen thermal conductivity and latent heat effects. Active circulation of water above, within and beneath permafrost can also maintain taliks, promote thawing or retard new permafrost for forming (Hopkins et al. 1955 as cited by Williams, 1970; Woo 2012).

The findings for these two alpine tundra sites correspond with those from a previous resistivity investigation near Site 6. A 360-m long ERT profile across the Mt McIntyre summit and onto the north-eastern slope of the mountain exhibited no obvious resistivity layering (Lewkowicz et al. 2011). The resistivity values modeled for that long profile are within the range of values obtained for sites 1 and 6 in the present study, but are often lower. This may be because the current profiles were obtained in more ice-rich deposits or because they were undertaken two months earlier in the thaw season, which would mean near-surface ground temperatures were lower (e.g. the temperature of the 4 m sensor in the Mt McIntyre borehole increases from below 0°C to about +2°C over the two summer months). The 2011 tomogram also includes a large negative resistivity anomaly, less than 1 kΩm, which coincided with the start of a nearby blockstream and the presence of *Cassiope* sp. (Lewkowicz et al. 2011). It was suggested that this could represent an open talik caused by deep, late-lying snow cover and groundwater flow (Lewkowicz et al. 2011). The low resistivity anomaly at Site 1 is interpreted similarly, but it could also be permafrost since most of the resistivity values are within the range interpreted as permafrost for Mt McIntyre in Lewkowicz et al. (2011).

Overall, even though vegetation changes sometimes reflect changes in permafrost, other surface changes occur at these transitions as well, notably in micro-topography or surficial materials. These likely affect snow cover patterns and potentially groundwater patterns. Both can be linked to permafrost conditions (Otto et al. 2012; Woo 2012). At the limited number of sites sampled, changes in shrub density or height in the tundra shrub ecotone do not consistently correspond with observed or inferred changes in permafrost.

At Site 7, permafrost changes (Figure 87) are more closely linked to topographic changes than to variations in shrub height or density.

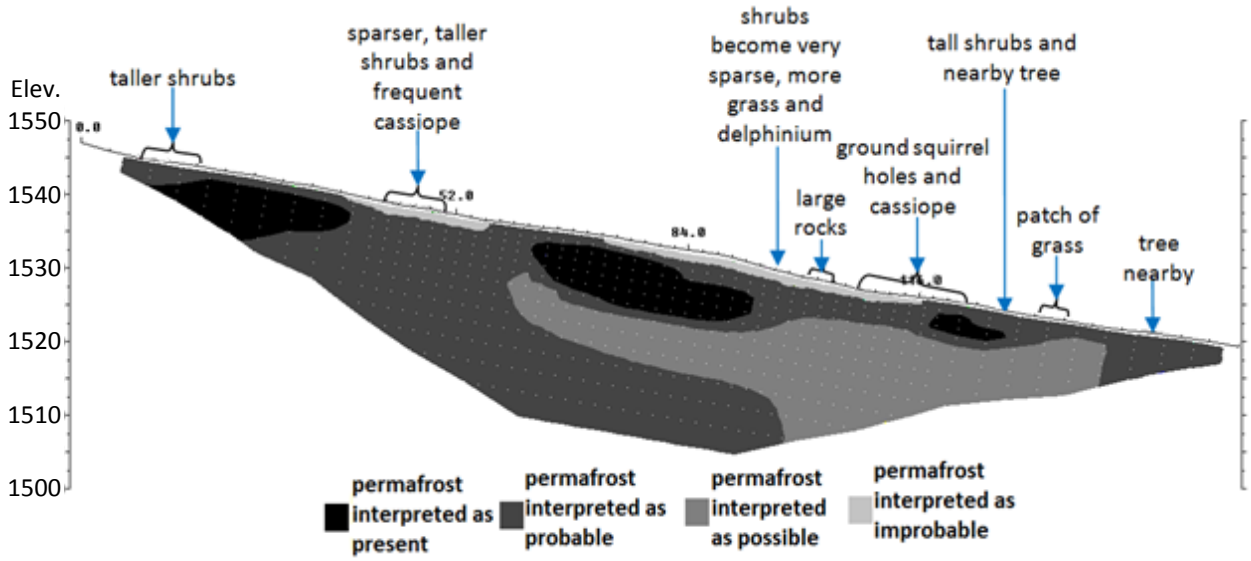

Figure 87: Permafrost interpretation image annotated with vegetation notes for Site 7

This site samples a part of the Mt McIntyre slope dominated by shrubs and no notable vegetation transitions, other than small-scale variations in shrub height and density, are traversed. Approximately only half of the small-scale vegetation variations correspond to noticeable changes in resistivity. Slope changes, possibly corresponding to the presence of solifluction steps, fit better with the transitions to and from areas of higher resistivity that occur at intervals

down the slope. Since permafrost is deemed possible in most of the profile, the higher resistivity values likely indicate areas with greater ice content or colder temperatures. The lower resistivity values in this profile are interpreted as unlikely for permafrost and may correspond to a talik, or they may simply reflect changes in the geology.

Site 7's results can be compared with the few other resistivity investigations completed on solifluction slopes (e.g. Kneisel 2010; Onaca et al. 2011). These studies suggest that resistivity patterns do reflect the solifluction process and permafrost conditions. Onaca et al. (2011) reported that a tongue-shaped lobe, which they had surveyed, had its own unique structure. They describe it as several individualized and undulating layers of variable thicknesses that they believe were created by solifluctional processes (Onaca et al. 2011). Kneisel (2010) found ERT to be "a valuable tool to map the spatial variability of frozen ground and soil moisture at solifluction/gelifluction slopes or terraces" (p.90). In tomograms from solifluction lobes and terraces, Kneisel found high resistive anomalies greater than 27 kΩm, and even greater than 100 kΩm in places. He reports that these higher resistivity areas indicate permafrost with variable ice content. These highly resistive, ice-rich permafrost areas tended to correspond with different solifluction lobes even though they were not always directly aligned. The results from Mt McIntyre also indicate clear alignment of highly resistivity areas with the steps attributed to solifluction, but whether these represent ice-rich zones is not known.

6.3 Transition through treeline

Five of the sites sample the vegetation transition from shrubs to forest, but only four provide insight into the changes in permafrost conditions occurring at that transition (Figure 88). The results from some of these sites suggest changes in permafrost that directly oppose initial expectations. Specifically, it was hypothesised that the active layer would deepen and that permafrost would thin or disappear as profiles extended from above to below alpine treelines. However, most of the results do not support these two hypotheses.

The active layer thickness, which is central to the first hypothesis, could not be adequately assessed across any of the four profiles with the methods used. One limitation was that surveying did not take place during maximum thaw. In addition, frost probe and resistivity data were of limited use in assessing active layer thickness due to the sites' surficial geology. The high clast content prevented the probe from reaching the frost table, and it also increased the near-surface resistivity values in the tomograms, obscuring the typical "active layer over permafrost" resistivity signal, which has lower resistivity values above higher values.

Surficial geology posing a problem for active layer measurements is a challenge researchers often face at mountain and slope sites (e.g. Harris 1987; Oldenborger 2010). To overcome the challenge, researchers may conduct ERT surveys with smaller spacing between electrodes (e.g. Hauck et al. 2007) and apply saltwater to the electrodes for improved contact (e.g. Hauck and Mühll 2003), use buried temperature sensors (e.g. Adlam et al. 2010) or drill boreholes (e.g. Marchenko et al. 2007). The methods in the present study were limited due to logistical constraints. Still, the depth of the frost table was measured at a few locations.

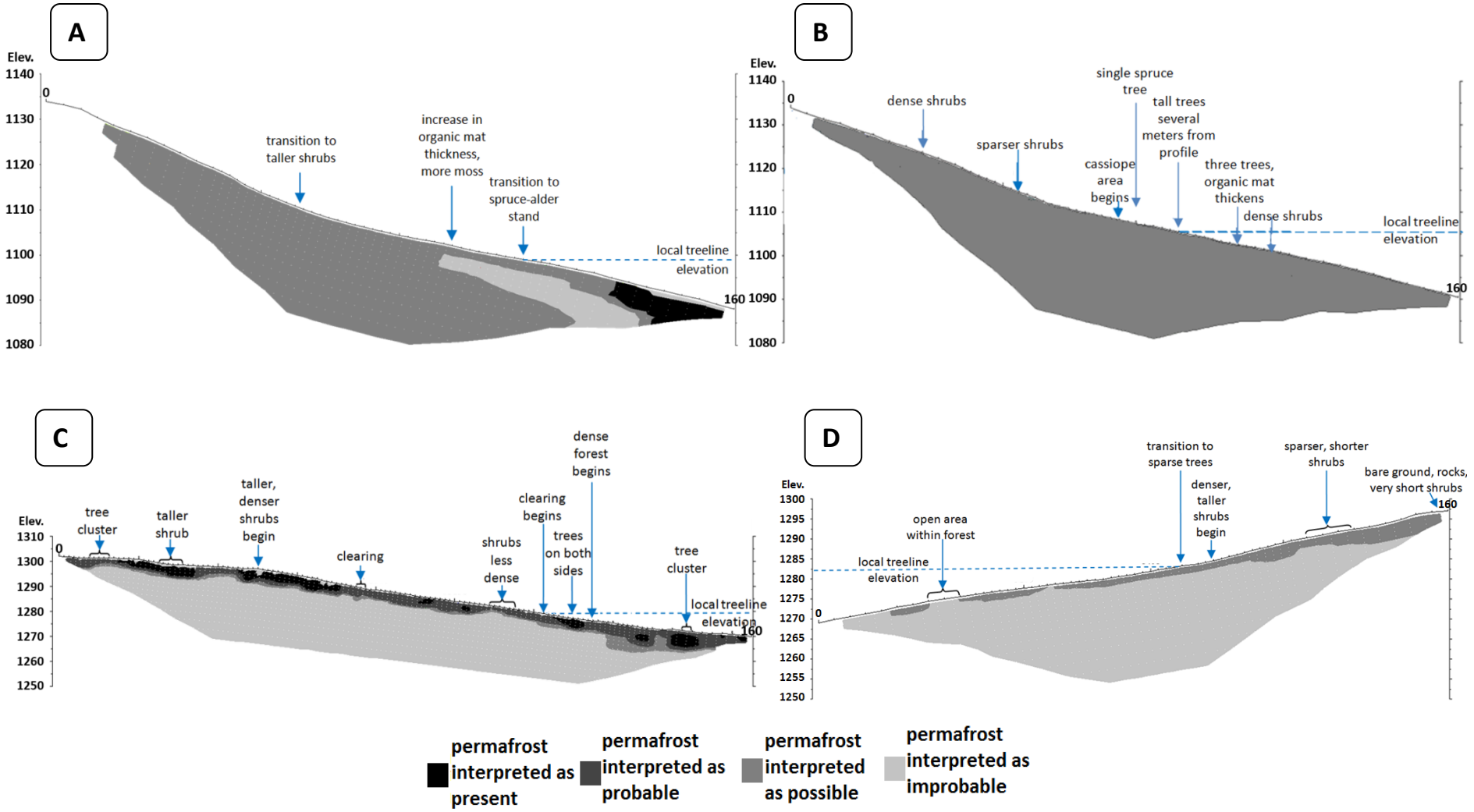

Figure 88: Permafrost interpretation images annotated with vegetation notes for sites sampling treeline transitions near Dawson, (A) Site 9 and (B) Site 10, and near Whitehorse, (C) Site 4 and (D) Site 5.

The limited findings do not seem to support the hypothesis of active layer deepening. Indeed, permafrost was interpreted as the cause of probe refusal at least once within the forest at every one of the four sites. Permafrost might not have been encountered through probing at all if the active layer was significantly deeper. However, false positive probe interpretations can occur and a confident interpretation of permafrost requires other sources of validation. For some sites, Site 8 and Site 5 for instance, the only indication of permafrost came from probe data. For other sites, like Site 9 and Site 4, high resistivity layers, temperature data and/or pit verification strongly supported the interpretation of near-surface permafrost. At Site 4, permafrost even occurred near the surface in the forest while the ground was confirmed unfrozen at similar depths upslope. All this evidence supports the interpretation of a thinning of the active layer. Such a change in the active layer is contrary to the first hypothesis.

Similarly, the four sites offer evidence, though limited, of a change in permafrost that opposes the second hypothesis. The results either lack permafrost being interpreted as present or probable, or they suggest that permafrost became thicker below treeline. The permafrost interpretations for Site 5 and Site 10 (Figure 88 B and D) are very uncertain and no firm interpretation of permafrost thickness or depth is made. At Site 9, a body of permafrost is interpreted with more confidence (Figure 88 A). This inferred body appears under the forest adjacent to an area of low resistivity that likely represents a talik. This potential talik extends near the surface upslope, but below the treeline it is only interpreted at greater depths. The extents of the potential talik and of the permafrost body that is interpreted with confidence suggest a thickening permafrost below treeline at Site 9. In the thin body of permafrost interpreted at Site 4 (Figure 88 C), some thinning or breaks occur. However permafrost appears

to thicken once the profile passes into the dense forest. A thicker organic mat also occurs within the forested part of the profile where the trees likely impact the rate of organic matter decomposition (Jorgenson et al. 2010). At Site 4, the thicker mat coincides with an area of higher resistivity that likely indicates colder or more ice-rich permafrost. Indeed, visible ice was exposed in a within the forest, although this was further along the profile.

Several possible causes exist for the increase in permafrost thickness and decrease in ground temperatures within the forest. These include increased shading from the forest canopy, more gradual snow accumulations contributing to more rapid freezeback (O'Neill et al. 2015) or the greater accumulation of organic matter. The change could be a local occurrence or be part of a larger trend.

Overall, the findings for transitions through treelines represent unexpected results and may provide new insights to the existing body of knowledge. Little is known about permafrost conditions directly at treeline. We found no other published work that examined permafrost thickness across treeline at the same scale so the ERT profiles appear to be the first of their kind. The hypothesis that the permafrost would thin or disappear was based mainly on the large scale concept of altitudinal zonation of permafrost. The breakdown of continuous permafrost into smaller patches was thought to perhaps coincide with a vegetation transition. The fact that permafrost did not seem to thin or disappear below treeline at the investigated sites does not mean that this does not occur and perhaps longer or additional profiles downslope within the forest might reveal such a trend.

The hypothesis that active layers would thin was strongly based in the literature. A number of studies, conducted in both vegetated and unvegetated regions, suggest that the average

active layer depth usually decreases with increasing elevation (e.g. Harris 1987; Marchenko et al. 2007; Adlam et al. 2010). However, as discussed above, active layer thickness could not be adequately assessed from the results. It is possible that several of the studies commenting on active layer thickness in mountain environments also provide only a limited view of active layer trends. The studies' findings may be constrained to their sampling sites or conditions specific to their area. For instance, boreholes in the Ak-Shiyrak Mountain Range revealed a decrease in active layer thickness within 3200-4000 m asl (Marchenko et al. 2007), but the active layer at higher elevations was not assessed. Similarly, Harris (1987) encountered problems probing above 1211 m asl in Alberta and did not examine active layer depth above that. In addition, he found an anomalous relationship between the active layer thickness and altitude on Outpost Mountain, Yukon (Harris 1987). Thus, the evidence for thinning active layers with increased elevations is compelling, but not without exceptions.

A more complex model of permafrost and its active layer (Figure 89) may better represent trends on certain mountains underlain by permafrost.

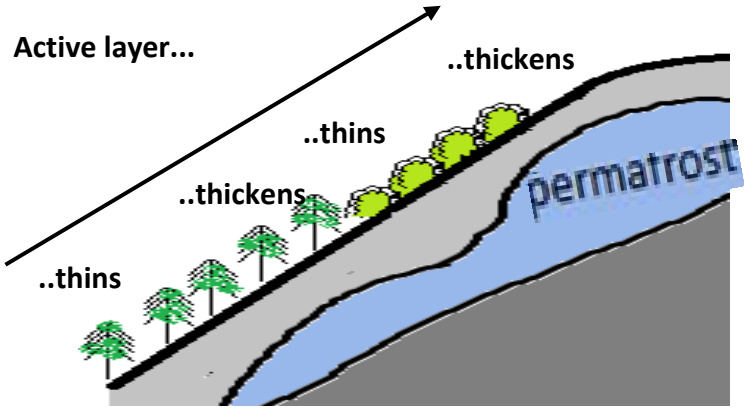

Figure 89: Conceptual model of possible active layer changes with elevation in mountain permafrost

Active layers could initially thin with increased elevation due to the general slow decrease in air temperature. But, they then might increase in thickness as changes in surficial geology, vegetation cover/organic mat and snow distribution occur.

Such a conceptual model (Figure 89) would fit with various diverging findings. The trends of active layers thinning with elevation would fit when corresponding to lower parts of slopes (e.g. Harris 1987). The deepening active layer upslope through treeline at Site 4 would match the mid-slope portion of the model. The deep active layer on Mt McIntyre's summit would correspond well with the model. Even the schematic landscape cross-section describing permafrost in the Klondike Plateau ecoregion (see Figure 8) fits in with the idea of active layers initially thinning with elevation and then thickening further upslope.

In summary, at the scale examined, treeline was not as important a demarcation point for changes in the permafrost characteristics examined. This is probably because the factors controlling permafrost distribution and characteristics are somewhat different than the factors controlling treeline. Climate and air temperatures may impact both permafrost and treelines. However, vegetation characteristics are more greatly influenced by summer climate than winter climate, while ground surface temperatures are critically affected by the winter regime (Palmer et al. 2012, O'Neill et al. 2015).

6.4 Comparison of altitudinal and latitudinal permafrost changes

An important aim of the study was to investigate whether the changes in permafrost contiguity over a few hundred meters of elevation differ from the changes that take place with latitude over hundreds of kilometers. Changes in permafrost contiguity remain poorly understood

for latitudinal and altitudinal transitions. Still, there appear to be both similarities and differences between permafrost trends across altitudinal and latitudinal forest-tundra ecotones.

One similarity is the importance of local controls on permafrost boundaries. Results from the present study and from others reveal that snow cover, organic mat, and surficial geology impact permafrost characteristics and extent in altitudinal and latitudinal forest-tundra ecotones. This study's results indicate many instances where small-scale changes in micro-topography create, sometimes in combination with shrub patches, protected areas that favour snow accumulation. The influence of changes in micro-topography on snow and ground temperature may be of greater importance to permafrost distribution and characteristics than the transition from one vegetation type to another. Other, more detailed investigations into snow and permafrost ecotone dynamics report that marked changes in snow conditions across the ecotonecan cause significant differences in ground temperatures at tundra and forest sites (e.g. Burn and Kokelj 2009; Palmer et al. 2012; O'Neill et al. 2015). In the present study, changes in mapped surficial geology and measured organic mat thickness also appear to correspond with changes in the permafrost characteristics examined. For example, thickening of the organic layer often occurred where permafrost was interpreted to begin (Site 2), or to become thicker or more ice-rich (Sites 4, 7, 11 and 12). Similarly, in a latitudinal transect in the sporadic/discontinuous permafrost zone, local controls influencing permafrost boundaries included organic mat thickness, changes in surficial deposits and the presence of standing or running water (Bellehumeur-Génier, 2016). All of these local factors are likely responsible for the "significant variability of thermal regime and thickness of permafrost within short distances even at the same altitudinal level" (Ermolin et al. 1989; Gorbunov et al. 1996; as cited by Marchenko et al. 2007).

Even though significant spatial variability in ground temperatures may appear in both altitudinal and latitudinal forest-tundra ecotones, more variability may be present in altitudinal ecotones. Graae et al. (2012) found a significant increase in the intra-site variation in soil surface mean annual temperature with altitude. The range of mean annual soil surface temperatures between microsites above altitudinal treeline was larger than the range between microsites below treeline. This altitudinal variability could be a source of difference in permafrost conditions between the latitudinal and altitudinal ecotones. However, an increase in the range of permafrost temperatures has also been reported for a latitudinal treeline (Smith et al. 2010). More research would be required to determine if altitudinal variability differs significantly from latitudinal variability.

Another difference between the permafrost trends across altitudinal and latitudinal ecotones results from the propensity of alpine environments for cold air drainage and surface lapse rate inversions. The occurrence of continuous bodies of permafrost interpreted within the forested slopes and valleys of the present study is often attributable to cold-air drainage. O'Neill et al. (2015) recently published similar findings from their study on permafrost conditions across an alpine treeline in the continuous permafrost zone. With sites between 30 and 500 m asl, on Peel Plateau, Northwest Territories, they found higher annual temperatures at the permafrost surface in the alpine tundra than the lowland forest (O'Neill et al. 2015). This, as the authors point out, contrasts with the northward decrease in permafrost temperatures found across latitudinal and altitudinal treelines elsewhere in the western Arctic (e.g. Burn and Kokelj 2009; Bonnaventure and Lewkowicz 2012b; Palmer et al. 2012). However, they suggest that annual temperatures at the permafrost surface increasing with elevation may be common in Arctic mountain environments, due to the frequent winter inversions (O'Neill et al. 2015). The results

from the present study support the importance of inversions on permafrost distribution in mountainous areas within the discontinuous permafrost zone. This influence on permafrost is not present in latitudinal forest-tundra ecotones.

Overall, this comparison of altitudinal and latitudinal permafrost changes revealed three ideas. First, local controls on permafrost boundaries play a significant role on permafrost distribution across both altitudinal and latitudinal forest-tundra ecotones. Second, there may be more spatial variability in permafrost conditions with increased altitude than with increased latitude. Third, inversions can modify altitudinal permafrost trends further differentiating altitudinal permafrost changes from latitudinal changes.

6.5 Challenges and limitations

There were several key challenges and limitations for this study that limit the strength of the conclusions. These challenges were both conceptual and practical, and include the semi-qualitative nature of modeled resistivity interpretation, the technical difficulties experienced in the field, the limited sample size, and the dynamic nature.

Tomograms and modeled resistivity profiles always contain some degree of measuring and modelling errors. For the purposes of permafrost interpretation, precise values are not needed since overall resistivity patterns and changes are key. Still, an awareness of modelling errors helps prevent erroneous interpretations. Determining the source and possible impact of tomogram errors often requires experienced judgement.

Even without tomogram errors, interpreting permafrost extent from resistivity values can be quite challenging. Resistivity values alone do not indicate permafrost absence or presence, since the resistivity of frozen ground can vary significantly and can change spatially and

temporally with ground conditions. Furthermore, many different combinations of ground conditions can create the same range of resistivity values or the same type of resistivity pattern.

Certain surficial geologies can produce high resistivity surface layers similar to thin permafrost layers. Notably, areas of colluvium over till surveyed in Pangnirtung, Nunavut, revealed resistive surface layers with more conductive underlying material (Oldenborger 2010). The active layer could not be resolved even where 1 m thick, and upslope increases in resistivity were thought to relate to high boulder occurrence (Oldenborger 2010). Similar resistivity patterns consisting of high resistivity near-surface layers occur at Site 2 and Site 4, and in the upslope portions of Site 5 and Site 10. Even on Site 3's south-facing inferred permafrost-free slope, colluvium produced higher resistivity values near the surface upslope than elsewhere in the profile. Careful examination of the extent of a high resistive layer, of its transition to lower resistivity values, and of the surficial geology along with additional ground-truthing was required to interpret either thin layers of near-surface permafrost or highly resistive unfrozen surficial material. In some cases, the lack of information prevented confident interpretations.

Technical difficulties also prevented the collection of sufficient information for permafrost interpretation at Site 8. At this site, problems arose during the ERT survey. Acceptable resistivity values repeatedly failed to be measured between multiple electrodes even after attempts to establish better ground contact. Due to time constraints, the survey was continued without obtaining measurements for the problematic data points. Unfortunately, more than half the data points in the profile were missing by the end and the modeled resistivity profile could not be used. What caused so many measurement errors remains unclear. Poor ground

contact at this site may be one of the reasons. The loss of data for this site particularly hindered the analysis since Site 8 was the only site that sampled treeline on Mt McIntyre.

The sample size was already smaller than originally planned as each survey was logistically challenging in the terrain sampled. The results obtained, however, varied from site to site and even at sites that sampled the same slope (Sites 4 and 5 by the Mt Sima Trail, and 9 and 10 near Dawson). The objective was to better understand how permafrost changes as vegetation cover transitions down slopes. But in order to obtain a realistic understanding, increased sampling across slopes at vegetation transition is needed. The changes in permafrost observed at a few sites need to be observed consistently at many more sites before it can be concluded that the changes are part of a landscape trend and not simply due to local conditions. Additional profiles further down slope within the forest might also assist in understanding the relation between permafrost elevation and vegetation.

The dynamic nature of permafrost also limits confidence in the findings. A permafrost body's genesis conditions and its history strongly influence permafrost characteristics. Indeed, a recent project initiating measurements of permafrost patch size in the sporadic/discontinuous zone found that permafrost patch size depended on local site settings, the current site climate, and the time since the permafrost became climatically unsustainable (Olivier Bellehumeur-Génier, 2016). If a permafrost body is a recent phenomenon, it will have different characteristics and distribution than if it is an older degrading body of permafrost previously part of a larger permafrost body. Thus, the changes in permafrost contiguity along both altitudinal and latitudinal gradients would vary as a function of the permafrost history.

The study scope was necessarily limited and excluded detailed investigations of the permafrost history or climatic sustainability. There are some indications that the air temperatures are increasing at the study sites based on data from climate stations, however it is unclear if the temperatures are warming at the top of permafrost. On the geologic scale, changes in permafrost distribution in North America are still proceeding to bring it into equilibrium with contemporary climates (Shur and Jorgenson 2007), and respond to the climate's warming since the Little Ice Age. Thus, at the small spatial scale examined, permafrost extents may not all be at equilibrium either. Therefore, the distribution of permafrost across alpine vegetation transitions is likely different in mountainous areas with different permafrost histories. It could be worthwhile to examine alpine permafrost conditions at vegetation transitions in other areas where permafrost is known to currently be climatically sustainable and to have been so for a significant time.

7.0 Conclusions

This research aimed to investigate the relationships between permafrost, elevation and vegetation cover in mountainous areas within the discontinuous permafrost zone of the Yukon. The need for a better understanding of the permafrost characteristics at vegetation transitions and for increased knowledge about boundaries between permafrost and non-permafrost terrain provided the context for this project. Such knowledge is needed for the development of models representing the responses of the permafrost zone to climate change. The primary objective was to gather preliminary information on permafrost contiguity conditions at vegetation transitions on select slopes. Where possible hypotheses based on the known impact of different vegetation covers on ground thermal regimes were also tested.

ERT profiles and site surveys were completed at 12 sites that sample various vegetation transitions. Organic layer thickness and vegetative species composition were recorded along each profile. Ground-truthing via frost probing, pit digging, and ground temperature data records from on-site climate stations aided in the analysis of ERT profiles. Permafrost conditions and contiguity were characterized with varying confidence. These were compared to surficial changes such as observed variations in vegetation, organic mat, slope, and sediment, as well as inferred changes in snow cover.

Following these analyses, the following conclusions were reached:

(1) ERT can be used to improve understanding of the complex relations between elevation, vegetation and permafrost, but with important challenges and limitations.

(2) Where permafrost with indicator vegetation occurred, changes in permafrost characteristics occurred at the boundaries of indicator vegetation. However, the indicator vegetation is not part of the altitudinal zonation model.

(3) Cold air drainage explains the presence of permafrost at elevations lower than expected by a linear altitudinal zonation model and differentiates altitudinal permafrost changes from latitudinal changes.

(4) Changes in organic mat, surficial geology, and snow cover (via micro-topography) appeared more important that vegetation changes. Even where vegetation changes sometimes did reflected changes in permafrost at the sites, other surficial changes also usually occurred at the permafrost transitions.

(5) Local controls on permafrost boundaries appear to play a significant role on permafrost distribution across both altitudinal and latitudinal forest-tundra ecotones.

(6) At the scale examined, treeline was not as important a demarcation point for changes in permafrost distribution as initially thought. Hypotheses regarding permafrost and active layer thickness changing at treeline were not supported.

(7) A more complex spatial model of permafrost and its active layer may be required to represent the trends on certain mountains underlain by permafrost.

Due to its scope, this thesis did not examine the permafrost's climatic sustainability, or permafrost contiguity at the larger slope-wide scale. Furthermore, interpretations were limited due to limited ground-truthing. Future research possibilities to further our understanding of the

relationship between permafrost, elevation and vegetation cover in the study area could include the completion of additional surveys across and down slopes and improved ground-truthing. A closer examination of snow cover regimes might also yield findings that could help improve understanding of the complex interactions between elevation, vegetation and permafrost.

References

Adlam, L.S. et al., 2010. Temporal and Spatial Variation in Active Layer Depth in the McMurdo Sound Region, Antarctica. *Antarctic Science*, 22(1), pp.45–52.

Bellehumeur-Génier, O., 2014. M.Sc Thesis Proposal.[Word document] Unpublished.

Bellehumeur-Génier, O., 2016. *Trends in permafrost patch size near the margins of discontinuous permafrost, southern Yukon and northern B.C.*, University of Ottawa.

Benkert, B.E. et al., 2015. Dawson City Landscape Hazards: Geoscience Mapping for Climate Change Adaptation Planning. Northern Climate ExChange, Yukon Research Centre, Yukon College. 166 p. and 2 maps.

Bevington, A., 2016. Database.[Excel files] Unpublished.

Bevington, A., 2015. *Towards a TTOP-Model of Permafrost Distribution for Three Areas in Yukon and Northern British Columbia*, University of Ottawa.

Biskaborn, B.K., et al., 2015. The new database of the Global Terrestrial Network for Permafrost (GTN-P), Earth System Science Data, 7 , pp.245-259 . doi: 10.5194/essd-7-245-2015

Bond, J., 2004. Late Wisconsinan McConnell glaciation of the Whitehorse map area (105D), Yukon. In: Yukon Exploration and Geology 2003, D.S. Emond and L.L. Lewis (eds.), Yukon Geological Survey, pp.73-88.

Bonnaventure, P.P. et al., 2012. A Permafrost Probability Model for the Southern Yukon and Northern British Columbia, Canada. *Permafrost and Periglacial Processes*, 23, pp.52–68. Available at: http://permafrost.gov.yk.ca/data/arcgis/.

Bonnaventure, P.P. and Lamoureux, S.F., 2013. The active layer: a conceptual review of monitoring, modelling techniques and changes in a warming climate. *Progress in Physical Geography*. 37, pp.352-376..

Bonnaventure, P.P. and Lewkowicz, A.G., 2013. Impacts of mean annual air temperature change on a regional permafrost probability model for the southern Yukon and northern British Columbia, Canada. *The Cryosphere (Online),* (3), pp.935-946.

Bonnaventure, P.P. and Lewkowicz, A.G., 2012. Permafrost probability modeling above and below treeline, Yukon, Canada. *Cold Regions Science and Technology*, 79-80, pp.92–106.

Bonnaventure, P.P. and Lewkowicz, A.G., 2011. Modelling climate change effects on the spatial distribution of mountain permafrost at three sites in northwest Canada. *Climatic Change*, 105(1-2), pp.293–312.

Bonnaventure, P.P. and Lewkowicz, A.G., 2008. Mountain permafrost probability mapping using the BTS method in two climatically dissimilar locations, northwest Canada. *Canadian Journal of Earth Sciences*, 45(4), pp.443-455.

Brown, J., Hinkel, K.M. and Nelson, F.E., 2000. The circumpolar active layer monitoring (calm) program:

Research designs and initial results 1. *Polar geography*, 24(3), pp.166–258.

Brown, R.J.E., 1966. Influence of vegetation on permafrost. In *Permafrost international conference: proceedings 11-15 November 1963 Lafayette, Indiana*. National Academies, pp.20–25.

Burgess, M.M., Judge, A.S. and Taylor, A.E., 1982. Yukon ground temperature data collection — 1966 to August 1981. Open File 82–1.

Burn, C.R. and Kokelj, S. V, 2009. The environment and permafrost of the Mackenzie Delta area. *Permafrost and Periglacial Processes*, 20(2), pp.83–105.

Carey, S.K. and Woo, M., 2005. Freezing of Subarctic Hillslopes, Wolf Creek Basin, Yukon, Canada. *Arctic, Antarctic, and Alpine Research*, 37(1), pp.1–10.

Chabot, B., 2012. *Physiological Ecology of North American Plant Communities*, Springer Science and Business Media.

Cody, W.J., 2000. *Flora of the Yukon territory*, NRC Research Press.

Colette, A., Chow, F.K. and Street, R.L., 2003. A numerical study of inversion-layer breakup and the effects of topographic shading in idealized valleys. *Journal of Applied Meteorology*, 42(9), pp.1255-1272.

Cooper, C.F. et al., 1986. Carbon dioxide enhancement of tree growth at high elevations. *Science*, 231(4740), pp.859–860.

Corte, A.E., 1985. Comparative study of geocryogenic (periglacial) conditions, features and processes in the Andes and Himalayas. The Andes. *Acta Geocriogenica*, 3, pp.35–48.

Danby, R., 2011. Monitoring Forest–Tundra Ecotones at Multiple Scales. *Geography Compass,* 5(9), pp.623-640.

Danby, R., and Hik, D., 2007a. Variability, contingency and rapid change in recent subarctic alpine tree line dynamics. *Journal of Ecology,* 95(2), pp.352-363.

Danby, R., and Hik, D., 2007b. Evidence of Recent Treeline Dynamics in Southwest Yukon from Aerial Photographs. *Arctic,* 60(4), pp.411-420.

DJI, 2014. Phantom 2 Vision+. Available at: http://www.dji.com/product/phantom-2-vision-plus/spec [Accessed January 1, 2015].

Duk-Rodkin, A. and Barendregt, R.W., 2011. Stratigraphical Record of Glacials/Interglacials in Northwes Canada. *Developments in Quaternary Science*, 15, pp.691–698.

Duk-Rodkin, A. 1996. Surficial geology, Dawson, Yukon Territory. Geological Survey of Canada, Open File 3288, scale 1:250,000.

EBA Engineering Consultants Ltd, 1989. *Geotechnical evaluation, C-2 Land Claim area, Dawson City, Yukon*, Whitehorse, Yukon.

EBA Engineering Consultants Ltd, 1995. *Geotechnical evaluation, Fox Street sewer extension and airport*

subdivision sewer servicing, Whitehorse, Yukon.

EBA Engineering Consultants Ltd, 2003. *Regional Ecosystem Classification and Mapping of the Southern Lakes and Pelly Mountains Ecoregions*, Whitehorse, Yukon.

Echotech, 2005. Electrical resistivity. [Image] Available at: http://www.echotech.com/electrical_resistivity.htm [Accessed January 1, 2015]

Environment Canada, 2016. Canadian Climate Data.[Data] Available at: http://climate.weatheroffice.gc.ca/climateData/canada_e.html.

Ermolin, E.D., Nemov, A.E. and Popov, M.V., 1989. Geotermicheskaya harakteristika mestorojdeniya Kumtore, (Geothermal characteristic of the Kumtor gold mine). *Geocryological Investigations in the Mountains of USSR. (in Russian)*, pp.31–40.

Etzelmller, B. and Frauenfelder, R., 2009. Factors Controlling The Distribution of Mountain Permafrost in The Northern Hemisphere and Their Influence on Sediment Transfer. *Arctic, Antarctic, and Alpine Research*, 41(1), pp.48–58.

Etzelmüller, B. et al., 2006. Mountain permafrost distribution modelling using a multi-criteria approach in the Hövsgöl area, northern Mongolia. *Permafrost and Periglacial Processes*, 17(2), pp.91–104.

Farbrot, H. et al., 2011. Air and ground temperature variations observed along elevation and continentality gradients in Southern Norway. *Permafrost and Periglacial Processes*, 22(4), pp.343–360.

Francis, S., Smith, S. and Janowicz, R., 1999. Intégration des données et la zonation écologique du bassin versant du ruisseau Wolf, In: *Bassin de recherche du ruisseau Wolf - hydrologie, écologie, environnement - Compte rendu de l'atelier tenu du 5 au 7 mars 1998 à Whitehorse (Yukon)*, J.W. Pomeroy and R.J. Granger (eds.) National Water Research Institute, pp.97-104.

French, H.M., 1998. An appraisal of cryostratigraphy in north-west Arctic Canada. *Permafrost and Periglacial Processes*, 9(4), pp.297–312.

French, H.M. and Heginbottom, J.A., 1983. *Guidebook to permafrost and related features of the Northern Yukon Territory and Mackenzie Delta, Canada*, Fairbanks: Fourth Internation Conference on Permafrost, University of Alaska.

Froese, D. et al. 2008. Ancient Permafrost and a Future, Warmer Arctic. *Science*, 321(5896), p.1648.

Gisnas, K. et al., 2014. A statistical approach to represent small-scale variability of permafrost temperatures due to snow cover. *Cryosphere,* 8(6), pp.2063-2074.

Gorbunov, A.P., 1978. Permafrost Investigations in High-Mountain Regions. *Arctic and Alpine Research*, 10(2), pp.283–294.

Gorbunov, A.P., Seversky, E.V. and Titkov, S.N., 1996. Geocriologiches- kie Usloviya Tyan-Shanya i Pamira (Geocryological Conditions of the Tien Shan and Pamir) Permafrost Institute publishers. (in Russian).

Gordey, S.P., 2008. Bedrock geology, Whitehorse (105D), Yukon. Geological Survey of Canada, Open File

5640, scale 1:250 000.

Graae, B.J. et al., 2012. On the use of weather data in ecological studies along altitudinal and latitudinal gradients. *Oikos*, 121(1), pp.3–19.

Grace, J., Berninger, F. and Nagy, L., 2002. Impacts of Climate Change on the Tree Line. *Annals of Botany*, 90(4), pp.537–544.

Gravis, G.F. et al., 1978. The Geocryological Characteristics of the Mongolian People's Republic and some Characteristics of Permafrost Development in the Past. In: Permafrost: Second International Conference, July 13-28, 1973: USSR Contribution, F.J. Snager and P.J. Hyde (eds.) National Academy of Science, pp.81-86.

Green, L.H. and Roddick, J.A., 1961. Geology, Dawson, Yukon Territory. Geological Survey of Canada, Map 1284A, scale 1:250 000.

Gruber, S. and Haeberli, W., 2007. Permafrost in steep bedrock slopes and its temperature-related destabilization following climate change. *Journal of Geophysical Research: Earth Surface*, 112(F2S18).

Gruber, S., Hoelzle, M. and Haeberli, W., 2004. Permafrost thaw and destabilization of Alpine rock walls in the hot summer of 2003. *Geophysical Research Letters*, 31(L13504). Gustavsson, T. et al., 1998. Development of temperature patterns during clear nights. *Journal of Applied Meteorology*, 37(6), pp.559-571.

Haeberli, W., 1973. Die Basis-Temperatur der winterlichen Schneedecke als moglicher Indikator fur die Verbreitung von Permafrost in den Alpen. *Z.Gletscherk.Glazialgeol.*, 9, pp.221–227.

Haeberli, W., 2013. Mountain permafrost — research frontiers and a special long-term challenge. *Cold Regions Science and Technology*, 96, pp.71–76.

Harper, K.A. et al., 2011. Tree spatial pattern within the forest-tundra ecotone: a comparison of sites across Canada. *Canadian Journal of Forest Research*, 41(3), pp.479-489.

Harris, C. et al., 2009. Permafrost and climate in Europe: Monitoring and modelling thermal, geomorphological and geotechnical responses. *Earth Science Reviews*, 92(3), pp.117–171.

Harris, C. et al., 2003. Warming permafrost in European mountains. *Global and Planetary Change*, 39(3), pp.215–225.

Harris, S.A., 1987. Altitude Trends in Permafrost Active Layer Thickness, Kluane Lake, Yukon Territory. *Arctic*, 40(3), pp.179–183.

Harris, S.A. and Brown, R.J.E., 1978. Plateau Mountain: a case study of alpine permafrost in the Canadian Rocky Mountains. *Proceedings of the 3rd International Conference on Permafrost, 10–13 July 1978, Edmonton, Alberta, Canada*, 1, pp.385–391.

Harsch, M.A. et al., 2009. Are treelines advancing? A global meta-analysis of treeline response to climate warming. *Ecology Letters*, 12(10), pp.1040–1049.

Hauck, C. et al., 2007. Geophysical identification of permafrost in Livingston Island, Maritime Antarctica.

Journal of Geophysical Research: Earth Surface, 112(2), pp.1–15.

Hauck, C. and Kneisel, C., 2008. *Applied geophysics in periglacial environments*, Cambridge University Press Cambridge.

Hauck, C. and Mühll, D.V., 2003. Inversion and interpretation of two-dimensional geoelectrical measurements for detecting permafrost in mountainous regions. *Permafrost and Periglacial Processes*, 14(4), pp.305–318.

Hauck, C., Vonder Mühll, D. and Maurer, H., 2003. Using DC resistivity tomography to detect and characterize mountain permafrost. *Geophysical Prospecting*, 51(4), pp.273–284.

Heginbottom, J.A., Dubreuil, M.A. and Harker, P.T., 1995. Canada -- Permafrost National Atlas of Canada. Map 2.1.

Hoelzle, M., 1992. Permafrost occurrence from BTS measurements and climatic parameters in the eastern Swiss Alps. *Permafrost and Periglacial Processes*, 3(2), pp.143–147.

Hopkins, D.M. et al., 1955. Permafrost and ground water in Alaska: U.S. Geological Survey, Professional Paper 264-F, pp.113-146.

Hughes, O.L. and Van Everdingen, R.O., 1978. Central Yukon- Alaska: guidebook for field trip No. 1. In *Third International Conference on Permafrost, Edmonton, July 10-13 1978*. National Research Council of Canada.

Isaksen, K. et al., 2011. Degrading Mountain Permafrost in Southern Norway: Spatial and Temporal Variability of Mean Ground Temperatures, 1999–2009. *Permafrost and Periglacial Processes*, 22(4), pp.361–377.

Isaksen, K. et al., 2002. Mountain permafrost distribution in Dovrefjell and Jotunheimen, southern Norway, based on BTS and DC resistivity tomography data. *Norsk Geografisk Tidsskrift - Norwegian Journal of Geography*, 56(2), pp.122–136.

Isaksen, K. et al., 2007. Recent warming of mountain permafrost in Svalbard and Scandinavia. *Journal of Geophysical Research: Earth Surface (2003–2012)*, 112(F2S04).

Ishikawa, M. and Hirakawa, K., 2000. Mountain permafrost distribution based on BTS measurements and DC resistivity soundings in the Daisetsu Mountains, Hokkaido, Japan. *Permafrost and Periglacial Processes*, 11(2), pp.109–123.

Jean, M. and Payette, S., 2014. Effect of Vegetation Cover on the Ground Thermal Regime of Wooded and Non-Wooded Palsas. *Permafrost and Periglacial Processes,* 25(4), pp.281-294.

Jorgenson, M. et al., 2010. Resilience and vulnerability of permafrost to climate change This article is one of a selection of papers from The Dynamics of Change in Alaskas Boreal Forests: Resilience and Vulnerability in Response to Climate Warming. *Canadian Journal of Forest Research,* 40(7), pp.1219-1236.

Karunaratne, K.C. and Burn, C.R., 2004. Relations between air and surface temperature in discontinuous permafrost terrain near Mayo, Yukon Territory. *Canadian Journal of Earth Sciences*, 41(12), pp.1437–1451.

King, L., 1990. Soil and rock temperatures in discontinuous permafrost: Gornergrat and unterrothorn, wallis, swiss alps. *Permafrost and Periglacial Processes,* 1(2), pp.177-188.

King, L., 1986. Zonation and Ecology of High Mountain Permafrost in Scandinavia. *Geografiska Annaler. Series A, Physical Geography,* 68(3), pp.131-139.

Kneisel, C., 2010. Frozen ground conditions in a subarctic mountain environment, Northern Sweden. *Geomorphology*, 118(1), pp.80–92.

Kokelj, S.V. et al., 2014. Distribution and activity of ice wedges across the forest-tundra transition, western Arctic Canada. *Journal of Geophysical Research: Earth Surface*, 119(9), pp.2032–2047.

Körner, C., 2012. *Alpine treelines: functional ecology of the global high elevation tree limits*, Springer Science and Business Media.

Körner, C., 2007. Climatic Treelines: Conventions, Global Patterns, Causes (Klimatische Baumgrenzen: Konventionen, globale Muster, Ursachen). *Erdkunde*, 61(4), pp.316–324.

Kremer, M., 2010. *Incorporation of vegetation into mountain permafrost distribution models, southern Yukon Territory*, University of Ottawa.

Kremer, M. et al., 2011. Utility of classification and regression tree analyses and vegetation in mountain permafrost models, Yukon, Canada. *Permafrost and Periglacial Processes*, 22(2), pp.163–178.

Kuntz, Z. 2016. *SDD Template Explanation*, [Video] Youtube. https://www.youtube.com/watch?v=jVN65umBhdk

Lacelle, D. et al., 2016. Solar Radiation and Air and Ground Temperature Relations in the Cold and Hyper-Arid Quartermain Mountains, McMurdo Dry Valleys of Antarctica. *Permafrost and Periglacial Processes,* 27(2), pp.163-176.

LaMarche, V.C. et al., 1984. Increasing atmospheric carbon dioxide: tree ring evidence for growth enhancement in natural vegetation. *Science*, 225(46666), pp.1019–1021.

Moffat, N. et al., 2016. Recent vegetation change (1980-2013) in the tundra ecosystems of the Tuktoyaktuk Coastlands, NWT, Canada. *Arctic Antarctic And Alpine Research,* 48(3), pp.581-597.

Lewkowicz, A.G. et al., 2013. *Electrical Resistivity Tomography (ERT) as an essential tool to investigate sites in discontinuous permafrost*, [Powerpoint] Department of Geography. University of Ottawa.

Lewkowicz, A.G. et al., 2012. Spatial and thermal characteristics of mountain permafrost, northwest Canada. *Geografiska Annaler, Series A: Physical Geography*, 94(2), pp.195–213.

Lewkowicz, A.G. and Coultish, T.L., 2004. Beaver damming and palsa dynamics in a subarctic mountainous environment, Wolf Creek, Yukon Territory, Canada. *Arctic, Antarctic, and Alpine Research*, 36(2), pp.208–218.

Lewkowicz, A.G. and Ednie, M., 2004. Probability mapping of mountain permafrost using the BTS method, Wolf Creek, Yukon Territory, Canada. *Permafrost and Periglacial Processes*, 15(1), pp.67–80.

Lewkowicz, A.G., Etzelmüller, B. and Smith, S.L., 2011. Characteristics of discontinuous permafrost based on ground temperature measurements and electrical resistivity tomography, Southern Yukon, Canada. *Permafrost and Periglacial Processes*, 22(4), pp.320–342.

Lewkowicz, A.G. and Bonnaventure, P.P., 2011. Equivalent elevation: a new method to incorporate variable lapse rates into mountain permafrost modelling, Permafrost Periglacial Processes, 22, pp.153–162.

Lliboutry, L., 1961. Phénoménes cryoniveaux dans les Andes de Santiago (Chili). *Biuletyn Peryglacjalny*, 10, pp.209–224.

Loke, M.H., 1999. Electrical imaging surveys for environmental and engineering studies. A practical guide to 2-D and 3-D surveys. Available at: http://moho.ess.ucla.edu/~pdavis/ESS135_2013/LITERATURE/LokeDCREsistivity.pdf [Accessed October 6, 2015].

Loke, M.H., 2004. Tutorial 2D and 3D Electrical Imaging Surveys. Available at: https://sites.ualberta.ca/~unsworth/UA-classes/223/loke_course_notes.pdf [Accessed May 11, 2016].

Long, P., 2016. Yukon Views -- Yukon plant photographs. Available at: http://www.yukonviews.com/yukon/flowers/ [Accessed July 6, 2016].

Loranty, M.M. and Goetz, S.J., 2012. Shrub expansion and climate feedbacks in arctic tundra. *Environmental Research Letters*, 7(1), 011005(3pp).

Mackay, J.R., and Black, R.F., 1973. Origin, composition, and structure of perennially frozen ground and ground ice: a review. In *North American Contribution, Permafrost Second International Conference* pp.185-192.

Marangunic, C.D., 1976. El glaciar de roca Pedregoso, río Colorado, V Región. In *1 Congreso Geológico Chile Santiago, Chile, 2-7 Agosto*. pp.D71–D80.

Marchenko, S.S., Gorbunov, A.P. and Romanovsky, V.E., 2007. Permafrost warming in the Tien Shan Mountains, Central Asia. *Global and Planetary Change*, 56(3), pp.311–327.

Matsuoka, N., 2001. Solifluction rates, processes and landforms: A global review. *Earth-Science Reviews*, 55(1-2), pp.107–134.

Matyssek, R. et al., 2009. Transpiration of forest trees and stands at different altitude: consistencies rather than contrasts? *European Journal of Forest Research*, 128(6), pp.579–596.

McConnell, R.G., 1905. Report on the Klondike goldfields. *Annual report of the Geological Survey of Canada*, 14, pp.1–71.

McKenna, K. et al., 2010. *Bioclimate, Ecodistrict and Ecologically Significant Features Mapping for the Dawson Planning Region, Yukon*, Available at: http://www.env.gov.yk.ca/animals-habitat/elc/documents/dawson_ecodistrict.pdf.

Morison, S.R. and Klassen, R.W., 1991. Surficial Geology, Whitehorse, Yukon Territory. Geological Survey of Canada, Map 12-1990, scale 1:250 000.

Nicolussi, K., Bortenschlager, S. and Körner, C., 1995. Increase in tree-ring width in subalpine Pinus cembra from the central Alps that may be CO 2 -related. *Trees*, 9(4), pp.181–189.

Noetzli, J. et al. 2007. Three-dimensional distribution and evolution of permafrost temperatures in idealized high-mountain topography.*J. Geophys. Res.,* 112(F2), F02S13.

O'Neill, H.B. et al., 2015. "Warm" Tundra: Atmospheric and Near-Surface Ground Temperature Inversions Across an Alpine Treeline in Continuous Permafrost, Western Arctic, Canada. *Permafrost and Periglacial Processes*, 26(2), pp.103–118.

Oelke, C. and Zhang, T., 2007. Modeling the Active-Layer Depth over the Tibetan Plateau. *Arctic, Antarctic, and Alpine Research*, 39(4), pp.714–722.

Oldenborger, G.A., 2010. *Electrical Geophysics Applied to Assessing Permafrost Conditions in Pangnirtung, Nunavut*, Nunavut, Geological Survey of Canada, Open File 6725.

Onaca, A.L. et al., 2011. Electrical resistivity measurements in sensitive periglacial environment from Southern Carpathians (Romania). In: B. Katalinic (ed.) *Annals of DAAAM for 2011 and Proceedings of the 22nd International DAAAM Symposium, Volume 22, No. 1*. Vienna, Austria: DAAAM International, pp. 885–886.

Otto, J.C. et al., 2012. Detection of mountain permafrost by combining high resolution surface and subsurface information - an example from the glatzbach catchment, austrian alps. *Geografiska Annaler, Series A: Physical Geography*, 94(1), pp.43–57.

Palmer, M.J. et al., 2012. Factors influencing permafrost temperatures across tree line in the uplands east of the Mackenzie Delta, 2004–2010. *Canadian Journal of Earth Sciences*, 49(8), pp.877–894.

Paulsen, J. and Weber, U.M., 2000. Tree Growth near Treeline: Abrupt or Gradual Reduction with Altitude? *Arctic, Antarctic, and Alpine Research*, 32(1), pp.14–20.

Payette, S. et al., 1985. Secular climate change in old-growth tree-line vegetation of northern Quebec. *Nature*, 315(6015), pp.135–138.

Péwé, T., 1983. Alpine permafrost in the contiguous United States: A review. *Arctic and Alpine Research,* 15(2), pp.145-156.

Reasoner, M. and Tinner, W., 2009. Holocene Treeline Fluctuations. In: V. Gornitz (ed.) *Encyclopedia of Paleoclimatology and Ancient Environments*. Encyclopedia of Earth Sciences Series. Springer Netherlands, pp. 442–446.

Roadhouse, E., 2010. *Air and Ground Surface Temperature Relations in a Mountainous Basin, Wolf Creek, Yukon Territory*. University of Ottawa.

Salzer, M.W. et al., 2009. Recent unprecedented tree-ring growth in bristlecone pine at the highest elevations and possible causes. *Proceedings of the National Academy of Sciences of the United States*, 106(48), pp.20348–20353.

Shur, Y.L. and Jorgenson, M.T., 2007. Patterns of permafrost formation and degradation in relation to climate and ecosystems. *Permafrost and Periglacial Processes*, 18(1), pp.7–19.

Smith, M.W., 1975. Microclimatic Influences on Ground Temperatures and Permafrost Distribution, Mackenzie Delta, Northwest Territories. *Canadian Journal of Earth Sciences*, 12(8), pp.1421–1438.

Smith, M.W. and Riseborough, D.W., 2002. Climate and the limits of permafrost: a zonal analysis. *Permafrost and Periglacial Processes*, 13(1), pp.1–15.

Smith, S.L. et al., 2005. Recent trends from Canadian permafrost thermal monitoring network sites. *Permafrost and Periglacial Processes*, 16(1), pp.19–30.

Smith, S.L. et al., 2010. Thermal state of permafrost in North America: a contribution to the international polar year. *Permafrost and Periglacial Processes*, 21(2), pp.117–135.

Tabony, R.C., 1985. Relations between minimum temperature and topography in great britain. *Journal of Climatology*, 5(5), pp.503–520.

Tape, K., Sturm, M. and Racine, C., 2006. The evidence for shrub expansion in Northern Alaska and the Pan-Arctic. *Global Change Biology*, 12(4), pp.686–702.

Thompson, B.W., 1986. Small-scale katabatics and cold hollows. *Weather*, 41(5), pp.146–153.

Throop, J. et al., 2012. Climate and ground temperature relations at sites across the continuous and discontinuous permafrost zones, northern Canada. *Canadian Journal of Earth Sciences*, 49(8), pp.865–876.

Transport Canada, 2015. Flying an unmanned aircraft recreationally. Available at: http://www.tc.gc.ca/eng/civilaviation/standards/general-recavi-uav-2265.htm?WT.mc_id=1zfhj#safety [Accessed October 6, 2015].

Vernon, P. and Hughes, O.L., 1966. Surficial Geology, Dawson, Yukon Territory. Geological Survey of Canada, Map 1170A, scale 1:253 440.

Villalba, R. et al., 1997. Recent trends in tree-ring records from high elevation sites in the Andes of northern Patagonia. *Climatic Change*, 36(3), pp.425–454.

Walther, G.-R., 2003. Plants in a warmer world. *Perspectives in Plant Ecology, Evolution and Systematics*, 6(3), pp.169–185.

Way, R.G. and Lewkowicz, A.G., 2015. Investigations of discontinuous permafrost in coastal Labrador with DC electrical resistivity tomography. In: *Proceedings of GéoQuebec: 68th Canadian Geotechnical Conference and 7th Canadian Permafrost Conference*. Quebec City, Canada.

Williams, J.R., 1970. *Groundwater in the permafrost regions of Alaska*. Professional paper 696, U.S. Geological Survey, Washington DC.

Woo, M.-K., 2012. *Permafrost Hydrology*, Springer, Berlin.

Wu, Q. et al., 2007. Responses of Permafrost on the Qinghai-Tibet Plateau, China, to Climate Change and Engineering Construction. *Arctic, Antarctic, and Alpine Research*, 39(4), pp.682–687.

Yukon Ecoregions Working Group, 2004a. Yukon Plateau-Central. In: C.A.S. Smith, J.C. Meikle, and C.F. Roots (eds.) *Ecoregions of the Yukon Territory: Biophysical Properties of Yukon Landscapes*.

Summerland, British Columbia: Agriculture and Agri-Food Canada, PARC Technical Bulletin No. 04-01, pp.187–196.

Yukon Ecoregions Working Group, 2004b. Yukon Southern Lakes. In: C.A.S. Smith, J.C. Meikle, and C.F. Roots (eds). *Ecoregions of the Yukon Territory: Biophysical properties of Yukon landscapes*. Summerland, British Columbia: Agriculture and Agri-Food Canada, PARC Technical Bulletin No. 04-01, pp.63–72.

Zhang, T., 2005. Influence of the seasonal snow cover on the ground thermal regime: An overview. *Reviews of Geophysics*, 43(4), RG4002.

Appendix A – Site Information

Profile	General description	Location[1] (Lat, Lon) Starting	Ending	Elevation (m asl)	Slope aspect[2]	Slope gradient[3]	Length (m)	Vegetation transition	Ground truthdata[4]	Field Day[5]
1	Wolf Creek basin alpine profile.	60.56846, -135.15686	60.56902, -135.15948	1472 - 1494	W	Varies. Very gentle to Strong mostly. Nearly level or Very strong in some locations. Average Moderate.	160	Tundra shrub vegetation and large areas of bare rocky ground.	Temp probe with pit.	19/07/2015 - 20/07/2015
2	Coal Ridge long profile.	60.49982, -135.21710	60.49870, -135.21310	1240 - 1330	NW	Lower slope: Gentle to Moderate. Mid slope: Moderate to Strong. Upper slope: Very strong to Extreme.	280	Primarily scattered stunted *Picea mariana* trees, dense *Betula nana* and *Salix sp.* shrubs of varying height. A lower treeline, due to cold air drainage, is at 1250 m asl	CR-1, CR-2, CR-3 along profile.	09/07/2015 - 10/07/2015
3	Wolf Creek basin south-facing slope.	60.46954, -135.21754	60.47044, -135.21956	1214 - 1250	S	Initially, Gentle to Moderate. Upslope, Strong to Very strong.	160	Dense shrubs near the base of the slope transition upslope to an open canopy, mixed forest including *Juniper sp.*, *Pinus banksiana*, *Picea glauca*, and *Populus sp.*.	none	13/07/2015
4	Long profile at top of mount Sima trail sampling WC-T4.	60.57771, -135.08490	60.57907, -135.08086	1270 - 1302	NE	Varies. Level to Strong. Average Moderate.	240	*Abies lasiocarpa* forest transitions upslope to shrub vegetation with sparse trees at roughly 1275 m asl The profile is about 400 m from Site 5 and on the same slope.	WC-T4 along profile, pit and temp probe.	14/07/2015 - 15/07/2015
5	Shorter duplicate profile same slope as profile 4.	60.58191, -135.08653	60.58095, -135.08847	1269 - 1297	NE	Mostly moderate to strong, with very strong and gentle upslope at end of profile.	160	*Abies lasiocarpa* forest transitions upslope to shrub vegetation with sparse trees at roughly 1282 m asl The profile is about 400 m from Site 4 and on the same slope.	Temp probe, WC-T4 nearby	17/07/2015 - 18/07/2015
6	Mt McIntyre profile starting at backup climate station MtMC-BK	60.62165, -135.14153	60.62233, -135.13924	1554 - 1569	NE	Varies. Nearly level to Very strong. Average Strong.	160	Tundra shrub vegetation and areas of bare ground. Lichen and moss covered rocky area transitions downslope to area with grass, *Cassiope sp.*, and short shrubs, further downslope dense *Betula nana* and *Salix sp.* shrub stand more than 1 m tall occurs.	MtMC-BK along profile, pit and temp probe, borehole nearby.	22/07/2015, 24/07/2015
7	Mt McIntyre downslope from backup climate station	60.62308, -135.13763	60.62381, -135.13525	1519 - 1547	NE	Strong to Very strong with Extreme in some locations.	160	*Salix sp.* and *Betula nana* shrub patches of various heights and densities throughout the profile and noted patches of *Cassiope sp.*.	none	23/07/2015

[1]Coordinates in NAD83 [2] North (N) South (S) West (W) Northwest (NW) Northeast (NE) Southeast (SE)

[3] Level (0-0.5%) Nearly Level (0.5-2%), Very gentle (2-5%) Gentle (5-9%) Moderate (9-15%) Strong (15-30%) Very strong (30-45%), Extreme (45-70%), Steep (70-100%), Very steep (>100%)

[4]Groundtruth data from temperature (temp) measurements, climate station data (abbreviations shown, see appendix B for station names), probing, pits, or borehole data.

[5] Date(s) fieldwork completed at each given site.

Profile	General description	Location[1] (Lat, Lon) Starting	Ending	Elevation (m asl)	Slope aspect[2]	Slope gradient[3]	Length (m)	Vegetation transition	Ground truth data[4]	Field Day[5]
8	Mount McIntyre dense treeline profile	60.62602, -135.12981	60.62666, -135.12740	1385 - 1415	NE	Varies. Mostly Strong to Very strong. Gentle and Moderate in some locations.	160	Tall dense *Betula nana* and *Salix sp.* shrubs transition to dense *Abies lasiocarpa* forest around 1400 m asl	none	25/07/2015
9	Dawson area profile sampling TOW-08 climate station.	64.12711, -139.69930	64.12843, -139.69881	1088 - 1134	N	Varies. Strong to Extreme. Downslope mostly strong. Average Very strong.	160	An open canopy mixed *Picea sp.-Alnus sp.* stand transitions upslope, at roughly 1100 m asl, to an area of shrub patches and sparse *Picea sp.* trees. The profile is about 40 m from profile 9 on the same slope.	TOW-8 along profile	28/07/2015, 29/07/2015
10	Duplicate profile same slope as profile 8.	64.12715, -139.70012	64.12849, -139.69963	1091 - 1134	N	Varies. Strong to Extreme. Downslope mostly strong. Average Strong.	160	An open canopy mixed *Picea sp.-Alnus sp.* stand transitions upslope, at roughly 1100 m asl, to an area of shrub patches and sparse *Picea sp.* trees. The profile is about 40 m from profile 8 on the same slope.	TOW-8 nearby	29/07/2015
11	Dawson cold air drainage valley, succession site, northwest-facing slope.	64.07634, -139.47890	64.07745, -139.48062	458 - 500	NW	Upper slope: Strong to Very strong, with Extreme section. Lower slope: Level to Moderate.	160	Stunted *Picea mariana*, scattered shrubs, and sparse *Alnus* sp. in valley bottom transitions upslope (around 480 m asl) to shrubless tall *Picea* sp. stand with few senescing *Betula papyrifera*.	temp probe, TOW-4 and TOW-5 nearby	31/07/2015
12	Dawson cold air drainage valley, succession site, southeast-facing slope	64.07787, -139.48296	64.07719, -139.47994	471 - 501	SE	Upper slope: Gentle. Mid-slope: Strong to Extreme. Lower slope: Moderate to Level.	160	Stunted *Picea mariana*, shrubs, and *Alnus* sp. in valley bottom transition upslope (around 475 m asl) to a mixed stand of tall *Picea* sp. and senescing *Betula papyrifera*. On the steepest section of the slope, *Betula papyrifera* dominates. In the upper slope, the vegetation transitions to a *Picea* sp. dominated forest.	temp probe, TOW-4 and TOW-5 nearby	30/07/2015

[1]Coordinates in NAD83 [2] North (N) South (S) West (W) Northwest (NW) Northeast (NE) Southeast (SE)
[3] Level (0-0.5%) Nearly Level (0.5-2%), Very gentle (2-5%) Gentle (5-9%) Moderate (9-15%) Strong (15-30%) Very strong (30-45%), Extreme (45-70%), Steep (70-100%), Very steep (>100%)
[4]Groundtruth data from temperature (temp) measurements, climate station data (abbreviations shown, see appendix B for station names), probing, pits, or borehole data.
[5] Date(s) fieldwork completed at each given site.

Appendix B – Climate station and borehole positions (modified from Bevington, 2014)

Station Name Abbreviation Study Area	Latitude (°N) Longitude (°W) Elevation (m asl)	Depth below ground surface of TTOP sensor (cm)	Relevant Profile(s)
Coal Ridge 01 CR-1 Whitehorse	60.4996 135.2162 1260	75	2
Coal Ridge 02 CR-2 Whitehorse	60.4994 135.2153 1271	75	2
Coal Ridge 03 CR-3 Whitehorse	60.4988 135.2134 1363	100	2
Mount McIntyre MtMC Whitehorse	60.6217 135.1414 1567	n/a *see borehole	6, 7, 8
Mount McIntyre Backup MtMC-BK Whitehorse	60.6204 135.1445 1565	unknown	6, 7, 8
Sima Trail 04 WC-T4 Whitehorse	60.5778 135.0844 1290	25	4, 5, 1
Top of the World 04 TOW-04 Dawson	64.0766 139.4808 484	50	11, 12
Top of the World 05 TOW-05 Dawson	64.0768 139.4784 503	100	11, 12
Top of the World 08 TOW-08 Dawson	64.1274 139.6993 1119	50	9, 10
Additional stations used only to estimate mean annual air temperature at sites without stations.			
Inversion Valley 01 WC2006-01 Whitehorse	60.538 135.1384 1266	n/a	1
Permafrost Mound WC-APM-WS Whitehorse	60.4814 135.1935 1202	n/a	3
Drained Lake WC-DR Whitehorse	60.474 135.1894 1225	n/a	3
Borehole			
Mount McIntyre MtMC Whitehorse	60.6217 135.1414 1567	400	6

Appendix C – ERT Acquirement Settings

Acquirement Settings Generally Used

- AGC_TimeSec: 0.060000
  - Acq_DelaySec: 0.300000
  - Acq_TimeSec: 0.600000
  - AutoStack: 1
  - BaseFreqHz: 60.000000
  - CurrentLimitHighAmpere: 0.020000
  - CurrentLimitLowAmpere: 0.000500
  - DoInitialAGC: 0
  - ElectrodeResistanceBadLimitHighOhm: 200000.000000
  - ElectrodeResistanceBadLimitLowOhm: 10000.000000
  - ElectrodeTest: 1
  - ElectrodeTestCurrentAmpere: 0.020000
  - ErrorLimit: 0.001000
  - Fullwaveform: 0
  - IPSP_TimeSec: 0.500000
  - IP_MinOffTimeSec: 0.500000
  - IP_OffTimeSec: 0.000000
  - IP_WindowSecList: 0.01 0.1 0.02
  - MarginLimitHigh: 1.200000
  - MeasureMode: 2
  - Measure_SNR: 0
  - PowerLimitHighWatt: 250.000000
  - PowerLimitLowWatt: 0.000000
  - PowerLossLimitHighWatt: 25.000000
  - SNR_TimeSec: 0.020000
  - SP_TimeSec: 1.000000
  - SampleRateHz: 1000.000000
  - StackLimitsHigh: 2
  - StackLimitsLow: 2
  - StackNorm: 0
  - VoltageLimitHighVolt: 300.000000
  - VoltageLimitLowVolt: 0.000000

Appendix D – Snow Data

Station CR-1

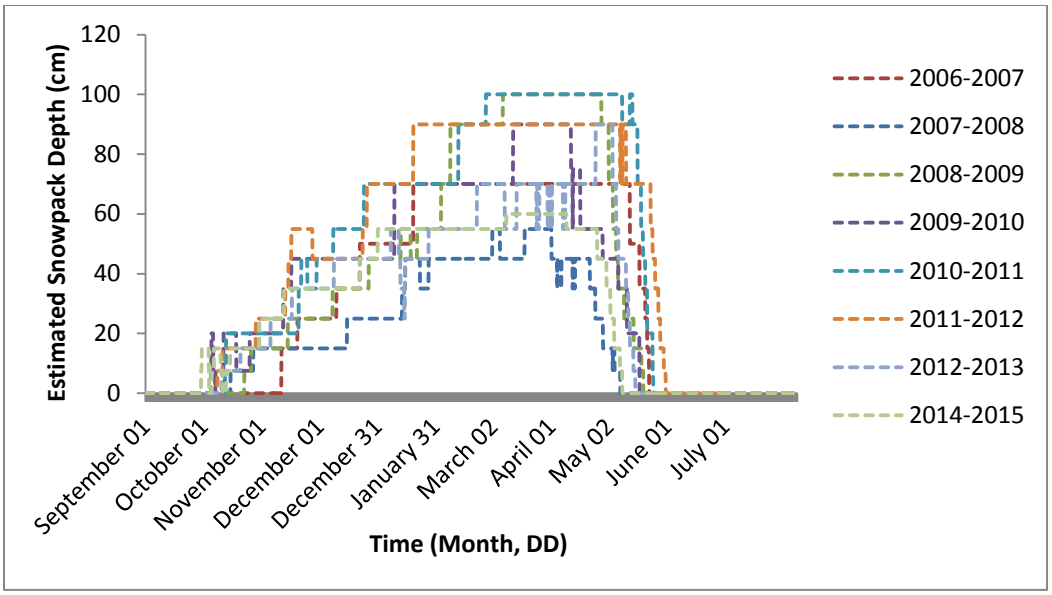

Station CR-2

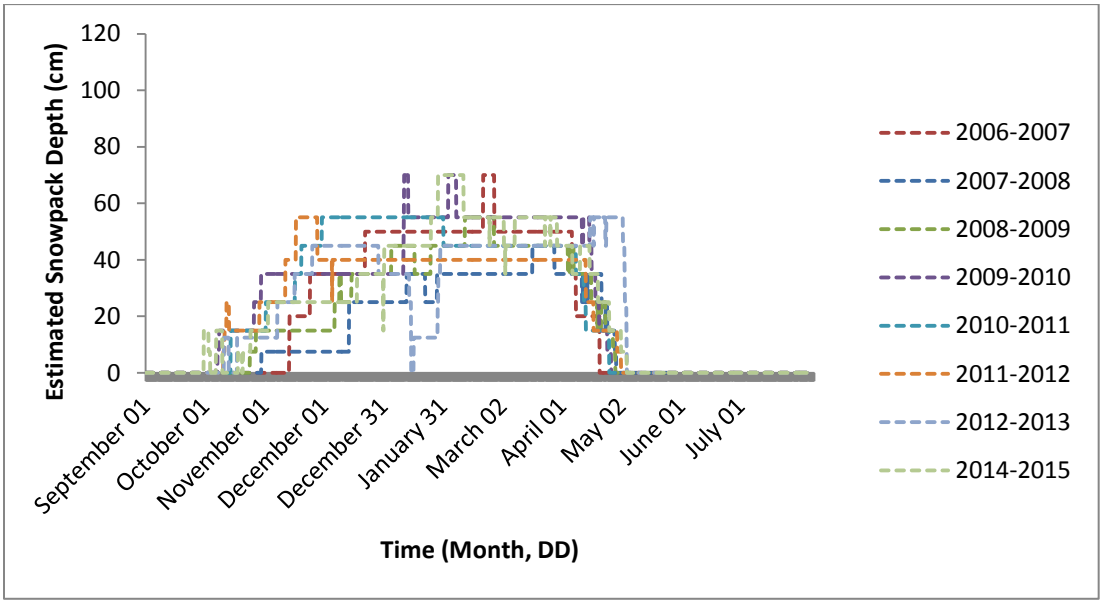

Station CR-3

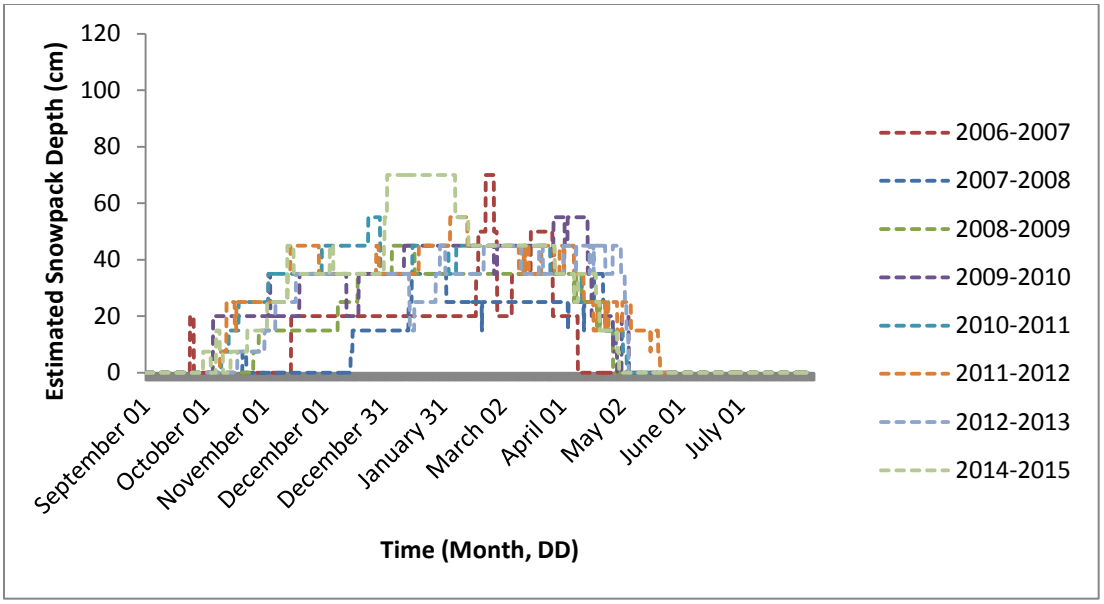

Station WC-T4

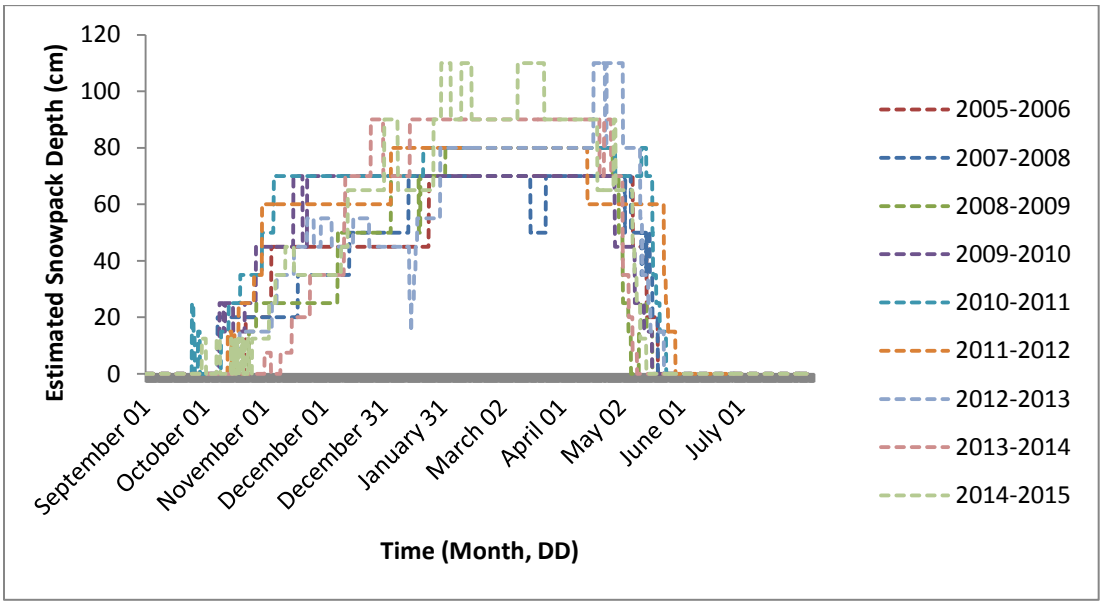

Station MtMC

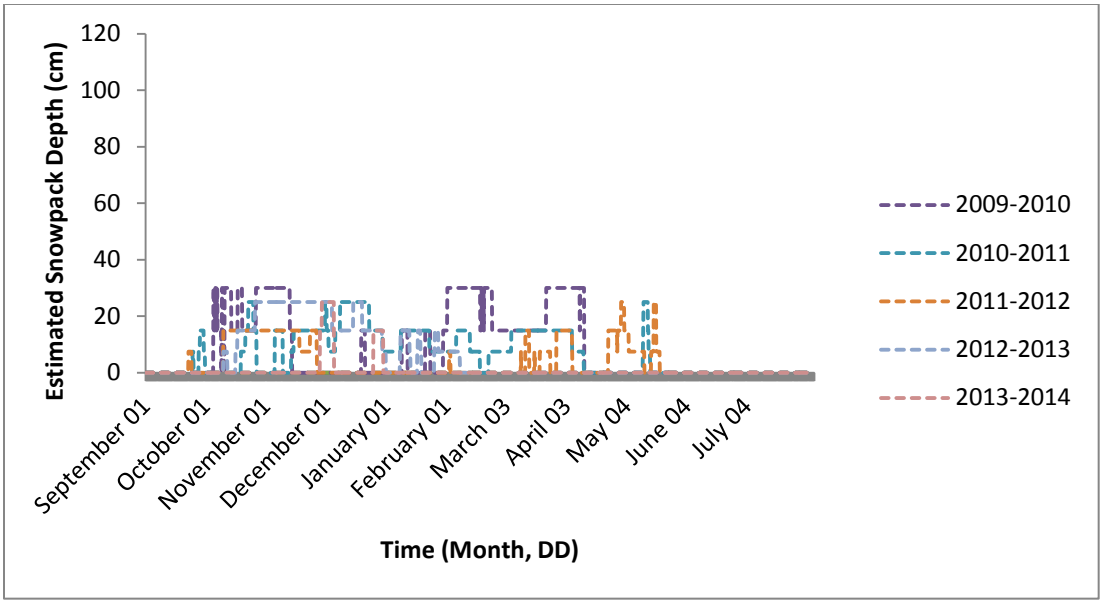

Station MtMC-BK

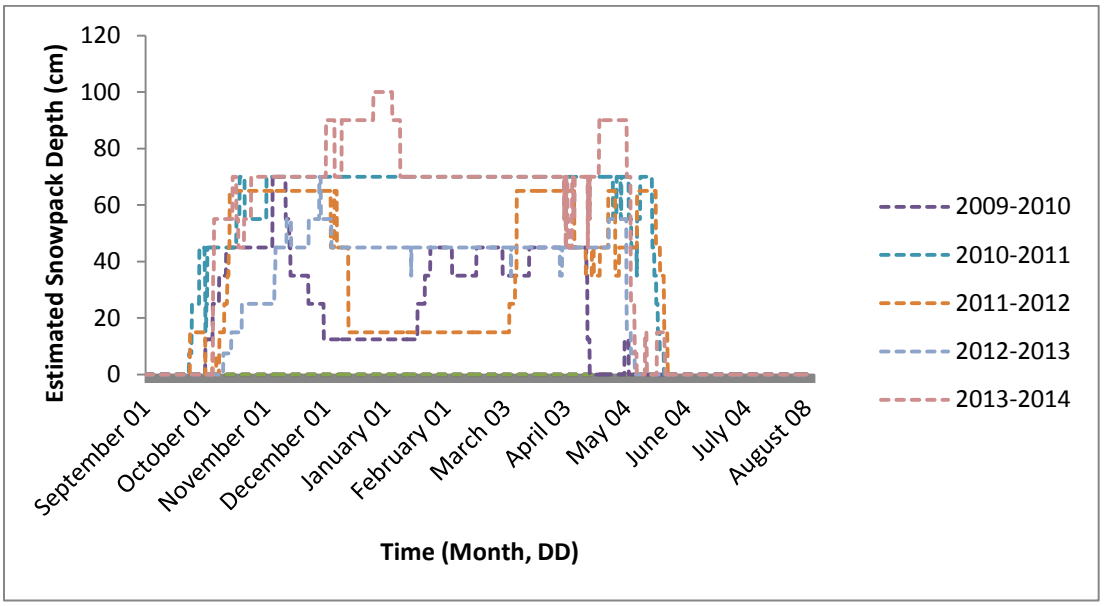

Station TOW-08

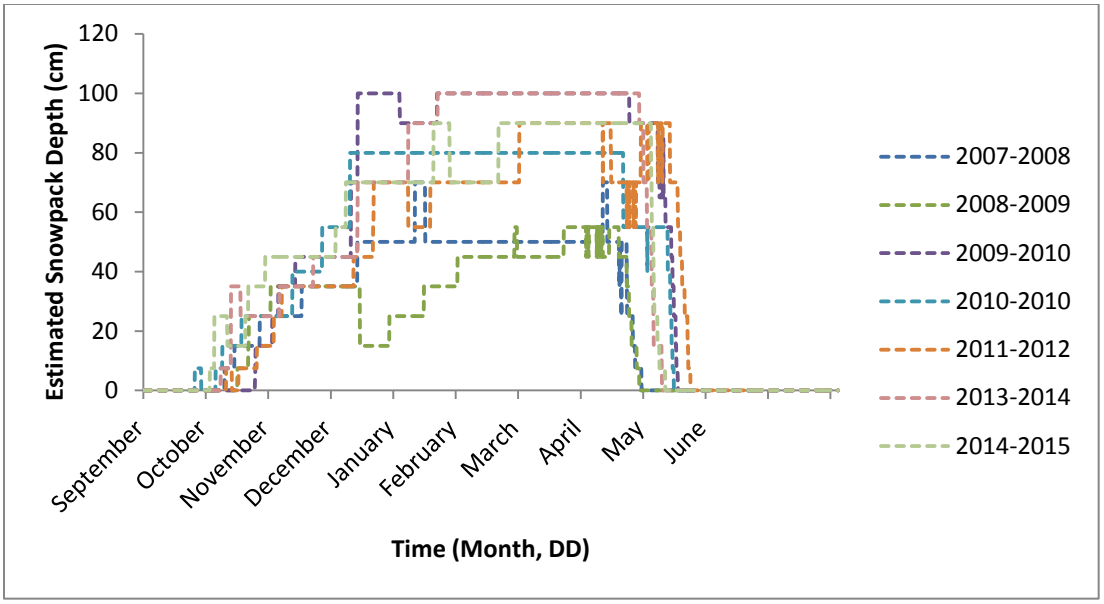

Station TOW-04

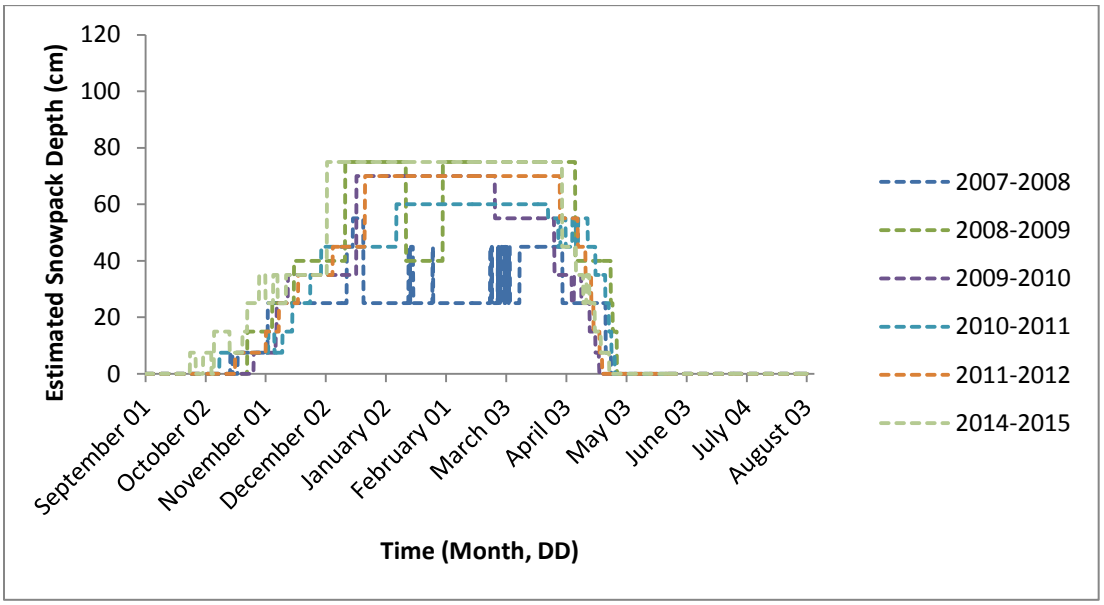

Station TOW-05

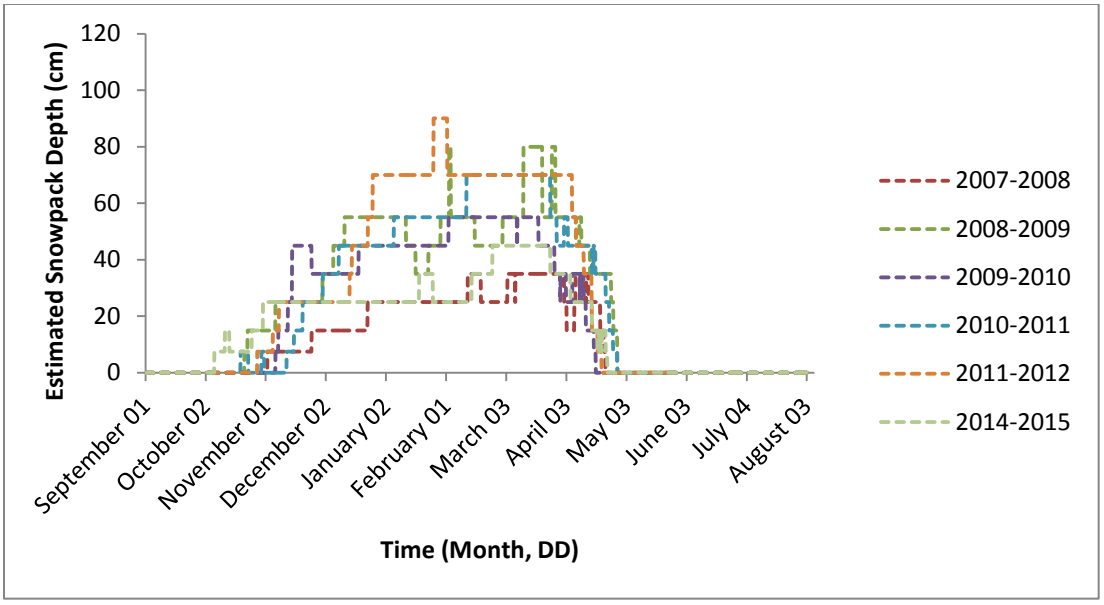

Appendix E – Site 1

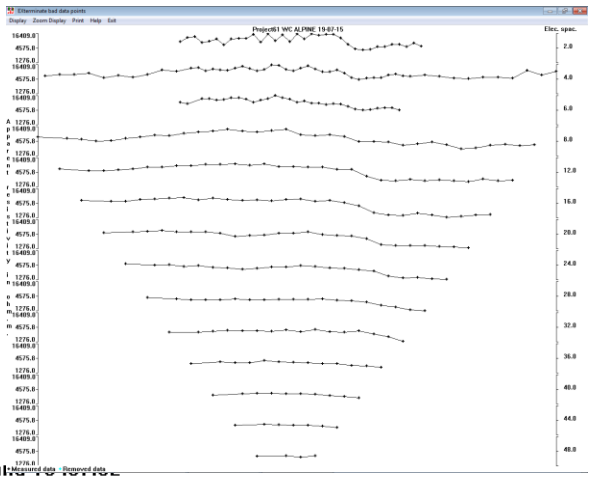

Project61 WC ALPINE 19-07-15
Electrode spacing is 2.000.
General array
Wenner array arrangement
Measurements are in resistances.
No user defined model depths.
Total number of datum points is 324.
X-distances are surface distances.
324 352.0600
Topographic data present in separate list.
The number of topographical datum points is 41.
Topography present type 2
Minimum and maximum electrode locations are 0.00 and 160.00.
Minimum electrode spacing is 2.00.
No fixed regions.
Total number of data levels is 14.
Total number of electrodes is 59.
First electrode is located at 0.00.
Last electrode is located at 160.00
Minimum and maximum apparent resistivity values are 1277.05 and 16409.0
Minimum, maximum and average geometric factors used in data set are 12.6, 301.6 and 96.7

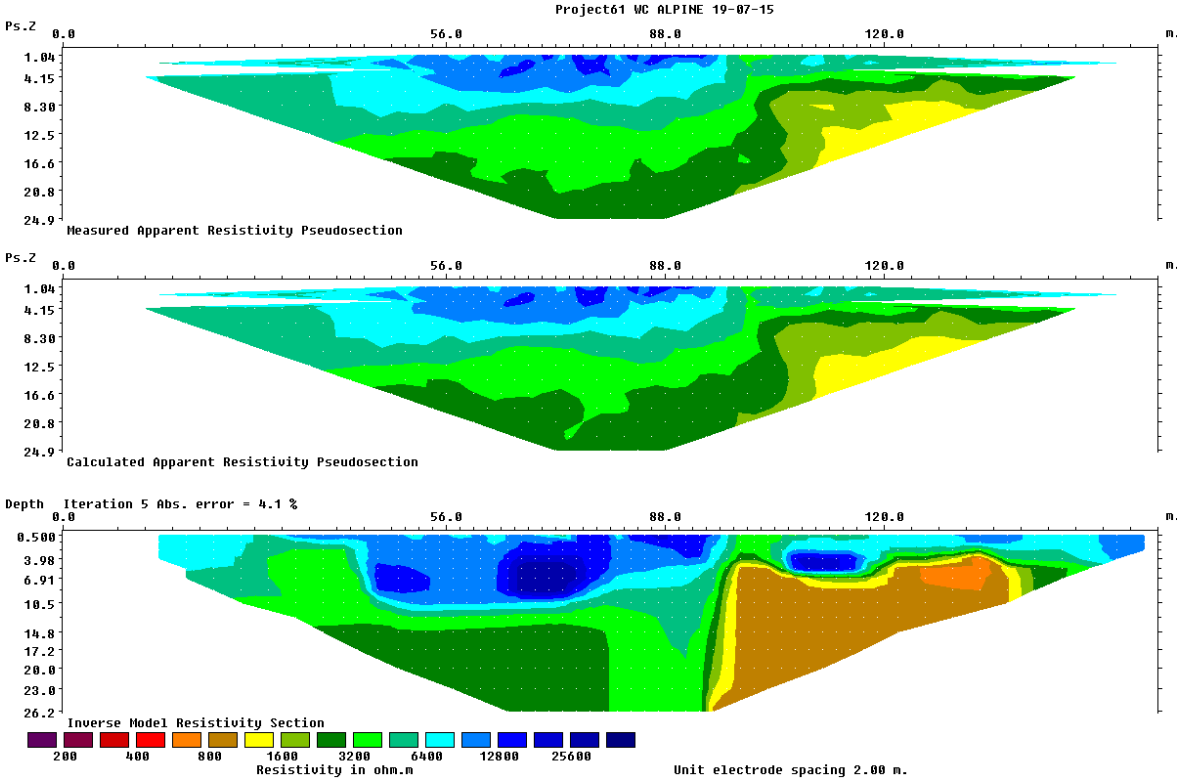

The model has 14 layers and 620 blocks.
Iteration 1 : RMS error 13.08.
Iteration 2 : Abs. error 9.05.
Iteration 3 : Abs. error 6.09.
Iteration 4 : Abs. error 5.08.
Iteration 5 : Abs. error 4.06.
Iteration 6 : Abs. error 3.89.
Iteration 7 : Abs. error 3.57.
Reference resisivity used is 4963.615
Topographical data present in inversion file.
Damped topography was incorporated into inversion model.
Blocks sensitivity information present.
Average sensitivity is 1.003.
Inversion constraints information present.

Appendix F – Site 2

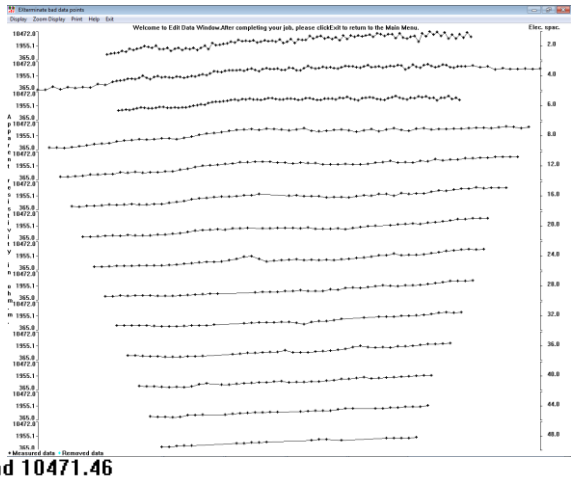

Project61 CL20 10-07-15
Electrode spacing is 2.000.
General array
Wenner array arrangement
Measurements are in apparent resistivity.
No user defined model depths.
Total number of datum points is 812.
X-distances are surface distances.
812 1677.255
Topography present type 2
Minimum and maximum electrode locations are 0.00 and 280.00.
Minimum electrode spacing is 2.00.
No fixed regions.
Total number of data levels is 14.
Total number of electrodes is 121.
First electrode is located at 0.00.
Last electrode is located at 280.00
Minimum and maximum apparent resistivity values are 366.22 and 10471.46

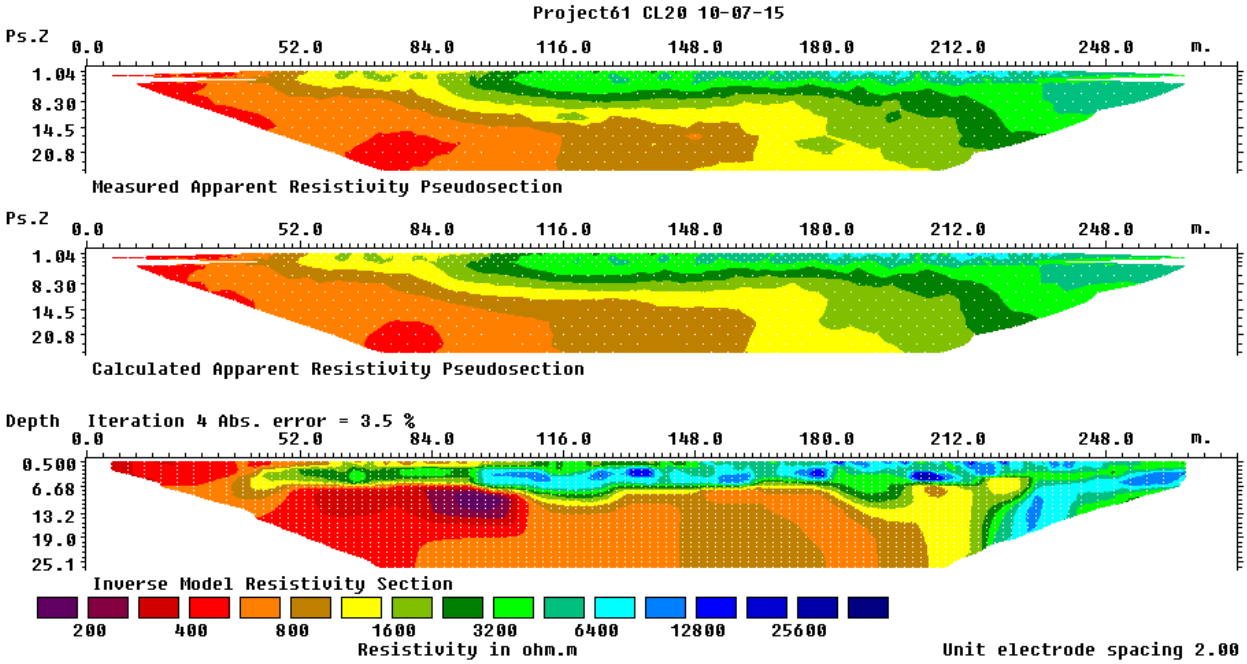

The model has 24 layers and 2377 blocks.
Iteration 1 : RMS error 11.67.
Iteration 2 : Abs. error 6.54.
Iteration 3 : Abs. error 4.53.
Iteration 4 : Abs. error 3.47.
Iteration 5 : Abs. error 3.01.
Iteration 6 : Abs. error 2.69.
Iteration 7 : Abs. error 2.57.
Reference resisivity used is 1931.702
Topographical data present in inversion file.
Damped topography was incorporated into inversion model.
Blocks sensitivity information present.
Average sensitivity is 0.637.
Inversion constraints information present.

Appendix G – Site 3

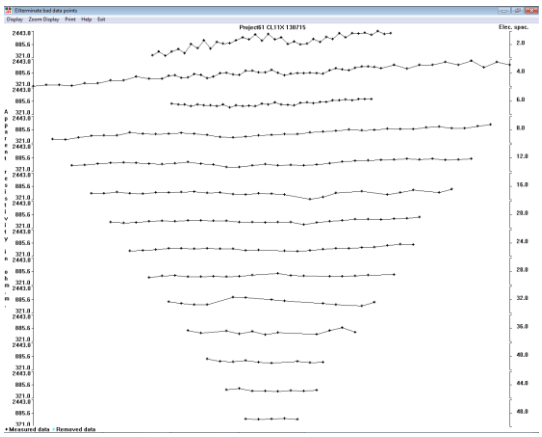

Project61 CL11X 130715
Electrode spacing is 2.000.
General array
Wenner array arrangement
Measurements are in apparent resistivity.
No user defined model depths.
Total number of datum points is 326.
X-distances are surface distances.
326 558.9183
Topography present type 2
Minimum and maximum electrode locations are 0.00 and 160.00.
Minimum electrode spacing is 2.00.
No fixed regions.
Total number of data levels is 14.
Total number of electrodes is 61.
First electrode is located at 0.00.
Last electrode is located at 160.00
Minimum and maximum apparent resistivity values are 322.40 and 2442.22

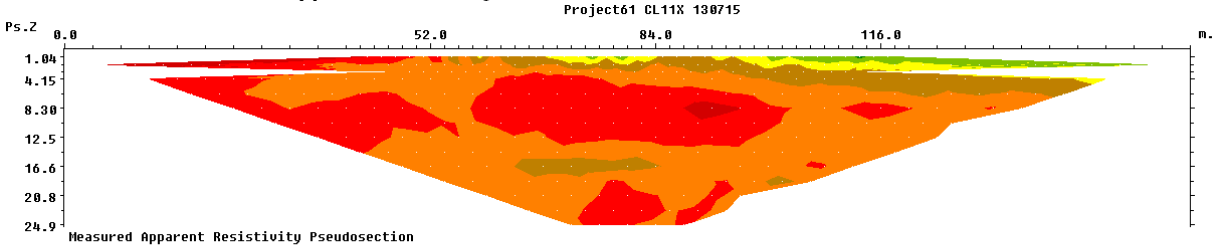

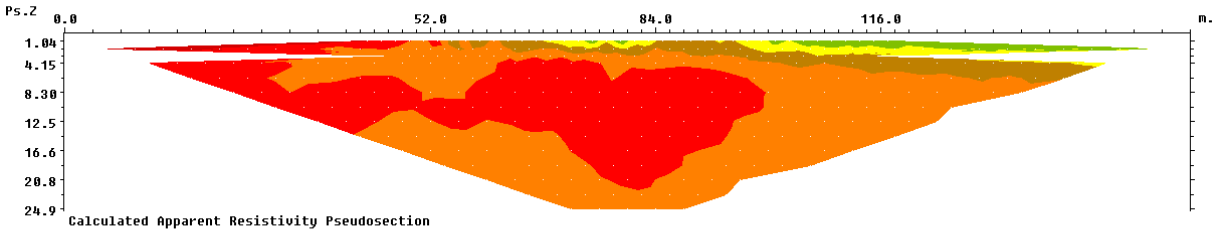

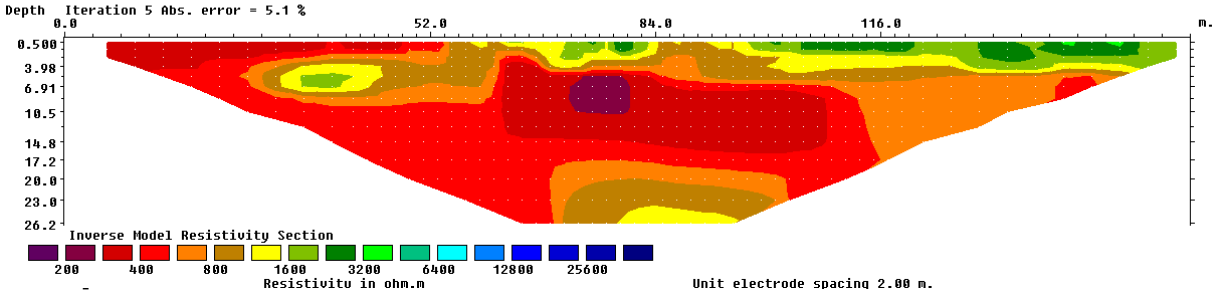

The model has 14 layers and 638 blocks.
Iteration 1 : RMS error 12.14.
Iteration 2 : Abs. error 9.29.
Iteration 3 : Abs. error 6.53.
Iteration 4 : Abs. error 5.42.
Iteration 5 : Abs. error 5.12.
Iteration 6 : Abs. error 4.61.
Iteration 7 : Abs. error 4.54.
Reference resisivity used is 709.273
Topographical data present in inversion file.
Damped topography was incorporated into inversion model.
Blocks sensitivity information present.
Average sensitivity is 0.919.
Inversion constraints information present.

Appendix H – Site 4

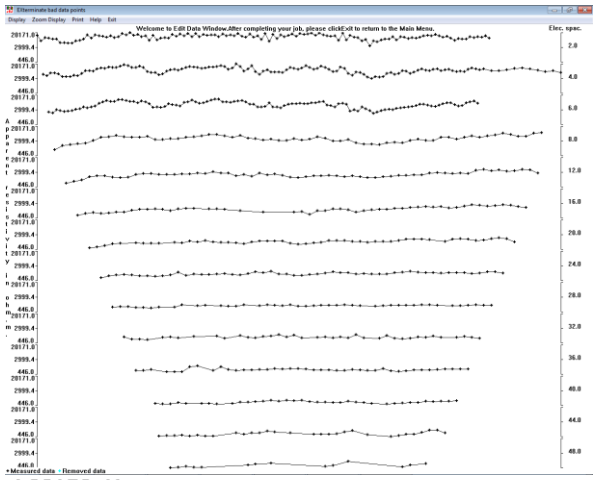

Project61 WC TRAIL 150715
Electrode spacing is 2.000.
General array
Wenner array arrangement
Measurements are in apparent resistivity.
No user defined model depths.
Total number of datum points is 845.
X-distances are surface distances.
845 782.16689
Topography present type 2
Minimum and maximum electrode locations are 0.00 and 280.00.
Minimum electrode spacing is 2.00.
No fixed regions.
Total number of data levels is 14.
Total number of electrodes is 131.
First electrode is located at 0.00.
Last electrode is located at 280.00
Minimum and maximum apparent resistivity values are 446.94 and 20170.41
Minimum, maximum and average geometric factors used in data set are 12.6, 301.6 and 98.8

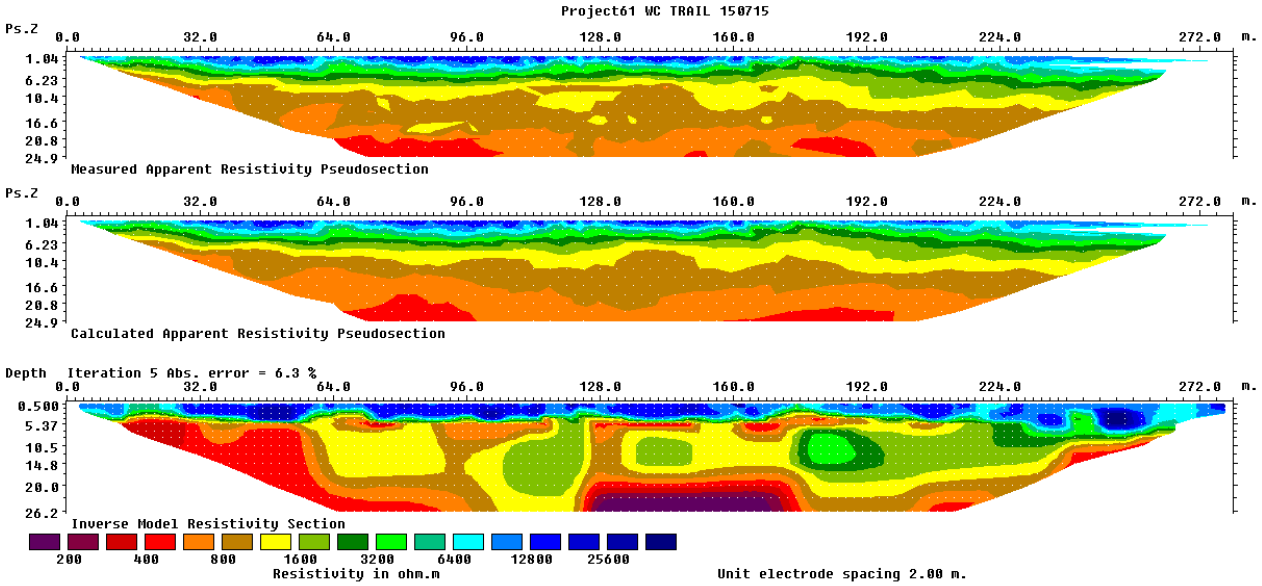

The model has 14 layers and 1541 blocks.
Iteration 1 : RMS error 23.19.
Iteration 2 : Abs. error 11.32.
Iteration 3 : Abs. error 8.46.
Iteration 4 : Abs. error 7.07.
Iteration 5 : Abs. error 6.25.
Iteration 6 : Abs. error 5.79.
Iteration 7 : Abs. error 5.39.
Reference resisivity used is 2771.647
Topographical data present in inversion file.
Damped topography was incorporated into inversion model.
Blocks sensitivity information present.
Average sensitivity is 1.161.
Inversion constraints information present.

Appendix I – Site 5

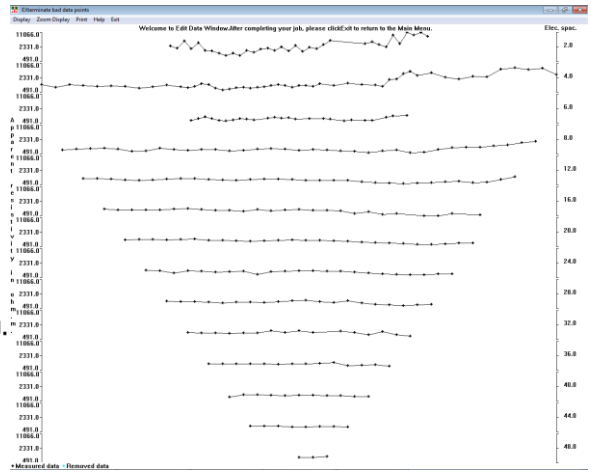

Project61 WC TRAIL-B 17-07-15
Electrode spacing is 2.000.
General array
Wenner array arrangement
Measurements are in apparent resistivity.
No user defined model depths.
Total number of datum points is 324.
X-distances are surface distances.
324 986.9080
Topography present type 2
Minimum and maximum electrode locations are 0.00 and 160.00.
Minimum electrode spacing is 2.00.
No fixed regions.
Total number of data levels is 14.
Total number of electrodes is 60.
First electrode is located at 0.00.
Last electrode is located at 160.00
Minimum and maximum apparent resistivity values are 492.40 and 11065.03
Minimum, maximum and average geometric factors used in data set are 12.6, 301.6 and 98.6

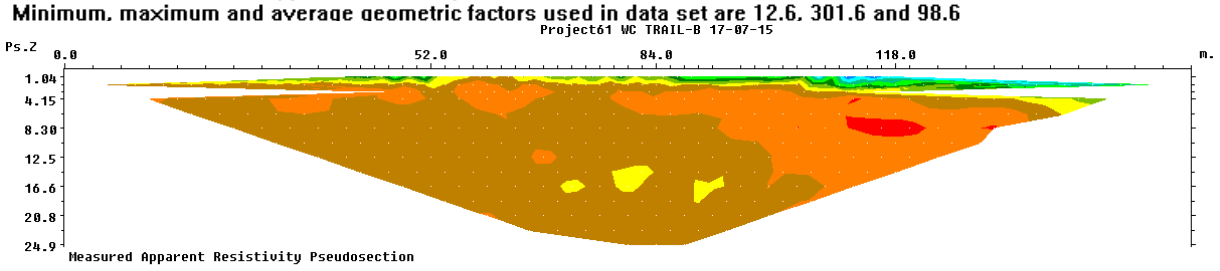

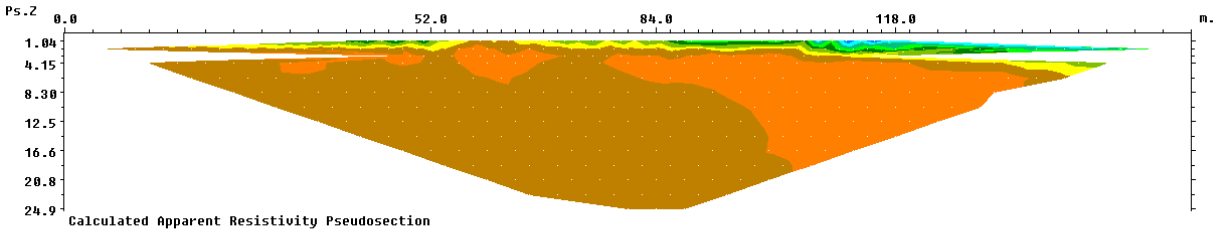

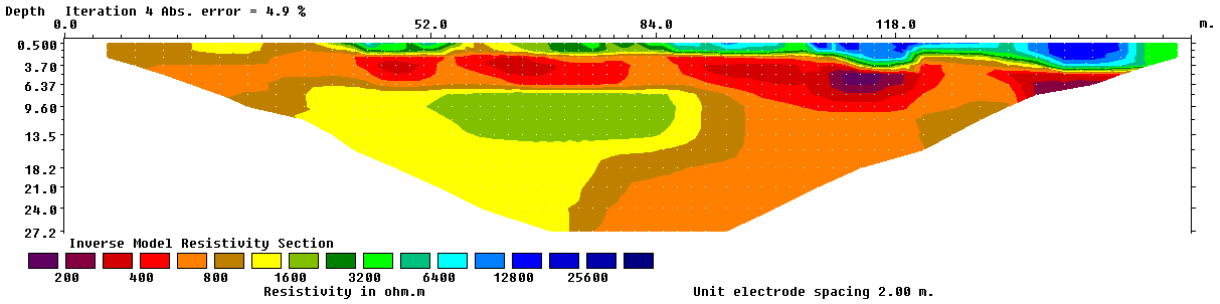

The model has 15 layers and 652 blocks.
Iteration 1 : RMS error 21.04.
Iteration 2 : Abs. error 11.49.
Iteration 3 : Abs. error 6.64.
Iteration 4 : Abs. error 4.95.
Iteration 5 : Abs. error 4.26.
Iteration 6 : Abs. error 4.00.
Iteration 7 : Abs. error 3.81.
Reference resisivity used is 1034.366
Topographical data present in inversion file.
Damped topography was incorporated into inversion model.
Blocks sensitivity information present.
Average sensitivity is 0.899.
Inversion constraints information present.

Appendix J – Site 6

Project61 MM00 22-07-15
Electrode spacing is 2.000.
General array
Wenner array arrangement
Measurements are in resistances.
No user defined model depths.
Total number of datum points is 345.
X-distances are surface distances.
345 407.276
Topographic data present in separate list.
The number of topographical datum points is 41.
Topography present type 2
Minimum and maximum electrode locations are 0.00 and 160.00.
Minimum electrode spacing is 2.00.
No fixed regions.
Total number of data levels is 14.
Total number of electrodes is 61.
First electrode is located at 0.00.
Last electrode is located at 160.00
Minimum and maximum apparent resistivity values are 734.88 and 10235.96
Minimum, maximum and average geometric factors used in data set are 12.6, 301.6 and 97.0

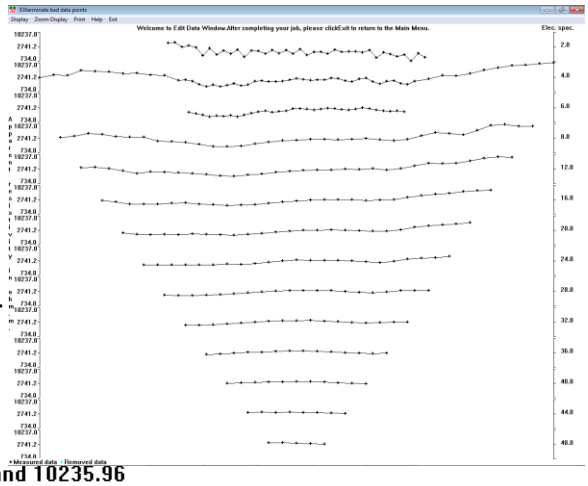

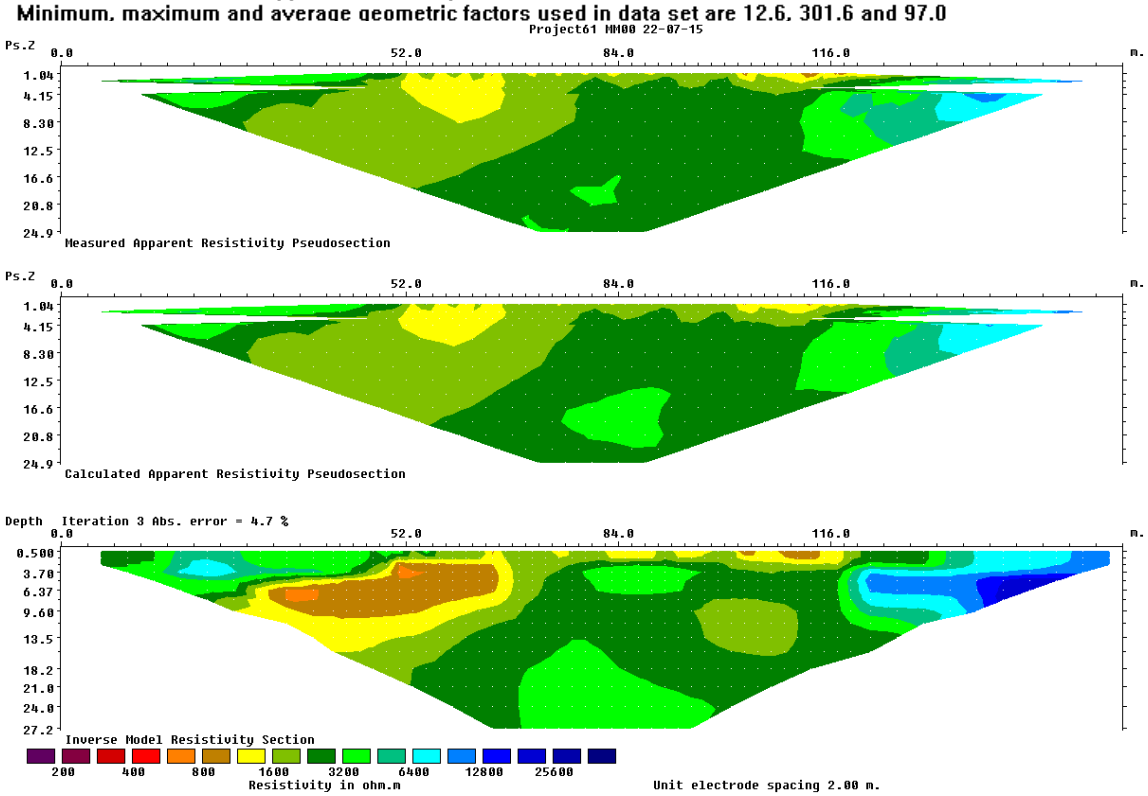

The model has 15 layers and 671 blocks.
Iteration 1 : RMS error 10.51.
Iteration 2 : Abs. error 6.67.
Iteration 3 : Abs. error 4.70.
Iteration 4 : Abs. error 3.86.
Iteration 5 : Abs. error 3.46.
Iteration 6 : Abs. error 2.90.
Iteration 7 : Abs. error 2.79.
Reference resisivity used is 2467.302
Topographical data present in inversion file.
Damped topography was incorporated into inversion model.
Blocks sensitivity information present.
Average sensitivity is 0.910.
Inversion constraints information present.

Appendix K – Site 7

Project61 MM01 23-07-15
Electrode spacing is 2.000.
General array
Wenner array arrangement
Measurements are in apparent resistivity.
No user defined model depths.
Total number of datum points is 344.
X-distances are surface distances.
344 3622.7649
Topographic data present in separate list.
The number of topographical datum points is 41.
Topography present type 2
Minimum and maximum electrode locations are 0.00 and 160.00.
Minimum electrode spacing is 2.00.
No fixed regions.
Total number of data levels is 14.
Total number of electrodes is 61.
First electrode is located at 0.00.
Last electrode is located at 160.00

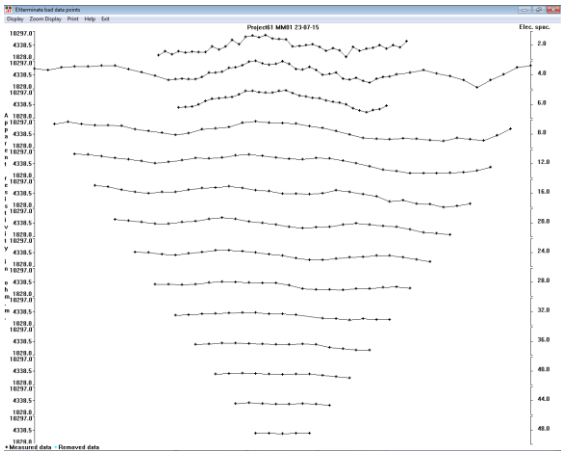

Minimum and maximum apparent resistivity values are 1829.12 and 10296.16
Minimum, maximum and average geometric factors used in data set are 12.6, 301.6 and 96.7

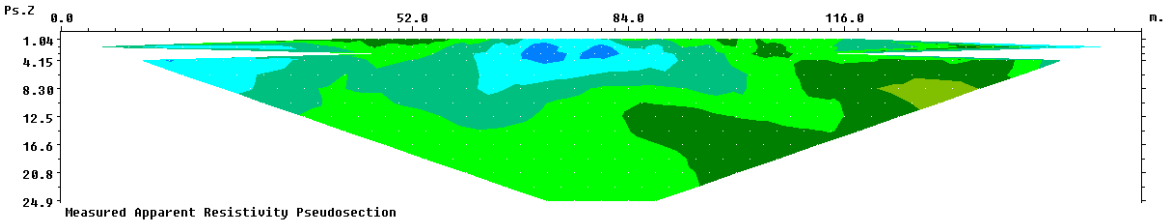

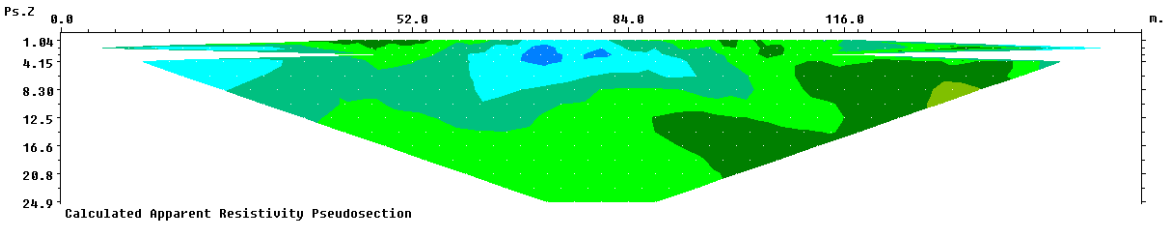

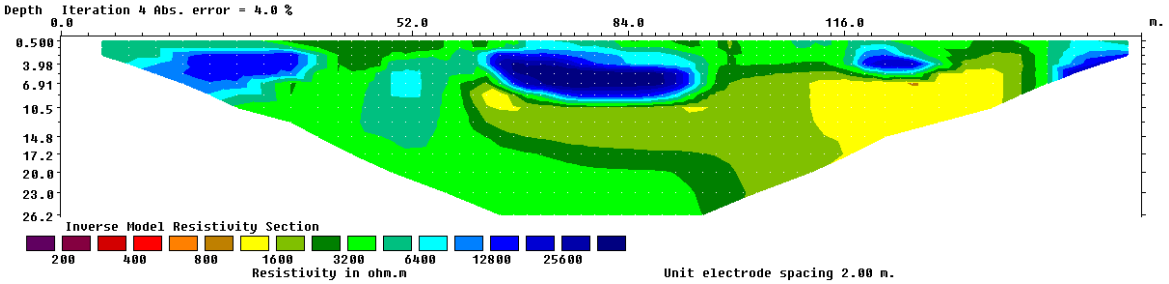

The model has 14 layers and 639 blocks.
Iteration 1 : RMS error 12.77.
Iteration 2 : Abs. error 8.13.
Iteration 3 : Abs. error 5.45.
Iteration 4 : Abs. error 3.99.
Iteration 5 : Abs. error 3.06.
Reference resisivity used is 4322.625
Topographical data present in inversion file.
Damped topography was incorporated into inversion model.
Blocks sensitivity information present.
Average sensitivity is 0.989.
Inversion constraints information present.

Appendix L – Site 8

Project61 MM03 26-07-15
Electrode spacing is 2.000.
General array
Wenner array arrangement
Measurements are in apparent resistivity.
No user defined model depths.
Total number of datum points is 143.
X-distances are surface distances.
143 3501.343
Topography present type 2
Minimum and maximum electrode locations are 0.00 and 160.00.
Minimum electrode spacing is 2.00.
No fixed regions.
Total number of data levels is 14.
Total number of electrodes is 58.
First electrode is located at 0.00.
Last electrode is located at 160.00
Minimum and maximum apparent resistivity values are 0.44 and 4048.08
Minimum, maximum and average geometric factors used in data set are 12.6, 301.6 and 124.1

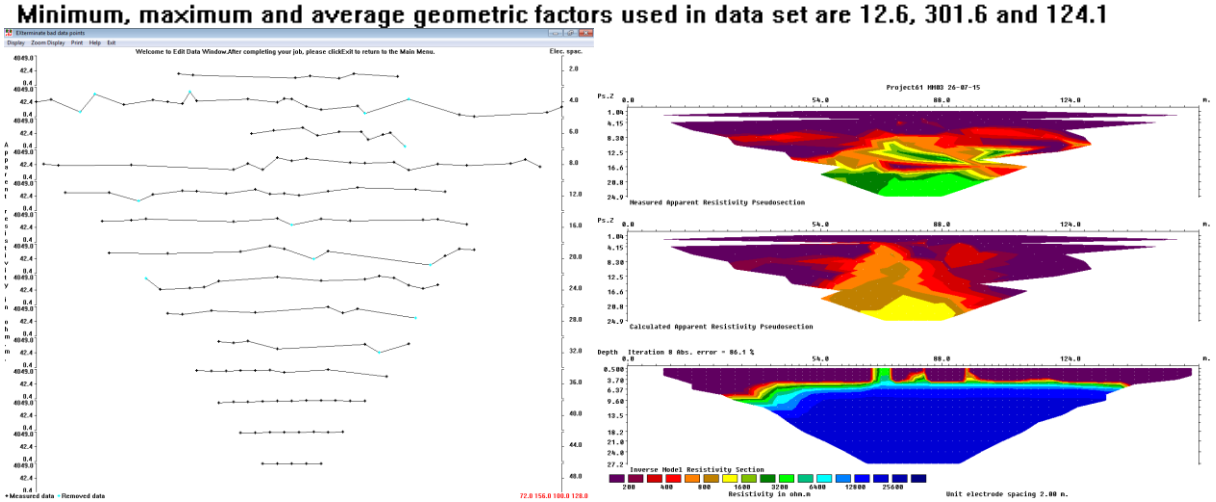

The model has 15 layers and 607 blocks.
Iteration 1 : RMS error 158.27.
Iteration 2 : Abs. error 121.24.
Iteration 3 : Abs. error 110.83.
Iteration 4 : Abs. error 104.17.
Iteration 5 : Abs. error 97.72.
Iteration 6 : Abs. error 92.44.
Iteration 7 : Abs. error 89.05.
Iteration 8 : Abs. error 86.12.
Reference resisivity used is 224.825
Topographical data present in inversion file.
Damped topography was incorporated into inversion model.
Blocks sensitivity information present.
Average sensitivity is 0.348.
Inversion constraints information present.

Appendix M – Site 9

Additional bad points were removed from data shown here and data re-inverted for final model used

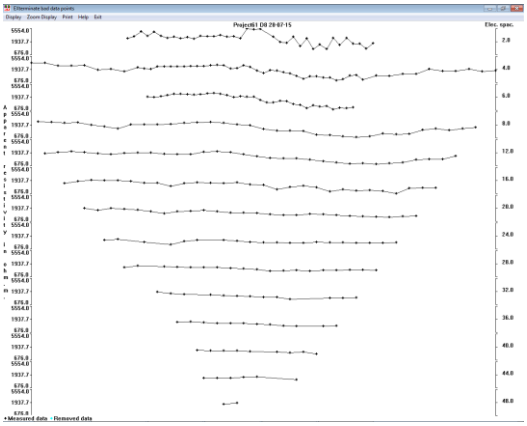

Project61 D8 28-07-15
Electrode spacing is 2.000.
General array
Wenner array arrangement
Measurements are in apparent resistivity.
No user defined model depths.
Total number of datum points is 324.
X-distances are surface distances.
324 1878.200
Topography present type 2
Minimum and maximum electrode locations are 0.00 and 160.00.
Minimum electrode spacing is 2.00.
No fixed regions.
Total number of data levels is 14.
Total number of electrodes is 61.
First electrode is located at 0.00.
Last electrode is located at 160.00
Minimum and maximum apparent resistivity values are 677.28 and 5552.61
Minimum, maximum and average geometric factors used in data set are 12.6, 301.6 and 91.1

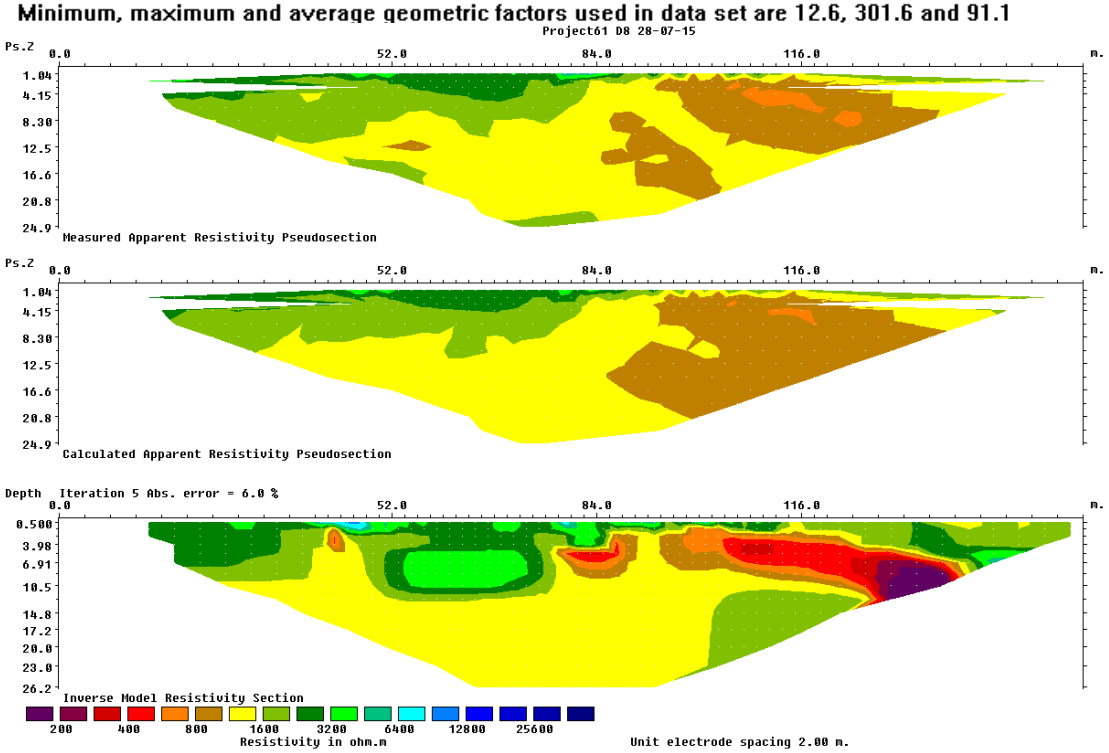

The model has 14 layers and 626 blocks.
Iteration 1 : RMS error 14.42.
Iteration 2 : Abs. error 9.60.
Iteration 3 : Abs. error 7.44.
Iteration 4 : Abs. error 6.66.
Iteration 5 : Abs. error 6.04.
Iteration 6 : Abs. error 5.24.
Iteration 7 : Abs. error 4.90.
Reference resisivity used is 1534.761
Topographical data present in inversion file.
Damped topography was incorporated into inversion model.
Blocks sensitivity information present.
Average sensitivity is 0.933.
Inversion constraints information present.

Appendix N – Site 10

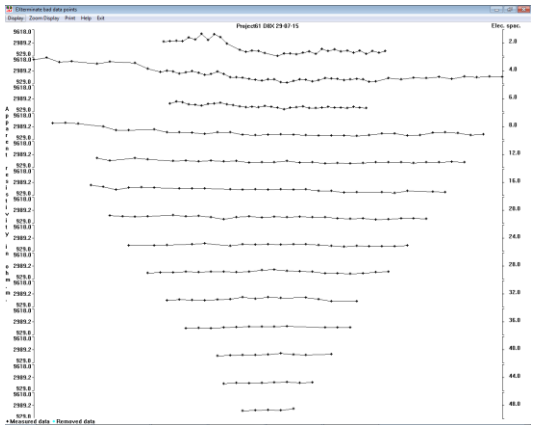

Project61 D8X 29-07-15
Electrode spacing is 2.000.
General array
Wenner array arrangement
Measurements are in apparent resistivity.
No user defined model depths.
Total number of datum points is 318.
X-distances are surface distances.
318 2253.348
Topography present type 2
Minimum and maximum electrode locations are 0.00 and 160.00.
Minimum electrode spacing is 2.00.
No fixed regions.
Total number of data levels is 14.
Total number of electrodes is 61.
First electrode is located at 0.00.
Last electrode is located at 160.00
Minimum and maximum apparent resistivity values are 930.07 and 9616.67
Minimum, maximum and average geometric factors used in data set are 12.6, 301.6 and 95.7

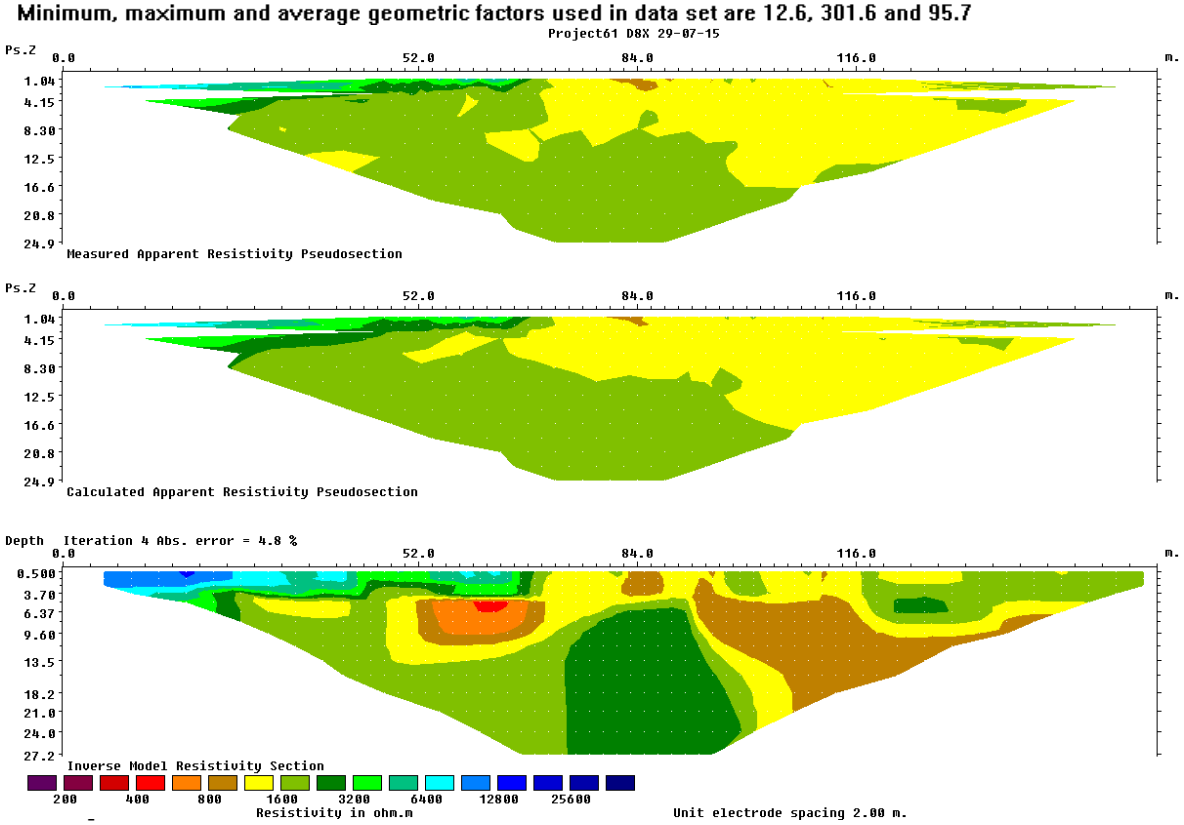

The model has 15 layers and 664 blocks.
Iteration 1 : RMS error 10.74.
Iteration 2 : Abs. error 6.44.
Iteration 3 : Abs. error 5.27.
Iteration 4 : Abs. error 4.79.
Iteration 5 : Abs. error 4.52.
Iteration 6 : Abs. error 4.23.
Iteration 7 : Abs. error 4.11.
Reference resisivity used is 1743.442
Topographical data present in inversion file.
Damped topography was incorporated into inversion model.
Blocks sensitivity information present.
Average sensitivity is 0.844.
Inversion constraints information present.

Appendix O – Site 11

Project61 DS NW 31-07-15
Electrode spacing is 2.000.
General array
Wenner array arrangement
Measurements are in apparent resistivity.
No user defined model depths.
Total number of datum points is 333.
X-distances are surface distances.
333 4903.8102
Topography present type 2
Minimum and maximum electrode locations are 0.00 and 160.00.
Minimum electrode spacing is 2.00.
No fixed regions.
Total number of data levels is 14.
Total number of electrodes is 61.
First electrode is located at 0.00.
Last electrode is located at 160.00

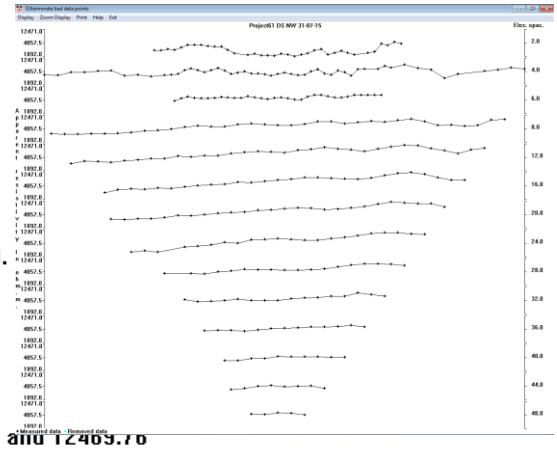

Minimum and maximum apparent resistivity values are 1892.95 and 12469.76
Minimum, maximum and average geometric factors used in data set are 12.6, 301.6 and 96.4

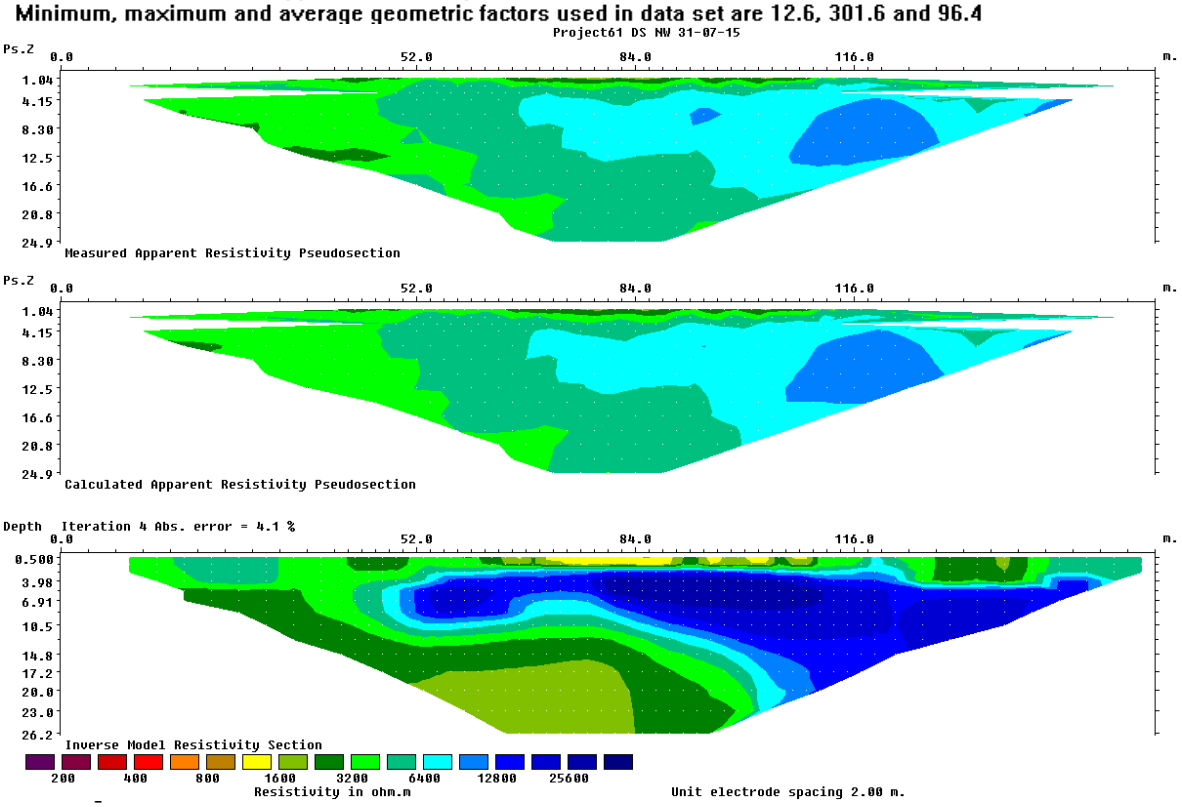

The model has 14 layers and 626 blocks.
Iteration 1 : RMS error 14.04.
Iteration 2 : Abs. error 7.72.
Iteration 3 : Abs. error 5.25.
Iteration 4 : Abs. error 4.12.
Iteration 5 : Abs. error 3.72.
Iteration 6 : Abs. error 3.62.
Reference resisivity used is 5247.439
Topographical data present in inversion file.
Damped topography was incorporated into inversion model.
Blocks sensitivity information present.
Average sensitivity is 0.954.
Inversion constraints information present.

Appendix P – Site 12

Project61 DS SE 30-07-15
Electrode spacing is 2.000.
General array
Wenner array arrangement
Measurements are in apparent resistivity.
No user defined model depths.
Total number of datum points is 335.
X-distances are surface distances.
335 2372.9969
Topography present type 2
Minimum and maximum electrode locations are 0.00 and 160.00.
Minimum electrode spacing is 2.00.
No fixed regions.
Total number of data levels is 14.
Total number of electrodes is 61.
First electrode is located at 0.00.
Last electrode is located at 160.00
Minimum and maximum apparent resistivity values are 767.99 and 1
Minimum, maximum and average geometric factors used in data set are 12.6, 301.6 and 97.2

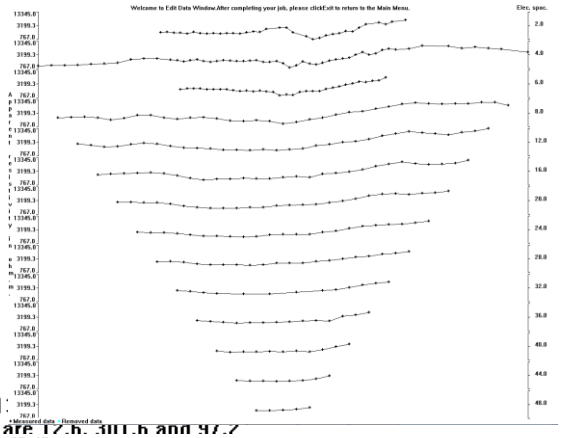

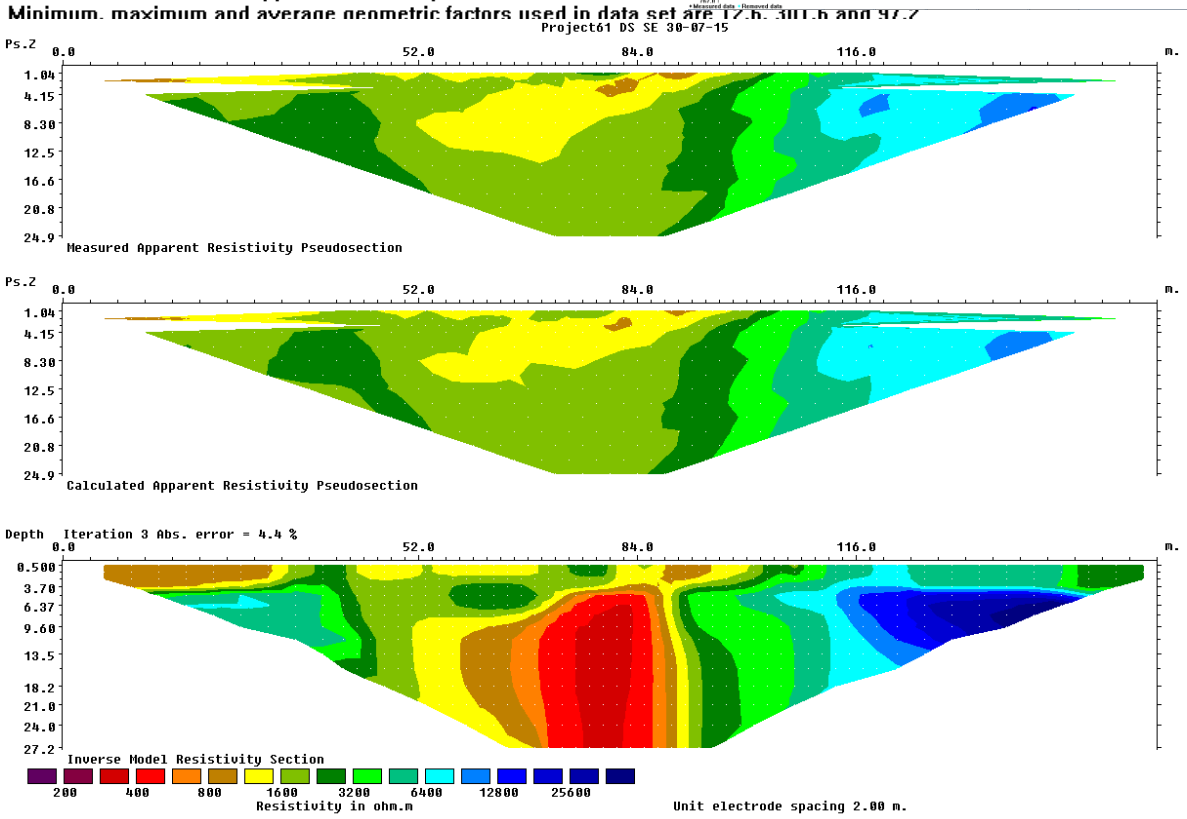

The model has 15 layers and 671 blocks.
Iteration 1 : RMS error 15.12.
Iteration 2 : Abs. error 8.55.
Iteration 3 : Abs. error 4.40.
Iteration 4 : Abs. error 3.63.
Iteration 5 : Abs. error 2.92.
Iteration 6 : Abs. error 2.75.
Iteration 7 : Abs. error 2.58.
Reference resisivity used is 2431.578
Topographical data present in inversion file.
Damped topography was incorporated into inversion model.
Blocks sensitivity information present.
Average sensitivity is 0.915.
Inversion constraints information present.